Molecular basis for digit patterning in the vertebrate limb

Digit patterning is controlled by a BMP-Sox9-Wnt Turing network modulated by morphogen gradients

Jelena Raspopovic

TESI DOCTORAL UPF / ANY 2014

DIRECTOR DE LA TESI: DR: JAMES SHARPE

DEPARTMENT OF SYSTEMS BIOLOGY EMBL/CRG

To my family and to Luciano

Agraïments

I first would like to thank my family for the love and support that they give me in all my life decisions. I want to thank particularly my father for having influenced me on my choice to become a scientist. It is one of the best professions one can have, of course with all the pros and cons that I have learned during my PhD. I want to thank my mother for having pushed me to go to Barcelona in the first place. Mom always knows best! I want to thank my sister Ana for teaching me that nothing is more important than clear thinking and being honest to yourself, and of course for the sense of humor we can only share as sisters, that helped me to cheer up in my grey moments! I want to thank my brother Nikola for his kindness and for being an inspiration as a patient artist and my sister Simona for her love and for bringing up Vida into our lives!!

Milica, Mico moja bez tebe nemoze ni da se zamisli ovaj PhD. Doneo nas zivot u Barcelonu, smestile smo se tu i ludovale ko klinci, pa onda malo porasle, pa se menjale, pa dozivele, i postale drugarice… onako bas! Sve ti dopustam samo da mi ne organizujes svadbu ali i to moze malo… mnogo te volim a ti to vec znas… samo da mi budes srecna!

This PhD would not be the same without my crazy Emre! There are so many nice memories that I will carry with me forever, and hope we will share them very soon, somewhere… maybe London? Ozzy you are the best! Tübingen waits for you whenever you want a little bit of fresh air but I guess I´ll be going to visit the Big-Ben much more often!

I want to thank the entire lab, the past and new members, for their support, friendship and the scientific discussions. I want to thank all the amazing people that I met at the CRG and outside the CRG that made my life during my PhD unique such as Natalia, Adam, Mirko, Alba, Lucia, Alessa, Xavi and Xavi, Vale, Anna y Ananta.

I want to give a special thanks to my supervisor James for his scientific vision and for giving me the opportunity to work on a project that opened my mind on the complex behavior of self-organization.

And last, I want to thank Luciano for his love, for being the most incredible person I ever met, and for sharing life with me.

"…giving a scientific explanation for a remarkable phenomenon does not make it any less miraculous."

V. A. Worwood

Abstract

This thesis focuses on the identification of the Turing network that underlies digit patterning in the mouse limb. Traditionally, digit specification has been explained by positional information models based on the temporal-spatial gradient of Sonic Hedge Hog (Shh). However embryonic and genetic manipulations have shown that Shh is dispensable for digit specification and have suggested that this process may be instead controlled by a reaction-diffusion Turing network. Despite extensive theoretical work, the identity of the molecules that implement the Turing network is still unknown. In this work I combine descriptive and functional experiments with modeling predictions to show that a Turing network implemented by Bmps, Sox9 and Wnts underlies digit patterning. From a broader point of view, this study provides an example of a systems biology approach to identify and evaluate Turing networks that underlie spatial patterning during development. Finally, I propose a retrospective interpretation of previous experiments under the light of a new digit patterning model that integrates growth, positional information signals and a Turing mechanism.

Resum

Aquesta tesi es centra en la identificació de les molècules de la xarxa de Turing que controla el patró dels dits en l'extremitat del ratolí. L'especificació dels dits ha estat explicada a la llum del model de Positional Information i el gradient temporal-espacial de Sonic Hede Hog (Shh). No obstant, manipulacions embrionàries i genètics han demostrat que Shh no és necessari per l'especificació dels dits i han proposat que en lloc aquest procés pot ser controlat per una xarxa de reacció-difusió de Turing. Malgrat l'extens modelatge teòric, les molècules de la xarxa de Turing va romandre desconegudes. Aquest estudi combina experiments descriptius i funcionals amb el modelatge per mostrar que una xarxa de Turing implementada per Bmps, Sox9 i Wnts controla el patró dels dits. Mes en general, aquest estudi proporciona un exemple d'una estratègia que usa la biologia de sistemes per identificar i avaluar les xarxes de Turing que controlen els patrons espacials durant el desenvolupament. Finalment, proposa una interpretació retrospectiva dels experiments realitzats prèviament a la llum d'un nou model de especificació dels dits que integra el creixement, els senyals d'informació de posició i un mecanisme de Turing.

Prefaci

This thesis focuses on the molecular mechanism that drives the specifications of the digits during mouse limb development. Digit specification has been explained by two fundamentally different models: the Positional Information model (Wolpert, 1969) and the self-organizing Turing model (Turing, 1990). During the last two decades, the Positional Information model has been the most prominent theory thanks to experimental evidence that supported the Sonic Hedgehog morphogen (SHH) as a positional information gradient that specifies the digits. In contrast, the Turing model has lacked the support of strong molecular and genetic data and has remained an interesting theoretical possibility, rather than a central concern of the developmental biology community. Recent genetic data however, have strengthened the Turing hypothesis and have suggested that distal Hox genes expressed in the limb modulate the Turing network that specifies the digits. Nevertheless, the molecules that implement the network have not yet been identified.

This thesis provides the first experimental evidence that Bmps, Sox9 and Wnts implement the Turing network that controls digit specification. An original aspect of this work is the systems biology approach that we developed by combining experiments and mathematical modeling. All the experimental work in this study was performed by me, while the mathematical modeling has been done by Luciano Marcon, another PhD student in the lab.

This thesis is structured in four chapters that are organized as follows. The first introductory chapter begins with a brief history of pattern formation and discusses the Turing and the Positional Information model in details. In this part of my thesis, I emphasize the conceptual differences between these two models and I present the experimental evidence that support the two theories in other model systems. The chapter follows with an introduction to limb development which mostly focuses on the anterior-posterior (AP) patterning of the limb. In this section, I review the evidence in favor of a Turing model and a Positional Information model for digit specification. I continue the chapter by describing the earliest chondrogenic marker Sox9 and its importance for the study of skeletal patterning. In this section, I also give an overview of the signaling pathways involved in the regulation of Sox9. Finally I highlight the importance of an accurate staging system for the study of limb development and I discuss the significance of a detailed three dimensional gene expression analysis to study pattern formation.

In the second and third chapter I present the main objectives of this thesis and the results of my work respectively. In the results chapter, I present unpublished detailed 3D expression patterns

obtained by Optical Projection Tomography (OPT). This data provides a detailed description of molecules that play an important role during the early digit patterning process. In this chapter I also present my two publications with the respective supplementary material.

My first publication with the title **"A GDF5 Point Mutation Strikes Twice - Causing BDA1 and SYNS2"**, is a collaboration with the laboratory of Petra Seemann at the Berlin-Brandenburg Center for Regenerative Therapies (BCRT). I collaborated with the Seemann lab, to describe the expression patterns of the BMP/GDF family genes and related molecules. This analysis confirmed that changes in BMP signaling activity underlie the development of skeletal malformations observed in brachydactyly type A1 (BDA1) and the synostoses syndrome 2 (SYNS2). My contribution to this work is a detailed description of the 3D expression patterns of *Gdf5*, *Noggin*, *Bmpr1a* and *Bmpr1b* showed in Figure 6 of this paper. This analysis shows that the genes are co-localized in the digital rays from E11.5 to E13.5 suggesting possible interaction that may underlie the malformations observed when GDF5 has a point mutation in the overlapping interface of antagonist and receptor binding site.

The second publication **"Digit patterning is controlled by a Bmp-Sox9-Wnt Turing network modulated by morphogen gradients"** is the main paper of my thesis. This paper provides molecular evidence that a Turing network involving Bmp, Sox9 and Wnt genes controls digit specification in the mouse limb. To pinpoint the candidate genes for the Turing network, I use several different experimental techniques: live imaging of Sox9-EGFP mouse limb micromass cultures, gene expression microarray analysis of Sox9-EGFP positive and negative cells, time-course of gene expression patterns and immunohistochemistry of signaling pathway activities. Together with mathematical modeling, these experiments contribute to the elaboration of a Turing network consisting of Bmps Sox9 and Wnts for the specification of the digits. Numerical simulations performed by Luciano Marcon show that this network is able to accurately capture the spatio-temporal dynamics of digit patterning in a realistic model of the wild type limb development. I also show that the effect of perturbations predicted by the model agrees with the perturbations performed in limb cultures treated with BMP and WNT signaling inhibitory drugs.

To conclude, in the fourth chapter of this thesis, I discuss the results of my work and I present possible future directions.

Index

Llista de figures

1. INTRODUCTION

1.1 Pattern formation in development

One of the most fascinating questions in developmental biology is how a complex multicellular organism forms from an initially single fertilized cell. From the egg to the embryo and from the embryo to the adult, cells and tissues organize spatially to form organs with specific size, pattern and function, despite the fact that all cells contain the same genetic code. By definition, pattern formation is the generation of temporal and spatial organization of cell fates during development. This is a key developmental process and together with morphogenesis, cell proliferation, cell death and cell differentiation contributes to create the body plan of the embryo in a reliable manner (Wolpert, 1971). Pattern formation is directly connected to but different from cell differentiation. While pattern formation defines the spatial distribution of cell fates, cell differentiation is the process that describes how cells are able to differentially activate genes as consequence of their acquired cell fate (Wolpert, 1971, Wolpert, 1969) and thus to turn into different cell types.

Although the concepts that underlie pattern formation during development seem relatively easy to us today, it has been necessary to accumulate a lot of scientific knowledge throughout history to enable us to pose the problem in the correct way.

"The key to the problem of pattern formation lies in the correct posing of the problem so that an answer can be obtained in terms of cellular behavior" (Wolpert, 1969).

1.1.1) Conceptual foundations of pattern formation throughout history

The first questions regarding pattern formation were phrased already in ancient Greece. The famous philosopher Aristotle proposed a theory called "epigenesis" by observing the development of the chick embryo. His theory proposed that during development, the different parts of an embryo were created from an undifferentiated state by hierarchical events. Unfortunately Aristotle's epigenesis was replaced by preformationist theories, up to the 18th century. Preformationists claimed that the embryo came from a preexisting miniature human called the "Homunculus" that was contained in the father's semen, an idea that was more consistent with a religious creationist view rather than empirical observations.

In the mid of the 17th centrury, the advances in microscopy led to the creation of the cell theory proposing that cells were the units of life. This theory and the discovery of the mammalian ovum by Karl Ernst von Baer radically changed the view on embryonic development. The fertilized egg became the main focus of developmental biologists that wanted to explain how the zygote could develop into a complex organism.

By the end of the 19th century, August Weismann proposed the first theory to explain early embryonic patterning. In his mosaic model he assumed that the zygotic nucleus contained factors that directed the development of the embryo and were asymmetrically distributed to each daughter cell during cleavage. The "mosaic development" was supported by experiments done in frog embryos by Wilhelm Roux, who showed that the destruction of one cell in the 2 cell-stage of the zygote resulted in half an embryo. However, in 1924, famous experiments done by Spemann and Mangold, showed that cells situated in specific regions of the embryo had an inductive role to other cells and directed their differentiation. These experiments pioneered the view of "regulative development" where the specification of a group of cells was highly dependent on global interactions in the developmental field, rather than on the growth of the whole embryo from a single cell (Wolpert, 1969). By the 1950's, with the discovery of the DNA molecule and the advances in molecular biology, the study of development focused on genes and how they related to the molecular nature of the organizers and morphological changes of the embryo.

The two most recent models of pattern formation were proposed in the mid of the last century and are still today important theoretical frameworks in developmental biology. The first model was presented by Alan Turing in 1952, who proposed the reaction-diffusion model (Turing, 1990). In his simplest formulation the reaction-diffusion model was based on two diffusible molecules, called morphogens, which reacted together and were able to spontaneously form periodic patterns starting from a homogenous state. The second model, called Positional Information, was presented by Lewis Wolpert in 1969 (Wolpert, 1969) who proposed that morphogen gradients released from organizing regions could induce different cell fates according to different morphogen concentrations.

1.1.2) Turing reaction-diffusion model

Alan Turing was an English mathematician born in 1912. He is best known as the founder of computer science and for his help in code breaking the German ciphers during Second World War. However, Turing was also one of the first mathematical biologists (Murray, 2012). In 1952, he published the paper "The Chemical Basis of Morphogenesis" (Turing, 1990), where he proposed the reaction-diffusion model (RD) as a possible mechanism to explain pattern-formation during embryonic development. Turing´s model suggested that a system of two diffusible morphogens that reacted together could generate ordered patterns from an initial homogenous state by amplifying stochastic fluctuations.

In his simplest model, Turing hypothesized a two cell system in which each cell produces two diffusible substances: X and Y. These two substances, that he called morphogens, can diffuse and react following normal chemical laws of reaction and diffusion. Their production is governed by the following equations:

$$(X) = 5X - 6Y + 1 \qquad (1.1)$$

$$(Y) = 6X - 7Y + 1 \qquad (1.2)$$

The diffusion rate of X is 0.5 (for unit difference of concentration between cells) and the diffusion rate of Y is 4.5. In the case when both X =1 and Y=1, according to (1.1) and (1.2), the system remains unchanged because the production terms of X and Y are zero and no diffusion occurs. In this case, the two cells are in a homogenous state and no spatial pattern of X and Y is formed between the two cells. If the concentrations of X and Y become slightly different due to random fluctuations, the system is able to deviate from the homogenous steady state and form a spatial pattern of X and Y concentrations. Let's assume for example that, $X_1 = 1.06$ and $Y_1 = 1.02$ in the first cell, and that $X_2 = 0.94$ and $Y_2 = 0.98$ in the second cell. Then the production rate of X and Y, according to (1.1) and (1.2) is going to be $X_1 = + 0.18$, $Y_1 = + 0.22$ in the first cell and X2 = -0.18, Y2 = -0.22 in the second cell, and the rate of diffusion from the first cell to the second cell is going to be 0.6 and 0.18 for X and Y respectively. By summing the contribution of reaction and diffusion we obtain a flow of the morphogens from the second cell to the first cell at the rate of 0.12 and 0.04 for X and Y respectively. This difference exponentially increases at every step drifting away from the equilibrium condition and accentuating the asymmetry between the two cells.

Turing extended this idea to a general reaction-diffusion system composed of a ring of cells and revealed that depending on the parameter values, the system could exhibit six different behaviors (Figure 1).

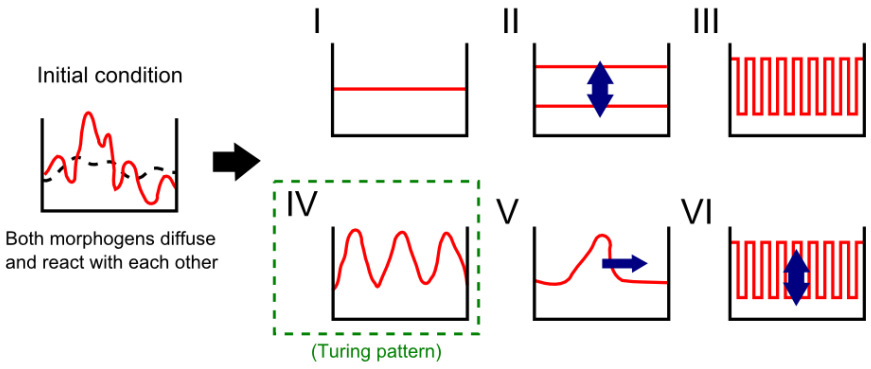

Figure 1. Schematic representation of the states that a Turing reaction-diffusion model can achieve. From the initial condition (right) the system can assume the following states: I) *Stationary case with extreme long wavelength* II) *Oscillatory with extreme long wave-length* III) *Stationary waves of extreme short wave-length* IV) *Stationary waves of finite wave-length*. This state is commonly called the Turing instability or Turing pattern. V) *Travelling waves* VI) *Out of phase oscillations with extreme short wavelength*. Note that the state V and VI need three (or more) morphogens. Figure adapted from (Kondo and Miura, 2010).

These six behaviours can be described as follows:

I-"*Stationary case with extreme long wavelength"*: In this case, the system converges to a stable and uniform state where all cells are the same: there is no flow of morphogens from cell to cell, (no diffusion), cells behave as if they are isolated.

II-"*Oscillatory with extreme long wavelength".* In this case the system oscillates homogenously, it is the same as in case I but with the oscillation of the morphogens.

III-*"Stationary waves of extreme short wavelength".* Cells have alternated identities like in a chessboard or in a lateral inhibition pattern.

IV-*"Stationary waves of finite wavelength".* Cells show a periodic stationary wave pattern in space. The number of peaks formed depends on the diffusion constants and on the radius of the ring of cells. This case is typically referred as a *Turing pattern*.

The last two dynamic states only occur if the equations are written for three or more morphogens:

V-*"Travelling waves".* This state generates a travelling wave.

VI-*"Out of phase oscillations with extreme short wavelength"*. This case generates a similar pattern to case II but with oscillations.

The main result of the analysis of Turing is the dynamic state IV, *"Stationary waves of finite wavelength",* and it is usually referred to as the Turing pattern or diffusion-driven instability. Turing showed that in this case, the system was able to form periodic spatial patterns without the need for any preexisting asymmetry besides small initial random fluctuations of the morphogen concentrations (Figure 2). Depending on the reaction rates and the diffusion coefficients, the system formed patterns with specific wavelength (periodicity).

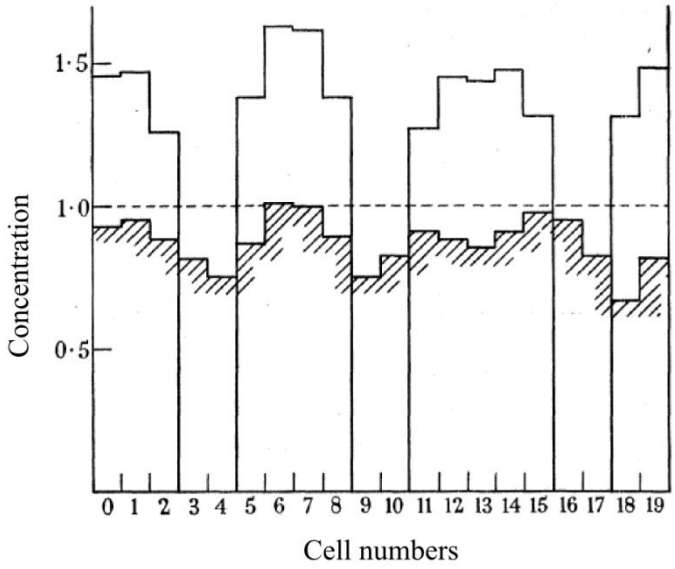

Figure 2. The concentration of the morphogen Y in a numerical simulation performed by Turing. The horizontal dashed line is the starting homogeneous steady state, the continuous line is the final equilibrium periodic pattern. The line highlighted by oblique lines is an intermediate state. Figure taken from (Turing, 1990).

In his original paper Turing proposed that the stationary wave patterns could explain the patterning of Hydra tentacles and whorled leaves. Turing also went further and considered his reaction-diffusion model in a three dimensional sphere as a model for gastrulation. The discovery of Turing and his extensive analysis was and still is a breakthrough for the study of pattern formation.

1.1.3) Gierer and Meinhardt Activator-Inhibitor (AI) and Substrate-Depleted (SD) models

A very important contribution to the study of reaction-diffusion models was proposed by Gierer and Meinhardt in (Gierer and Meinhardt, 1972). They proposed more biologically realistic reaction-diffusion models made of two morphogens: one being an activator and the other an inhibitor. They formulated their model showing that two necessary conditions are required for a diffusion-driven instability: (a) a short-range autocatalysis of the activator (b) a production by the activator of its long-range inhibitor (Gierer and Meinhardt, 1972, Gierer, 1981).

Gierer and Meinhardt developed two basic models that could satisfy these two conditions, the Activator-Inhibitor Model and the Substrate-Depleted Model:

(A) The Activator-Inhibitor model (AI): an activator *u* activates itself and stimulates the production of its own inhibitor *v*. The model is equivalent to the original model proposed by Turing model and its equations are:

$$\frac{\partial u}{\partial t} = \rho_u \frac{u^2}{(1 + k_u u^2)v} - \mu_u u + \sigma_u + D_u \nabla^2 u$$

$$\frac{\partial v}{\partial t} = \rho_u u^2 - \mu_v v + \sigma_v + D_v \nabla^2 v$$

The term $\frac{u^2}{(1+k_u u^2)v}$ represents the auto-activation of *u* (u^2), the inhibition from *v* (that is at the denominator) and the saturation on the auto-activation depending on k_u. The terms μ_u and μ_v are the decay of *u* and *v* respectively. σ is the production term of u and v. The diffusion rate is given by $D_u \nabla^2 u$ and $D_v \nabla^2 v$ being D_u and D_v the diffusion constants of *u* and *v* respectively. The source density or competence ρ describes the ability of the cells to perform the auto-catalysis and is usually set to obtain absolute concentrations around one. Superimposed small fluctuations (+/-1%) are sufficient to trigger the onset of pattern formation. A schematic representation of this model is shown in Figure 3.

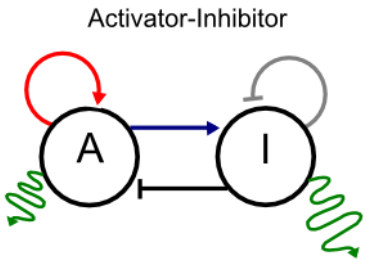

Figure 3. Topology of the AI model.

A activates itself (red arrow) and its own inhibitor I (blue arrow). I diffuses faster than A (green curved arrows). A linear decay (gray inhibition arrow) limits the growth of I.

To illustrate the process of pattern formation driven by the AI model, I will describe a hypothetical simulation in one dimension (1D) over time (Figure4). Starting from the homogenous steady-state if there are no perturbations, u and v will not form any pattern (Figure 4I). If due to random fluctuations, the concentration of the activator (u) raises slightly (Figure 4II), the auto-activation on u allows it to increase further (A in figure 4III) and diffuse into the surroundings; u is able to activate the inhibitor (v) that diffuses faster due to its higher diffusion rate (B in Figure 4IV); because of this fast diffusion, v is able to substantially accumulate in the lateral neighboring regions of u (C in Figure 4V). This locally depresses the activator function, resulting in the decrease of the activator concentrations (C in Figure 4V). Subsequently the decrease of activator causes the decrease of inhibitor in the surrounding regions (D in Figure 4V). As the inhibitor concentration goes lower, the activator becomes relatively more dominant than the inhibitor, and allows again the start of the auto-activation (E in Figure 4VI). In the final periodic pattern, u and v are in-phase, their peaks of high concentration are overlapping in the same region.

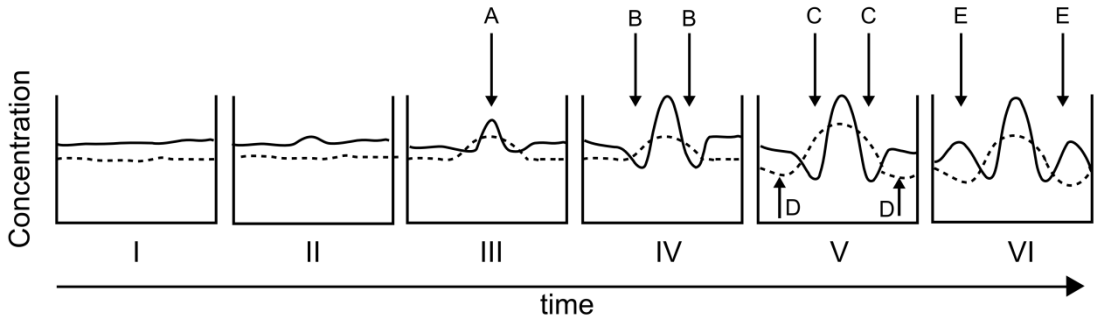

Figure 4. Hypothetical 1D simulation for the AI model.

The activator (u) is represented with full black line and the inhibitor (v) with dashed line. I) Homogenous steady-state. II) u rises slightly due to random fluctuations. III) The autoactivation of u allows it to rise further (A) IV) The rise of u promotes the up-regulation of the inhibitor v that diffuses faster in the surroundings (B). V) The inhibitory effect of v downregulates u in (C) which provokes u downregulation

further apart in (D). VI) The downregulation of v allows for a new auto-activation and up-regulation of u in (E). Figure adapted from (Kondo and Miura, 2010).

(B) The Substrate-Depleted model (SD): In this model the activator *u* activates itself but at the same time depletes a substrate *v*. The equations for this model are the following:

$$\frac{\partial u}{\partial t} = \rho_u \frac{u^2 v}{(1 + k_u u^2)} + \sigma_u + D_u \nabla^2 u$$

$$\frac{\partial v}{\partial t} = -\rho_v \frac{u^2 v}{(1 + k_u u^2)} + \sigma_v + D_v \nabla^2 v$$

Where the term $\frac{u^2 v}{(1+k_u u^2)}$ in both equations represent that *u* activates itself (u^2) by consuming *v* with a saturation of the auto-activation k_u. A schematic representation of this model is shown in Figure 5.

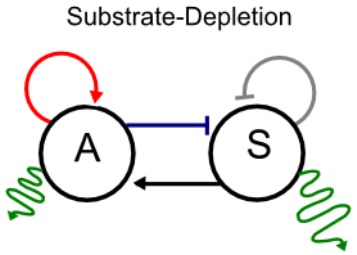

Figure 5. Topology of the SD model.
A activates itself (red arrow) and consumes the substrate S (blue arrow). S diffuses faster than A (green curved arrows). The linear decay of S (gray inhibition arrow) limits the growth of A.

To illustrate the dynamics of the SD model, I will again describe a hypothetical simulation in time and space. Starting from the homogenous steady-state, u and v will not form any pattern in the absence of perturbations (Figure 6I). If due to random fluctuations, the activator concentration raises slightly (Figure 6II), the auto-activation on u allows it to increase further (A in Figure 6III) and to diffuse in the surroundings; this time in the A region, u is going to consume the substrate v (Figure 6IV); in a neighboring region B the substrate concentration is still high (Figure 6V). The higher levels of the substrate in B, result in the increase of the

activator concentration in C (Figure 6VI). At the region C, the activator grows due to auto-activation and again depletes the substrate v (Figure 6VII). Contrary to the AI model, in the SD model the two morphogen patterns are out-of-phase (their periodic patterns are opposite, where u is high v is low and vice-versa).

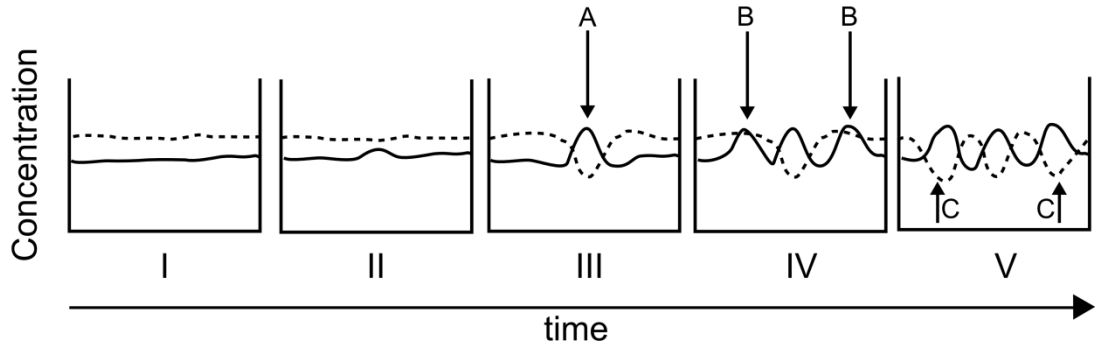

Figure 6. Hypothetical 1D simulation for the SD model.

The activator (u) is represented with full black line and the substrate (v) with dashed line. I) Homogenous steady-state of u and v. II) u rises slightly due to random fluctuations. III) The auto-activation further increases u that consumes v in (A). IV) The high concentrations of v in the surroundings (B) up-regulates u V) . Again, u raises further by autoactivation and deletes v (C).

To conclude, Turing pioneered the discovery that spatial patterns can be generated by a reaction-diffusion model. In particular, he proposed that two or more morphogens with different diffusivities can spontaneously from a periodic pattern of concentrations from small perturbations of a homogeneous state. On the other hand, Gierer and Meinhardt showed that the generation of a diffusion-driven instability only occurs if two conditions are satisfied, short range auto-activation and long range lateral inhibition. These conditions describe in more general terms which reaction-diffusion systems can produce stable patterns and lead to the creation of models with more biologically realistic interactions (Meinhardt, 2012). Finally, Gierer and Meinhardt defined two classes of models: the Activator-Inhibitor and Substrate-Depleted model. The first creates periodic concentration patterns with the two morphogens in-phase while the second create out-of-phase concentrations patterns.

1.1.5) Experimental evidence for Turing models in Biology

Turing´s model gained new popularity two decades after his publication, when studies of Prigogine and his co-workers on theoretical thermodynamic (Prigogine and Lefever, 1968, Glansdorf and Prigogine, 1971, Nicolis and Prigogine, 1977) proposed that chemical reactions could behave as a reaction-diffusion systems. This led to the first experimental evidence for a diffusion-driven instability: a chemical reaction system between malonic acid and chlorite-iodide in a gel reactor (Castets et al., 1990) usually referred to as the CIMA reaction (Figure 7)(De Kepper and Epstein, 1982).

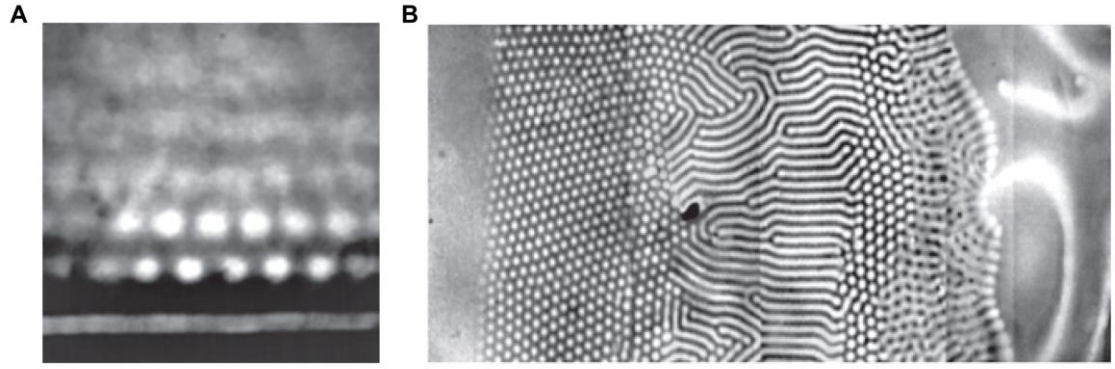

Figure 7. The CIMA reaction.

A) The original CIMA reaction from (Castets et al., 1990). The change of parameters results in the observation of different Turing patterns, from stripes (bottom) to spots (middle). B) A more complex setting for the CIMA reaction with a ramp of different parameters, show the variety of possible Turing patterns that can be formed: spots, stripes, bifurcations and "anti spots". Figure adapted from (Szalai et al., 2012).

Although CIMA experiments showed that chemical reactions could indeed form Turing instabilities, a step further was needed to prove that a reaction-diffusion mechanism could pattern living systems. During the 80´s and 90´s, a major drawback for the acceptance of Turing´s model by the developmental biology community, was the discovery that the body-plan of *Drosophila* was not controlled by a self-organizing system but rather by a maternal determinant that acted as a positional information gradient (Driever and Nüsslein-Volhard, 1988), further discussed in section 1.1.7.

However, in the last decade, several studies that combined modeling and experiments have revived the interest in Turing´s model (Marcon and Sharpe, 2012). On one side, modern genetic and molecular techniques have suggested new gene networks that could produce Turing

patterns. On the other hand, the creation of realistic mathematical models that can predict the non-intuitive dynamical behavior of Turing mechanisms, have allowed biologists to interpret and design new experimental perturbations to verify the Turing networks. I will briefly describe some of the studies that have proposed Turing mechanisms to explain patterning process during development.

The early left-right asymmetry in bilaterian vertebrate embryos, such as zebrafish, mouse and frog, is governed by TGF-β family members Nodal and Lefty (Solnica-Krezel, 2003, Nakamura et al., 2006). Functional experiments showed that Nodal behaves as an activator and Lefty as an inhibitor implementing the Activator-Inhibitor network of Gierer and Meinhardt (Nakamura et al., 2006, Hamada, 2012, Shen, 2007) . This was supported by genetic assays that proposed that auto-activation of Nodal and the negative feedback of Lefty could produce a Turing instability (Chen and Schier, 2002, Hamada et al., 2002, Saijoh et al., 2000) . In addition, simulations of the Nodal-Lefty system (Nakamura et al., 2006) showed that a model similar to the AI model of Gierer and Meinhardt was able to reproduce the phenotypes observed in the experimental perturbations. Finally, fluorescence recovery after photo bleaching (FRAP) showed that Lefty diffuses fourteen times faster than Nodal in agreement with the differential diffusivity required to form a Turing pattern (Muller et al., 2012).

For a long time it was hypothesized that skin appendages (such as hairs, feathers, scales, sensory bristles and pigmentation markings) are patterned by Turing mechanisms. However, experimental data that confirmed this hypothesis was provided only in the last two decades (Painter et al., 2012). In particular a reaction-difusion model proposed that Shh and Fgf4 act as the activators and Bmp2, Bmp4 as the inhibitors of the Turing network that specifies the periodic pattern of feathers in the skin (Jung et al., 1998). By performing bead experiments in chick, this study showed that FGF4 and SHH induced local expression of *Bmp4*, while BMP4 suppressed local expression of both *Fgf4* and *Shh*. The study also showed that a computer simulation of the Turing model could reproduce feather pattern formation. In more recent years, another model of feather development proposed Bmp2 as the inhibitor and Bmp7 as the activator in an activator-inhibitor (AI) reaction-diffusion network (Michon et al., 2008). This study showed that Bmp7 was implicated in the chemotaxis of progenitor feather cells, whereas Bmp2 lead to an arrest of the migration. A mathematical model that considered an AI Turing network between Bmp2 and Bmp7, as well as cell proliferation and chemotaxis, was proposed to recapitulate *Bmp2* and *Bmp7* expression during wild-type feather patterning. However, this model could not explain the feather bud fusions caused by transformation of inter bud region (Jung et al., 1998, Widelitz et al., 1996). Recent studies on feather patterning (Mou et al., 2011, Painter et al., 2012) showed that the difference between the pattern in the neck of a normal

chick and the pattern of a natural mutant with bare neck was due to elevated production of BMPs. These studies considered an Activator-Inhibitor model where Bmps acted as the inhibitors, retinoic acid (RA) as a BMP signaling modulator and an unknown molecule as the activator. The model was able to explain loss of feathers upon addition of exogenous BMP and appearance of a stripy feather pattern when the BMP sensitivity was lowered by the addition of RA. These studies concluded that a lower threshold of BMP signaling obtained by RA modulation was able to completely suppress feather development in the neck region.

Similar to feather patterning, already in the 80s it was proposed that hair follicle specification was regulated by a reaction-diffusion mechanism (Nagorcka, 1983, Nagorcka and Mooney, 1985). However, molecular evidence supporting this hypothesis was found only in recent years. The first molecular model proposed Wnts as the activators and Dkks as the inhibitors of the Turing mechanism that controls hair follicle specification (Sick et al., 2006). It was shown that WNT signaling was active in the forming hair follicle and that it promoted the expression of its inhibitor Dkk4. A WNT/DKK mathematical model was able to predict the reduced appendage density observed upon *Dkk* over-expresssion and the increase on appendage density observed upon exogenous activation of WNT signaling. However, a parallel study proposed an alternative Activator-Inhibitor network to explain the same process (Mou et al., 2011, Headon and Painter, 2009) suggesting that Eda acted through its receptor Edar to stimulate both its own production as well as production of its inhibitors, Bmp4 and Bmp7. This model was able to reproduce the wild-type periodic pattern of hair follicles as well as experimental manipulations that produced a stripy hair follicle pattern when high concentrations of exogenous Eda were added. These two alternative models for hair specification, the WNT/DKK and Edar/BMP networks were also suggested to be connected since Edar can induce expression of *Wnt10a*, *Wnt10b* while WNT canonical pathway stimulates the expression of *Edar* itself (Bazzi et al., 2007, Fliniaux et al., 2008, Zhang et al., 2009).

A very well-known study on Turing patterns, is the work of Kondo and Asai (Kondo and Asai, 1995) that demonstrated that the stripy arrangement of pigmented scales in the fish *Pomacanthus imperator* could be explained by a Turing mechanism. Later studies from Kondo´s lab showed that the stripe regeneration, that followed laser-ablation of the pigment cells in zebrafish, was in agreement with the dynamics predicted by a reaction-diffusion two-dimensional simulation (Yamaguchi et al., 2007). Based on these observations, this study proposed that the pigmentation pattern of Zebrafish was specified by a Turing mechanism of interacting diffusible morphogens. However, following studies showed that the pattern was rather formed by the interaction of different pigmented cell types (Nakamasu et al., 2009) that physically migrated to re-arrange following cell to cell signaling mediated by dendrite contacts

(Inaba et al., 2012). It was proposed that the contact-repulsion observed between two pigmented cell-types could act as a short range auto-activation and long-range lateral inhibition, therefore not contradicting the Turing hypothesis. Interestingly, another study showed that by mutating connexin41.8, a gap-junction component, the pigmented stripes of Zebrafish were transformed into spots (Watanabe et al., 2006).

Lung branching has also been suggested to be controlled by reaction-diffusion system (Miura and Shiota, 2002) and in a recent work, a model was proposed for this hypothesis, implemented by FGF10 as an Activator and SHH as a Substrate in a Substrate-Depleted Turing network (Menshykau et al., 2012). This network was simulated on a model of the growing lung bud and predicted that different growth speeds would change the type of branching formed by the lung buds.

Finally a recent study proposed that FGF and SHH signaling can drive rugae formation in the mammalian palate by implementing an Activator-Inhibitor Turing network (Economou et al., 2012). Similar to the stripe ablation in zebrafish, this study showed that when rugae were removed their regeneration followed dynamics that fitted with two-dimensional simulations of a Turing model. It was also found that the pattern of FGF signaling activity (as revealed by Spry2 expression) reflected the rugae pattern. Genetic and pharmacological functional experiments showed that reduction of Fgf signaling caused a disorganized pattern. Similarly, when SHH signaling was inhibited the rugae pattern was disrupted.

1.1.6) The Positional Information model.

The basic idea of the Positional Information model is that there is a cellular parameter, a positional value, which is related to a cell´s position in the developing system (Wolpert, 1969). This concept was elaborated by Lewis Wolpert in 1969, that influenced by early experimental work on sea urchin embryos and Hydra regeneration, proposed a basic idea to explain patterning during development. Previous work by Hans Driesch had proposed the basic idea of a mechanism that specified cell positional values to induce specific differentiation (Driesch, 1893). Later, the works of Child (Child, 1941) suggested that physiological gradients were essential for embryological development and experiments performed by Hörstadius (Hörstadius, 1935, Olsson, 2007) showed that cell fates were specified in a graded manner: cells in the anterior pole of the sea urchin embryo had a graded fate of ´animalness´ (epidermal determination) while cells in the posterior pole had a graded fate of ´vegetalness´ (endodermal determination). Lewis Wolpert was originally studying hydra and was fascinated by the fact that

when parts of the hydra were dissected they could give rise to an almost complete adult animal. This lead him to formalize questions about pattern formation and to propose the French Flag problem (Wolpert, 1969) to explain universal principles governing pattern formation in development.

He illustrated the problem by questioning how a row of identical cells could be able to differentiate into blue, white, or red cell fate to form a French Flag pattern irrespectively of the number of cells (Figure 8). Wolpert proposed that the French flag problem could be solved by assuming that positional information in form of a morphogen gradient was giving to each cell their fate according to their position along the gradient (see Figure 8). Wolpert proposed that the French Flag problem could be solved in two phases:

I- *Specification*: The first phase is the formation of the morphogen gradient that confers positional values to cells. The gradient can be formed by alternative mechanisms, by local production and diffusion or by active transport. Different mechanisms can produce different gradient profiles. Wolpert gave an example of a local morphogen (source on one extreme whose sink is at the other extreme) which results in a linear gradient; however a more realistic gradient in terms of biological gradient profiles would be exponential (Figure 8). This phase requires cell communication or diffusion.

II- *Interpretation*: In the second phase cells interpret their positional value and differentiate. Different morphogen concentrations or thresholds are able to trigger different genetic responses in the cells and can be interpreted to form a spatial pattern (such as the hypothetical pattern of blue, white and red state of cells in the French Flag problem see Figure 8). The interpretation phase is not dependent on cell communication. It is a cell-autonomous process that depends only on the positional value and historical background of each cell (Wolpert, 1969).

In summary the concept of positional information defined the hypothesis that molecular gradients can determine different cell fates in a group of identical cells thus originating a spatially organized pattern.

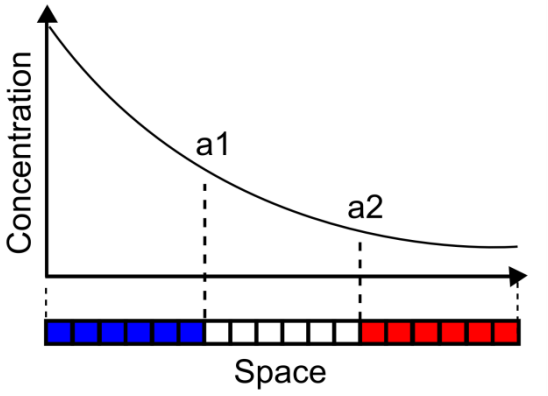

Figure 8. Schematic representation of the Positional Information model.

The graph shows an exponential morphogen gradient profile along the space with two thresholds highlighted: a1 and a2. A line of cells (bottom) interprets the morphogen gradient concentration and translates it into distinct cell fates: cells that experience morphogen concentration higher than a1 become blue, cells that experience morphogen concentrations between a1 and a2 become white and cells that receive concentrations of the morphogen bellow a2 become red.

1.1.7) Experimental evidence for the Positional Information model.

The first experimental evidence in support of the Positional Information model was found in the chick limb. The pioneering experiment of Saunders and Gasseling (Saunders and Gasseling, 1968) that showed that the grafting of a posterior part of the limb to the anterior region was able to generate a mirror duplication of the digits, was interpreted by Wolpert as the evidence for the specification of anterior-posterior positional values (Wolpert, 1969). Successively, Tickle and colleagues (Tickle et al., 1975) suggested that the posterior region of the limb secreted a morphogen gradient that was responsible for the specification of the digits. On the other hand Summerbell and Wolpert (Summerbell et al., 1973) proposed that a gradient coming from the distal ectoderm of the limb provided positional values to pattern the proximo-distal axis. The patterning of the limb along the proximo-distal and anterior-posterior axis will be discussed in more detail in sections 1.2.4) and 1.2.5) respectively.

While the experiments in the chick limb indirectly inferred to the existence of morphogens that confer positional information, the most direct evidence in support of the positional information model was the discovery of the morphogen gradient that controls the anterior-posterior patterning of the *Drosophila* embryo. Several studies (Frohnhöfer and Nüsslein-Volhard, 1986, Johnston et al., 1989) found that a maternal gradient of the gene *bicoid* (Bcd) along the anterior posterior axis of the *Drosophila* egg provided the positional values for the patterning of the

body plan during development. It was later proposed, that the BCD gradient was formed from an anterior source of accumulated maternal *Bcd* mRNA, which diffuses and leads to the establishment of an antero-posterior protein gradient that is higher at the anterior pole (Driever and Nüsslein-Volhard, 1988). However, recent studies have also proposed that the mRNA itself forms a gradient which is than translated into the BCD protein gradient (Spirov et al., 2009). The interpretation of the BCD gradient leads to patterning of gap, pair-rule and segment polarity genes (Akam, 1987, Ingham, 1988). This process is best described as a hierarchical patterning system that consists of consecutive and independent steps responsible for the establishment of a segmented body plan: from the initial maternal gradient to segment polarity gene expression. The step that is better described is the gap-gene network system that implements the first interpretation phase from the maternal gradient to the broad non-overlapping gap gene domains (Jaeger, 2011). A model of this network was reverse-engineered from experimental data (Reinitz et al., 1998) and could recapitulate the gap gene dynamics with a purely cell-autonomous (without cell-communication) mechanism. A following study even showed that the same cell autonomous process could also recapitulate the posterior shifts that that gap gene domain showed over time (Jaeger and Martinez-Arias, 2009).

These results supported the basic Positional Information model of Wolpert where cell-autonomous interpretations of morphogen thresholds can account for the complex patterning observed during development.

Further confirmations to Wolpert's ideas were revealed by studying the mechanism that control the specification of the main body axes in the Xenopus embryo. The patterning along the dorso-ventral axis in Xenopus embryos is controlled by a gradient of BMP4 which is higher in the ventral region (Niehrs, 2010). The BMP4 gradient is formed through the dorsal diffusion of BMP antagonists (expressed in the Spemann organizer in the dorsal midline) and the action of the Chordin protease Tolloid, which regulate gradient polarity and shape by establishing and maintaining a dorsal BMP sink. Perpendicular to the Xenopus dorso-ventral BMP gradient, a Wnt/β-catenin gradient controls patterning along the antero-posterior axis (Kiecker and Niehrs, 2001). Similarly to the BMP gradient, the WNT signaling gradient is formed through the diffusion of antagonists. It has been also proposed that the dorso-ventral and anterior-posterior gradients are integrated at the level of Bmp signaling complex, Smad1/5/8, (Eivers et al., 2008), supporting the idea that cells at different positions may interpret these two orthogonal morphogens to determine the embryonic body plan. While the molecular nature of the morphogen gradients in Xenopus and qualitative aspects of the diffusion/transport of morphogens are being revealed, less is known about the quantitative aspects of these gradients, particularly about their timing and how the concentration varies along the axis.

Other systems, such as the regeneration of hydra embryos and of the amphibian limbs, have also been used to highlight the importance of positional information gradients during organogenesis. For example, it is well known that amputated limbs of salamanders have the capacity to regenerate via a complex process that takes place at the site of injury. Intercalation experiments (Pescitelli Jr and Stocum, 1981) supported the idea that a continuous set of positional values must exist along the amphibian limb. The regeneration of the lost segments was thus interpreted as a specification of new positional values. Recently, it has been discovered that a membrane bound molecule named Prod1 is graded from one end of the regenerated limb to the other along the proximo distal axis, and was proposed to be the basis for the morphogen gradient that specifies positional values (Kumar et al., 2007). This was supported by experiments that showed that when Retinoic Acid was applied at the distal end of a cut, it promoted the regeneration of a whole new limb by increasing Prod1 concentration (Kumar et al., 2007, da Silva et al., 2002).

1.1.8) Turing model versus Positional Information model.

The two models of pattern formation that I have described – the self-organizing Turing model and the Positional Information model—explain patterning during development with different conceptual principles. While the Turing model is based on cell-cell interactions and random fluctuations, the Positional Information model relies on an already specified source of a morphogen and requires cell-cell interactions only for the specification of the gradient. In accordance to this, a cell in a Turing pattern does not "know" its position, while a cell specified by positional information "knows" its position with respect to one or more points in the system.

In addition, Positional information models are often described as hierarchical mechanism emphasizing the fact that the interpretation phase is usually a cell autonomous translation of a morphogen gradient that does not feedback to the specification phase. This is in contrast with the Turing models, were the pattern emerges spontaneously by a feedback mechanism.

These two mechanisms can however work in conjunction since they are not mutually exclusive. This is well described in (Wolpert, 1989), where Lewis Wolpert discusses the idea that a pre-patterning mechanism could work together with Positional Information. Wolpert explains that repeated isomeric structures such as digits could be specified by a wave-like pre-patterning mechanism (Turing) that would be more robust and easier to evolve. Indeed, while Turing-like mechanisms can pattern several peaks at the same time with one threshold (Figure 9A), the positional information model requires to interpret many thresholds of the morphogen gradient to

create the isomorphic pattern (Figure 9B). From an evolutionary point of view, it is therefore more likely that a repeated pattern is formed with the interpretation of one threshold than multiples ones.

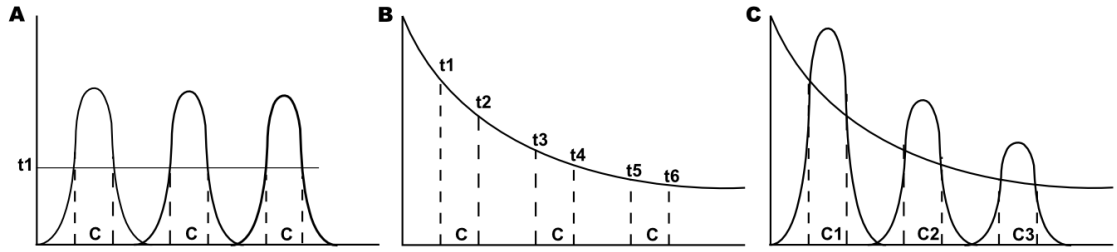

Figure 9. Positional Information and Turing models combined.

(A) A Turing mechanism specifies three repetitive fates such as digits by requiring the interpretation of only one threshold t1. (B) A Positional Information model needs six thresholds t1-t6 to create three repetitive fates. By combining the two models (C) a Turing mechanism could specify non-equivalent regions if modulated by a gradient, Figure adapted from (Wolpert, 1989).

However wave-like pre-patterning mechanisms does not totally illustrate the variety of patterns that can be formed during development. For example, in case of the digits, they are all specified as digits but they differ between each other in their identity. Therefore Wolpert suggests that the waves of a Turing pattern could be combined with Positional Information model to generate non-equivalent waves: the digits could be formed by a pre-patterning Turing mechanism while the anterior-posterior identity could be given by a morphogen gradient (Figure 9C). Such combination of the two models could generate the variety of patterns observed during development. More recently, this idea has gained new popularity (Kondo and Miura, 2010; Miura, 2013).

1.2 Mouse limb development: a model system for patterning and morphogenesis

The vertebrate limb is an excellent model system for the study of pattern formation and morphogenesis during development. One of its main advantages is that it is an external organ not necessary for the survival of the embryo, which allows for experimental manipulation without impairing the embryonic survival. An important part of the knowledge concerning limb development comes from classical experimental manipulations in the chick wing. These studies have contributed to various seminal discoveries about pattern formation and laid the theoretical

foundations for future molecular studies. During the last three decades, with the development of molecular genetics, the mouse limb has expanded our knowledge of the genes and molecules that control patterning during development (Logan et al., 2002).

1.2.1) Anatomy of the skeletal pattern

The mouse limb starts to develop around 9 days post coitum (dpc) (Wanek et al., 1989, Fernández-Terán et al., 2006). It protrudes from the lateral plate mesoderm (LPM) as a bulge, named the limb bud, at very specific sites along the embryo main body axis (Figure 10)(Burke et al., 1995, Cohn et al., 1995). At E9.0 the young limb bud is constituted of undifferentiated mesenchymal cells covered with an ectodermal layer. In 72h, this simple structure is able to develop into a complex organ with many patterned tissue types: cartilage, bone, tendons and the dermis. The muscles and the circulatory system are developed from a migratory cell population originated from the somites (Chevallier et al., 1977, Christ et al., 1983, Brand-Saberi et al., 1996, Ambler et al., 2001) while the nervous system originates from the neural tube (Whitelaw and Hollyday, 1983).

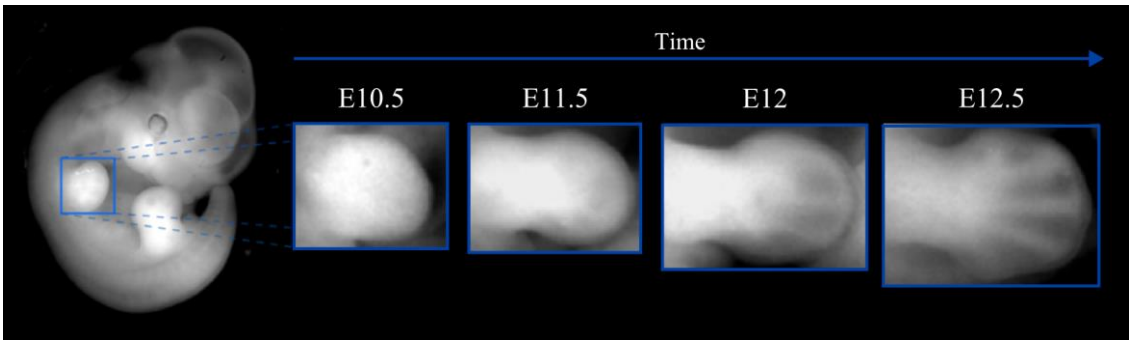

Figure 10. Limb bud development.
On the left, a magnified image from a dissecting microscope of a mouse embryo at Embryonic day (E) 10.5. The limb bud (highlighted with a blue square) protrudes from the body flank. On the right, a time-course of limb bud development with magnified photos of limbs at E10.5, E11.5, E12 and E12.5.

The limb anatomy can be described along three main axes: proximal to distal (PD), anterior to posterior (AP) and dorsal to ventral (DV) (Figure 11). As the bud grows and elongates, the skeletal pattern is laid down in a sequential manner along the PD axis (Summerbell et al., 1973). The stylopod develops first and has one element: the humerus in the forelimb (FL) and the femur in the hindlimb (HL). The zeugopod forms next with two elements, radius and ulna (FL) or tibia and fibula (HL). Finally the distal part of the limb bud changes into a paddle shape to form the autopod which contains metacarpals (FL) or metatarsals (HL) and the digits. The

stylopod and zeugopod elements are highly conserved in evolution contrary to the autopod that is variable across the species (Mariani and Martin, 2003). It is traditionally believed that the common tetrapod ancestor had five digits (pentadactyl limbs) and that many species have reduced the number of digits or even lost the limb (Cohn and Tickle, 1999). For example, human and mouse are pentadactylous while the chick forms only 3 digits in the forelimb. The identity of the digits is associated to the size, length, position and the number of phalanges. In the mouse, the thumb is identified as digit 1 and possesses 2 phalanges while the digits 2 to 5 have 3 phalanges. Controversy arises for species with a reduced number of digits, as for example in chick, where embryological evidence identifies the remaining digits as II, III and IV, while gene expression data and fossil record as I, II and III (Vargas and Fallon, 2005).

Growth and patterning of the limb are highly dependent on interactions between the mesenchyme and the ectoderm. These interactions are controlled by essential signaling centers or organizing regions. There are three signaling centers in the limb, and each one mainly controls growth and patterning along one of the limb axes: the apical ectodermal ridge (AER) controls the PD axis, the zone of polarizing activity (ZPA) the AP axis and the non-AER ectoderm the DV axis (Figure 11).

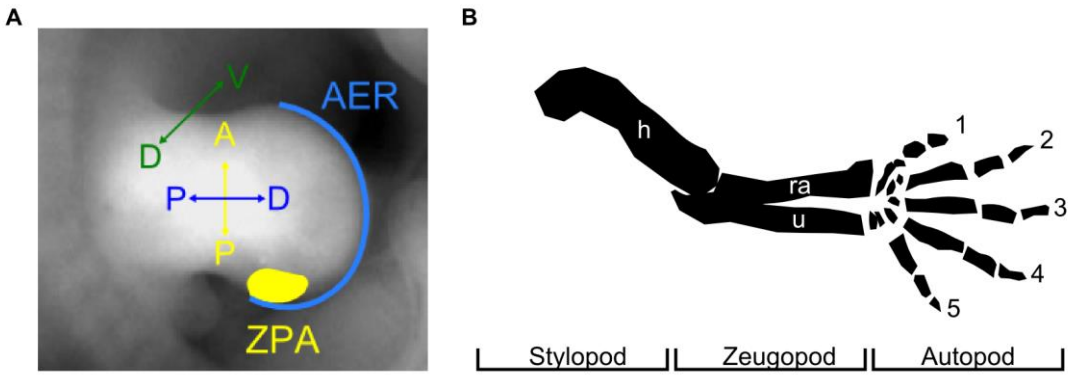

Figure 11. Limb axes and the skeletal elements.

A) The limb develops along 3 main axes which are controlled by specific signaling centers: the ZPA (yellow region), is situated in the posterior region of the limb bud and controls patterning along the anterior-posterior axis (A, P, highlighted with yellow); the AER (blue curved line) controls limb outgrowth and patterning along the proximo-distal axis (P, D highlighted with blue) and the dorso-ventral axis (D,V highlighted in green) is controlled by an interplay between genes expressed in the dorsal or ventral ectoderm. B) A schematic drawing of the skeletal elements of a mouse forelimb. From proximal to distal: the stylopod, contains one element, the humerus (h). The zeugopod contains two elements, the radius (ra) and ulna (u). The distal autopod contains multiple elements such as the carpals, metacarpals, and phalanges. Digit-1 to digit-5 are highlighted by numbers.

1.2.2) Dorso-ventral (DV) patterning and formation of the AER.

During early limb development the establishment of dorso-ventral fates is tightly connected to the induction of the AER. WNT canonical pathway acts upstream or together with BMP signaling to induce the transcription factor *Engrailed1* (*En1*) that is expressed in the ventral ectoderm (Ahn et al., 2001, Pizette et al., 2001, Soshnikova et al., 2003). *En1* represses the expression of *Wnt7a* , thereby restricting *Wnt7a* to the dorsal ectoderm (Figure 12) (Logan et al., 1997, Loomis et al., 1996). Mis-expression experiments in chick and mutations in mouse have shown that *Wnt7a* is a major regulator of dorsal fate (Parr and McMahon, 1995, Riddle et al., 1995, Vogel et al., 1995). Indeed, when *En1* is knocked out, limbs with bi-dorsal fates are formed because of ectopic expression of *Wnt7a* in the ventral ectoderm. On the other hand, *Wnt7a* mutants have bi-ventral limbs. Moreover *En1;Wnt7a* double mutants display a bi-ventral limb phenotype similar to the *Wnt7a* mutant, suggesting that *En1* regulates the D-V polarity by preventing ventral expression of *Wnt7a* (Cygan et al., 1997, Loomis et al., 1996). Wnt7a specifies the dorsal fates by induction of the LIM domain homeobox gene, *Lmx1b*, in the underlying dorsal limb mesenchyme. *Lmx1b* mis-expression in chick leads to bi-dorsal limbs whereas *Lmx1b* inactivation in mouse results in a bi-ventral phenotype (Chen et al., 1998, Cygan et al., 1997, Parr and McMahon, 1995, Riddle et al., 1995, Vogel et al., 1995) indicating that *Lmx1b* function is both necessary and sufficient to specify the dorsal limb fate.

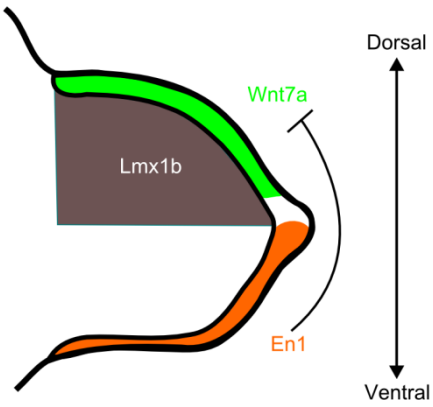

Figure 12. DV patterning.

En1 (orange) is expressed in the ventral ectoderm, and restricts *Wnt7a* expression (green) to the dorsal ectoderm. *Wnt7a* specifies the dorsal fate of the mesenchyme by regulating *Lmx1b* (gray region covering the dorsal part of the mesenchyme).

The WNT canonical signaling in the lateral plate mesoderm also restricts the *Fgf10* expression in the presumptive limb field. Subsequently *Fgf10* signals to the overlaying ectoderm and induces the Apical Ectodermal Ridge (AER) formation by activating and maintaining

ectodermal *Wnt* expression. WNT signaling induces *Fgf8* expression in the AER progenitor cells (Barrow et al., 2003, Kawakami et al., 2001) which is then responsible for maintenance of *Fgf10*. Mutations that affect the canonical WNT, BMP and FGF signaling, result in defective AER formation (Ahn et al., 2001, Barrow et al., 2003, Min et al., 1998, Sekine et al., 1999, Soshnikova et al., 2003, Revest et al., 2001, Xu et al., 1998). The AER is formed through the movement and compaction of progenitors that arise from the ventral limb ectoderm, a process controlled by *En1* (Crossley and Martin, 1995, Fernandez-Teran and Ros, 2008, Loomis et al., 1996). Indeed, *En1* mutants show defective AER morphogenesis (Loomis et al., 1998).

1.2.3) Proximo-distal (PD) patterning

The Apical Ectodermal Ridge (AER), discovered by Saunders in the late 40s, is an ectodermal thickening at the most distal tip of the limb bud (Saunders, 1948). In mouse, the AER forms by with the bulging of the limb at 9.5 dpc and reaches its maturity at E11. At this stage can be seen as a compacted band of polystratified epithelium running along the distal tip (Fernandez-Teran and Ros, 2008). After reaching its maximal elevation, the AER starts to flatten until it is not distinguished from the ventral end dorsal ectoderm. This process is called "AER regression", and occurs first at the level of the interdigits and finally at the level of the digits around E12.5. (Jurand, 1965, Milaire, 1974, Wanek et al., 1989, Guo et al., 2003).

Classical removal experiments of the AER from the wing buds of chick embryos showed that it is essential for the outgrowth of the limb along the PD axis (Saunders, 1948, Summerbell et al., 1973). These experiments also revealed a correlation between the level of the truncation and the time at which the AER was removed: when removed early, only proximal structures were developed; when removed later, more distal wing structures were formed. Further studies from Saunders and colleagues showed that the AER had a permissive rather than an instructive role, as interchanging a late chick limb bud AER with an early AER did not alter limb growth (Rubin and Saunders Jr, 1972, Saunders, 1948, Summerbell et al., 1973). Based on these experiments Summerbell and Wolpert formulated the Progress Zone Mode (Summerbell et al., 1973). This model postulated that as the limb grows along the PD axis, positional values are specified depending on how much time cells spend in the Progress Zone, the region under the influence of AER signals. In other words, the model suggested a "clock" mechanism that became fixed when cells exited the influence of the AER. Cells that spend a short time in the Progress Zone were specified to form proximal structures, whereas cells that spend longer time would form more distal structures. Thus, this model depends highly on growth, timing and length of exposure of

undifferentiated cells to a permissive AER signal (Figure 13A). An important evidence for the Progress Zone model was based on X-irradiation experiments done in chick (Wolpert et al., 1979). The chick mesenchyme was irradiated with X-rays at different developmental stages which resulted in a different level of limb truncations. Irradiation of young limbs led to the loss of more proximal structures, while irradiation of older limbs led to the loss of more distal structures (Wolpert et al., 1979). This was interpreted in the context of the Progress Zone Model by assuming that the X-rays affected the pool of undifferentiated cells in the Progress zone which led to the loss of more distal structures when the limb was irradiated at an older stage.

The Fibroblast Growth Factors, FGFs, were discovered as the molecular signals secreted by the AER due to their ability to restore chick limb bud outgrowth and patterning after AER removal (Niswander et al., 1993, Fallon et al., 1994). Four FGF ligands are expressed in the AER: Fgf8 is expressed along the whole AER, while Fgf4, Fgf9 and Fgf17 are first expressed in the posterior AER and later expand anteriorly (Martin, 1998, Fernandez-Teran and Ros, 2008, Lewandoski et al., 2000, Mariani et al., 2008). Genetic removal of *Fgf4*, *Fgf9*, or *Fgf17* alone do not show any AER related limb phenotype (Mariani et al., 2008). However Fgf8 is essential for limb development since genetic inactivation of *Fgf8* results in a smaller AER, delayed limb bud outgrowth, and lack of the stylopod element (Lewandoski et al., 2000, Moon and Capecchi, 2000). It was consecutively shown that *Fgf4* is up-regulated in the *Fgf8* null mutant, probably due to a compensation mechanism, and the transient loss of proximal structured was associated to the time required for the Fgf8 compensation (Lu et al., 2006, Sun et al., 2002). Early genetic inactivation of both *Fgf4* and *Fgf8* lead to complete agenesis of the limb (Boulet et al., 2004, Sun et al., 2002). Moreover, transient expression of *Fgf4* and *Fgf8* in early limb buds was sufficient to correctly specify the PD axis although subsequent proliferation of skeletal progenitors was disrupted (Sun et al., 2002).

These results were difficult to explain with the Progress Zone Model as they suggest that the PD axis was specified by the AER-FGFs at an early stage (Mariani et al., 2008). Taking this into account the Early Specification Model was proposed as an alternative model for the patterning along the proximo-distal axis (Dudley et al., 2002). This model postulated that the PD identities were specified early and that the specified progenitors pools progressively expanded as the limb grew under the influence of AER (Figure 13B) (Dudley et al., 2002). This model was used to re-interpret the AER removal experiments in chick by proposing that limb truncations were due to cell death under the AER rather than the time cells spent under the influence of the Progress Zone (Dudley et al., 2002). In addition a re-evaluation of the X-ray irradiation experiment, by using molecular analysis and cell tracking, showed that the resulting truncations were not due to a patterning defect but rather resulted from a time-dependent loss of skeletal progenitors. This

was not consistent with the Progress Zone model and was in support of the Early Specification model (Galloway et al., 2009). Finally the Early Specification model was also supported by the early ability of limb mesenchymal cells to sort out according to their PD position (Barna and Niswander, 2007).

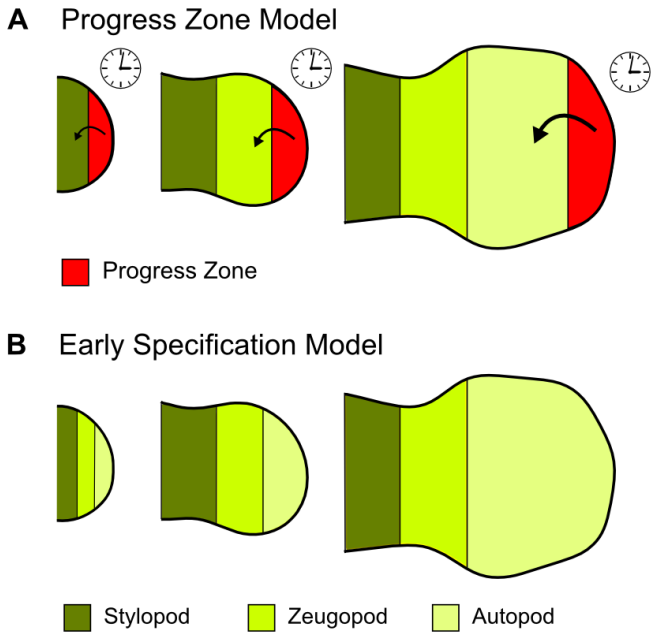

Figure 13. The Progress Zone and the Early Specification models.

A) The Progress Zone Model. The progress zone (PZ) (red) encompasses a region of unspecified cells which are under influence of the AER signals. As the limb grows cells that are no longer in the PZ can acquire their proximo-distal identity: zeugopod, stylopod and autopod, highlighted with green, yellow and beige respectively. The PD positional values depend on the time (illustrated by the clock) that cells spend under the influence of the AER signals: cells that spend a shorter time in the PZ acquire more proximal fates, while cells that spend more time in the PZ acquire more distal fates. B) The Early Specification Model postulates that the PD identities are specified early in development and progressively expand as the limb grows.

The Early Specification model presented a new conceptual framework for the specification of the PD identities however it did not propose any mechanistic solution. Moreover, molecular markers for the early specification were not found (Tabin and Wolpert, 2007). A more mechanistic model was introduced in (Mercader et al., 2000) by showing that a gradient of RA from the body flank promoted proximal fates, while the AER-FGF gradient promoted more distal fates. This study also showed that RA induced proximal cell identity by promoting expression of *Meis1* and *Meis2* which mark the stylopod. Indeed, misexpression of *Meis* caused either reduction or truncation of distal structures and induced expression of proximal genes (Mercader et al., 1999, Mercader et al., 2000). On the other hand AER-FGFs lead to activation

of *Hoxa11* and *Hoxa13* which mark the zeugopod and autopod respectively, and repress Meis expression (Mercader et al., 2000, Capdevila et al., 1999, Tabin and Wolpert, 2007). This evidence was used to suggest that the overlap between the two opposing gradients, which is reduced as the limb elongates along the PD axis, could underlie the specification of the PD segments and their molecular markers (Figure 14) (Mariani et al., 2008, Mercader et al., 1999, Mercader et al., 2000). This model was successively named as the Two Signal model (Tabin and Wolpert, 2007, Mariani et al., 2008). The two signal model is also supported by an extensive genetic study on FGF functions (Mariani et al 2008). Inactivation of *Fgf8* alone led to mild limb phenotype, but double and triple knockouts were made with, *Fgf17, Fgf9* or *Fgf4* and resulted in increasing severity of limb phenotypes. This suggested that each AER-Fgf differentially contribute to the total AER-FGF signal (Mariani et al., 2008). Analysis of these mutants also revealed that the AER-FGFs are required for cell survival and for the distal fate specification having an instructive rather than permissive role. While in triple knockouts of *Fgf4,Fgf8* and *Fgf9* all the three limb segment were missing, in the *Fgf4/Fgf8* double mutant heterozygotic for *Fgf9*, proximal and distal most structure were present but intermediate structures were absent. This limb phenotype was interpreted as evidence in favour of the Two Signal model, since the loss of intermediate positional values would depend on the impairment of growth that normally drives the correct intercalation of RA and FGF. (Mariani et al., 2008).

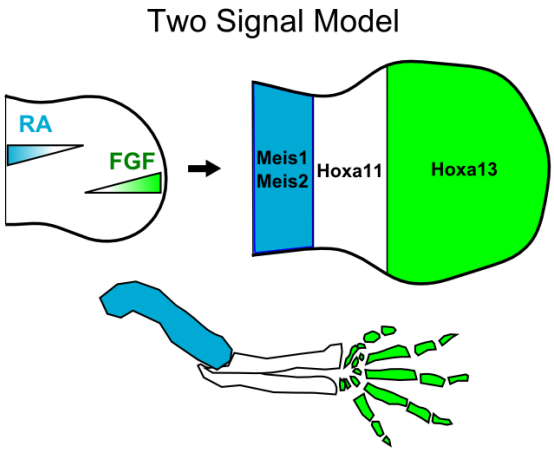

Figure 14. The Two-Signal model.

Proximal and distal positional values are specified by the RA gradient (blue triangle) and AER-FGF signaling gradient (green triangle) respectively. The intermediate positional values are intercalated by local growth. The *Meis1/2*, *Hoxa11*, and *Hoxa13* expression domains mark the three P-D territories. Figure adapted from (Bénazet and Zeller, 2009).

In order to integrate the new molecular data about the two opposing gradients with the classical AER-removal experiments, Tabin and Wolpert (Tabin and Wolpert, 2007) proposed the

Differentiation Front model as a description of the molecular and cellular events occurring during the specification of the PD identities. This idea postulated that the limb started to develop with proximal identities, but this was counteracted by the AER-FGF signals that induced distal cell fates. The role of the AER-FGFs was to maintain distal cells in a proliferative and undifferentiated state while in the proximal cells were progressively determined allowing chondrogenic condensation and differentiation to occur. The border between the proximal committed segments and the undifferentiated distal cells defines the differentiation front, hat goes to more distal positions with the progression of limb bud development.

In summary, while the exact mechanism that specifies the PD limb segments remains elusive (Towers and Tickle, 2009), so far the Two Signal model provides the best molecular basis for a PD specification model. It is important to notice that some studies have shown that the expression domains of the Meis genes, Hoxa11 and Hoxa13 do not exactly define the prospective stylopod, zeugopod and autopod, even if they are currently used as the best markers for these segments (Mariani et al., 2008, Galloway et al., 2009). Moreover, other studies claim that RA does not play a role as the proximal signal (Zhao et al., 2009). Therefore, it is still a matter of debate whether RA is indeed one of the essential signals in the Two Signal model.

1.2.4) Anterior-posterior (AP) patterning

The anterior-posterior (AP) patterning of the limb is one of the aspects of limb development that has been most extensively studied in the last four decades. A seminal discovery in this field was made in the late 60s by Saunders and Gasseling (Saunders and Gasseling, 1968) that identified a posterior part of the limb that could induce a mirror duplication of the digits when grafted anteriorly. This posterior region was named the Zone of Polarizing Activity (ZPA) and it was proposed that it specified the digits by releasing a morphogen gradient as described by the French Flag model of Lewis Wolpert (Tickle et al., 1975). According to this hypothesis the anterior grafting of the ZPA resulted in a duplication of the morphogen gradient that in turn induced a mirror duplication of the digits (Figure 15).

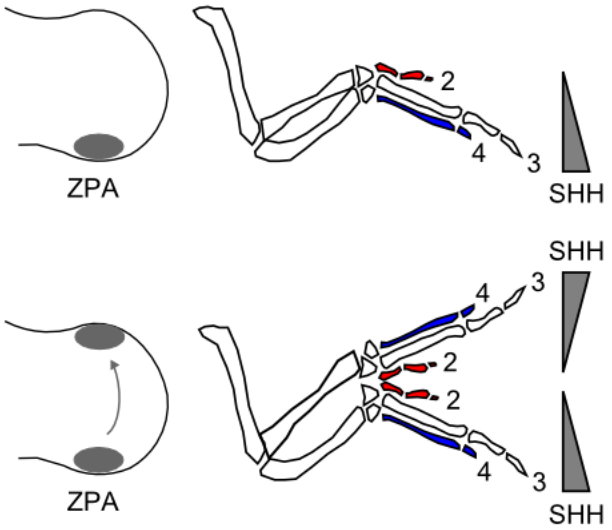

Figure 15. A schematic drawing explaining the ZPA grafting experiment.

Top: The zone of polarizing activity (ZPA) (grey region) in the posterior limb mesenchyme produces a gradient of SHH morphogen from posterior to anterior (grey triangle) which specifies the identities of the three digits, 4 , 3 and 2 depicted by the French Flag colors. Bottom: grafting ZPA cells to the anterior region of the chick limb, generates a duplicated SHH gradient and a mirror image duplication of the digits. Adapted from (Bénazet and Zeller, 2009, Zeller et al., 2009).

The molecular identity of the gradient was found only two decades later, with the identification of Sonic Hedge Hog (Shh) (Riddle et al., 1993), which was expressed in the posterior part of the limb and induced digit duplications when applied anteriorly. Following studies (Ros et al., 1996, te Welscher et al., 2002, Cohn, 2000) showed that the posterior expression of *Shh* was controlled by an early anterior-posterior asymmetry determined by the opposite expression of *Hand2* (on the posterior region of the limb) and *Gli3* (on the anterior region of the limb). It was subsequently shown that the activation of *Shh* by Hand2 was mediated by distal 5´Hox genes (such as Hoxa11 and Hoxd13) (Capellini et al., 2006, Kmita et al., 2005, Tarchini and Duboule, 2006). The formation of the anterior-posterior SHH gradient was assumed to result from the posterior expression coupled with diffusion. This view was consistent with the anterior digit duplications that were observed when SHH diffusion was increased by preventing SHH-cholesterol modifications (Li et al., 2006). However, a recent study (Sanders et al., 2013) has proposed that SHH does not directly diffuse in the extracellular matrix but seems to be traveling along actin-based filopodia of mesenchymal cells that can span several cell diameters. SHH co-receptors, such as CDO and BOC, co-localize in filopodia of SHH-responding cells. Thus interactions between filopodia containing SHH ligand and those containing co-receptors could control the long range SHH signaling.

SHH signals through the patched 1 (*Ptch1*) receptor (Yang et al., 1997) and blocks the cleavage of Gli transcription factors. Uncleaved Gli transcription factors directly activate or repress transcription of hedgehog target genes such as *Gli2* and the *Ptch1* receptor (Vokes et al., 2008, Vokes et al., 2007). In particular, SHH prevents the processing of Gli3 to its repressing form (Gli3R). The SHH gradient is therefore translated in an inverse gradient of Gli3R (Wang et al., 2000) which is higher on the anterior part of the limb. The inhibition of Gli3R by SHH is also important for the maintenance of HoxA and HoxD gene expression (Litingtung et al., 2002, te Welscher et al., 2002).

Manipulations of the SHH gradient, by ZPA grafting or bead implantation, were usually performed in chick embryos where the limb bud could be more easily accessed. These experiments induced digits duplications and only more rarely resulted in duplications of the zeugopod skeletal elements (Saunders and Gasseling, 1968). For this reason, most of the studies that investigated AP patterning focused on the specification of the digits. The chicken wing (forelimb) has only three digits, while the chicken leg (hindlimb) has four. Numbering of chick digits from anterior to posterior with Roman numerals I to V has been used as a classical way to identify homologies with the pentadactylous archetype. It is indeed assumed that chick digits have emerged due to evolutionary loss of digits from the pentadactylous state. While a consensus exists for the numbering of the digits in the chick hindlimb, from anterior to posterior as I to IV, a controversy exists for the digit numbering in chick wings. For a long time, it was considered that the anterior to posterior digit sequence in the wing was II and III (both with two phalanges), and then IV (with three phalanges). However, a recent study has re-discussed the meaning of digit identities and has proposed to number the chick forelimb digits as I, II, III (Carkett and Logan, 2011). The meaning of digit identity is indeed ambiguous: on one side, it has often referred to the position of digit progenitors along the anterior posterior axis, and on the other side, to the subsequent morphological identity of each digit. These two concepts are not necessarily coupled: the first concept mainly relates to the specification of the "digit fates" versus the "interdigit fates", while the second refers to unique morphology (E.g. number of phalanges) that is subsequently associated to each digit (Figure 16).

As I discussed in section 1.1.8, Wolpert himself proposed that the repeated isomeric "digit fates" were more likely to be specified by a pre-patterning mechanism like a Turing model, while the difference between each digit could be specified by a positional information gradient. Nevertheless, most digit patterning models implicitly assumed that the Shh positional information gradient controlled both digit specification and digit identity. This hypothesis was consistent with the observation that *Shh* inactivation resulted in the formation of only one digit (Chiang et al., 2001, Kraus et al., 2001). The remaining digit was usually identified as digit 1

(the thumb) and was interpreted as a default digit, independent of SHH signaling. Following studies proposed that the development of this digit was instead dependent on Sall4, Tbx5 and HOX genes (Koshiba-Takeuchi et al., 2005, Montavon et al., 2008).

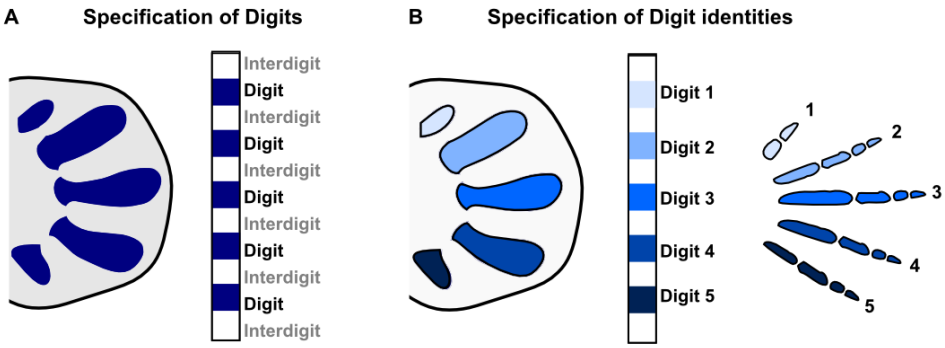

Figure 16. Specification of digits versus Specification of digit identities.
A) The concept of digit specification involves the determination of the digital fate in a field of undifferentiated cells. The digital fate is identical for all digits. A pattern of digital fates is periodic as it is repetitive and intercalated by the interdigital fate. B) The specification of digit identities is a process of attributing a specific quality to each digit which will result in their differences, for example in the number of phalanges and the morphology of digits (left).

A number of studies have extended the classic Shh positional information model to explain how SHH signaling specifies each digit. A first extension was made by performing fate maps of Shh descendent cells at different time of development (Harfe et al., 2004). The fate maps showed that Shh expressing cells contributed to digits 5, 4 and to half of digit 3. In addition, it was showed that from posterior to anterior the digits expressed Shh for progressively shorter times. Based on these observations, a model called temporal-spatial-gradient model (Zeller, 2004) proposed that each posterior digit was specified depending on how long the cells had expressed *Shh* (Figure 17). Cells that contributed to digit 5 had expressed *Shh* for long times, while cells that formed digit 4 and 3 had expressed it for shorter times. The fate maps also revealed that digit 2 cells never expressed *Shh*. It was therefore proposed that digit 2 was the only digit specified completely by the long range SHH paracrine signaling (Figure 17). Finally, since Shh fate maps overlapped only partially with digit 3, it was proposed that this digit was specified by a combination of Shh expression duration and Shh paracrine signaling. Digit 1 was considered to be SHH-independent as proposed by previous studies. The temporal-spatial-gradient model was also supported by another study which showed that brief exposure to SHH was sufficient to

specify anterior but not posterior digits and that mutants with reduced SHH signaling-range lacked digit 2 (Scherz et al., 2007).

Another extension of the classical SHH positional information model, called the Growth-Morphogen model, suggested a dual role for SHH in chick: control of digit specification and control of limb proliferation (Towers et al., 2008). This hypothesis was based on the observation that application of a SHH inhibitor or an inhibitor of proliferation at different times lead to a smaller limb with loss of different digits. In particular, SHH inhibition at progressively earlier times caused loss of more posterior digits, while transient proliferation inhibition caused loss of anterior digits. The study concluded that the duration/dose of SHH signaling controlled both growth and the specification of digit progenitors.

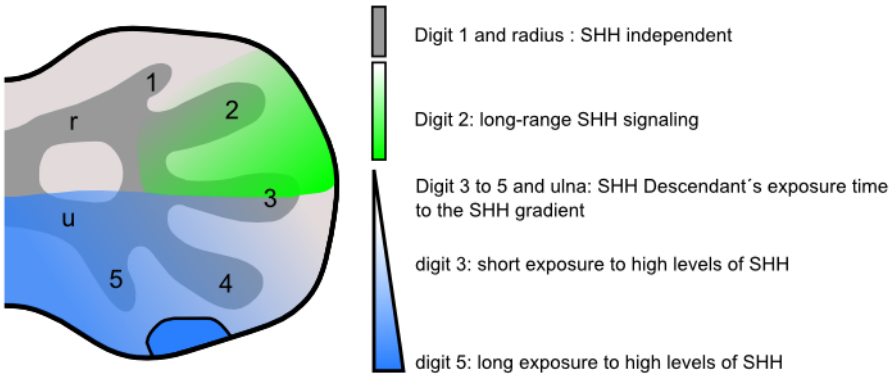

Figure 17. The Temporal-Spatial gradient model.

Digit 1 and the radius are formed independently of the SHH gradient while digit 2 specification depends on the long-range of SHH signaling. Half of the digit 3, digit 4, digit 5 and the ulna are composed of *Shh*-descendants and they are specified based on the length of time cells are exposed to the high level of SHH signaling. (Figure adapted from adapted from (Zeller, 2004).

Another study in mouse (Zhu et al., 2008), showed that upon inactivation of *Shh* at progressively earlier time points, digit 3 was lost first than digit 5, than digit 2 and finally digit 4. This order reflected the inverse temporal sequence of formation of digital condensations (digit 4, than 2, than 5 and finally 3). To explain these results it was suggested that SHH specified the anterior-posterior digit identities already during early limb bud development while it controlled the proliferation of the specified progenitors in subsequent events. This new model was referred as the Biphasic model (Figure 18) (Zhu et al., 2008) and explained the digit loss sequence by assuming that SHH signaling was required to ensure enough expansion of digit progenitors at later stages.

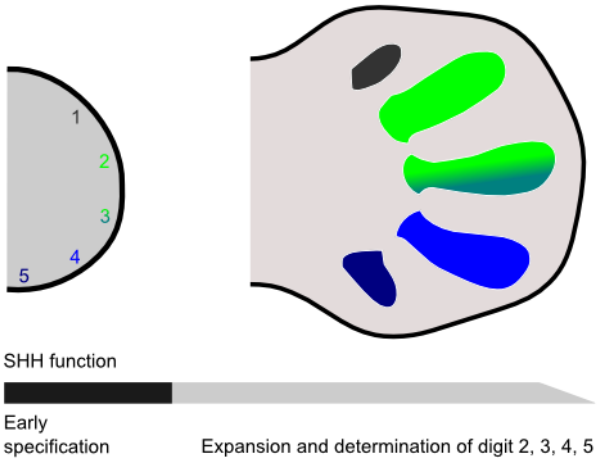

Figure 18. The Biphasic model.

On the left, SHH specifies digit identities in the early limb bud. Later SHH signaling is required for expansion of digit progenitors from digits 2 to 5. Figure adapted from (Bénazet and Zeller, 2009).

All the extensions to the classical Shh positional information model presented above assumed a tight link between the specification of digits and the specification of digit identities. This however contrasted with an early study which revealed that Shh was dispensable for digit specification (Litingtung et al 2002). This study showed that although *Shh* mutants had only one digit (Figure 19), limb lacking *Gli3* (the main mediator of Shh signaling) had eight digits (polydactyly). This important result showed that the mechanism that controlled digit specification was not affected when SHH signaling was compromised. This lead to the idea that SHH signaling was dispensable for digit specification and that its main role was to prevent the formation of Gli3R which otherwise reduced the number of digits (te Welscher et al., 2002). This idea was also re-enforced by the polydactyly phenotypes of double mutants of *Shh* and *Gli3* (Litingtung et al., 2002) that were indistinguishable from those observed in *Gli3* mutants (Figure 19).

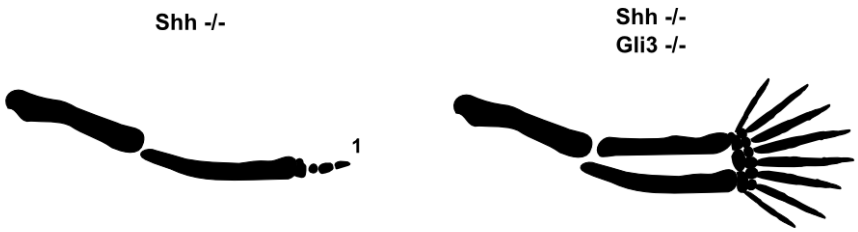

Figure 19. Dispensability of Shh for digit specification.

On the left, a schematic drawing of the *Shh* null mutant limb. Only digit 1 is formed which is thought to be SHH-independent. The phenotype observed is consistent with Positional information models that assume that SHH is necessary for digit specification. On the right, a schematic drawing of the skeletal elements of the *Shh/Gli3* double mutant. The polydactyly phenotype with 6-8 digits of equal identity shows that Shh is dispensable for digit specification.

The eight digits formed in these mutants had all the same identity, suggesting that Shh was however important for specification of digit identity. In relation to this, previous studies showed that anterior-posterior digit identities are not fixed at early limb stages since their identity could still be reprogrammed at later stages by the mesenchyme posterior to each digit (Dahn and Fallon, 2000). More recent studies (Suzuki et al., 2008, Montero et al., 2008) showed that when the digits are already specified, a high BMP signaling region called the phalanx forming region (PFR) or the digit crescent forms at the tip of the digit. A model was proposed (Suzuki et al., 2008) where phalanxes were specified in a proximo-distal direction by PFR cells, that formed the most proximal phalanx first, and subsequently another PFR gave rise to the next phalanx (Figure 20). The determination of the fate of PFR cells, the number, size and shape of phalanges was proposed to be controlled by is BMP signaling from the interdigits. Which ligands mediate the BMP signaling is not clear but it was proposed that GDF, a member of the BMP family of proteins, could be a good candidate (Suzuki et al., 2008). Finally, there is also evidence that the number of phalanxes is controlled by FGF signaling (Sanz-Ezquerro and Tickle, 2003).

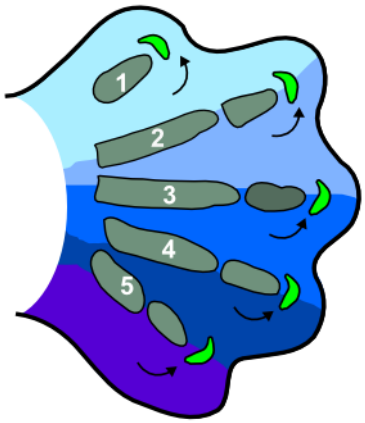

Figure 20. Schematic drawing of the phalanx forming region model.

Bmp signaling in the interdigital region posterior to each digit (blue colors) signal (black arrow) to the phalanx forming region (green) at the top of the formed digit ray. This results in the specification of digit identities by controlling the number, size and shape of the phalanxes.

The Gli3 mutant revealed a previously unappreciated SHH-independent potential of the limb to pattern the digits. Moreover, it suggested that the main action of Shh was to constrain the limb to pentadactyly and to specify digit identities. The intrinsic potential of the limb to form digits is more easily explained by the long-standing proposal that a self-organizing Turing mechanism controls digit specification. This hypothesis is based on the idea that the alternating sequence of digits and interdigits along the anterior-posterior axis could be specified as a periodic pattern established by a Turing mechanism. This concept was first discussed by Lauder and Bard in (Bard and Lauder, 1974) that nevertheless proposed that the intrinsic variability showed by Turing patterns would not fit the reproducibility and robustness of digit specification. However, the authors admitted that it was still unclear if the variability of Turing patterns could be reduced when a Turing mechanism was coupled with a pre-existing polarity (E.g. the SHH gradient). A later pioneering theoretical study (Wilby, 1977) showed that the polydactyl phenotype of the Talpid chick mutant could be explained by a Turing-like mechanism that would naturally predict the formation of more digits on a limb with bigger AP length. Similarly, it was later proposed that the polydactyly observed in the *Gli3* mouse mutant could also be explained by the behavior of a Turing mechanism on bigger limbs (Tickle, 2005, Sheth et al., 2012). The Turing hypothesis was popularized again by Stuart Newman in 1979 (Newman and Frisch, 1979) which proposed a Turing model to explain digit patterning in chick. However, for more than two decades this hypothesis was explored mainly from a theoretical point of view (Hentschel et al., 2004, Miura et al., 2006, Badugu et al., 2012). Important classical experimental evidence in favor of the Turing hypothesis are re-aggregation experiments in chick, that show the intrinsic capacity of the limb cells to self-organize (Zwilling, 1964). These experiments consist of removing and mixing the mesenchymal cells

from a donor limb bud and to graft them inside another ectodermal layer to into a neutral side of the embryo (Figure 21A). In these conditions the re-aggregated limbs were still able to grow and form two digits. This suggests that limb cells that have already received positional cues from the organizers like the ZPA, are still able to be re-specified and to self-organize to form digits. The same experiments done in Xenopus led to limbs with up to thirty digits (Yokoyama et al., 1998) providing a strong evidence for the self-organizing capacity of the mesenchyme to form a periodic digit pattern. Another type of experiments that supports the self-organizing capacity of the limb mesenchymal cells is the micromass culture system (Cottrill et al., 1987). This high density in-vitro culture of limb mesenchymal cells spontaneously forms a chondrogenic periodic pattern which is strikingly reminiscent of a Turing simulation (Figure 21B). For this reason, it has been used as an in-vitro model of digit patterning to identify the diffusible molecules that implement the Turing network (Newman, 1996). Micromass experiments (Leonard et al., 1991, Miura and Shiota, 2000) proposed that TGFβs act as an Activator molecule in the Turing network that controlled the chondrogenic periodic pattern. However, later studies (Pryce et al., 2009, Shull et al., 1992, Kaartinen et al., 1995, Sanford et al., 1997, Dünker et al., 2002) showed that impairment of TGFβ signaling affected only the recruitment and maintenance of tendon progenitors and did not affect the digit pattern. This suggested that TGFβ signaling was mostly important for the formation of tendons and their musculoskeletal counterparts at later stages. More recently, the idea that digit specification is controlled by a Turing mechanism was strengthened by the experimental evidence that showed that distal Hox genes control the width (wavelength) of the digits (Sheth et al., 2012). This study showed that the progressive reduction of distal Hox genes (Hoxa13, Hoxd11-Hoxd13) caused a progressively higher number of supernumerary thinner digits and proposed that these phenotypes could be explained by a Turing model modulated by Hox genes. This observation was more evident in the *Gli3* mutant background that had a bigger handplate size that was not reduced when Hox genes were removed. The complete allelic series of Hox genes removal showed polydactyly phenotypes that ranged from 7 /8 digits up to 14 digits in one limb. In agreement with the hypothesis that Hox genes increased the wavelength of the Turing mechanism, the mutants had narrower digits as the Hox gene dosage was reduced. A Turing model implemented by two unknown diffusible molecules was simulated inside realistic limb shape to show that when the wavelength of the Turing mechanism was modulated by Hox and Fgf, all the experimental manipulations could be re-capitulated. Nevertheless the identity of the diffusible Turing molecules remained unknown.

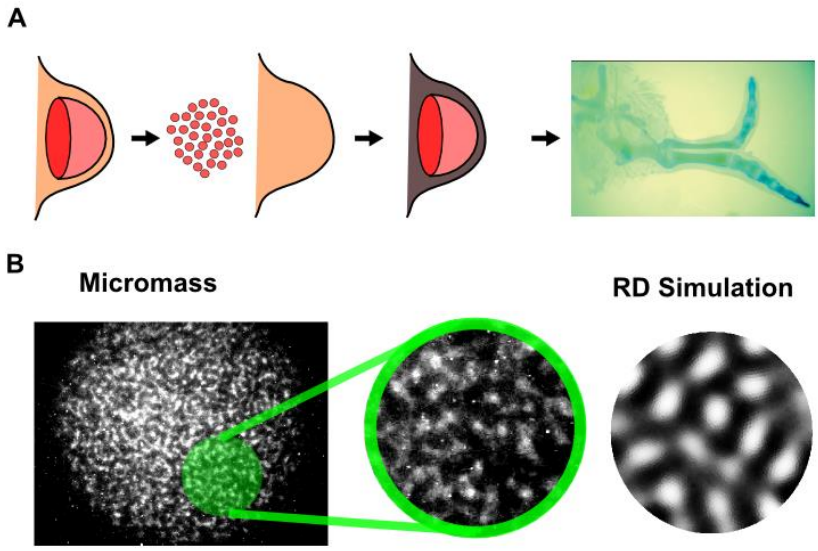

Figure 21. Experiments supporting a Turing mechanism for digit patterning.

A) The re-aggregation experiment: mesenchymeal cells of a donor limb (pink) are extracted from the ectoderm (beige), mixed and re-aggregated into an ectodermal jacket of another limb (grey). When grafted to a neutral side of the embryo, the re-aggregated limb is able to form two digits. B) On the left, a 20h micromass culture of mesenchymal limb cells forms a periodic chondrogenic pattern marked by Sox9 (immuno-staining against Sox9). The periodic pattern is strikingly similar to a reaction-diffusion simulation of the AI Turing model.

In summary, digit patterning along the AP axis has been traditionally explained in the light of a positional information model based on the SHH morphogen gradient. This hypothesis was strongly supported by the digit duplications observed when the ZPA cells were grafted anteriorly. However, *Shh/Gli3* double mutants showed that Shh was mostly responsible for controlling digit identities and growth, and was not required to specify the digits. This study also suggested that another mechanism was underlying an intrinsic propensity of the limb mesenchyme to specify digits that could easily produced polydactyly. It was proposed that such mechanism could be a Turing system that specified the digits in a periodic manner along the AP axis. Recent genetic perturbations have confirmed this hypothesis and have showed that in the absence of *Gli3*, the main mediator of SHH signaling, limbs with reduced distal Hox dosage form up to 14 digits. However, the identities of the diffusible molecules that implement the Turing mechanism remain unknown.

1.2.5) Coordination between AP and PD axis

Already in the pioneering times of grafting experiments, several evidences suggested a possible crosstalk between the AER and the ZPA. The first evidence was showed by revealing that ZPA grafts had stronger effects once placed under the AER (Tickle, 1981). This suggested that the two organizers could coordinately regulate AP and PD patterning. Support for this hypothesis was provided by showing that in absence of the AER, FGF-soaked beads were able to rescue *Shh* expression and that SHH-soaked beads were able to induce the AER and *Fgf* expression (Niswander, 2002, Tickle, 2005). Subsequently it was discovered that a positive feedback loop between ZPA and AER cells was mediated by *Gremlin1* (*Grem1*) which is expressed in the mesenchyme (Khokha et al., 2003, Michos et al., 2004). Indeed, inactivation of *Grem1* led to a dysfunctional AER, with lack of *Fgf4-9-17* expression, reduced *Fgf8* expression and shorter time of *Shh* expression in the ZPA. As an antagonist of BMP, *Grem1* was proposed to lower BMP activity, which is essential for the maintenance of the positive feedback loop between Shh and FGFs (Bénazet et al., 2009, Michos et al., 2004). Consistently, BMP signaling was required for the AER initiation (Ahn et al., 2001). In addition, it was also shown that BMP signaling promoted the expression of its inhibitor *Grem1* (Nissim et al., 2006) which in turn reduced *Shh* expression (Bastida et al., 2009). By combining mouse molecular genetics and mathematical modeling, it was proposed that during early stages of limb development a fast negative feedback loop between BMP4 and GREM1 allows for the initial up-regulation of AER-Fgfs that is responsible for the initiation of the positive feedback loop between Shh and AER-Fgfs (Figure 22A) (Bénazet et al., 2009, Zeller et al., 2009). Subsequently, SHH, FGFs and GREM1 form a slower positive feedback loop that permits a phase of limb expansion, specification of skeletal elements and differentiation (Figure 22B). During this phase, low but persistent mesenchymal BMP signaling is necessary for restricting the AER to its correct length, as inactivation of *Bmp4* during this period in mouse leads to anterior expansion of the AER-FGF signaling and results in digit polydactyly (Bénazet et al., 2009, Selever et al., 2004). When the limb expands, the core mesenchyme exits the range of ectodermal WNT and FGF signals, allowing for the activation of *Sox9* expression and initiation of chondrogenesis (ten Berge et al., 2008). On the other hand the progressive expansion of the cells that express *Shh* leads to specification of digit 4 and 5 (Harfe et al., 2004, Zhu et al., 2008). In a final phase, the positive feedback loop self-terminates when FGFs increase beyond a certain threshold and lead to Grem1 inhibition (Figure 22C) (Verheyden and Sun, 2008, Scherz et al., 2004, Bénazet et al., 2009, Zeller et al., 2009).

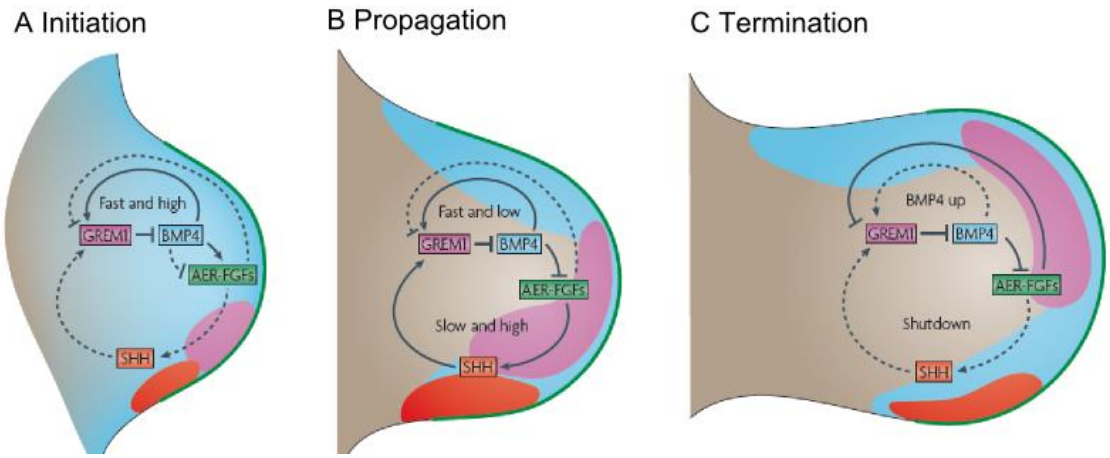

Figure 22. Two feedback loops control limb patterning and growth.
Schematic representation of the expression domains of Bmp4 (BMP4; light blue), Shh (SHH; red), Grem1 (GREM1; purple) and FGFs (AER-FGF; green) at three stages of limb development. Active feedback loops are represented with a solid line. A) In the initiation phase, BMP4 induces its own repressor *Grem1* in a fast manner. The expression of *Shh* is independent from GREM1 and AER-FGFs signaling. B) During the propagation phase, two feedback loops are interconnected to control the distal outgrowth and patterning of the limb bud. SHH upregulates GREM1 that reinforces the AER-FGF and ZPA activities by inhibiting BMP4. This epithelial–mesenchymal feedback loop is slower. During this period the activity of the fast Grem1-BMP4 loop is low to allow maintenance of the AER. C) During the termination phase the separation of the expression domains of *Shh* and *Grem1*, together with the onset inhibition of *Grem1* by AER-FGFs, allows to the signaling system to self-terminate. This promotes the increase of the BMP4 activity. Figure taken from (Zeller et al., 2009).

1.3 Sox9 and skeletal patterning

Sox9 is a transcription factor that belongs to the SRY (sex-determining region on the Y chromosome) family and contains the HMG (high mobility group) box DNA binding domain. During the development of the mouse embryo, *Sox9* is expressed in all chondroprogenitors and chondrocytes except the hypertrophic chondrocytes, in the male gonad, otic vesicle, heart, kidney, pancreas, intestine, and neural crest (Figure 23). Genetic studies, as well as human mutations, have shown that Sox9 is a master regulator of chondrogenesis. Sox9 haploinsufficiency in humans and mice causes campomelic dysplasia, characterized by a severe skeletal dysmorphology and XY reversal (Foster et al., 1994, Wagner et al., 1994, Wunderle et al., 1998). Similarly, heterozygous Sox9 mouse embryos exhibit severe hypoplasia of the cartilage associated to lower levels of cartilage matrix genes (Bi et al., 2001) which are directly activated by Sox9, such as *Col2a1*, *Col11a2*, and *Aggrecan* (Lefebvre et al., 1997, Bridgewater

et al., 1998, Sekiya et al., 2000). More precisely, Sox9 induces the expression of its downstream targets and co-factors, *Sox5* and *Sox6* (Akiyama et al., 2002) required for Sox9 induction of *Col2a1*, *Col9a2* and *Col11a2* (Smits et al., 2001). *Sox5/Sox6* double-null mutant mice have normal *Sox9* expression and mesenchymal condensation but no chondrocyte differentiation due to severe reduction in the expression of *Col2a1*, *Col9a2*, *Col11a2* (Smits et al., 2001). Other studies also showed that Sox9 is the earliest marker for chondrogenesis as it is expressed in chondrogenic cells before the outbreak of chondrogensis (Healy et al., 1999) and is able to ectopically induce chondrogenic fates.

Figure 23. Sox9 expression domains during development of the mouse embryo.
Notice the clear outline of the skeletal pattern in the limb buds (white arrowheads) at E12.5.(Figure taken from (Akiyama, 2008)

In the limb, Sox9 is the earliest known gene that reflects the skeletal pattern: marking the onset of the stylopod , the zeugopod and the digits in the autopod (Wright et al., 1995). At the sites of Sox9 expression, mesenchymal condensations are successively marked by Col2a1, from E10.5 to E12.5. From E12.5 onwards the chondrogenic differentiation is marked by expression and secretion of cartilage matrix genes (e.g. Agreccan ,Versican,Col9a1,Col11a2 and CD-Rap). The differentiated chondrocytes then undergo a series of sequential changes that include unidirectional proliferation, conversion to hypertrophic chondrocytes, ability to calcify the extracellular matrix, cell death, and replacement by bone (Hall and Miyake, 2000, Pizette and Niswander, 2000). During chondrogenesis, *Sox9* is expressed in all chondroprogenitors and in all differentiated chondrocytes, but not in hypertrophic chondrocytes (Ng et al., 1997, Zhao et al., 1997). Conditional inactivation of *Sox9* in the limb results in complete absence of chondrogenic mesenchymal condensations and subsequent cartilage and bone fromation (Akiyama et al., 2002, Akiyama et al., 2004) showing that *Sox9* prefigures the formation of all mesenchymal condensations that initiate chondrogenesis and give rise to the skeletal primordia (Bi et al., 2001, Akiyama et al., 2005). Furthermore, *Sox9* gain of function experiments in chick and mouse result in ectopic digit formation (Healy et al., 1999, Akiyama et al., 2007b). These

experiments show the importance of Sox9 for the formation of the chondrogenic pattern in the limb. Moreover, they suggest that Sox9 can feedback into the skeletal patterning mechanism rather than just being a downstream chondrogenic marker. However, the several aspects of the regulation of Sox9 are still unknown.

1.3.1) BMP pathway and the regulation of *Sox9*

Bone morphogenetic proteins (BMP) were originally discovered for their ability to induce the formation of bone and cartilage (Urist, 1965, Wozney et al., 1988) and for triggering cartilage formation when implanted at ectopic sites in adult animals (Hogan, 1996). They are secreted cytokines and have been classified as a subfamily of the larger TGFβ growth factor family due to their structural similarities. They are synthesized as larger precursor molecules with an amino-terminal signal sequence and a pro-domain usually cleaved at a RXXR site to release a mature carboxy-terminal segment. The active signaling molecule is made up of hetero- or homo-dimers of the final mature domain (Massague, 1990, Massagué, 2012).

Several members of the BMP family are expressed in the limb, namely *Bmp2/4/5/7/8* (Geetha-Loganathan et al., 2006) as well as a subgroup of growth/differentiation factors *(Gdf) 5/6/7*, (Ducy and Karsenty, 2000). I will focus this review mainly on Bmp2, Bmp4 and Bmp7, as these are the main ligands that control patterning and chondrogenesis in the limb bud. Other members of the family as Gdf5 and Gdf6 are instead associated to joint development (Storm and Kingsley, 1996, Storm et al., 1994, Seemann et al., 2005, Settle Jr et al., 2003, Degenkolbe et al., 2013) while Bmp5 is important for interdigital cell death (Zuzarte-Luıs et al., 2004).

Bmp2 and Bmp4 belong to the same group and are homologus to the Drosophila Dpp gene, while Bmp7 belongs to another Bmp subgroup called the osteogenic protein-1, OP-1group (Hogan, 1996, Ducy and Karsenty, 2000). In Xenopus and Zebrafish development, all three Bmps can form heterodimers which promote stronger signal activation than homodimers (Nishimatsu and Thomsen, 1998, Schmid et al., 2000). Bmps bind and activate transmembrane serine-threonine kinase receptors of type I and II, both of which are required for signal transduction (Shi and Massagué, 2003, Heldin et al., 1997). Type II receptors are constitutively active, and phosphorylate the type I receptors upon ligand binding, leading to the activation of type I receptor kinases. Therefore, the specificity of the intracellular signals is mainly determined by type I receptors. BMPs bind to three distinct type II receptors: BMP type II receptor (BMPR-II), activin type II receptor (ACVR-II) and activin type IIB receptors (ACVR-

IIB). Regarding type I receptors, BMPs bind to three distinct type I receptors, called activin receptor-like kinase, ALK2 (also termed ACVR1), ALK-3 (also termed BMPR-IA), and ALK-6 (BMPR-IB). Bmp canonical signaling involves phosphorilation of different SMAD proteins, namely SMAD1, SMAD5 and SMAD8 by the activated receptor type I, see Figure 24. Once SMADs are phosphorilated, they associate into a complex with the co-factor Smad4 and translocate into the nucleus where they bind to the DNA to transcribe target genes (Yang et al., 2002, Feng and Derynck, 2005). In addition to the Smad pathway, BMP signaling activates non-canonical pathways which include Rho-like small GTPases, phosphatidylinositol 3-kinase/Akt (P3K/Akt) and/or various types of MAPK (Moustakas and Heldin, 2005, Zhang, 2008), see Figure 24. The aspect of the non-canonical BMP signaling that is best understood is the activation of the TGFβ-activated kinase 1 (Tak1)/p38 pathway (Sorrentino et al., 2008, Yamashita et al., 2008). It has been suggested that cooperation between canonical and non-canonical signaling determines the final outcome of cellular responses to BMP (Moustakas and Heldin, 2005, Zhang, 2008). For a detailed review of the Bmp signaling pathways see (Chen et al., 2004a, Dutko and Mullins, 2011, Moustakas and Heldin, 2005, Zhang, 2008).

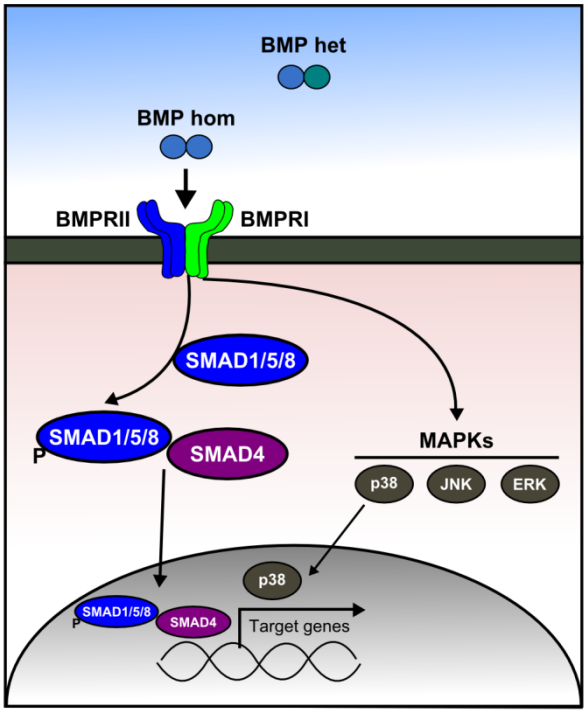

Figure 24. Schematic drawing representing BMP signaling pathways.

BMP homodimers (BMP hom) or BMP heterodimers (BMP het) bind to receptor type II (BMPRII) and type I (BMPRI). The canonical SMAD pathway is represented on the left: the activation of BMPRI by BMPRII allows for the phosphorilation of SMAD1/5/8. The activated SMAD1/5/8 binds to co-SMAD4 (SMAD4) and is transported to the nucleus where the complex can bind to DNA and regulate the expression of target genes. The non-canonical BMP pathways are represented on the right: BMP signaling activates MAPKs such as p38, JNK or ERK which control directly or indirectly target gene expression in the nucleus.

The use of retroviral vectors (RCAS system) in chick limb has strengthened the evidence that Bmps regulates chondrogenesis. First, retroviral-mediated misexpression of dominant negative versions of BMP receptors resulted in limbs that lack Alcian blue-stained cartilage elements (Kawakami et al., 1996, Zou et al., 1997). Secondly, retroviral misexpression of the secreted BMP antagonist *Noggin* (Zimmerman et al., 1996) resulted in loss of *Sox9* expression or complete absence of skeletal elements (Healy et al., 1999, Pizette and Niswander, 2000, Capdevila and Johnson, 1998), suggesting that BMP signaling was not only important for chondrogenic differentiation and bone development but also for the early steps of the commitment to the chondrogenic fate through activation of Sox9. Finally, BMP gain-of-function experiments in the chick embryos by retroviruses encoding *Bmp2, Bmp4,* or activated type I *BmpRs*, resulted into an increase in volume of cartilage elements (Duprez et al., 1996, Zou et al., 1997). In addition, application of exogenous BMP2-soaked beads to chick limbs up-regulated *Sox9*, which confirmed the capability of BMPs to induce ectopic cartilage (Healy et al., 1999).

Studies done in primary cell cultures of chondrocytes, the mesenchymal progenitor cell line C3H10T1/2 and chondrogenic cell line ATDC5, showed that BMPs induce chondrocyte differentiation and promote the expression of cartilage-specific genes (Wang et al., 1993, Shukunami et al., 1998, Haas and Tuan, 1999) by directly stimulating induction of Sox9 expression in a dose dependent manner (Zehentner et al., 1999). Moreover, a more recent study (Pan et al., 2008) showed that in pluripotent mouse embryonic fibroblasts (MEFs) cell cultures, BMP2 signaling directly activates Sox9 through a CCAAT box binding in the proximal promoter. This study also suggested that, while Tak1/p38 non-canonical BMP pathway is needed for the expression and activation of Sox9, SMAD signaling only regulates SOX9 activity without affecting its expression.

Genetic studies have also been crucial to investigate the role of BMP signaling during limb development. In the mouse, removal of *Bmp2* and *Bmp4* or *BmprI* and *BmprII* cause early embryonic lethality (Mishina et al., 1995, Winnier et al., 1995, Zhang and Bradley, 1996, Beppu et al., 2000), which impedes the study of the role of BMP signaling. For this reason, conditional mutants created with the Crelox-P technology (Le and Sauer, 2000, Nagy, 2000) have been extremely useful in depicting the role of the Bmp pathway during mouse development (Robert, 2007). Conditional mutants of individual Bmps in the limb, were generated using Prx1-Cre transgenic line that drives Cre recombinase activity in the limb mesoderm (Logan et al., 2002, Selever et al., 2004, Bandyopadhyay et al., 2006). *Bmp4*-deficient limbs show a variable penetrance of preaxial and postaxial polydactyly, but otherwise normal patterned digit (Selever

et al., 2004). *Bmp2*-deficient limbs do not show any deficiency, neither in the skeletal pattern nor in the chondrogenic and osteogenic differentiation (Bandyopadhyay et al., 2006). However they show malformations of the scapula and syndactyly with variable penetrance (Bandyopadhyay et al., 2006). Finally Bmp7 null mutants have no defects in the skeletal elements but show occasional preaxial polydactyly (Dudley et al., 1995). In contrast to the mild effects of single mutants, *Bmp2/Bmp4* double conditional mutant show down-regulation of *Sox9* expression and loss of the most posterior digits (2 digits in the forelimb, 3 digits in the hindlimb) (Bandyopadhyay et al., 2006) . The lack of phenotypes in single Bmp mutants and the loss of *Sox9* expression in double conditional mutant strongly support the idea that BMPs have redundant roles in chondrogenesis (Karsenty, 2003). However, the conditional inactivation of *Bmp2* in a *Bmp7* mutant background does not show any skeletal defect beside occasional loss of the final phalanx of digit 3 (Bandyopadhyay et al., 2006).

Two BMP receptors type I are expressed in the limb mesenchyme: *Bmpr1A* is expressed ubiquitously while *Bmpr1B* is expressed in the cartilage condensations (Dewulf et al., 1995, Yi et al., 2000). Conditional knockout of *Bmpr1A* in the mesenchyme, results in the absence of digits and severe defects in *Sox9* expression (Ovchinnikov et al., 2006). BMPR1A has a much higher affinity to BMP2-BMP4 heterodimer than other BMPs (Yamaji et al., 1994). This correlates with the stronger phenotype of the *Bmp2/Bmp4* double knockout with respect to the conditional inactivation of *Bmp2* in a *Bmp7* mutant background. In contrast to *Bmpr1A,* null mutants of *Bmpr1B* show normal *Sox9* expression but defects in later chondrogenic events (Yi et al., 2000), suggesting that while *BmprIA* is essential for induction of *Sox9* and commitment to the chondrogenic fate during early limb development, *Bmpr1B* is important for later chondrogenic differentiation. The activin receptor type I, *Acvr1,* is also expressed ubiquitously in the limb mesenchyme (Verschueren et al., 1995). Misexpression of constitutively active *Acvr1* in chick led to enhanced chondrogenesis and enlarged cartilage elements; however its function has mainly been associated with later chondrogenic events and ossification. Indeed, *Acvr1* is one of the main genes associated to Fibrodysplasia ossificans progressiva (FOP), a rare autosomal dominant disorder of skeletal malformations and progressive extraskeletal ossification (Shore et al., 2006). Finally, the type II receptor, *BmprII*, conditional knockout in the limb mesenchyme show normal formation of chondrogenic condensations and no skeletal defect (Gamer et al., 2011) suggesting that other type II receptors like ACVR-II or ACVR-IIB are likely to be involved in limb development. However, single genetic inactivation of *AcvrII* or *AcvrIIB* does not show limb pattern defects (Robert, 2007) . The double null mutants of *AcvrII* and *AcvrIIB* die at gastrulation and *AcvrII*+/– :*AcvrIIB*–/– survive only up to E9.5, precluding the study of the developing limb (Song et al., 1999). Therefore, it is still unkown if these receptors play an important role in skeletal pattern formation.

A mutant that gives insight into the control of *Sox9* expression by canonical BMP signaling is the conditional inactivation of Smad4 in the limb (Bénazet et al., 2012). *Smad4* inactivation prevents BMP signaling in the limb autopod and results in absence of *Sox9* expression and impairment of digit formation. SMAD4 is also a known co-factor of the TGFbeta pathway, however genetic inactivation of TGF-beta signaling in mouse embryos does not produce similar phenotypes (Sanford et al., 1997, Seo and Serra, 2007).

In summary, from the genetic studies referred above it is clear that BMP signaling is essential for the induction of Sox9 and consequently regulates the onset of chondrogenesis in the limb. However, it is still not clear how Bmps activate *Sox9* in a periodic manner along the anterior-posterior axis to specify chondrogenic and non-chondrogenic fates.

1.3.2) TGFβ´s, Activins and the regulation of *Sox9*

TGFβs and Activins are also secreted cytokines of the TGF-β superfamily. Similarly to BMPs they signal through serine-threonine type I and type II receptors. TGFβs signal through TGFβreceptor 2 (TGFβR2) and TGFβ receptor 1 (TGFβR1). Activins signal through type II Activin receptor 2A, and 2B, (ACVR2A, ACVR2B), and type I Activin receptor 1, 1B and 1C (ACVR1, ACVR1B, ACVR1C). Type I activin receptors are also shared by some BMP proteins, for review see (Massagué, 2012). Contrary to BMPs, TGFβs and Activins signal through SMAD2 and SMAD3 proteins, that when phosphorilated by activated type I receptors form complexes with co-factor SMAD4 and are transported into the nucleus where they regulate transcription of target genes.

Three ligands of the TGFβ family are expressed in the limb: TGFβ1, TGFβ2 or TGFβ3. Two of these ligands, Tgfβ2 and Tgfβ3, have been found expressed in the condensing digits (Lorda-Diez et al., 2010), in the developing joints and in the differentiating tendon blastemas (Millan et al., 1991, Merino et al., 1998, Kuo et al., 2008). TGFβs are able to induce chondrogenesis. Indeed application of TGFβ1, TGFβ2 or TGFβ3 in the interdigital regions of chick embryos inhibits apoptosis and promotes chondrogenesis with the formation of ectopic digits (Ganan et al., 1996). Consistently, addition of TGFβs to the medium of micromass cultures increases chondrogenesis (Miura and Shiota, 2000, Leonard et al., 1991, Schofield and Wolpert, 1990, Chimal-Monroy and Díaz, 1997, Zhang et al., 2004).

Studies in micromass culture (Miura and Shiota, 2000, Leonard et al., 1991) also proposed that TGFβ1 and TGFβ2 could be the activators of the Turing network that controlled the skeletal patterning. Nevertheless, other studies have shown that TGFβs inhibited chondrogenesis (Seo and Serra, 2007, Tsuiki and Kishi, 1999, Jin et al., 2008) or that had both a positive and negative influence on chondrogensis (Roark and Greer, 1994). It was suggested that this dual effect could be explained by the capacity of TGFβs to coordinate cartilage and tendon differentiation in the developing limb mesenchyme (Lorda-Diez et al., 2009). This was confirmed by a recent study in chick, that analyzed the expression of chondrogenic and connective tissue markers around a TGFβ1-soaked bead (Lorda-Diez et al., 2011). This study showed that 3h after bead implantation tendon progenitor markers like *Scleraxis* were up-regulated around the bead (Lorda-Diez et al., 2011). In agreement with this study, conditional inactivation of TGFβ signaling in the limb mesenchyme impaired tendon development and showed that TGFβ signaling was essential for recruitment and maintenance of tendon progenitors through regulation of *Scleraxis* expression (Pryce et al., 2009). This study also showed that at stage E12.5, *Tgfβ2* or *Tgfβ3* were expressed in tendon progenitors, muscles and prechondrogenic skeletal condensations, suggesting a possible role for TGFβ as coordinators between the forming tendons and their musculoskeletal counterparts.

Neither the *Tgfβ1*, *Tgfβ2*, or *Tgfβ3* null mutants nor the double null mutants for *Tgfβ2* and *Tgfβ3* show any phenotype in digit formation (Shull et al., 1992, Kaartinen et al., 1995, Sanford et al., 1997, Dünker et al., 2002). However, conditional deletion of *Tgfβr2* in the limb results in long bones only and in impaired joint development (Seo and Serra, 2007). In addition, mice expressing dominant negative *Tgfβr2* in the developing chondrocytes develop hypoplastic cartilage (Hiramatsu et al., 2011) and local application of TGFβs in the chick limb interdigit activates the expression of *Bmpr1B* which is essential for chondrogenic differentiation but not for induction of *Sox9* (Ganan et al., 1996, Merino et al., 1998).

In summary, TGFβ signaling appears to be connected more to the specification of later chondrogenic differentiations rather than the specification of the early *Sox9* pattern. This is consistent with the requirement of TGFβs for joint and tendon development through the regulation of *Scleraxis* at later stages. Different target genes of the TGFβ signaling could be controlled by several cofactors (Wotton and Massague, 2001, Inoue and Imamura, 2008). For example, it was suggested that the TGF-interacting factor *Tgif1* and SKI-like oncogene *SnoN* could be the cofactors that mediate the inhibition of *Sox9* favoring the specification of joints and tendon progenitors (Lorda-Diez et al., 2009). However a recent study has suggested that TGFβs could act before BMPs to induce chondrogenesis in a transient way (Karamboulas et al., 2010).

Activins are expressed in the digit primordia and exogenous application of Activins A, B or AB induces ectopic digits in the interdigital chick mesenchyme (Merino et al., 1999). In addition, blocking Activin function by local treatments with its antagonist Follistatin inhibits the formation of digits in chick limb bud (Merino et al., 1999). As observed for TGFβs, digit induction mediated by Activins resulted in upregulation of *Bmpr1b* (Ganan et al., 1996, Merino et al., 1998, Merino et al., 1999) which mediates chondrogenic differentiation through BMP signaling (Yi et al., 2000). According to *in vitro* data, Activins might be modulating cell aggregation by regulating the adhesive properties of prechondrogenic precursors (Jiang et al., 1993). It was also shown that establishment of the digit crescent (Montero et al., 2008) or phalanx forming region (Suzuki et al 2008) is directed by Activin/TGFβ signaling. This was shown by inhibiting Smad6 and Bambi, two specific BMP antagonists, and thus allowing BMP signaling to activate *Sox9* and chondrogenesis in that region (Merino et al 2008). However, Activins or Follistatin-deficient mice show several developmental alterations but no digit phenotype (Matzuk et al., 1995a, Matzuk et al., 1995b, Oh et al., 2002). Early lethality in *Acvr1a* and *Actr1b* null mice do not allow to study their function in the limb and up-to-date no conditional mutant was made (Mishina et al., 1999, Gu et al., 1998). This is also the case for the *Smad2* mutant mice (Nomura and Li, 1998). *Smad3* mutants instead survive but they do not show any digital phenotype (Zhu et al., 1998). Misexpression in chick of constitutively active *Acvr1* led to enhanced chondrogenesis and enlarged cartilage elements, however its function has mainly be associated with later condrogenic events and ossification, being one of the main genes associated to Fibrodysplasia ossificans progressiva (FOP) (Shore et al., 2006). In summary, Activins seem to play an important role to control late chondrogenic events similar to the case of TGFβs. However, it is still not clear if they play a role in early Sox9 patterning.

1.3.3) WNT pathway and regulation of *Sox9*

WNTs are secreted glycoproteins that signal through the canonical β-catenin dependent pathway and two known non-canonical pathways (Figure 25) (Barrow, 2006, Kühl et al., 2000, Logan and Nusse, 2004). In the canonical pathway, in the absence of WNT signaling , β-catenin is degraded by a β-catenin destruction complex constituted of Axin, adenomatosis polyposis coli (APC), protein phosphatase 2A (PP2A), glycogen synthase kinase3 (GSK3) and casein kinase 1α (CK1α). Within this complex, CK1 α and GSK3 phosphorylate β-catenin allowing for its ubiquitination and proteasome mediated degradation (He et al., 2004). When WNT ligands bind to its receptor Frizzled and co-receptor LRP5/6, Frizzled activates its cytoplasmatic target

Dishevelled (DVL) which suppresses GSK-3 activity. As a result, β-catenin is not phosphorylated and thus not degraded, resulting in accumulation of β-catenin in the cytoplasm and translocation to the nucleus (Hatsell et al., 2003). In the nucleus β-catenin binds to transcription factors of the LEF/TCF family allowing for target gene transcription (Peifer and Polakis, 2000, Nusse, 2005).

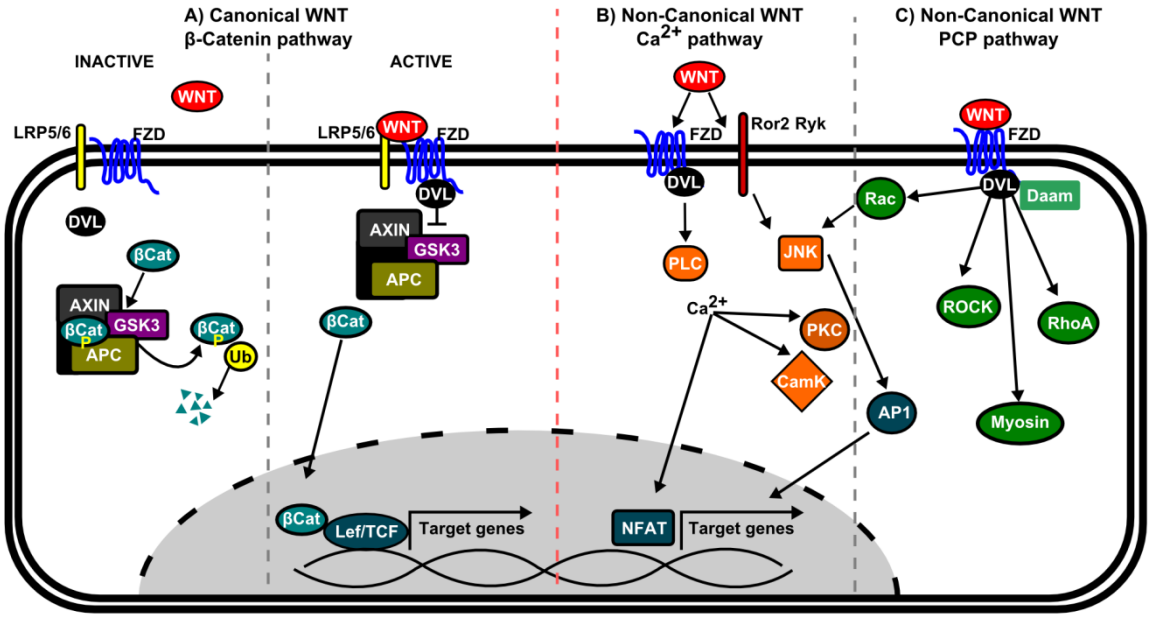

Figure 25. WNT signaling pathways.

A) The canonical WNT/β-catenin pathway: without the binding of the WNT ligands to the receptor FZD and co-receptors LRP5/6 the pathway is inactive. Cytosolic β-Catenin (β-Cat) is targeted to proteolytic degradation through phosphorylation by the APC–Axin–GSK3β complex and further ubiquitination through action of the ubiquitin ligase complex (Ub). When WNT ligands bind to FZD receptors and LRP5/6, FZD recruits DVL. DVL will inhibit APC–Axin–GSK3β complex formation by the recruitment of GSK3β, CK1γ and Axin to the cytoplasmic membrane. Consequently, β-catenin can accumulate in the cytoplasm and enter the nucleus, activating transcription of target genes through association with Lef/TCF transcription factor family. B) Non-Canonical WNT/Ca^{2+} pathway: WNT binding to FZD receptors can lead to an increase in intracellular calcium level, through possible activation of PLC. Intracellular calcium subsequently activates CAMKII and PKC, as well as the transcription factor NFAT. This pathway is particularly important for convergent-extension movements during gastrulation. Additionally, Fzd receptors in association with Ror2 or Ryk receptors can also activate JNK promoting expression of specific genes through activation of AP-1. C) Non-Canonical WNT/PCP pathway: WNT-signaling activates Rho GTPases such as RhoA and Rac1 and ROCK leading to cytoskeleton rearrangement, with the participation of Daam1 (Daam). Rac1 can also activate JNK, and modulate gene transcription through AP-1. Figureadapted from (Franco et al., 2009) .

Two β-catenin–independent or non-canonical WNT pathways also require activation of Dishevelled (DVL): the planar cell polarity pathway (PCP pathway) and the WNT/Ca^{2+} pathway. The PCP pathway controls asymmetric actin cytoskeletal organization, coordinated polarization of cells within the plane of epithelial sheets, and directed cell migration (Boutros et al., 1998, Li et al., 1999). On one side DVL activates JNK through Rac GTPase (Habas et al., 2003, Habas et al., 2001). This pathway is used in *Drosophila* planar cell polarity (Gao, 2012) and by Wnt11 in convergent extension movements during Zebrafish gastrulation (Heisenberg et al., 2000). On the other side the DVL-Daam1 complex activates the small GTPase Rho, Rho-associated kinase (ROCK) (Marlow et al., 2002) and myosin (Weiser et al., 2007) which leads to modification of the actin cytoskeleton and cytoskeletal rearrangement. Since no downstream regulation of gene transcription is known through Rho and Rac mediated WNT signaling, it seems that their primary role is indeed to control the cytoskeletal modulation (Keller, 2002). The other non-canonical pathway, Wnt/Ca^{2}+ pathway, leads to release of intracellular calcium possibly via G-proteins (Kohn and Moon, 2005, Slusarski and Pelegri, 2007). This pathway involves activation of phospholipase C (PLC) and protein kinase C (PKC). Elevated Ca^{2}+ can activate the phosphatase calcineurin, which leads to dephosphorylation of the transcription factor NFAT and its accumulation in the nucleus. In the Xenopus embryos, NFAT activity suppresses canonical Wnt signals during axis formation (Beals et al., 1997, Chevallier et al., 1977).

The canonical WNT pathway has essential roles in early embryogenesis and organogenesis of several organ systems, while the non-canonical pathways has been more associated to cell migration and morphogenesis (van Amerongen and Nusse, 2009).

In the limb, there are eleven different Wnts and seven Fzds (Summerhurst et al., 2008) and the canonical WNT pathway is known to play essential roles in skeletogenesis (Parr et al., 1993, Guo et al., 2004, Day et al., 2005, Hill et al., 2005, Hu et al., 2005).

A previous study has shown that expression of *Wnt4*, *Wnt14*, and *Wnt16* in the presumptive mouse joints is associated with up-regulation of β-catenin protein levels and inhibition of *Sox9* expression (Guo et al., 2004). In addition it was shown that the inhibition of β-catenin signaling in micromass cultures leads to upregulation of chondrogenesis, while ectopic expression of an active form of β-catenin or *Wnt14* in chondrocytes results in loss of *Sox9* expression and promotion of the expression of joint markers such as *Gdf5* and *Scleraxis*. Using the same conditional mutant with overexpression of *Wnt14*, a subsequent study showed that Wnt/β-catenin signaling was sufficient to block chondrocyte differentiation and to enhance

endocondral bone formation and chondrocyte hypertrophy or maturation (Day et al., 2005). Moreover conditionally inactivated β-*catenin* in chondroprogenitors using Dermo1:Cre promoter, induced ectopic cartilage formation at the expense of diminished ossification. This suggested again that canonical WNT pathway is inhibiting chondrocyte formation and promotes osteoblast differentiation. The authors proposed that during the initial phase of ossification, chondrocytes are formed inside mesenchymal condensations that have low WNT/βcatenin signaling and express *Sox9*. Then in a second phase, osteoblast are formed in the periphery of *Sox9* expressing cells where WNT signaling is upregulated (Guo et al., 2004). In agreement with this, it was showed that Sox9 promotes degradation of β-catenin (Akiyama et al., 2004). Furthemore over-expression of *Sox9* or inactivation of β-*catenin* in chondrocytes resulted in inhibition of chondrocyte proliferation and delayed the transition of proliferating chondrocytes to hypertrophy. In addition, expression of a stabilized β-catenin in chondrocytes produced a phenotype of severe chondrodysplasia, with strong loss of *Sox9* expression and a marked inhibition of chondrocyte differentiation.

The genetic studies presented above (Akiyama et al., 2004, Guo et al., 2004, Day et al., 2005) used the *Col2a1:Cre* (Long et al., 2004) or *Dermo1:Cre* (Yu et al., 2003) to drive genetic over-expression or inactivation of WNT signaling. These promoters drive expression during the chondrogenic and osteogenic differentiation, respectively, (from E13 onwards) that begins much later than the initial expression of *Sox9*. Therefore, they do not allow drawing conclusions about the involvement of canonical WNT signaling in the early patterning events that regulate Sox9 expression. In contrast, a following study used the Prx1:Cre promoter to create conditional β-catenin over-expression and inactivation in the limb mesenchyme from the onset of limb bud formation (Logan et al., 2002, Hill et al., 2005). These mutants were analyzed at early time points (E11) and revealed that upon β-*catenin* inactivation, *Sox9* was up-regulated in the whole limb, while upon β-*catenin* over-expression *Sox9* was completely lost. This is in agreement with the low levels of β-catenin protein found in the *Sox9* expressing region of E11.5 limbs (Guo et al., 2004) and suggests that mesenchymal WNT canonical signaling controls the specification of chondrogenic fates at early limb stages.

A more recent study proposed that a combination of canonical WNT signaling from the ectoderm (E.g Wnt3, Wnt6) and FGF signals from the AER, synergistically maintain cells in an undifferentiated proliferating state, therefore restricting *Sox9* expressing cells to the core mesenchyme (ten Berge et al., 2008). This was shown by different functional experiments where Wnt3a inhibited *Sox9*, promoted proliferation and induced connective tissue fates. This study proposed that in young limb buds, where both WNT and FGF signaling encompass the whole limb mesenchyme, all cells are maintained in an undifferentiated and proliferative state.

Successively, limb outgrowth allows the cells in the core mesenchyme to exit the influence of the FGF and WNT signals, which results in arrest of proliferation, *Sox9* expression, and subsequent differentiation of the chondrogenic core. The cells underling the ectoderm are still within the range of FGF and WNT signals from the ectoderm, which maintain a low proliferative state and drive cells towards soft connective tissue fates. This model was proposed to explain how the chondrogenic fate was confined to the core mesenchyme but it did not investigate the patterning of the skeleton along the AP axis. It is therefore difficult to conclude if ectodermal Wnts influence the *Sox9* periodic digit pattern as well. Unfortunately a previous genetic study (Barrow et al., 2003) which inactivated Wnt3 in the ectoderm in mouse using the *Msx1Cre* promoter, was also unable to investigate role of Wnt3 inhibition on skeletal patterning due to early limb bud truncations. This confirmed that Wnt3 is essential for AER formation and maintainance as previously proposed in chick (Kengaku et al., 1998).

A recent study in chick also confirmed that ectodermal Wnts have an inhibitory effect on *Sox9* and restrict its expression to the core mesenchyme (Geetha-Loganathan et al., 2010). In this study, it was shown that ectodermal removal promotes extension of *Sox9* expression towards the ectoderm. This did not appear to affect the patterning of the skeletal elements; however the experiments were analyzed only at early stages when only the stylopod and zeugopod were specified. Therefore it is still not clear if the ectoderm removal affects the digit patterning process.

Wnt5a is expressed in the distal limb mesenchyme (Yamaguchi et al., 1999) and has been mostly associated to the non-canonical Wnt/Ca^{2+} pathway, leading to the activation of Ca^{2+}–dependent effector molecules CamKII, NFAT, and PKC in a pertussis toxin (PTX)–sensitive manner (Slusarski et al., 1997, Kühl et al., 2000, Sheldahl et al., 1999, Murphy and Hughes, 2002). Moreover, it has been shown that WNT5a antagonizes canonical WNT pathway by promoting β-catenin degradation through a GSK3-independent pathway (Topol et al., 2003) . Wnt5a null mutants exhibit a strong limb phenotype with five digits that are truncated along the PD axis and are broader along the AP axis (Yamaguchi et al., 1999). A similar phenotype was observed by inactivating *Porcupine*, an Endoplasmic Reticulum (ER) protein essential for WNT secretion (Barrott et al., 2011). The Wnt5a null mutant shows loss of *Sox9* expression and up-regulation of β-catenin signaling in the distal region of the limb. This suggested that *Wnt-5a*, which is normally expressed at the highest level in the distal limb, inhibits the canonical Wnt activity to allow chondrogenesis to occur distally. To test if the upregulation of distal β-catenin signaling was indeed responsible for the inhibition of chondrogenesis, *Sfrp-2* expressing CEF cells were grafted into the interdigit area of the distal mesenchyme of *Wnt-5a* mutant limbs at E11.5. *Sfrp-2* is normally expressed in the surrounding mesenchyme of newly formed cartilage

in the distal limb (Lescher et al., 1998) and is considered a canonical-WNT antagonist during embryonic development (Lee et al., 2000). The grafted *Sfrp-2* expressing CEF cells were able to ectopically induce expression of *Col2a1*, in both wild-type and mutant limbs (Topol et al., 2003). These data suggested that suppression of canonical WNT signaling in the interdigital mesenchyme allows chondrogenesis to occur.

Using time-lapse video microscopy in GFP-electroporated chick embryos, a recent study demonstrated that mesenchymal cells in the limb move and divide according a specific orientation. By re-analyzing the Wnt5a null mutant they proposed that WNT5A/JNK was necessary for the proper orientation of cell movements and cell orientations (Gros et al., 2010). The short and broad digit phenotype in the Wnt5a null mutant can thus be explained due to a combined effect of loss of oriented growth (Gros et al., 2010) and up-regulation of anti-chondrogenic β-catenin signaling (Topol et al., 2003).

Wnt7a has also been shown to inhibit chondrogenesis in micromass culture through Fz7 receptor and MAPK pathway (Tufan and Tuan, 2001, Tufan et al., 2002b, Tufan et al., 2002a). This inhibition was correlated with maintenance of N-cadherin expression and cell adhesion (Tufan and Tuan, 2001). In the mouse limb, Wnt7a is expressed in the dorsal part of the ectoderm (Gavin et al., 1990, Parr et al., 1993) and controls the DV patterning of the limb (Parr and McMahon, 1995, Riddle et al., 1995), see also section 1.2.3. Wnt7a regulates *Lmx1b* expression which covers the whole dorsal mesenchyme, this suggests that ectodermal Wnts can diffuse and signal throughout the mesenchyme (Church and Francis-West, 2002). However, several evidences show that Wnt7a is not the only gene regulating *Lmx1b* expression (Cygan et al., 1997, Loomis et al., 1998) and that probably other WNTs signal through the canonical pathway to regualte *Lmx1b* (Hill et al., 2006). In the Wnt7a mutant the posterior digits are lost (Woods et al., 2006). However, rather than a direct influence on Sox9, this phenotype has been associated to the downregulation of *Shh* (Parr and McMahon, 1995, Parr et al., 1998). Wnt7a signaling may also depend on LRP6, since deletion of LRP6 results in dorso-ventral patterning and anterior-posterior patterning defects similar to those observed in the Wnt7a mutant (Pinson et al., 2000).

In summary, ectodermally expressed WNTs, such as WNT3, WNT6 and WNT7a (ten Berge et al., 2008, Geetha-Loganathan et al., 2010, Tufan and Tuan, 2001) as well as mesenchymal WNTs such as Wnt14 (Hartmann and Tabin, 2001), have been associated with an inhibitory function on *Sox9* expression in the limb and therefore with the regulation of the early chondrogenesis. Most of these Wnts, signal through the canonical β-catenin pathway. Consistently β-catenin inactivation results in over-expression of *Sox9* in the whole limb, while

its up-regulation inhibits *Sox9* expression (Hill et al., 2006, Hill et al., 2005). On the other hand, Sox9 is capable of counteracting the inhibitory effect of WNT/β-catenin signaling by directly promoting β-catenin degradation in the nucleus (Akiyama et al., 2004, Topol et al., 2003). While WNT3 and WNT6 signaling from the ectoderm limit the chondrogenic fate to the core mesenchyme (ten Berge et al., 2008, Geetha-Loganathan et al., 2010), the involvement of WNT signaling in the establishment of the Sox9 periodic pattern along the AP it is still not clear. It is known that Sfrp3 and Sfrp2 which are diffusible WNT antagonists are expressed within the Sox9 expression domain or at the periphery of Sox9 domains respectively (Wada et al., 1999, Baranski et al., 2000, Esteve et al., 2000, Ladher et al., 2000, Witte et al., 2009). Therefore, the presence of the antagonists in the Sox9 expressing region could allow chondrogenesis to proceed while inhibitory WNT signaling from the surrounding mesoderm and ectoderm could limits the chondrogenic fate (Rudnicki and Brown, 1997, Stott et al., 1999, Hartmann and Tabin, 2001).

1.4 Capturing 3D spatio-temporal dynamics of gene expression during development

Developmental processes such as patterning and morphogenesis are driven by a complex temporal and spatial regulation of gene expression. Therefore, the analysis of gene expression patterns during development is important to study the function of genes and their possible interactions. A gene can be essential at one stage for one specific function but its expression can reveal another function at another stage; if two genes are co-expressed in the same region they can interact, while complementary gene expression patterns can reflect an inhibitory effect.

To describe gene expression patterns during development, it is common to use whole mount *in situ* hybridization (WMISH) which visualizes the distribution of mRNAs at one particular developmental stage. The conventional way to analyze WMISH data is by taking 2D pictures of the embryo or organ with a specific orientation (E.g. a dorsal view in the case of the limb). In order to gain more insight into the 3D expression, it is also common to analyze gene expression patterns in tissue sections, see for example (Witte et al., 2009). Nevertheless, this data does not reveal the full 3D spatial distribution of a gene and can lead to false conclusions about its function.

The development of the Optical Projection Tomography (OPT) microscopy has enabled the 3D imaging of gene expression in specimens that range from 1 mm to 1 cm, such as the embryo

(Sharpe, 2003, Sharpe et al., 2002). The advantage of OPT over other 3D imaging methods, such as confocal microscopy and Single Plane Illumination Microscopy (Huisken et al., 2004), resides in its ability to image non-fluorescent stains commonly used in biochemical protocols, like X-gal/LacZ reporters or BCIP/NBT detection of *in situ* hybridization. The OPT scanner is able to capture high resolution 3D WMISH data thanks to several technical aspects, see also Figure 26. Firstly, OPT can reach depth of focus up to 15 mm while other microscopy techniques like confocal imaging can only image to a maximum 1 mm depth. Secondly, it combines images from many different angles by rotating the specimen of 360 degrees. This produces 3D data with the same focus in every part of the embryo despite different focus within single images. Thirdly, the OPT uses the principle of projection tomography to obtain the 3D data, which means that the raw data are mathematically transformed to reconstruct the original 3D object (Kak and Slaney). Finally, the OPT microscope uses visible light to detect colored stains (the light shines through the specimen and the camera detects how much light is absorbed by dark colored regions with regular stains) and it can also measure the emission from fluorescent compounds.

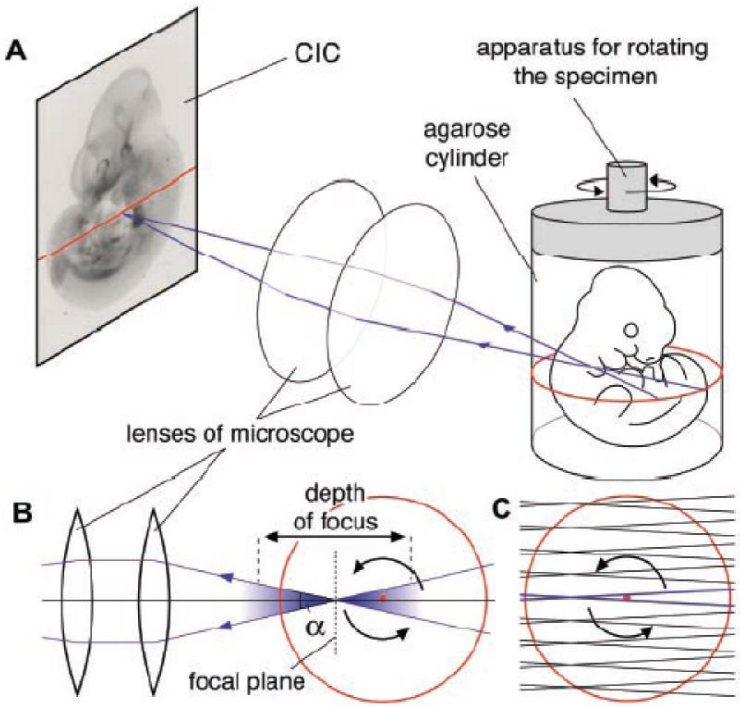

Figure 26. Schematic representation of the OPT microscopy.

(A) The specimen is rotated in an agarose cylinder while it is imaged by the microscope. The light transmitted from the specimen (blue lines) is focused by the lenses onto the camera-imaging chip (CIC or CCD). The apparatus is adjusted so that light emitted from a section that is perpendicular to the axis of rotation (red ellipse) is focused onto a single row of pixels on the CIC (red line). The section highlighted as a red ellipse in (A) is seen as a red circle in (B). The region of the specimen sampled by a single pixel of the CIC is shown as a double inverted cone shape (blue region). Points far from the focal plane will not

appear sharply focused in the image (pale blue shading), while those closer to the plane will be more focused (darker blue shading). The depth-of-focus is not always large enough to include the entire specimen, Therefore the position of the axis of rotation is adjusted so that only the front half of the specimen is in focus. This ensures that every part of the specimen is imaged in focus during a full 360 degree rotation. Figure adapted from (Sharpe et al., 2002).

All these characteristics make the OPT a powerful tool to analyze 3D gene expression patterns during development. However to obtain a detailed gene expression time-course data, it is necessary to analyze and combine data from many specimens at different developmental stages which requires an accurate determination of the developmental stages.

The age of an embryo (in days or hours) is often used to estimate the developmental stage. In mouse, this can be a source of variability because embryos from the same litter can develop at different speeds. This can be avoided by using a more accurate staging system such as the Theiler staging system (Theiler, 1972) or by counting somites (Michos et al., 2004). However these classical staging systems rely on qualitative biological features of the embryo. This creates a problem of subjective analysis, since two scientists can interpret the features in a different way. Another problem is that it still is unclear to which extent the development of the different organs is synchronized. Some organs indeed develop with great variability and become asynchronous from the rest of the embryo. For example, it was shown that mouse limb buds with the same Theiler stage differ greatly in their shape and size (Boehm et al., 2011). Finally, some staging systems consider stages that last for about half a day and cannot be used to stage developmental processes like limb development where important events occur within hours. Finer staging resolution can be achieved with somites counting (Michos et al., 2004) but this method is not suitable for later stages when the somites have already differentiated. To overcome these problems, previous work from our laboratory has contributed with the development of an accurate landmark-free morphometric staging system of the limb (Boehm et al., 2011). This staging system is based on morphometrics (the limb shape is quantified by calculating the curvature of limb outline) and provides accuracy of about ±2 hours from E10.5 to E12.5. The staging system comes with a user friendly graphical user interface available at http://limbstaging.crg.es.

A combination of OPT imaging and an accurate staging system allows for a detailed analysis of gene expression dynamics in 3D. This is crucial to expand our knowledge about limb development, which is currently represented mainly by 2D data that focuses on the patterning process of the AP and PD axis (Summerhurst et al., 2008). Finally, detailed 3D data will also establish the basis of more realistic computational models of limb development.

2. OBJECTIVES

The aim of this thesis is to explore to what extent digit patterning is controlled by a reaction-diffusion Turing mechanism as opposed to traditional Positional Information models. This study has four main objectives.

The first objective is to describe in detail the spatio-temporal dynamics of digit patterning. This defines exactly what the digit patterning mechanism has to achieve and which are its constraints. Previous studies had similar goals but described skeletal patterning by analyzing the differentiating tissue at later stages, when a number of subsequent events had modified the first molecular pattern. By using OPT imaging and *in-situ* hybridization, I provide a detailed three-dimensional description of the skeletal patterning process as soon as it is established.

The second objective of my work is to identify candidate molecular components for the reaction-diffusion Turing mechanism that controls digit specifications. The hypothesis that a Turing mechanism could drive the specification of the digits and interdigits along AP axis has been proposed more than three decades ago. However, due the lack of molecular evidence this theory has remained a theoretical proposal rather than a widely accepted digit patterning model. In conjunction with the theoretical work of another member of the lab, I develop a system biology approach to identify the molecular Turing network that controls digit patterning. I first screen the possible candidates using high throughput data from a comparative analysis made with the Sox9 reporter mice. This together with the analysis of expression patterns and signaling pathway activities identifies candidate genes that reflect the digit pattern as soon as it is established. This data represents the basis for a mathematical analysis that explores the possible Turing network that can explain digit patterning.

The third objective of my work is to design manipulative experiments to evaluate the Turing network. This study represents the first attempt for a systematic identification and evaluation of the Turing molecules that controls digit patterning. To evaluate the candidate molecules, I develop an in-vitro limb culture system with the Sox9 reporter mice. Within this set-up I perform bead experiments and pharmacological perturbations to compare perturbed Sox9 patterns with the predictions of the model.

Finally the fourth objective of my work is to relate the Turing hypothesis with the long-standing positional information models based on Shh. Following the predictions of the model, I propose

a retrospective interpretation of previous experiments under the light of a new digit patterning model that integrates growth, positional information signals and a Turing mechanism.

3. RESULTS

The main goal of my PhD was to identify the molecular Turing network that controls digit patterning. This ambitious project was divided in two phases.

In an initial phase, I analyzed the 3D spatio-temporal expression of several genes during early limb development. This analysis was used to describe the early molecular dynamics of digit specification and to identify possible candidates for the Turing network. The first gene that I analyzed was the transcription factor Sox9, which is the earliest known gene that marks the skeletal pattern. This analysis allowed me to describe the dynamics of digit specification with high spatial and temporal resolution. To investigate the involvement of BMP signaling in digit specification, I also analyze the expression patterns of *Bmp*s and their inhibitor *Noggin*. Furthermore, I collaborated with the laboratory of Petra Seemann to analyze the 3D expression patterns of Bmp/GDF family genes and the related inhibitors *Gremlin1* (*Grem1*), *Gremlin2* (*Grem2*), *Chordin* (*Chrd*), *Chordin–like 2* (Chrdl2) and activator *Crim2*. These unpublished results are presented in the first section of this chapter. Part of these expression patterns (*Bmpr1b, Bmpr1a, Gdf5, Noggin)* contributed to the publication presented in the second section, which investigates the role of BMP signaling in brachydactyly type A1 (BDA1) and synostoses syndrome 2 (SYNS2).

Finally, in the second phase of my project, I combined microarray data, analysis of gene expression patterns and pathway activities with perturbation experiments to identify the molecular Turing network that controls digit specification. This is the main work of my PhD and resulted in the publication presented in the third section.

3.1 3D gene expression patterns

Hereby I present a collection of unpublished 3D gene expression patterns of *Sox9*, *Bmp2*, *Bmp4*, *Bmp7*, *Noggin* , *Grem1*, *Grem2*, *Chordin*, *Chordin-like protein2* (*Chrdl2*) and *Crim2*. Individual limbs at different stages, ranging from E10.5 to E12.5, were scanned in the OPT to capture gene expression patterns showed by standard WMISH protocol using NBT/BCIP or BM/Purple substrate, and auto-fluorescence was captured to define the shape of the limb. The raw data from OPT scans was reconstructed to obtain 3D gene expression patterns that were analyzed in the Bioptonics software. I present several virtual sections for each 3D expression pattern (Figure 27). Scanned limbs are staged using the morphometric limb staging system presented in (Boehm

et al., 2011). The resulting stages are shown with the nomenclature “mE” (mouse embryonic) followed by the stage in days and hours, such that the stage mE10.12 represents a limb at 10 days and 12 hours which is equivalent to the classic E10.5 stage.

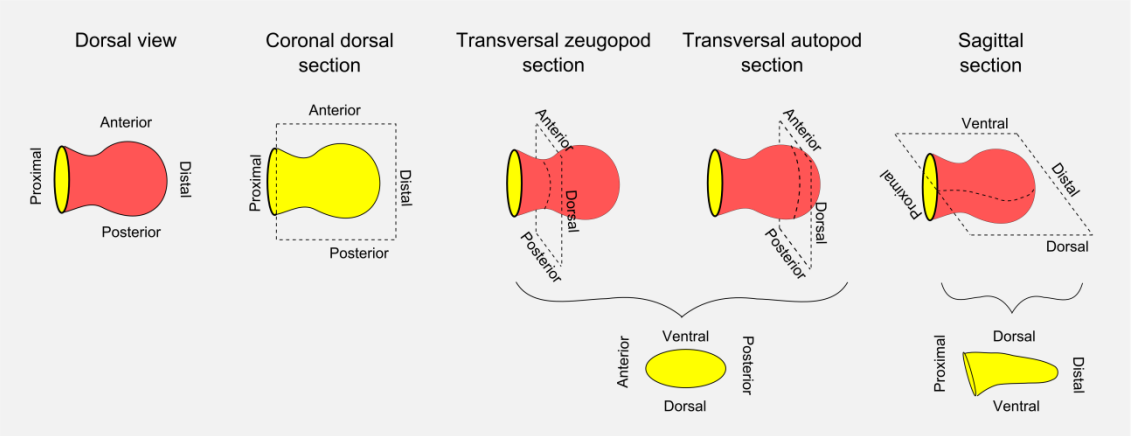

Figure 27. Schematic representation of the virtual sections performed with Bioptonics software.

3.1.1) *Sox9* expression pattern

From E10.5 to E12, the *Sox9* pattern appears as a continuous domain of expression where new skeletal elements arise from the previous ones: the stylopod appears first, then the two element of the zeugopod and finally the digits in the autopod. This order of appearance reflects the progressive proximo-distal patterning of the skeleton (Figure 28).

Around E10.5 (mE10.12), *Sox9* is expressed in the core mesenchyme of the limb bud and extends into the body. The proximal part of *Sox9* expression marks the stylopod and the distal part shows the first hints of the specification of the zeugopod (see dorsal view at mE10.14 Figure 28).

As the limb grows, around E11, Sox9 is down regulated in the center of the zeugopod region and forms two skeletal elements that unite distally forming doughnut-like shape.

From E11, the posterior part of the distal *Sox9* expression is separated in two regions: the most posterior demarcates the developing digit 4 and the most anterior region will develop into digit 2 and 3. These two digits form when *Sox9* is downregulated in the interdigit 3/2 around E11.12 (around E11.5).

Digit 5 forms slightly later around mE11.16 in the most posterior region of the limb and digit 1 forms around mE12.00 in the most anterior part of the limb. At mE12:00 the proximal part of *Sox9* expression that corresponds to the stylopod and the zeugopod is down-regulated.

The specification of the digits starts at mE11:00, with the branching of the distal continuous expression of *Sox9*, and down-regulation of *Sox9* in the interdigital regions. At mE11.12 (E11.5) digit 4, 3 and 2 become visible reflecting the first signs of the *Sox9* periodic pattern (see autopod section at mE11.13, Figure 28).

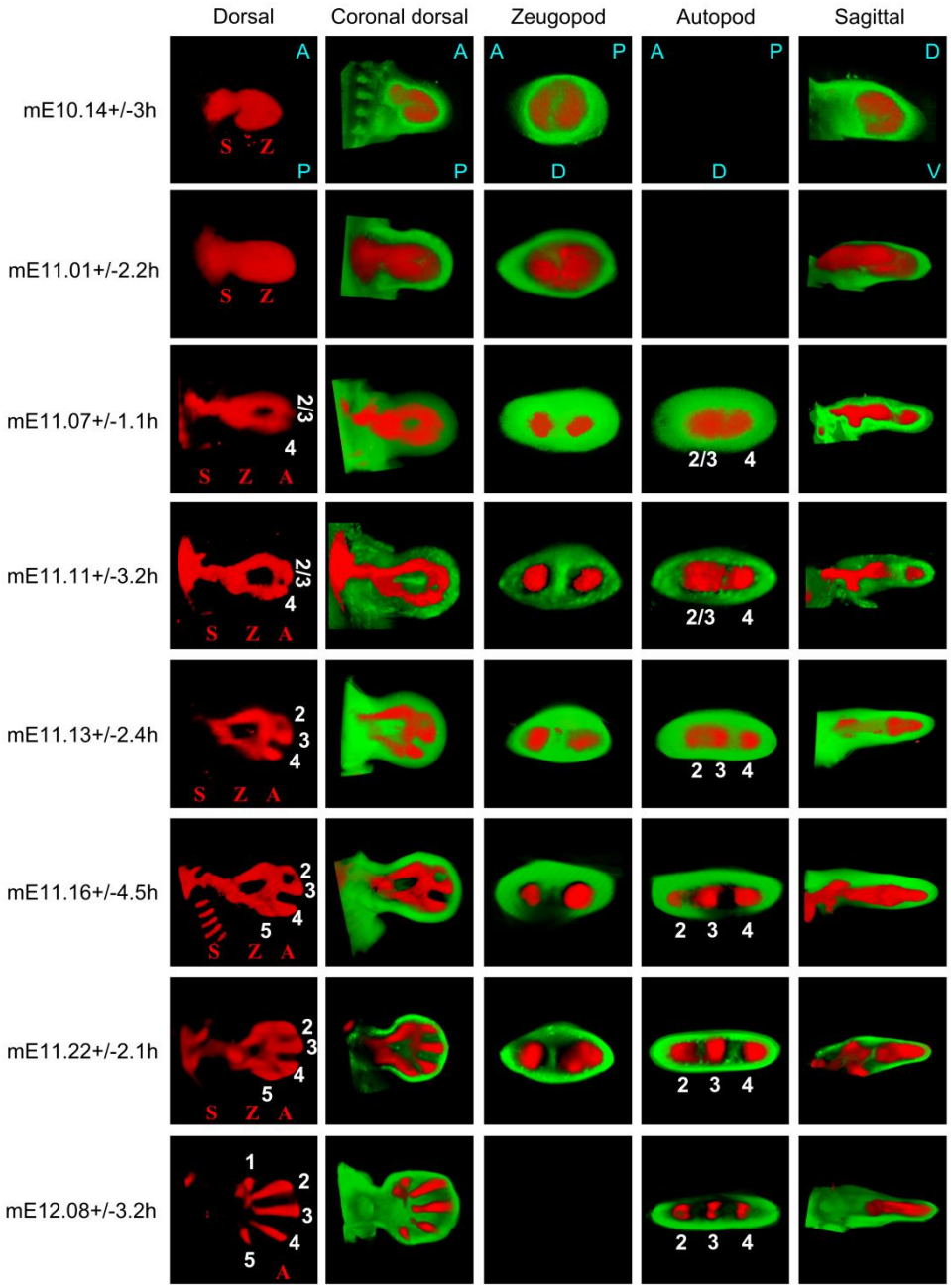

Figure 28. 3D *Sox9* expression patterns from mE10.14 to mE12.08, in the mouse forelimb.

From left to right: the first column shows a dorsal view of the *Sox9* expression in red; the second column shows a virtual coronal section centered along the DV, the limb shape in green, dorsal is to the front; the third and forth column show virtual transversal sections at the zeugopod and autopod level respectively; the fifth column shows a virtual saggital section crossing centered along the AP axis. Digits are highlighted with white numbers. The stylopod, zeugopod and autopod regions are highlighted with red letters, S, Z and A respectively. The order of digit formation is digit 4, digit 3 and digit 2, digit 5, digit 1. The periodic pattern of digit 4, digit 3 and digit 2 is first visible around E11.5 (mE11.12). A is anterior, P is posterior, D is dorsal and V is ventral.

3.1.2) *Bmp2* expression pattern

At E10.5 (mE10.12) *Bmp2* is strongly expressed in a region situated in the proximal/posterior/dorsal mesenchyme. *Bmp2* is expressed under the distal ectoderm and surrounds the core mesenchyme (see coronal view at mE10.13, Figure 29) and it is is expressed more strongly in the posterior mesenchyme. The saggital section shows how the expression of *Bmp2* is complementary to the expression of *Sox9* (compare the saggital section of *Bmp2* at mE10.12, Figure 29 with the saggital section of Sox9 at mE10.14, Figure 28).

At mE11, a new proximal region with high *Bmp2* expression is formed in the middle of the ventral and dorsal mesenchyme (saggital section at mE11.01, Figure 29). The distal expression of *Bmp2* has expanded anteriorly (see coronal section at mE11.01, Figure 29).

At mE11.12 (E11.5) the ventral and dorsal expressions in the proximal part become stronger, and are positioned at the level of the zeugopod (zeugopod section at mE11.12, Figure 29). The strong expression of Bmp2 in the porximal-posterior mesenchyme has expanded ventrally (zeugopod section at mE11.12, Figure 29). Moreover the anterior-proximal mesenchyme shows stronger expression as well (zeugopod section at mE11.12, Figure 29). Distally, Bmp2 is down-regulated at the region of the forming digit 4 and surrounds the region of the prospective digits 2 and digit 3 (compare coronal sections of *Bmp2* at mE11.12, Figure 29, and coronal section of *Sox9* at m11.11, Figure 28).

Around mE11.17 in the distal part, *Bmp2* is expressed in the interdigits, and in the dorsal mesenchyme and ventral mesenchyme surrounding digit 4, digit 3 and digit 2 (compare the autopod section of *Bmp2* at mE 11.17, Figure 29 with the autopod section of *Sox9* at mE11.16, Figure 28).

At mE11.20 the expression is similar to one observed at mE11.17 except for a clear downregulation at the level of digit 5 (compare the coronal section of *Bmp2* at mE11.17, Figure 29 and the coronal section of *Sox9* at mE11.22, Figure 28).

At E12 in the distal region, *Bmp2* is expressed in the interdigits (see autopod and coronal sections at mE12.06, Figure 29) and in the proximal region in different parts of the dorsal and ventral mesenchyme underlying the ectoderm (see zeugopod section at mE12.06, Figure 29). It is also possible to visualize a ventral expression centered on the digital rays (see dorsal view at mE12.06, Figure 29).

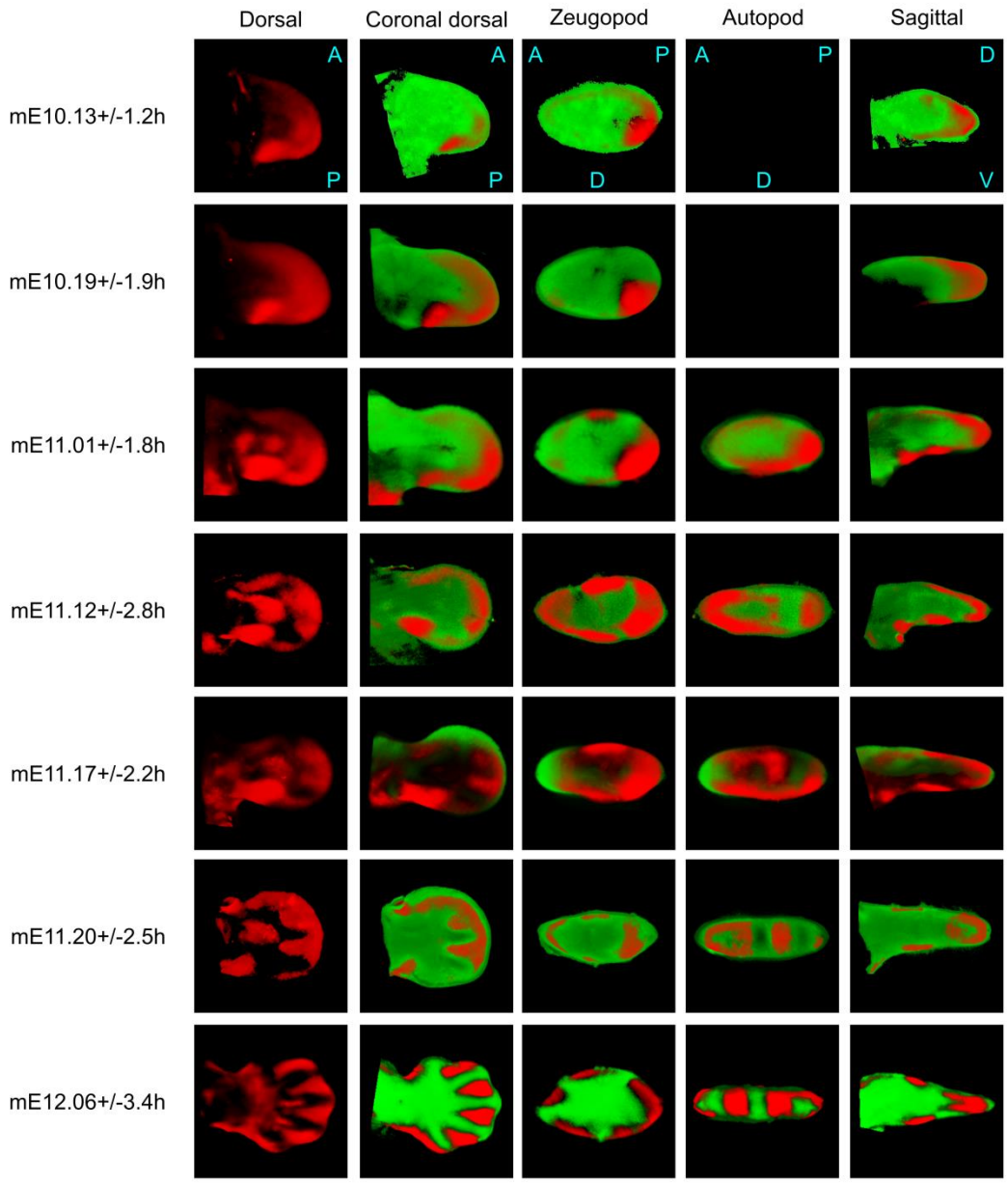

Figure 29. OPT timecourse of *Bmp2* expression pattern from mE10.13 to mE12.06, in the mouse forelimb.

From left to right: the first column shows the dorsal view of the *Bmp2* gene expression in red; the second column shows a virtual coronal section centered along the DV, the limb shape in green, dorsal is to the front; the third and forth column show virtual transversal sections at the zeugopod and autopod level respectively; the fifth column shows a virtual saggital section crossing the middle point of the AP limb axis. A is anterior, P is posterior, D is dorsal and V is ventral. Overall the expression of *Bmp2* appears strikingly complementary to expression of *Sox9*, see Figure 28.

3.1.3) *Bmp4* expression pattern

From mE11, *Bmp4* is expressed under the distal ectoderm and surrounds the core mesenchyme, with stronger expression at the proximal-posterior and proximal-anterior regions (see dorsal view at mE11.06, Figure 30).

At mE12, *Bmp4* is expressed in the interdigital, still surrounds the core mesenchyme and has a dorsal-proximal expression that underlies the ectoderm and seems to be located at the level of the forming tendons (see dorsal view at mE12.06, Figure 30).

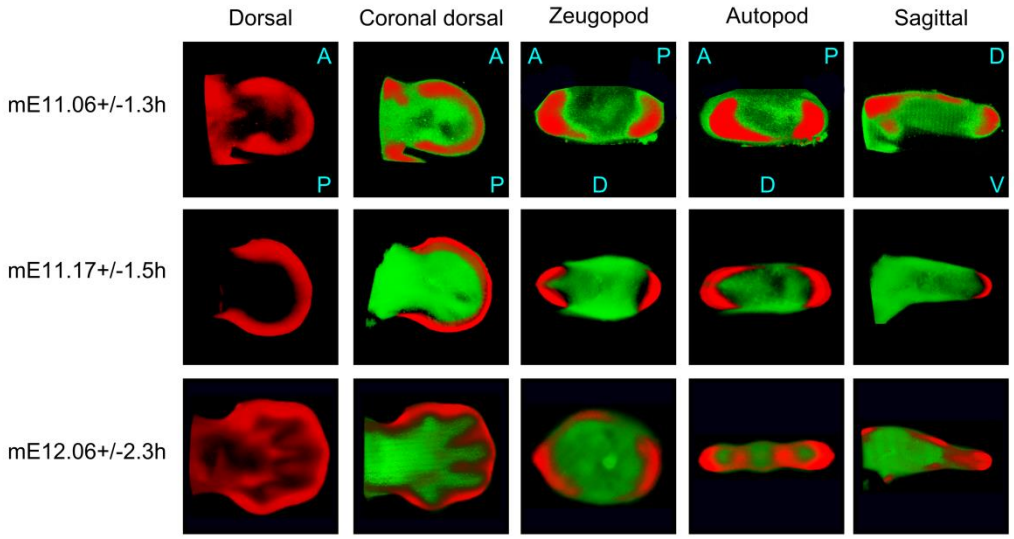

Figure 30. OPT timecourse of *Bmp4* expression pattern from mE11.06 to mE12.06, in the mouse forelimb.

From left to right: the first column shows the dorsal view of *Bmp4* expression in red; the second column shows a virtual coronal section centered along the DV axis, the limb shape in green, dorsal is to the front; the third and fourth column show virtual transversal sections at the zeugopod and autopod level respectively; the fifth column shows a virtual saggital section centered along the AP axis. A is anterior, P is posterior, D is dorsal and V is ventral.

3.1.4) *Bmp7* expression pattern

At E11, Bmp7 is expressed under the distal ectoderm and sorrounds the core mesenchyme. Moreover, it is expressed in two regions on the middle ventral and dorsal mesenchyme (see zeugopod and autopod sections at mE11.06, Figure 31).

At E12, Bmp7 is expressed in the interdigital regions (see coronal section at mE12.07, Figure 31) and in the ventral and dorsal mesenchyme underlying the ectoderm at the level of the digits (compare the autopod section of *Bmp7* at mE12.07, Figure 31 with the autopod section of Sox9 at mE12.08, Figure 28).

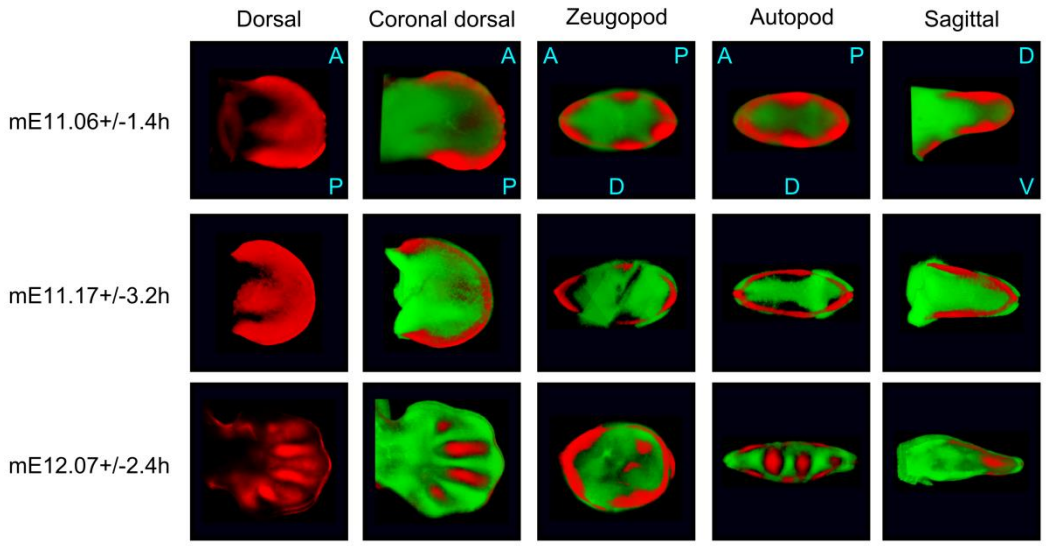

Figure 31. OPT timecourse of *Bmp7* expression pattern from mE11.06 to mE12.07 in the mouse forelimb.

From left to right: the first column shows the dorsal view of *Bmp7* expression in red; the second column shows a virtual coronal section centered along the DV axis, limb shape in green, dorsal is to the front; the third and forth column show virtual transversal sections at the zeugopod and autopod level respectively; the fifth column shows a virtual saggital section centered along the AP axis. A is anterior, P is posterior, D is dorsal and V is ventral.

3.1.5) *Noggin* expression pattern

At mE11, *Noggin* shows a fainted expression under the distal ectoderm (see coronal section at mE11.03, Figure 33) and in a region centered on the proximal dorsal mesenchyme (see dorsal view at mE11.03, Figure 32).

Around mE11.17, *Noggin* is also expressed in a region centered on the proximal-ventral mesenchyme (see zeugopod view at mE11.17, Figure 33). In the distal part, Noggin is expressed in digit 4 and digit 2 (compare coronal section of *Noggin* at mE11.17, Figure32, with the coronal section of *Sox9* at mE11.16, Figure 28).

At mE12, *Noggin* is expressed in all digital rays (compare dorsal view at mE12.05, Figure 32, with dorsal view of *Sox9* at mE12.08. Figure 28) and proximally at the level of the zeugopod (see zeugopod section at mE12.05).

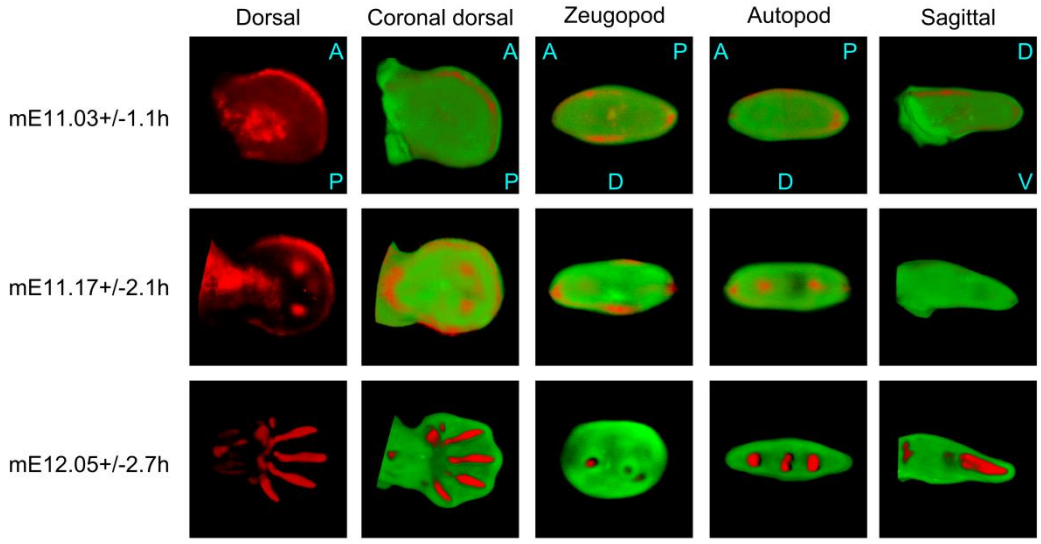

Figure 32. OPT timecourse of *Noggin* expression pattern from mE11.03 to mE12.05 in the mouse forelimb.

From left to right: the first column shows the dorsal view of the *Noggin* gene expression in red; the second column shows a virtual coronal section centered along the DV axis, the limb shape in green, dorsal is to the front; the third and forth column show virtual transversal sections at the zeugopod and autopod level respectively; the fifth column shows a virtual sagittal section centered along the AP axis. A is anterior, P is posterior, D is dorsal and V is ventral.

3.1.6) *Grem1* expression pattern

At E11, *Grem1* is expressed distally in the ventral and dorsal mesenchyme (see autopod section at mE11.01, Figure 33).

At E12, *Grem1* is still expressed distally in the ventral and dorsal mesencyme but it is restricted to the regions below and above the interdigits (see autopod section at mE12.03, Figure 33). A zone of proximal expression can be noticed underlying the ectoderm (see dorsal view and saggital section, at mE12.03, Figure 33).

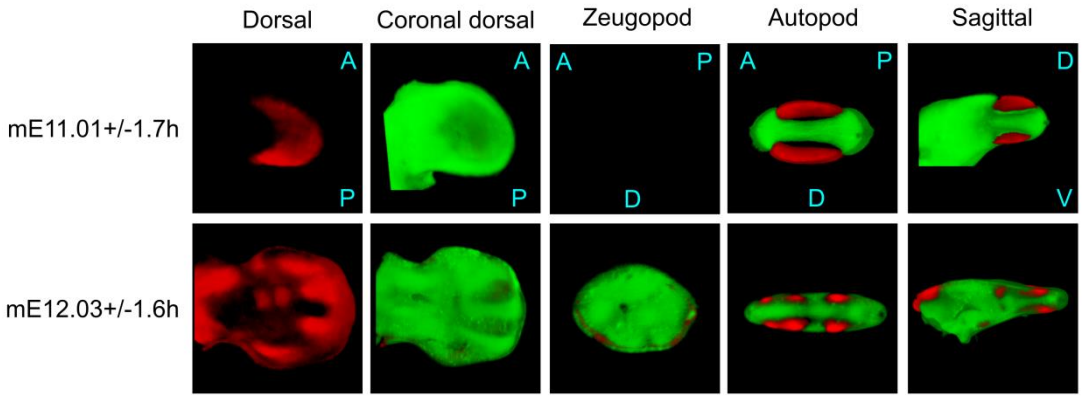

Figure 33. OPT *Grem1* expression pattern at mE11.01 and mE12.03 in the mouse hindlimb.
From left to right: the first column shows the dorsal view of the *Grem1* gene expression in red; the second column shows a virtual coronal centered along the DV axis, the limb shape in green, dorsal is to the front; the third and forth column show virtual transversal sections at the zeugopod and autopod level respectively; the fifth column shows a virtual sagittal section centered along the AP axis. A is anterior, P is posterior, D is dorsal and V is ventral.

3.1.7) *Grem2* expression pattern

At E11, *Grem2*, is expressed in the mesenchyme that underlies the ectoderm (see expression at mE11.04, Figure 34).

At E12, *Grem2* expression can also be seen in the digital rays and in the wrist region (see autopod and saggital sections at mE12.07, Figure 34).

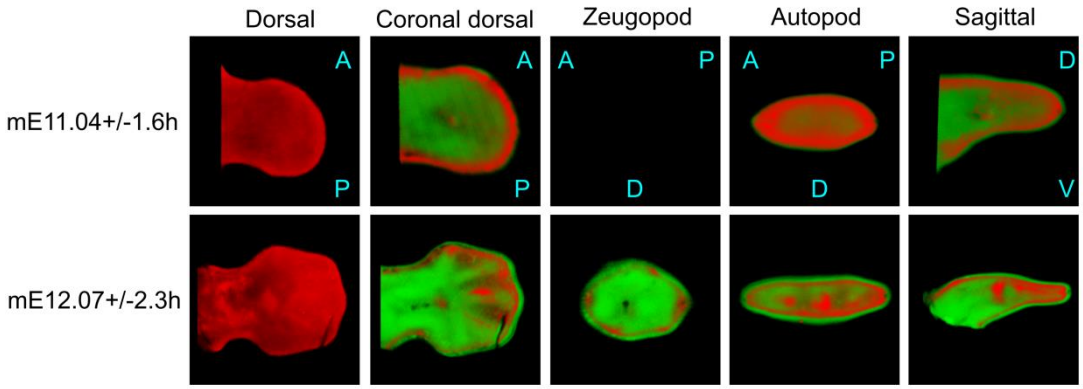

Figure 34. OPT *Grem2* expression pattern at mE11.01 and mE12.03 in the mouse hindlimb.
From left to right: the first column shows the dorsal view of the *Grem2* gene expression in red; the second column shows a virtual coronal section centered along the DV, the limb shape in green, dorsal is to the front; the third and forth column show virtual transversal sections at the zeugopod and autopod level respectively; the fifth column shows a virtual sagittal section centerd along the AP axis. A is anterior, P is posterior, D is dorsal and V is ventral.

3.1.8) *Chordin* expression pattern

At E11, *Chordin* is weakly expressed in the mesenchyme that underlies the ectoderm (see autopod and coronal sections at mE11.08, Figure 35) while it is strongly expressed in two regions centered on the dorsal and the ventral part that underlies the ectoderm (see dorsal view and zeugopod section at mE11.08, Figure 35). The dorsal region shows a stronger expression.

At E12, in the distal part, *Chordin* is expressed in the interdigits (see autopod and coronal sections at mE12.05, Figure 35) with stronger expression in the dorsal and ventral regions (see dorsal view and autopod section at mE12.05, Figure 35). The two regions centered on the proximal dorsal and the ventral part that underlie the ectoderm are maintained (see autopod section at mE12.05, Figure 25).

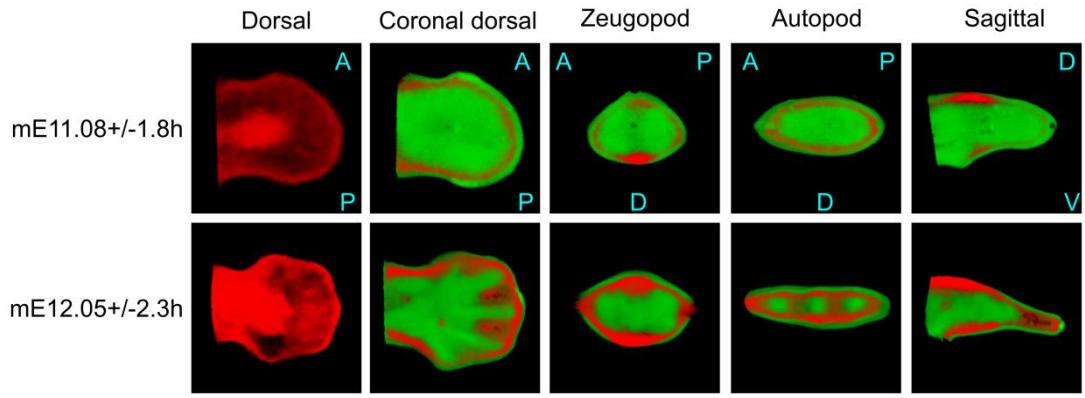

Figure 35. OPT *Chordin* expression pattern at mE11.01 and mE12.05 in the mouse hindlimb.
From left to right: the first column shows the dorsal view of the *Chordin* gene expression in red; the second column shows a virtual coronal section centered along the DV, limb shape in green, dorsal is to the front; the third and forth column show virtual transversal sections at the zeugopod and autopod level respectively; the fifth column shows a virtual sagittal section centered along the AP limb. A is anterior, P is posterior, D is dorsal and V is ventral.

3.1.9) *Chrdl2* expression pattern

Around E11.5, *Chrdl2* is weakly expressed in the mesenchyme underlying the ectoderm (see sections at mE11.13, Figure 36).

At E12, in the distal part, *Chrdl2* is expressed in the digital rays (see dorsal view and autopod section at mE12.08, Figure 26) and in the proximal part at different regions of the ventral and dorsal mesenchyme underlying the ectoderm (see zeugopod section at mE12.08, Figure 36).

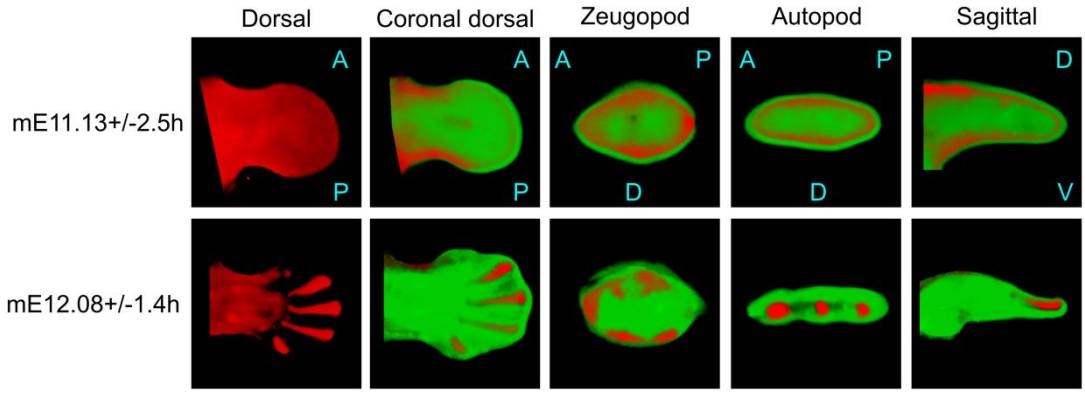

Figure 36. OPT *Chrdl2* expression pattern at mE11.13 and mE12.08 in the mouse forelimb.
From left to right: the first column shows the dorsal view of the *Chrdl2* gene expression in red; the second column shows a virtual coronal section centered along the DV axis the limb shape in green, dorsal is to the front; the third and forth column show virtual transversal sections at the zeugopod and autopod level respectively; the fifth column shows a virtual sagittal section centered along the AP axis. A is anterior, P is posterior, D is dorsal and V is ventral.

3.1.10) *Crim2* expression pattern

Around E11.5, *Crim2* is expressed in the proximal posterior and anterior mesenchyme underlying the ectoderm (see dorsal view at mE11.11, Figure 37). It is also expressed in the region of the forming digit 4 (compare the autopod section of *Crim2* at mE11.11, Figure 37 with the autopod section of Sox9 at mE11.11, Figure 28).

At E12, in the distal part, *Crim2* is expressed in the dorsal and ventral mesenchyme at the level of the interdigit 3/4 and interdigit 3/2 (compare the autopod section of *Crim2* at mE12.09, Figure 37 with the autopod section of Sox9 at mE12.08, Figure 28). In the proximal regions, *Crim2* continues to be expressed in the proximal anterior and posterior region (see dorsal view at mE11.11 and mE12.09, Figure 37).

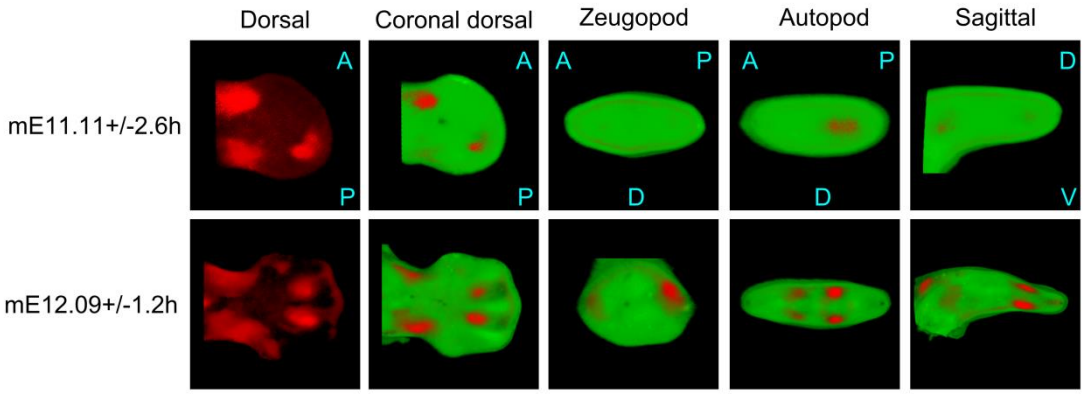

Figure 37. OPT *Crim2* expression pattern at mE11.01 and mE12.09 in the mouse hindlimb.

From left to right: the first column shows the dorsal view of the *Crim2* gene expression in red; the second column shows a virtual coronal section centered along the DV axis, limb shape in green, dorsal is to the front; the third and forth column show virtual transversal sections at the zeugopod and autopod level respectively; the fifth column shows a virtual saggital section centered along the AP axis. A is anterior, P is posterior, D is dorsal and V is ventral.

3.2 First paper : “A GDF5 Point Mutation Strikes Twice-Causing BDA1 and SYNS2”

This study was done in collaboration with the Seemann lab. It showed that changes in BMP signaling activity underlie the development of skeletal malformations observed in brachydactyly type A1 (BDA1) and synostoses syndrome 2 (SYNS2). My contribution to this work is a detailed description of the 3D expression patterns of *Gdf5*, *Noggin*, *Bmpr1a* and *Bmpr1b* showed Figure 6. This analysis reveals that these genes are co-localized in the digital ray from E11.5 to E13.5 suggesting possible interaction that may underlie the malformations observed when GDF5 has a point mutation in the overlapping interface of antagonist and receptor binding site.

Degenkolbe E, König J, Zimmer J, Walther M, Reißner C, Nickel J, Plöger F, Raspopovic J, Sharpe J, Dathe K, Hecht J, Mundlos S, Dolken S, Seemann P. "A GDF5 Point Mutation Strikes Twice-Causing BDA1 and SYNS2" PLOS Genetics. 2013 DOI: 10.1371/journal.pgen.1003846

OPEN ACCESS Freely available online

PLOS | GENETICS

A GDF5 Point Mutation Strikes Twice - Causing BDA1 and SYNS2

Elisa Degenkolbe[1,2☯], Jana König[1,2☯¤a], Julia Zimmer[1,2¤b], Maria Walther[1], Carsten Reißner[3], Joachim Nickel[4,5], Frank Plöger[6], Jelena Raspopovic[7,8], James Sharpe[7,8,9], Katarina Dathe[10], Jacqueline T. Hecht[11], Stefan Mundlos[1,10,12], Sandra C. Doelken[10], Petra Seemann[1,2,12]*

1 Berlin-Brandenburg Center for Regenerative Therapies (BCRT), Charité – Universitätsmedizin Berlin, Berlin, Germany, **2** Berlin-Brandenburg School for Regenerative Therapies (BSRT), Charité – Universitätsmedizin Berlin, Berlin, Germany, **3** Institute of Anatomy, Dept. Anatomy and Molecular Neurobiology, Universitätsklinikum Münster, Münster, Germany, **4** Lehrstuhl für Physiologische Chemie II, Theodor-Boveri-Institut für Biowissenschaften (Biozentrum) der Universität Würzburg, Würzburg, Germany, **5** Department of Tissue Engineering and Regenerative Medicine, Universitätsklinikum Würzburg, Würzburg, Germany, **6** Biopharm GmbH, Heidelberg, Germany, **7** EMBL-CRG Systems Biology Program, Centre for Genomic Regulation, Barcelona, Spain, **8** Universitat Pompeu Fabra (UPF), Barcelona, Spain, **9** Institució Catalana de Recerca i Estudis Avançats (ICREA), Barcelona, Spain, **10** Institut für Medizinische Genetik und Humangenetik, Charité – Universitätsmedizin Berlin, Berlin, Germany, **11** Department of Pediatrics, University of Texas Medical School at Houston, Houston, Texas, United States of America, **12** Research Group Development and Disease, Max Planck Institute for Molecular Genetics, Berlin, Germany

Abstract

Growth and Differentiation Factor 5 (GDF5) is a secreted growth factor that belongs to the Bone Morphogenetic Protein (BMP) family and plays a pivotal role during limb development. GDF5 is a susceptibility gene for osteoarthritis (OA) and mutations in *GDF5* are associated with a wide variety of skeletal malformations ranging from complex syndromes such as acromesomelic chondrodysplasias to isolated forms of brachydactylies or multiple synostoses syndrome 2 (SYNS2). Here, we report on a family with an autosomal dominant inherited combination of SYNS2 and additional brachydactyly type A1 (BDA1) caused by a single point mutation in GDF5 (p.W414R). Functional studies, including chondrogenesis assays with primary mesenchymal cells, luciferase reporter gene assays and Surface Plasmon Resonance analysis, of the GDF5^{W414R} variant in comparison to other GDF5 mutations associated with isolated BDA1 (p.R399C) or SYNS2 (p.E491K) revealed a dual pathomechanism characterized by a gain- and loss-of-function at the same time. On the one hand insensitivity to the main GDF5 antagonist NOGGIN (NOG) leads to a GDF5 gain of function and subsequent SYNS2 phenotype. Whereas on the other hand, a reduced signaling activity, specifically via the BMP receptor type IA (BMPR1A), is likely responsible for the BDA1 phenotype. These results demonstrate that one mutation in the overlapping interface of antagonist and receptor binding site in GDF5 can lead to a GDF5 variant with pathophysiological relevance for both, BDA1 and SYNS2 development. Consequently, our study assembles another part of the molecular puzzle of how loss and gain of function mutations in GDF5 affect bone development in hands and feet resulting in specific types of brachydactyly and SYNS2. These novel insights into the biology of GDF5 might also provide further clues on the pathophysiology of OA.

Citation: Degenkolbe E, König J, Zimmer J, Walther M, Reißner C, et al. (2013) A GDF5 Point Mutation Strikes Twice - Causing BDA1 and SYNS2. PLoS Genet 9(10): e1003846. doi:10.1371/journal.pgen.1003846

Editor: Gregory S. Barsh, Stanford University School of Medicine, United States of America

Received March 12, 2013; **Accepted** August 12, 2013; **Published** October 3, 2013

Funding: This work was supported by grants from the Deutsche Forschungsgemeinschaft [SE 1778/1-1 to PS and SFB760-A2 to PS and SM] and the Bundesministerium für Bildung und Forschung [Biochance plus3; 0313851A/B to FP and SM]. Contributions were made possible by DFG funding through the Berlin-Brandenburg School for Regenerative Therapies GSC 203 [ED, JK, JZ] and by FCT-Fundação para a Ciência e a Tecnologia [JR]. The funders had no role in study design, data collection and analysis, decision to publish, or preparation of the manuscript.

Competing Interests: Frank Plöger is an employee of the company Biopharm GmbH as indicated in the affiliation. Biopharm GmbH is a 100% privately owned company. All other authors have declared that no competing interests exist.

* E-mail: petra.seemann@charite.de

☯ These authors contributed equally to this work.

¤a Current address: Roche Diagnostics International AG, Rotkreuz, Switzerland.
¤b Current address: Section of Clinical Allergology, Paul-Ehrlich-Institut Federal Institute for Vaccines and Biomedicines, Langen, Germany.

Introduction

Growth and Differentiation Factor 5 (GDF5), which is also known as Cartilage-Derived Morphogenetic Protein 1 (CDMP1) belongs to the Transforming Growth Factor Beta superfamily (TGFB) and the subordinated group of Bone Morphogenetic Proteins (BMPs) [1]. GDF5 has a fundamental role during limb development, where it controls the size of the initial cartilaginous condensations as well as the process of joint development [2–4]. As a positive key regulator of early chondrogenesis, dimeric GDF5 initiates signaling by interacting preferably with two distinct BMP type I receptors, BMPR1A and BMPR1B, whereas binding via BMPR1B is favored over BMPR1A [5,6]. Upon receptor phosphorylation, intracellular SMAD transducer proteins are activated in order to regulate target gene transcription [7,8]. GDF5 activity is counteracted by BMP antagonists such as NOGGIN (NOG), which mask the receptor binding sites of GDF5 by a direct protein-protein interaction, thereby impeding receptor binding of the ligand and thus signaling [9,10].

Author Summary

Mutations can be generally classified in loss- or gain-of-function mutations depending on their specific pathomechanism. Here we report on a GDF5 mutation, p.W414R, which is associated with brachydactyly type A1 (BDA1) and Multiple Synostoses Syndrome 2 (SYNS2). Interestingly, whereas shortening of phalangeal elements (brachydactyly) is thought to be caused by a loss of function, bony fusions of joints (synostoses) are due to a gain of function mechanism. Therefore, the question arises as to how p.W414R in GDF5 leads to this combination of phenotypes. In our functional studies, we included two reported GDF5 mutations, which are associated with isolated forms of SYNS2 ($GDF5^{E491K}$) or BDA1 ($GDF5^{R399C}$), respectively. We demonstrate that an impaired interaction between the extracellular antagonist NOGGIN (NOG) and GDF5 is likely to cause a joint fusion phenotype such as SYNS2. In contrast, GDF5 mutations associated with BDA1 rather exhibit an altered signaling activity through BMPR1A. Consequently, the $GDF5^{W414R}$ mutation negatively affects both interactions in parallel, which causes the combined phenotype of SYNS2 and BDA1.

Alterations in GDF5 signaling due to specific point mutations have been associated with various diseases affecting bone and cartilage development [2,11,12]. Activating mutations in *GDF5* lead to a gain of function phenotype, resulting in increased chondrogenic activity as described for proximal symphalangism (SYM1, MIM #185800) and the multiple synostoses syndrome 2 (SYNS2; MIM #610017) [13–18]. The SYM1 phenotype is characterized by ankylosis of the proximal interphalangeal joints as well as fusion of carpal and tarsal bones. Additional symphalangism in the elbow and knee joint caused by *GDF5* mutations is a hallmark of the SYNS2 phenotype. In contrast to activating *GDF5* mutations, loss of function mutations result in hypoplastic or absent skeletal elements as described for the molecular disease family of brachydactylies. Depending on the affected phalanges, five different types of brachydactylies are categorized (A–E) including three subgroups (A1–A3) [11]. So far, mutations in *GDF5* have been linked to isolated traits of BDA1 (MIM #112500), BDA2 (MIM #112600) and BDC (MIM 113100) [16,18–21]. Extreme shortening of digits and limbs are caused by homozygous loss-of-function mutations in GDF5, which are associated with different types of acromesomelic chondrodysplasia (Grebe MIM #200700, Hunter Thompson MIM #201250, Du Pan MIM#228900) [22].

Here we describe a family carrying a mutation in the mature domain of GDF5, p.W414R, showing combined clinical features of BDA1 and SYNS2. In this work we unravel the unique pathomechanism behind $GDF5^{W414R}$ and thus demonstrate how one mutation in GDF5 confers a gain- and loss-of-function phenotype simultaneously.

Results

$GDF5^{W414R}$ results in SYNS2 and BDA1

We report on a family of Mexican descent with an autosomal dominant form of SYNS2 with additional BDA1 (Figure 1A). Sequencing of the *GDF5* gene revealed a c.T1240C mutation (p.W414R) in three affected individuals from three generations. A mutation in *NOG*, a candidate gene for SYNS1, was excluded. The

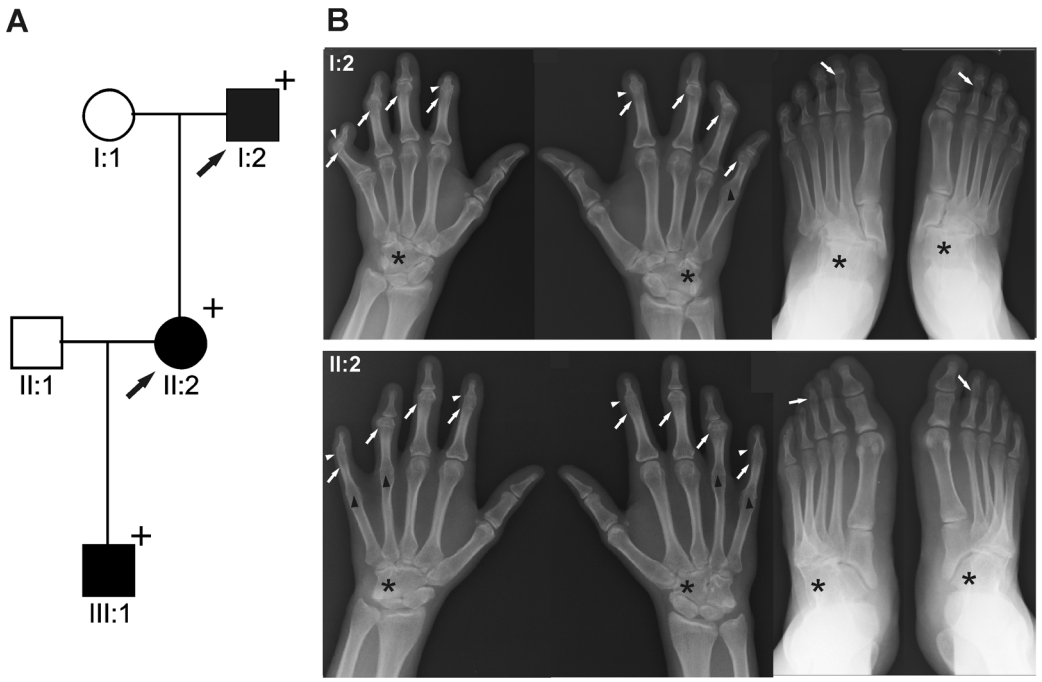

Figure 1. $GDF5^{W414R}$ is associated with SYNS2 and BDA1. A: Pedigree of a family affected by SYNS2 and BDA1. Filled symbols represent affected family members and plus symbols indicate a confirmed mutation. Arrows identify the probands who underwent X-ray analysis. **B** Radiographs of hands and feet of individuals I:2 and II:2 displaying phenotypic abnormalities marked as follows: white arrows - proximal symphalangism of all fingers; arrowheads - distal symphalangism of the 2nd and 5th fingers; black arrowheads -synostoses of the 4th and 5th metacarpals with the corresponding proximal phalanges; asterisks - carpal and tarsal fusions. Overall, the fused or partially fused middle phalanges appear hypoplastic or rudimentary, consistent with BDA1. For a detailed list of phenotypic abnormalities observed in this family see also Table 1.
doi:10.1371/journal.pgen.1003846.g001

affected individuals are presented with multiple synostoses including proximal and distal symphalangism, metacarpophalangeal synostosis, and synostosis of carpal and tarsal bones as well as BDA1 with severe hypoplasia and even aplasia of the middle phalanges (Figure 1B and Table 1). Additional symptoms such as hearing impairment or short stature were not observed.

GDF5^{W414R} is positioned within the NOG and BMPRI binding interface

The three mutations of interest (GDF5^{W414R}, GDF5^{R399C}, GDF5^{E491K}) were highlighted in the GDF5 structure model (Figure 2A). GDF5^{W414R} is positioned within the long loop of finger 1, whereas GDF5^{E491K} is located within the second finger of the GDF5 dimer. GDF5^{R399C} is located at the N-terminal end, right in front of the β1 sheet of the first finger [23]. As shown in Figure 2B, all mutated sites in GDF5 are conserved among different species (human, mouse, chicken). Based on the crystal structures of the BMP7:NOG, BMP2:BMPR1A and GDF5:BMPR1B complexes, we predicted residues of GDF5 that are involved in binding to NOG or to the BMP type I receptors (Figure 2B) [5,24–26]. Both SYNS2 associated variants, GDF5^{W414R} and GDF5^{E491K}, are located within the NOG interaction site. Contrary, GDF5^{R399C}, which is linked to an isolated BDA1 phenotype, is positioned outside of the NOG binding interface. Since all three mutations might also interfere with BMP type I receptor recruitment, we analyzed the interactions of the three mutations (GDF5^{W414R}, GDF5^{R399C}, GDF5^{E491K}) to NOG and to BMPR1A and BMPR1B.

GDF5^{W414R} is insensitive to inhibition by NOG

NOG, the main regulator of GDF5 activity, was initially identified to be mutated in patients with SYNS1 [27]. As GDF5^{W414R} is associated with the SYNS2 phenotype and furthermore located within the critical NOG binding site, we examined the signaling potency of the GDF5 mutations compared to wild type GDF5 in the absence and presence of NOG. We performed *in vitro* chondrogenesis assays and used the respective chicken *GDF5* constructs to infect chicken limb bud micromass cultures with and without *NOG*. Similar expression levels of wild type and mutant GDF5 were confirmed by Western blot (Figure S1, Text S1). As a chondrogenic marker, the extracellular matrix (ECM) produced by the limb bud cells was stained with Alcian blue (Figure 3).

In the absence of NOG, quantification of Alcian blue revealed a strong induction of early chondrogenesis for wild type GDF5 and GDF5^{W414R} as well as for the BDA1 causing variant GDF5^{R399C} and the SYM1/SYNS2-associated variant GDF5^{E491K}. However, co-infection of *NOG* suppressed chondrogenesis effectively in wild type *GDF5* expressing cells, while *GDF5*^{W414R} infected cells displayed a clear insensitivity towards NOG. NOG-resistance was also found for the GDF5^{E491K} variant. In contrast, cartilage formation was strongly inhibited in micromass cells expressing *GDF5*^{R399C}.

The reduced sensitivity of GDF5^{W414R} to NOG was also detected in Biacore measurements. In contrast to the high binding affinity of wild type GDF5 to NOG (apparent KD: ~2 nM), GDF5^{W414R} showed a markedly reduced (~12 fold) binding to NOG (apparent KD: ~25.5 nM) (Table 2).

GDF5^{W414R} shows specific loss of BMPR1A signaling

As GDF5^{W414R} is located in the overlapping interface of the high affinity BMP type I receptors and NOG, we analyzed subsequently signaling activities of wild type GDF5 and GDF5^{W414R} after co-expression of either one of the type I receptors, *Bmpr1a or Bmpr1b*. Signaling activities were determined in NIH/3T3 cells using a Smad Binding Element (SBE) luciferase reporter gene assay (Figure 4A–C).

Overexpression of wild type *GDF5* in combination with either one of the two type I receptors, *Bmpr1a* and *Bmpr1b*, resulted in a strong induction of luciferase activity. As expected from our Biacore data, wild type GDF5-induced signaling via Bmpr1b was stronger compared to signaling mediated via Bmpr1a (Figure 4B–C; Table 2). In case of GDF5^{W414R}, no reporter gene activity was observed when *Bmpr1a* was additionally transfected (Figure 4B). However, co-transfection of *Bmpr1b* led to a clear induction of the SBE reporter, even though to a slightly lesser extent compared to wild type *GDF5* (Figure 4C). For the BDA1 associated variant GDF5^{R399C}, we revealed the same signaling pattern in our luciferase assay as for GDF5^{W414R}, which leads to the assumption that the pathomechanism of BDA1 is presumably connected with an alteration of the GDF5:BMPR1A binding interaction. In contrast, the SYM1/SYNS2 causing GDF5 variant GDF5^{E491K} promotes GDF5 signaling via Bmpr1a and Bmpr1b to a similar extent when compared to wild type GDF5.

Biacore analysis supported the findings from our cell based assays since GDF5^{W414R} showed a clear deviation from the wild type GDF5 receptor binding pattern. We could demonstrate a 7-fold lower affinity of GDF5^{W414R} to BMPR1A (apparent KD: ~124 nM) compared to wild type GDF5 (apparent KD: ~17 nM)

Table 1. Clinical features of the affected family members with mutations in *GDF5*.

Feature	HPO:ID	W414R	E491K [14]	R399C [19]
Proximal symphalangism	HP:0100264	+	+	−
Distal symphalangism	HP:0100263	+	+	−
Metacarpophalangeal Synostosis	HP:0100325	+	−	−
Synostosis of carpal bones	HP:0005048	+	+	−
Synostosis of tarsal bones	HP:0100330	+	+	−
Tarsometatarsal synostosis	HP:0100329	−	+	−
Aplasia/Hypoplasia of the middle phalanges of the hand (Brachydactyly Type A1)	HP:0009843	+	−	+
Hypoplastic/short 1st metacarpal	HP:0010034	−	−	+

The features are coded using terms from the Human Phenotype Ontology [47]. + present; − absent. *GDF5* mutations are presented with either features of brachydactyly (GDF5 p.R399C) or features of synostosis (GDF5 p.E491K) or a combination of multiple synostosis with additional brachydactyly (GDF5 p.W414R).
doi:10.1371/journal.pgen.1003846.t001

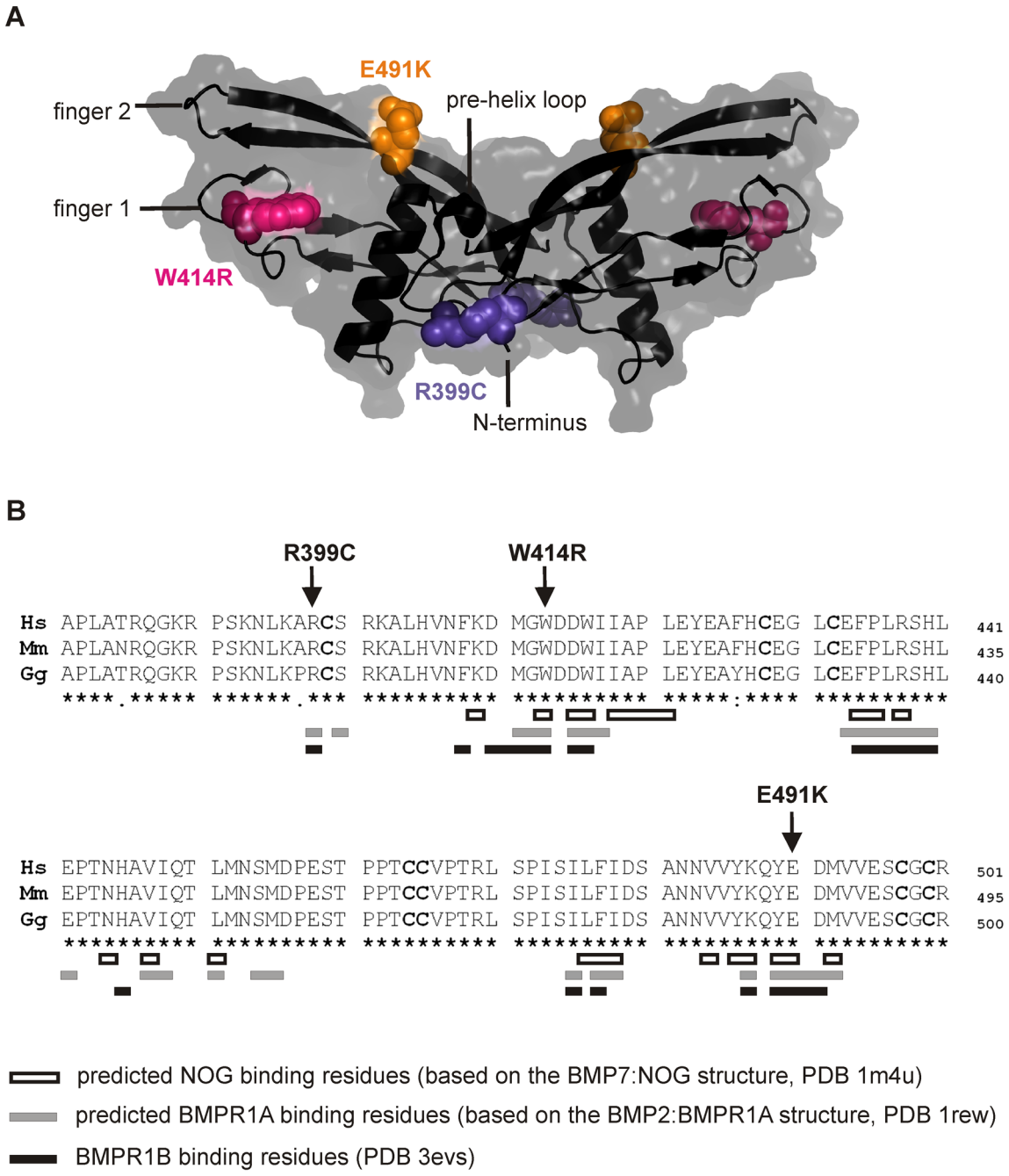

Figure 2. GDF5^{W414R} is positioned within the NOG and BMPR1A/B binding interface of the GDF5 dimer. A: 3D presentation of the human GDF5 homodimer (PDB 1waq). The topology of the GDF5 monomer comprises two ß-sheets forming the fingers as well as the four-turn α-helix with the preceding pre-helix loop. The mutations are highlighted in pink (GDF5^{W414R}), violet (GDF5^{R399C}) and orange (GDF5^{E491K}). The image of the GDF5 structure was visualized using PyMol (http://www.pymol.org/). **B**: Protein sequence alignment of human, mouse and chicken GDF5 comprising the seven cysteine residues (bold) of the mature domain. Numbering is referred to the pro-protein sequence. Amino acids predicted to form the NOG binding interface are depicted as framed white boxes and based on the BMP7:NOG complex (PDB 1m4u). Residues predicted to be involved in BMPR1A binding are shown as grey boxes and refer to the BMP2:BMPR1A structure (PDB 1rew). Black boxes mark amino acids that bind to BMPR1B (PDB 3evs). Arrows indicate the mutated sites for GDF5^{W414R}, GDF5^{R399C} and GDF5^{E491K}. Note that GDF5^{W414R} and GDF5^{E491K} are located within the NOG binding site. Moreover, all three mutations interfere with the BMP type I receptor (BMPR1A and BMPR1B) binding interface.
doi:10.1371/journal.pgen.1003846.g002

and only a 3-fold lower affinity for BMPR1B (apparent KD: ~3,3) compared to wild type GDF5 (apparent KD: ~1,1 nM) (Table 2).

In summary, Biacore analysis and *in vitro* overexpression studies indicate a functional link between the phenotypic features of BDA1 and an impaired BMPR1A signaling of BDA1 associated GDF5 variants.

Activity of GDF5^{W414R} is reduced in the absence of *Bmpr1b*

In order to confirm the previous hypothesis, that GDF5^{W414R} is not able to transduce signaling via BMPR1A, we conducted an *in vitro* chondrogenesis assay using primary mesenchymal cells derived from *Bmpr1b* null mice (Figure 5A–C). Assuming that in

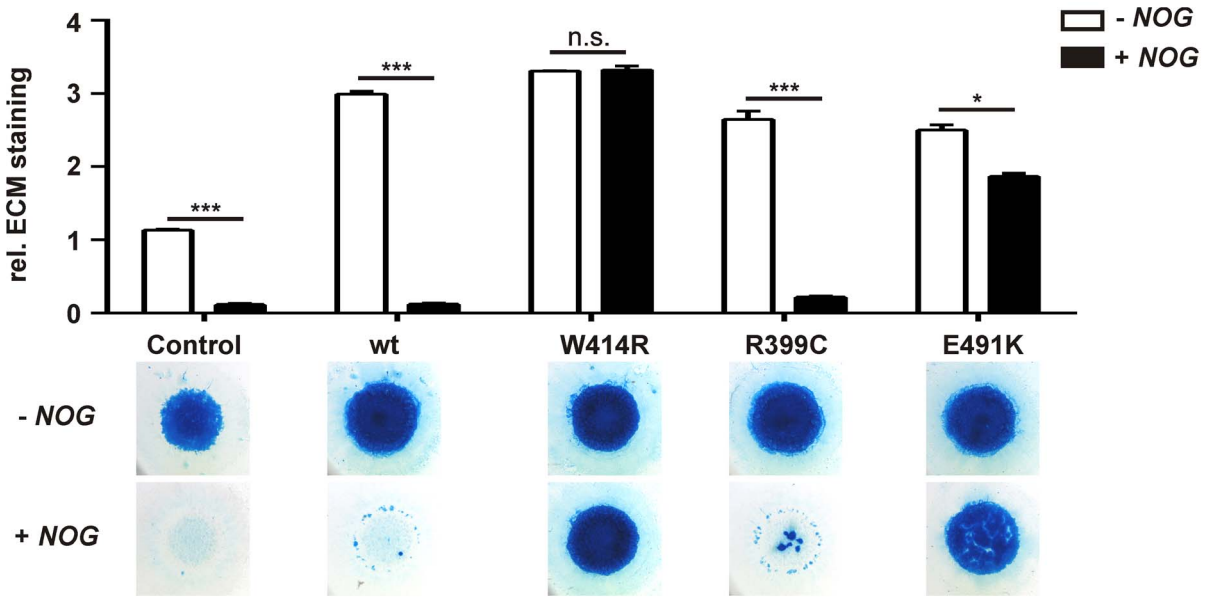

Figure 3. GDF5^{W414R} is resistant towards inhibition by NOG in chicken micromass cultures. Chicken micromass cells were infected with RCASBP(A) containing the coding sequence (cds) of either wild type *GDF5* or the GDF5 variants *GDF5^{W414R}*, *GDF5^{R399C}* or *GDF5^{E491K}*. RCASBP(B) contained the cds of *NOG* and was used for co-transfection. Chicken micromass cultures and quantification of Alcian blue incorporation at 595 nm into the extracellular matrix (ECM) are shown for day 5. In the chicken micromass system, wild type GDF5 strongly induced chondrogenesis compared to the untransfected control. Chondrogenic differentiation was completely blocked in both, the control and wild type GDF5 cultures, when *NOG* is co-transfected. A similar pattern was observed for GDF5^{R399C}. Contrary, GDF5^{W414R} and GDF5^{E491K} exhibited insensitivity towards the antagonist. Values represent the mean of triplicates and error bars indicate standard deviation. Statistical analysis was performed using a two-tailed Student's t test (n.s.: not significant; *p≤0.05; ***p≤0.001).
doi:10.1371/journal.pgen.1003846.g003

wild type cells GDF5 signaling is mediated via Bmpr1a and Bmpr1b, a *Bmpr1b* knock-out would lead to a situation where solely Bmpr1a transmits GDF5-specific signals. Hence, we hypothesized that GDF5^{W414R} would not able to stimulate chondrogenic differentiation in cells lacking *Bmpr1b*, due to its insufficiency in binding to Bmpr1a.

As anticipated, heterozygous and homozygous *Bmpr1b* cells resulted in decreased chondrogenic activity for both, wild type GDF5 as well as GDF5^{W414R}. However, wild type GDF5 stimulation led to an induction of chondrogenesis even in the complete absence of Bmpr1b, whereas GDF5^{W414R} stimulated cells displayed a complete loss of chondrogenic activity, indicating that a loss of binding of GDF5 to BMPR1A represents the centerpiece of the BDA1 pathomechanism.

Table 2. Binding affinities of GDF5^{W414R} to immobilized receptor ectodomains.

KD [nM]	BMPR1A	BMPR1B	NOG
GDF5^{wt}	17,0±4,6 [15]	1,1±0,2 [15]	2,0±0,6
GDF^{W414R}	124,0±30,8	3,3±0,8	25,5±9,0

GDF5^{W414R} shows altered NOG and BMP receptor type I binding affinities in the Biacore assay.
Mean values from two experiments using at least six different analyte concentrations are shown.
doi:10.1371/journal.pgen.1003846.t002

Gdf5 expression co-localizes with *Nog* and *Bmpr1b* during limb development

To reconstruct the progress of GDF5 dependent limb development we analyzed the gene expression of *Gdf5* and its main antagonist *Nog* as well as its BMP type I receptors *Bmpr1a* and *Bmpr1b* in mice limb buds at stages E11.5 to E13.5, which represent critical phases of limb development.

At stage E11.5, *Gdf5* is expressed in the anterior part of the limb bud (Figure 6A/E). Here, expression signals for *Nog* and *Bmpr1b* partly co-localize with *Gdf5* in the distal region (Figure 6B/F and D/H). Additionally, *Bmpr1b* and *Nog* show signals in the area of the later developing shoulder and *Nog* in the elbow joint as well. In contrast, *Bmpr1a* expression concentrates in the surrounding epithelium and underlying mesenchyme but sparing the central mesenchyme (Figure 6C/G). At stage E12.5 the expression pattern becomes more defined for *Gdf5*, *Nog* and *Bmpr1b* in the digital rays (Figure 6A′/E′, 6B′/F′ and 6D′/H′) and for *Bmpr1a* in direct proximity in the inter-phalangeal regions and the surrounding epithelium (Figure 6C′/G′). From stage E13.5 onwards, *Gdf5* expression concentrates in the joint interzones (Figure 6A″/E′), flanked by *Nog* and *Bmpr1b* expression (Figure 6B′/F′ and 6D′/H′). Apart from the distal tips, *Bmpr1a* is still expressed in the surrounding limb epithelium and interdigital mesenchyme.

The expression pattern analysis shows a co-localization for *Gdf5*, *Nog* and *Bmpr1b* and in case of *Bmpr1a*, expression in direct proximity to *Gdf5*.

Discussion

Here we describe a novel GDF5 Trp to Arg transition (p.W414R) in patients with multiple synostoses syndrome 2 (SYNS2), including

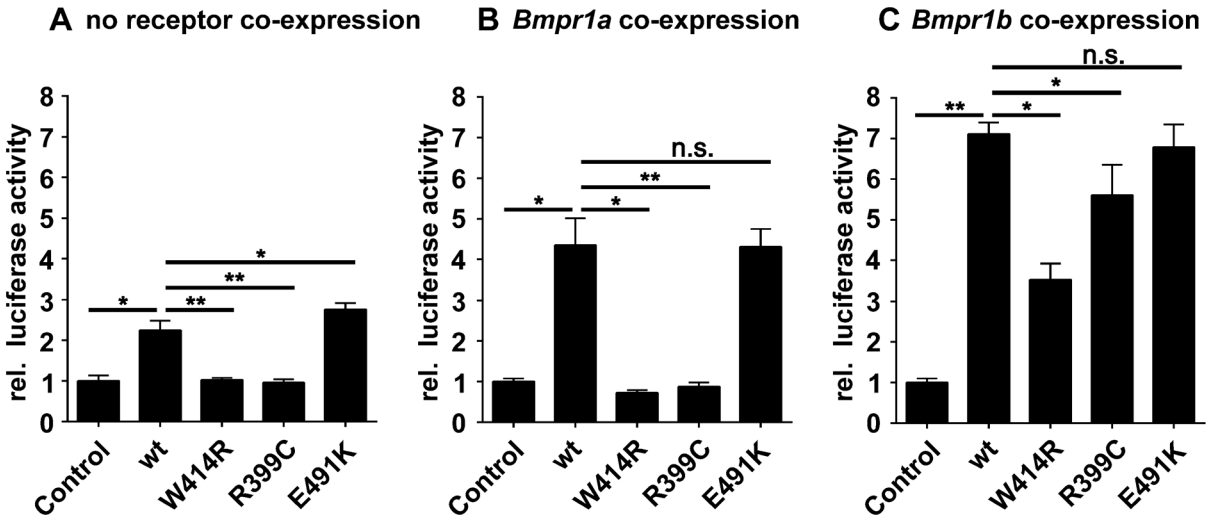

Figure 4. GDF5^{W414R} shows impaired Bmpr1a signaling in a SBE-Luciferase reporter gene assay. NIH/3T3 cells were transfected with the BMP type I receptors, *Bmpr1a* or *Bmpr1b,* as well as with wild type *GDF5* and the GDF5 variants *GDF5^{W414R}*, *GDF5^{R399C}* and *GDF5^{E491K}*. As reporter, the SMAD binding element (SBE) was used and firely luciferase was normalized against TK-Renilla luciferase. **A**: No Bmp type I receptor was co-expressed which resulted in a weak SBE reporter activation for wild type GDF5 and GDF5^{E491K}, whereas in case of GDF5^{W414R} and GDF5^{R399C} signaling activity was absent. **B**: *Bmpr1a* co-expression increased the signaling activity of wild type GDF5 and GDF5^{E491K}; however, GDF5^{W414R} and GDF5^{R399C} were not able to induce reporter gene expression. **C**: Co-expression of *Bmpr1b* further increased the signaling activity of wild type GDF5 and GDF5^{E491K} compared to co-expression with *Bmpr1a*. In case of GDF5^{W414R} and GDF5^{R399C}, *Bmpr1b* co-expression rescued their signaling activity. The means of triplicate measurements are shown, error bars indicate standard deviation and a represent experiment is shown. Statistical analysis was performed using a two-tailed Student's t test (n.s.: not significant; *p≤0.05; **p≤0.01). Significances are related to the respective wild type GDF5 value.
doi:10.1371/journal.pgen.1003846.g004

proximal and distal symphalangism, metacarpophalangeal synostosis, and synostosis of carpal and tarsal bones as well as BDA1 with severe hypoplasia and even aplasia of the middle phalanges. We identified that BDA1 and SYNS2 caused by GDF5^{W414R} are due to two independent molecular mechanisms involving specifically the BMP receptor BMPR1A and the BMP antagonist NOG, respectively.

Interestingly, mutations in *NOG* as well as in *GDF5* can lead to similar phenotypic characteristics of SYM1 and SYNS1/2

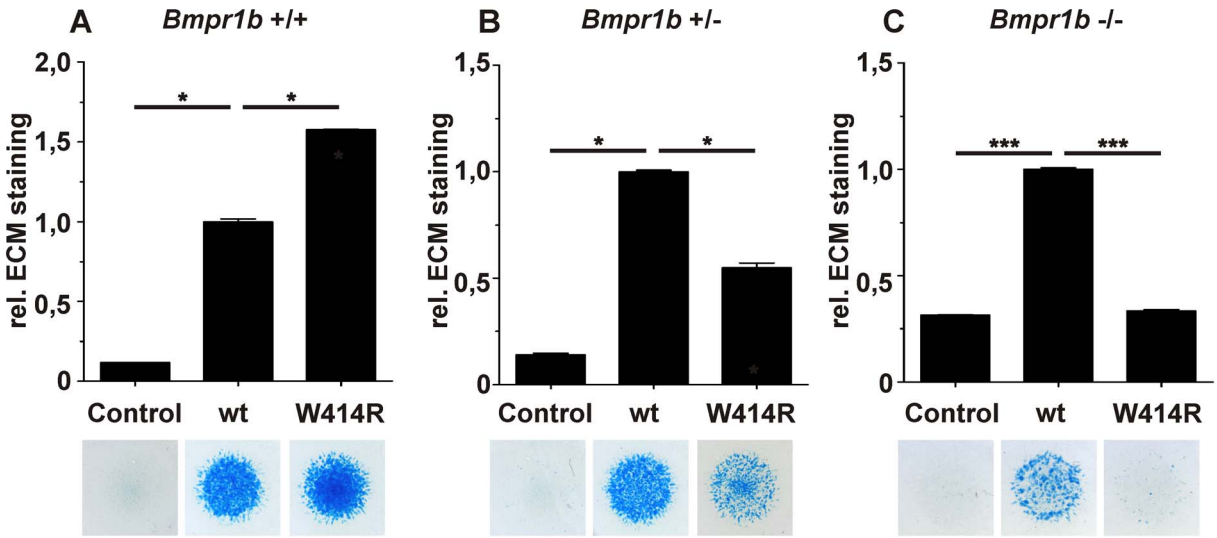

Figure 5. GDF5^{W414R} displays reduced chondrocyte differentiation in the absence of *Bmpr1b*. *Bmpr1b* wild type (*Bmpr1b$^{+/+}$*), heterozygous (*Bmpr1b$^{+/-}$*) and homozygous (*Bmpr1b$^{-/-}$*) mouse mesenchymal limb bud cells (E13.5) were stimulated with 5 nM recombinant human GDF5 protein (wild type GDF5 and GDF5^{W414R}). Alcian blue incorporation into the extracellular matrix (ECM) was measured at 595 nm after five days of cultivation and four days of stimulation. **A**: Alcian blue staining of *Bmpr1b$^{+/+}$* cells exhibited a strong induction of chondrogenesis upon stimulation with both recombinant GDF5 proteins. **B**: Stimulation of *Bmpr1b$^{+/-}$* cells resulted in a reduced chondrogenic activity of GDF5^{W414R} compared to wild type GDF5. **C**: In case of *Bmpr1b* knockout cells, stimulation with GDF5^{W414R} resulted in a complete loss of chondrogenic activity, compared to wild type GDF5. Values represent the mean of three replicates, error bars indicate standard deviation. Statistical analysis was performed using a two-tailed Student's t test (*p≤0.05; ***p≤0.001).
doi:10.1371/journal.pgen.1003846.g005

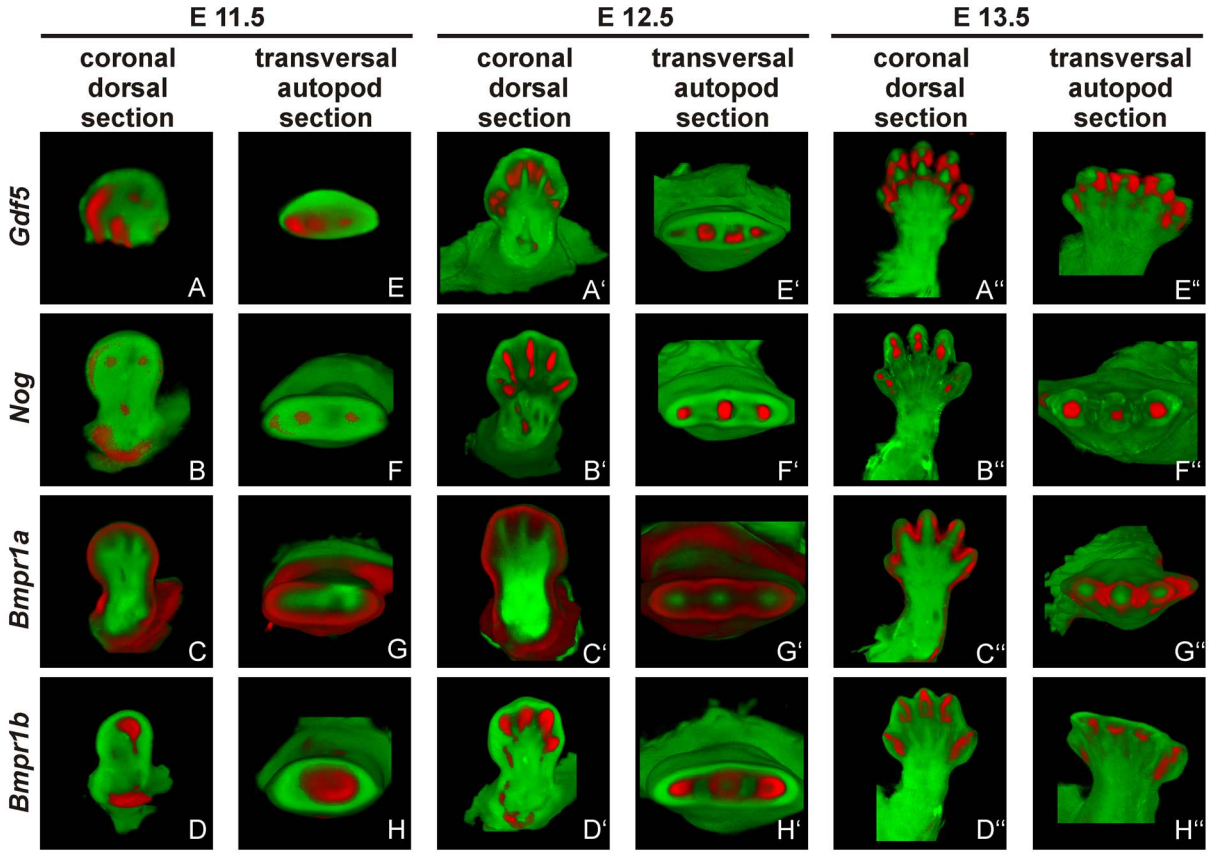

Figure 6. *Gdf5*, *Nog* and *Bmpr1b* are co-expressed during murine limb development. Mouse embryos with the C57BL/6 genetic background at embryonic stages 11.5 (A–H), 12.5 (A′–H′) and 13.5 (A″–H″) were labeled with probes of *Gdf5* (A and E), *Nog* (B and F), *Bmpr1a* (C and G) or *Bmpr1b* (D and H) and signals are shown in red. Representatively, two sections of the coronal dorsal axis (A–D) and the autopod transversal axis (E–H) are depicted. The signal for *Gdf5* strongly co-localizes with the *Nog* and *Bmpr1b* expression pattern, whereas *Bmpr1a* expression is in direct proximity in the surrounding epithelium and underlying mesenchyme.
doi:10.1371/journal.pgen.1003846.g006

[15,17,27]. However, joint fusions caused by NOG mutations often affect the ossicles leading to hearing impairment, whereas mutations in GDF5 including GDF5^{W414R} spare this feature [27–29]. Regarding the literature, SYM1- and SYNS2-associated mutations in *GDF5* like GDF5^{N445T} and GDF5^{S475N} were shown to destabilize the GDF5/NOG interaction thus leading to a severe insensitivity towards the antagonist, also called NOG resistance [15,17]. Therefore, we likewise analyzed GDF5^{W414R} concerning its interaction with NOG. W414 is located within the putative NOG binding interface, which was predicted based on the published superimposed GDF5:NOG complex [15,30]. Interaction analyses of GDF5^{W414R} using chondrogenic differentiation assays together with Biacore binding studies revealed a NOG resistance as molecular cause of the joint fusion phenotype similar to GDF5^{N445T} and GDF5^{S475N} [15,17]. In addition, we identified NOG insensitivity as the effect of the SYM1 associated GDF5^{E491K} mutation [14]. Hence, in case of SYM1 and SYNS2, an impaired GDF5/NOG interaction interferes with the negative feedback loop by which GDF5 is antagonized and thus balanced within the fine-tuned signaling network. Consequently, GDF5 variants associated with joint fusions exert an enhanced chondrogenic activity and can be referred to as gain of function mutations (Figure 7) [11]. The tight connection between GDF5 and NOG and their major importance for the development of joints become further visible as the results of our expression analyses of the developing mouse limb show overlapping temporal and spatial expression patterns of *Gdf5* and *Nog*.

To elucidate the underlying molecular mechanism by which GDF5^{W414R} causes joint fusions in combination with brachydactyly, we further analyzed how the mutation interferes with its cognate transmembrane BMP type I receptors. Situated in the long loop of finger 1 between the ß-sheets ß1/2 and ß3/ß4, W414 is positioned outside of the wrist epitope, which is mainly responsible for binding the BMP type I receptors BMPR1A and BMPR1B [5,6,23]. On the basis of the GDF5:BMPR1B crystal structure and the modeled GDF5:BMPR1A interaction, the contact of both BMP type I receptors with W414 was confirmed [5,23]. As suggested, a transition of hydrophobic Trp to hydrophilic Arg at this highly conserved position results in impaired BMP type I receptor activation as shown in reporter gene assays and Biacore binding studies. Most strikingly, GDF5^{W414R} displayed a complete loss of BMPR1A activation, whereas signaling via BMPR1B was only moderately decreased. Possibly, a mutation interfering with the BMP type 1 receptor binding has in general a more drastic effect for the BMPR1A than for the BMPR1B, because the interaction with BMPR1A is per se lower. The remaining signaling activity of GDF5^{W414R} via BMPR1B seems to be sufficient to preserve its biological functionality as seen in our chondrogenic differentiation assays. A recently published GDF5 mutation (GDF5^{R399C}) is likewise reported to cause BDA1. However, in this French

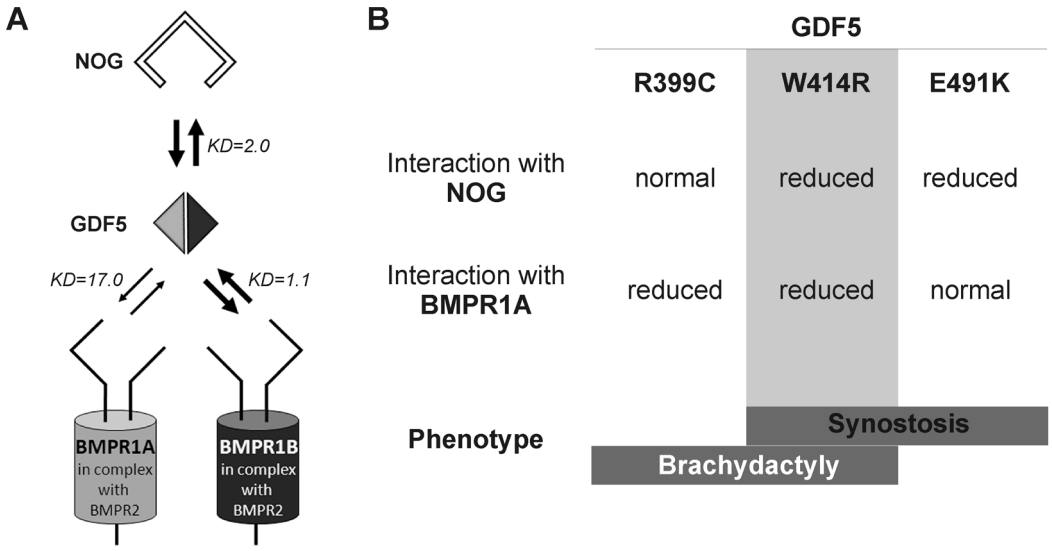

Figure 7. Disease model for SYNS2 and BDA1. A: During normal limb development, dimeric GDF5 (light/dark grey rhomb) is antagonized by NOG (black framed clamp) and thus balanced within the GDF5 signaling network. Downstream signaling is mediated via heteromeric receptor complexes consisting of each of the BMP type I receptors (BMPR1A and BMPR1B) in complex with the BMP type II receptor (BMPR2). Wild type GDF5 binds BMPR1A with a weaker affinity compared to BMPR1B as indicated by thin and thick arrows and additionally by Biacore binding affinities (KD). **B**: Summary of altered interaction of GDF5 mutations resulting in specific phenotypes. SYNS2 is characterized by GDF5 gain of function mutations, leading to an insensitivity of GDF5 towards its extracellular antagonist NOG. In contrast, BDA1 is caused by *GDF5* loss of function mutations, which result specifically in absent BMPR1A signaling.
doi:10.1371/journal.pgen.1003846.g007

Canadian family BDA1 occurs as an isolated trait in contrast to the phenotype of $GDF5^{W414R}$, which is combined with features of synostoses [19]. $GDF5^{R399C}$ is located at the N-terminus of the mature GDF5, right in front of the first β-sheet of finger 1, and is predicted to interfere with both BMP type I receptors [23]. Accordingly, we revealed a BMP type I receptor activation pattern similar to that of $GDF5^{W414R}$ indicating that the disruption of BMPR1A signaling is a hallmark of the BDA1 pathomechanism (Figure 7).

There are two studies which deal explicit with the analyses of specific functions of BMPR1A and BMPR1B, one was done in chicken and the other one was done in mice [31,32]. In the chicken study the expression patterns of both receptors were distinct during limb development. BMPR1B was strongly expressed in precartilaginous condensations, whereas BMPR1A was reported to be expressed throughout the limb mesenchyme. To rule out a functional difference between BMPR1A and BMPR1B, the authors overexpressed either constitutive active (c.a.) or dominant negative (d.n.) variants of BMPR1A and BMPR1B *in vivo* in the chicken limb bud or *in vitro* in chicken micromass cultures [32]. Interestingly, BMPR1B turned out to be necessary for early steps of cartilage formation, whereas BMPR1A was shown to elicit an important function in prehypertrophic chondrocytes. Expression of c.a. BMPR1A led to a delay of chondrogenic differentiation; similar to the phenotype caused by overexpression of IHH [33]. Another study indicated that the IHH-regulated process of chondrogenic differentiation indeed requires BMP signaling [34]. As both signals, IHH and BMP, are required for maintaining a normal proliferation rate and regular differentiation of chondrocytes, these findings could explain how BDA1 can be caused by mutations in IHH or the BMP pathway. A few years later a study was undertaken in mice, where authors concluded that Bmpr1a and Bmpr1b have mostly redundant functions in chondrogenesis [31]. This statement was made due to the observation that single knock outs of either Bmpr1a or Bmpr1b showed only subtle skeletal phenotypes, whereas the double knock out displayed a very strong phenotype with a nearly absent endochondral skeleton. Nevertheless, the phenotypes of each knock out are very distinct, for example Bmpr1b null mice displayed defects in the appendicular skeleton, whereas Bmpr1a cKO shows a generalized chondrodysplasia and the more severe phenotype seen in the double knock out could also be explained by an additive or synergistic effect. Therefore we suggest that both receptors have unique functions and loss of binding of the GDF5 mutants to one of the two receptors cannot be compensated by the other receptor.

Loss of GDF5 receptor binding in general plays a central role within the molecular disease family of brachydactylies. For example, the GDF5 variant $GDF5^{L441P}$ causes BDA2 due to an impaired BMPR1B binding [11,16]. Vice versa, specific mutations in *BMPR1B* are associated with BDA2 [35]. Compared to BDA1, where all middle phalanges are affected and distal symphalangism can occur, BDA2 is characterized by short or absent middle phalanges only of the second and sometimes fifth finger. BDC comprises features of BDA1 and BDA2 and primarily affects the middle phalanges of the second, third and fifth fingers and the first metacarpal bone. Interestingly, the molecular reason for BDC is functional haploinsufficiency of GDF5 [21]. The implication of GDF5 in chondrogenesis and joint formation can finally be highlighted in connection with osteoarthritis (OA; MIM #165720), the most common form of late-onset destruction of articular cartilage in synovial joints nowadays [36]. Among various genetic loci, GDF5 has been discovered as the most consistent and robust risk factor of OA, whereby decreased Gdf5 mRNA levels have been found to account for a murine OA-like phenotype [36–38]. Furthermore Masuya et al. identified a Trp to Arg transition in a large ENU mutagenesis screen, which was described to impair joint formation and thereby cause OA [39]. This mutation (p.W408R) is the mouse homologue to the $GDF5^{W414R}$ mutation we described in this work. Therefore, understanding the biology of

$GDF5^{W414R}$ might also give insights into the pathophysiology of OA.

In summary, we revealed that $GDF5^{W414R}$, in contrast to wild type GDF5, loses the BMPR1A signaling route and at the same time increases the alternative signaling via BMPR1B in the presence of NOG. Therefore, the reduced sensitivity of W414R to Noggin and its reduced interaction with BMPR1A do not actually "neutralize" each other, but lead to a misbalance of BMPR1A and BMPR1B signaling. Hence, our study assembles another part of the molecular puzzle how loss and gain of function mutations in GDF5 affect bone development in hands and feet and result in specific types of brachydactyly and SYNS2.

Materials and Methods

Clinical investigation and molecular analysis

All clinical investigations have been performed according to Declaration of Helsinki principles. The study was approved by the local institutional review board "Ethikkommission der Charité - Universitätsmedizin Berlin". Informed consent for genetic testing was obtained from the patient or their legal guardians respectively. Genomic DNA of affected family members were extracted from peripheral blood samples by standard methods. The coding regions of *NOG* and *GDF5* as well as the flanking intronic sequences were amplified by standard PCR protocols. The primer sequences and PCR conditions for the molecular testing were previously described [20,30]. PCR products were analyzed on 2% agarose gels. Sequencing was done using the ABI Prism BigDye Terminator Sequencing Kit (Applied Biosystems) with PCR primers used as sequencing primers. Products were evaluated on an automated capillary sequencer (Applied Biosystems).

Chicken micromass cultures

Cloning of the coding sequences of chicken *GDF5* and *NOG* into RCAS(BP)A or RCAS(BP)B, respectively was previously described [15]. Mutations ($GDF5^{W414R}$, $GDF5^{R399C}$, $GDF5^{E491K}$) were introduced into the coding sequence of chicken *GDF5* in pSLAX13 by *in vitro* mutagenesis. Primer sequences are available in the supplement (Table S1). Production of viral supernatant in DF1 cells and concentration of viral particles was performed as described previously [40]. Fertilized chicken eggs were obtained from VALO BioMedia GmbH (Osterholz-Scharmbeck, Germany) and incubated at 38°C in a humidified egg incubator for 4.5 days. Micromass cultures were plated in a drop containing 2×10^5 cells. Infection was performed with concentrated viral supernatants: RCASBP(A) containing cDNA encoding chicken wild type *GDF5* and the *GDF5* mutants $GDF5^{W414R}$, $GDF5^{R399C}$, and $GDF5^{E491K}$ with a titer of 1×10^7 plaque forming units (PFU)/ml. RCASBP(B) containing the cDNA encoding chicken wild type *NOG* was applied with a titer of $2{,}5\times10^6$ PFU/ml. Culture medium containing DMEM-F12 (Biochrom), 10% FBS (Biochrom), 0,2% chicken serum (Sigma), 2 mM L-Gln (Lonza), 100 U/ml penicillin, and 100 µg/ml streptomycin (Lonza) was replaced every 2 days. For each condition, three replicates were performed in parallel. Quantification of Alcian blue dye was performed at 595 nm after extraction with Guanidin-HCl.

Recombinant proteins

Recombinant human (rh) GDF5 and its variant $rhGDF5^{W414R}$ were dissolved in 10 mM HCl and provided by Biopharm GmbH.

BIAcore binding assay

The BIA2000 system (Biacore) was used to analyze the binding affinities of recombinant human GDF5 and its variant $GDF5^{W414R}$ to immobilized NOG and ectodomains of BMPR1A, BMPR1B and BMPR2, as previously described [16].

Luciferase activity assay

Coding sequences of human *GDF5* and mouse *Bmpr1a* and *Bmpr1b* were cloned into pSLAX13. Mutations ($GDF5^{W414R}$, $GDF5^{R399C}$, $GDF5^{E491K}$) were introduced into the coding sequence of human *GDF5* in pSLAX13 by *in vitro* mutagenesis. Primer sequences are available in the supplement (Table S1). Inserts were subcloned into pCS2+ via ClaI.

Luciferase reporter gene assays were performed using the murine fibroblast cell line NIH/3T3 (ATCC) which was maintained in DMEM high glucose (Lonza) with 10% FCS (Biochrom), 2 mM L-Gln (Lonza), 100 U/ml penicillin, and 100 µg/ml streptomycin (Lonza). Prior to transfection, cells were seeded in a 96-well plate at a density of 1×10^4 cells per well. BMP receptors and GDF5 constructs were transfected for 40 hours together with the Smad Binding Element luciferase construct SBE-pGL3 [41] and the normalization vector pRLTk (Promega) using Lipofectamine 2000 (Invitrogen). Luciferase activity was determined as described previously [42].

Mouse micromass cultures

Limb mesenchymal cells were isolated from stage E13.5 embryos resulting from matings of C57BL/6, $Bmpr1b^{tm1kml}$ heterozygous or homozygous knock-out mice on a C57BL/6 background [43]. Mouse embryos were genotyped using primers for *Bmpr1b* and *neomycin* (Table S2), if applicable embryos were pooled according to their phenotypes. Isolation of mouse micromass cells was performed as described for chicken micromass cultures with minor modifications. For mouse micromass cultures no additional chicken serum was used. After 24 h mouse micromass cultures were stimulated with 5 nM of recombinant human wild type GDF5 and $GDF5^{W414R}$.

Whole mount *in situ* hybridization

C57BL/6 mouse embryos were harvested at stages E11.5–13.5 and fixed in 4% PFA. Whole mount *in situ* hybridization was performed as previously described [44].

DIG-labeled RNA antisense-probes were generated by *in vitro* transcription using the coding sequences of mouse *Bmpr1a*, *Bmpr1b* and *Nog* as a template. The probe for mouse *Gdf5* was previously published [45]. Signal detection was performed with BMPurple (Roche). 3D imaging of labeled limbs was done by optical projection tomography (OPT) scans as previously described [46].

Statistics

Statistical analyses were performed using a two-tailed Student's T-test. Results are presented as mean ± SEM. P values of less than 0.05 were considered significant.

Supporting Information

Figure S1 Wild type and mutant GDF5 transcripts are expressed at comparable levels in chicken micromass cultures. Chicken micromass cultures were infected with empty RCASBP(A) as control and RCASBP(A) containing the cds of either wild type *GDF5* or the GDF5 variants ($GDF5^{W414R}$, $GDF5^{R399C}$, $GDF5^{E491K}$). After SDS-PAGE under non-reducing (GDF5) and reducing (ACTIN) conditions and subsequent Western Blot, GDF5 and ACTIN were detected at comparable levels using specific antibodies.
(TIF)

Table S1 Primers used for site-directed mutagenesis. *In vitro* mutagenesis of GDF5 mutations ($GDF5^{W414R}$, $GDF5^{R399C}$, $GDF5^{E491K}$) into the coding sequences of chicken *GDF5* and human *GDF5* were carried out by using the following primers.
(DOC)

Table S2 Primers used for mouse genotyping. Genotyping of *Bmpr1b* wild type ($Bmpr1b^{+/+}$), heterozygous ($Bmpr1b^{+/-}$) and homozygous ($Bmpr1b^{-/-}$) mouse embryos for mouse micromass assays was carried out using the following primers.
(DOC)

Text S1 Materials and Methods for anti-GDF5 Western blot.
(DOC)

Acknowledgments

The authors would like to thank Mareen Schmidt-von Kegler for excellent technical assistance. pGl3basic-SBE and chicken *NOG* in RCAS(BP)B were kindly provided by Peter ten Dijke and Andrea Vortkamp, respectively. Furthermore, we thank Daniel Graf for providing the genotyping protocol of $BmprIB^{tm1kml}$ mouse and Lutz Schomburg for critical remarks on the manuscript.

Author Contributions

Conceived and designed the experiments: PS. Performed the experiments: ED JK JZ MW JN JR. Analyzed the data: ED JK JZ MW CR JN FP JR JS KD JTH SM SCD PS. Contributed reagents/materials/analysis tools: CR JN FP JS JTH SM SCD PS. Wrote the paper: ED PS.

References

1. Chang SC, Hoang B, Thomas JT, Vukicevic S, Luyten FP, et al. (1994) Cartilage-derived morphogenetic proteins. New members of the transforming growth factor-beta superfamily predominantly expressed in long bones during human embryonic development. J Biol Chem 269: 28227–28234.
2. Stricker S, Mundlos S (2011) Mechanisms of Digit Formation: Human Malformation Syndromes Tell the Story. Developmental Dynamics 240: 990–1004.
3. Buxton P, Edwards C, Archer CW, Francis-West P (2001) Growth/differentiation factor-5 (GDF-5) and skeletal development. J Bone Joint Surg Am 83-A Suppl 1: S23–30.
4. Storm EE, Huynh TV, Copeland NG, Jenkins NA, Kingsley DM, et al. (1994) Limb alterations in brachypodism mice due to mutations in a new member of the TGF beta-superfamily. Nature 368: 639–643.
5. Kotzsch A, Nickel J, Seher A, Sebald W, Muller TD (2009) Crystal structure analysis reveals a spring-loaded latch as molecular mechanism for GDF-5-type I receptor specificity. EMBO J 28: 937–947.
6. Mueller TD, Nickel J (2012) Promiscuity and specificity in BMP receptor activation. FEBS Lett 586: 1846–1859.
7. Nohe A, Keating E, Knaus P, Petersen NO (2004) Signal transduction of bone morphogenetic protein receptors. Cell Signal 16: 291–299.
8. Schmierer B, Hill CS (2007) TGFbeta-SMAD signal transduction: molecular specificity and functional flexibility. Nat Rev Mol Cell Biol 8: 970–982.
9. Miyazono K, Kamiya Y, Morikawa M (2010) Bone morphogenetic protein receptors and signal transduction. J Biochem 147: 35–51.
10. Bragdon B, Moseychuk O, Saldanha S, King D, Julian J, et al. (2011) Bone morphogenetic proteins: a critical review. Cell Signal 23: 609–620.
11. Mundlos S (2009) The brachydactylies: a molecular disease family. Clin Genet 76: 123–136.
12. Lories RJ, Luyten FP (2005) Bone morphogenetic protein signaling in joint homeostasis and disease. Cytokine Growth Factor Rev 16: 287–298.
13. Dawson K, Seeman P, Sebald E, King L, Edwards M, et al. (2006) GDF5 is a second locus for multiple-synostosis syndrome. Am J Hum Genet 78: 708–712.
14. Wang X, Xiao F, Yang Q, Liang B, Tang Z, et al. (2006) A novel mutation in GDF5 causes autosomal dominant symphalangism in two Chinese families. Am J Med Genet A 140A: 1846–1853.
15. Seemann P, Brehm A, Konig J, Reissner C, Stricker S, et al. (2009) Mutations in GDF5 reveal a key residue mediating BMP inhibition by NOGGIN. PLoS Genet 5: e1000747.
16. Seemann P, Schwappacher R, Kjaer KW, Krakow D, Lehmann K, et al. (2005) Activating and deactivating mutations in the receptor interaction site of GDF5 cause symphalangism or brachydactyly type A2. J Clin Invest 115: 2373–2381.
17. Schwaerzer GK, Hiepen C, Schrewe H, Nickel J, Ploeger F, et al. (2012) New insights into the molecular mechanism of multiple synostoses syndrome (SYNS): mutation within the GDF5 knuckle epitope causes noggin-resistance. J Bone Miner Res 27: 429–442.
18. Ploger F, Seemann P, Schmidt-von Kegler M, Lehmann K, Seidel J, et al. (2008) Brachydactyly type A2 associated with a defect in proGDF5 processing. Hum Mol Genet 17: 1222–1233.
19. Byrnes AM, Racacho L, Nikkel SM, Xiao F, MacDonald H, et al. (2010) Mutations in GDF5 presenting as semidominant brachydactyly A1. Hum Mutat 31: 1155–1162.
20. Schwabe GC, Turkmen S, Leschik G, Palanduz S, Stover B, et al. (2004) Brachydactyly type C caused by a homozygous missense mutation in the prodomain of CDMP1. Am J Med Genet A 124A: 356–363.
21. Everman DB, Bartels CF, Yang Y, Yanamandra N, Goodman FR, et al. (2002) The mutational spectrum of brachydactyly type C. Am J Med Genet 112: 291–296.
22. Thomas JT, Kilpatrick MW, Lin K, Erlacher L, Lembessis P, et al. (1997) Disruption of human limb morphogenesis by a dominant negative mutation in CDMP1. Nat Genet 17: 58–64.
23. Nickel J, Kotzsch A, Sebald W, Mueller TD (2005) A single residue of GDF-5 defines binding specificity to BMP receptor IB. J Mol Biol 349: 933–947.
24. Keller S, Nickel J, Zhang JL, Sebald W, Mueller TD (2004) Molecular recognition of BMP-2 and BMP receptor IA. Nat Struct Mol Biol 11: 481–488.
25. Kirsch T, Sebald W, Dreyer MK (2000) Crystal structure of the BMP-2-BRIA ectodomain complex. Nat Struct Biol 7: 492–496.
26. Groppe J, Greenwald J, Wiater E, Rodriguez-Leon J, Economides AN, et al. (2002) Structural basis of BMP signalling inhibition by the cystine knot protein Noggin. Nature 420: 636–642.
27. Gong Y, Krakow D, Marcelino J, Wilkin D, Chitayat D, et al. (1999) Heterozygous mutations in the gene encoding noggin affect human joint morphogenesis. Nat Genet 21: 302–304.
28. Brown DJ, Kim TB, Petty EM, Downs CA, Martin DM, et al. (2002) Autosomal dominant stapes ankylosis with broad thumbs and toes, hyperopia, and skeletal anomalies is caused by heterozygous nonsense and frameshift mutations in NOG, the gene encoding noggin. Am J Hum Genet 71: 618–624.
29. Mangino M, Flex E, Digilio MC, Giannotti A, Dallapiccola B (2002) Identification of a novel NOG gene mutation (P35S) in an Italian family with symphalangism. Hum Mutat 19: 308.
30. Lehmann K, Seemann P, Silan F, Goecke TO, Irgang S, et al. (2007) A new subtype of brachydactyly type B caused by point mutations in the bone morphogenetic protein antagonist NOGGIN. Am J Hum Genet 81: 388–396.
31. Yoon BS, Ovchinnikov DA, Yoshii I, Mishina Y, Behringer RR, et al. (2005) Bmpr1a and Bmpr1b have overlapping functions and are essential for chondrogenesis in vivo. Proc Natl Acad Sci U S A 102: 5062–5067.
32. Zou H, Wieser R, Massague J, Niswander L (1997) Distinct roles of type I bone morphogenetic protein receptors in the formation and differentiation of cartilage. Genes Dev 11: 2191–2203.
33. Vortkamp A, Lee K, Lanske B, Segre GV, Kronenberg HM, et al. (1996) Regulation of rate of cartilage differentiation by Indian hedgehog and PTH-related protein. Science 273: 613–622.
34. Minina E, Wenzel HM, Kreschel C, Karp S, Gaffield W, et al. (2001) BMP and Ihh/PTHrP signaling interact to coordinate chondrocyte proliferation and differentiation. Development 128: 4523–4534.
35. Lehmann K, Seemann P, Stricker S, Sammar M, Meyer B, et al. (2003) Mutations in bone morphogenetic protein receptor 1B cause brachydactyly type A2. Proc Natl Acad Sci U S A 100: 12277–12282.
36. Reynard LN, Loughlin J (2012) Genetics and epigenetics of osteoarthritis. Maturitas 71: 200–204.
37. Liu J, Cai W, Zhang H, He C, Deng L (2013) Rs143383 in the Growth Differentiation Factor 5 (GDF5) Gene Significantly Associated with Osteoarthritis (OA)-A Comprehensive Meta-analysis. Int J Med Sci 10: 312–319.
38. Daans M, Luyten FP, Lories RJ (2011) GDF5 deficiency in mice is associated with instability-driven joint damage, gait and subchondral bone changes. Ann Rheum Dis 70: 208–213.
39. Masuya H, Nishida K, Furuichi T, Toki H, Nishimura G, et al. (2007) A novel dominant-negative mutation in Gdf5 generated by ENU mutagenesis impairs joint formation and causes osteoarthritis in mice. Hum Mol Genet 16: 2366–2375.
40. Morgan BA, Fekete DM (1996) Manipulating gene expression with replication-competent retroviruses. Methods Cell Biol 51: 185–218.
41. Jonk LJ, Itoh S, Heldin CH, ten Dijke P, Kruijer W (1998) Identification and functional characterization of a Smad binding element (SBE) in the JunB promoter that acts as a transforming growth factor-beta, activin, and bone morphogenetic protein-inducible enhancer. J Biol Chem 273: 21145–21152.
42. Hampf M, Gossen M (2006) A protocol for combined Photinus and Renilla luciferase quantification compatible with protein assays. Anal Biochem 356: 94–99.
43. Yi SE, Daluiski A, Pederson R, Rosen V, Lyons KM (2000) The type I BMP receptor BMPRIB is required for chondrogenesis in the mouse limb. Development 127: 621–630.
44. Pryce BA, Brent AE, Murchison ND, Tabin CJ, Schweitzer R (2007) Generation of transgenic tendon reporters, ScxGFP and ScxAP, using regulatory elements of the scleraxis gene. Dev Dyn 236: 1677–1682.
45. Sharpe J, Ahlgren U, Perry P, Hill B, Ross A, et al. (2002) Optical projection tomography as a tool for 3D microscopy and gene expression studies. Science 296: 541–545.
46. Quintana L, Sharpe J (2011) Preparation of mouse embryos for optical projection tomography imaging. Cold Spring Harb Protoc 2011: 664–669.
47. Robinson PN, Kohler S, Bauer S, Seelow D, Horn D, et al. (2008) The Human Phenotype Ontology: a tool for annotating and analyzing human hereditary disease. Am J Hum Genet 83: 610–615.

3.3 Second paper: “Digit patterning is controlled by a Bmp-Sox9-Wnt Turing network modulated by morphogen gradients”

This paper provides molecular evidence that a Turing network involving Bmp, Sox9 and Wnt genes controls digit specification in the mouse limb. To pinpoint the candidate genes for the Turing network I used several different experimental techniques: live imaging of Sox9-EGFP micrass cultures, gene expression microarray analysis of differential gene expression between Sox9-positive and Sox9-negative cells, time-course of gene expression patterns and immunohistochemistry of signaling pathway activities. Together with mathematical modeling, these experiments contribute to the elaboration of a Turing network consisting of Bmps Sox9 and Wnts for the specification of the digits. I also show that the effect of perturbations predicted by the model agrees with the perturbations performed in limb cultures treated with BMP and WNT signaling inhibitory drugs.

Raspopovic J, Marcon L, Russo L, Sharpe J. “Digit patterning is controlled by a Bmp-Sox9-Wnt Turing network modulated by morphogen gradients” Science, 2014 (In Press).

Raspopovic J, Marcon L, Russo L, Sharpe J. Digit patterning is controlled by a Bmp-Sox9-Wnt Turing network modulated by morphogen gradients. Science. 2014 Aug 1;345(6196):566-70. doi: 10.1126/science.1252960

Raspopovic J, Marcon L, Russo L, Sharpe J. Digit patterning is controlled by a Bmp-Sox9-Wnt Turing network modulated by morphogen gradients. Supplementary materials
Science. 2014 Aug 1;345(6196):566-70. doi: 10.1126/science.1252960

4. DISCUSSION

Digit patterning in the vertebrate limb has been interpreted in the light of two alternative models: the Positional Information and the reaction-diffusion Turing model. The Positional Information model has been vastly supported by classical ZPA grafting experiments and perturbations of the SHH signaling pathway. However, limb re-aggregation experiments and the *Shh/Gli3* double mutant, showed that digit specification is independent of *Shh* and may be instead controlled by a reaction-diffusion Turing model. Recent work has shown that Hoxd genes modulate the wavelength of the Turing mechanism that specifies the digits; nevertheless the diffusible molecules that implement the Turing network have not yet been identified.

This thesis provides experimental evidence that a Turing network implemented by Bmps, Sox9 and Wnts (the BSW model) controls digit specification. From a broader point of view, this study provides an example of a systems biology approach to identify and evaluate Turing networks that may underlie spatial patterning during development.

In the first part of this discussion I will examine the four aspects of our strategy, that combines experiments and modeling, which have been crucial to identify the Turing network. In the second section, I will discuss in more detail the role of the BMP and WNT signaling in our model. In the third section, I will reconcile the role of SHH with the BSW model and re-interpret previous models for digit specification based on the Shh positional information gradient. Finally I will discuss the future directions of this study and propose an integrative view on digit specification that coordinates patterning by a Turing mecanism, signaling gradients and growth.

4.1 The strategy to identify Turing molecules

4.1.1) Analysis of the early patterning process

Narrowing my analysis to the earliest time that showed a periodic digit pattern, which I identified as E11.5, I ensured that the experiments focused only on the first molecular patterning process and ignored later differentiation events. In contrast, previous studies have analyzed the skeletal pattern at late stages, with markers like Col2a1 or skeletal preparations, when the pattern has already been formed and cartilage has started to differentiate (from E12.5 onwards). This is useful to study the overall development of the skeleton but it can be potentially misleading to describe the early digit patterning process, since the pattern may have been modified by subsequent events. For example, a digit can be patterned correctly at early stages but can be missing at later stages due to lack of progenitor cells or impaired differentiation. Even genes that are expressed slightly later than the first markers are not an ideal choice to study the dynamics of early digit patterning. A previous study (Zhu et al., 2008) for example, analyzed the expression of *Noggin* to conclude that the digits were specified in the following order: digit 4 first, then digit 2, then digit 5 and finally digit3 and digit 1. This observation contrasts with the detailed 3D *Sox9* expression time course presented in section 3.1.1, which reveals that the digits are specified in the following order: first digit 4, than digit 3 and 2 simultaneously , than digit 5 and finally digit 1. Since it is known that *Noggin* is expressed later than *Sox9* (Zehentner et al., 2002, Akiyama et al., 2002), it is probable that *Noggin* is not depicting the earliest skeletal pattern and shows an order of digit formation that is not directly connected to the order of specification. Curiously, the authors of the same study (Zhu et al., 2008) compared the expression of *Noggin* and *Sox9* and did not observe any difference in the order of digit specification. This suggests that the analysis of *in-situ* hybridization by OPT can depict differences that are not easily detectable with classic 2D imaging techniques.

4.1.2) Combination of high throughput and theoretical analysis

A second important aspect to identify the candidate Turing molecules was to combine modeling predictions with a high throughput analysis. Previous theoretical studies have shown that two different classes of models can implement a Turing mechanism: the Activator-Inhibitor model

and the Substrate-Depleted model. These two simple topologies are implemented by two diffusible molecules that can form either overlapping periodic patterns (in phase), or opposite periodic patterns (out of phase). To find candidate Turing molecules, I therefore screened for genes or proteins that were expressed or active in a pattern that was overlapping or contrary to the pattern of Sox9. The screening was performed with a high throughput comparative analysis and was refined by analyzing gene expression patterns and pathway activities. Importantly, I focused the comparative analysis at E11.5, the stage that I previously identified as the earliest moment that showed a periodic digit pattern. This increased my confidence that the candidate molecules were involved in the establishment of the *Sox9* periodic pattern.

My initial aim was to group the results of the microarray data by signaling pathways. The number of differentially expressed genes in each group reflected the importance of each pathway in the patterning process. Successively, I analyzed the expression patterns of the best gene candidates with time course *in situ* hybridizations centered on stage E11.5. The gene expression patterns were used as a second level of verification to narrow down the results of the microarray. Indeed, the differential expression in the microarray was a necessary but not sufficient condition for an expression pattern completely in-phase or out-of-phase with *Sox9*. Some false positive are inevitable since genes that appear differentially expressed in Sox9 positive or Sox9 negative cells can be expressed only in sub-populations. For example, a gene that is differentially expressed in Sox9 negative cells can be expressed only under the apical ectodermal ridge. The overall analysis revealed that the BMP and WNT pathway had the highest number of genes expressed in phase or out-of-phase with *Sox9*.

An obvious question that was necessary to answer before further investigation of the Turing network was if *Sox9* itself was part of the feedbacks of the Turing mechanism, or it was a downstream readout. The experimental evidence from previous studies favored the former hypothesis. Firstly, when *Sox9* was conditionally inactivated in the limb all the genes that reflected a digital or inter-digital pattern lost their normal periodic expression (Akiyama et al., 2002). If *Sox9* was only downstream of the Turing mechanism, it would be possible to see genes that reflect the periodic expression even in the absence of *Sox9*, which is not the case. Secondly, extra digits were formed when *Sox9* was misexpressed in chick or mouse (Akiyama et al., 2002, Healy et al., 1999). Again if *Sox9* would be only a downstream gene, by definition it would only reflect the final pattern and should not be able to alter it. To further confirm that Sox9 was part of the Turing network, I performed micromass cultures experiments with Sox9-positive and Sox9-negative FACS-sorted cells from E11.5 Sox9-EGFP limb autopods. I could observe that

the micromass cultures formed a periodic Sox9 pattern even when initiated with Sox9-positive or with Sox9-negative cells. This meant that cells of E11.5 autopods (where the periodic Sox9 pattern was already visible) were still able to dynamically up-regulate or down-regulate Sox9 to create a periodic chondrogenic pattern. This degreed of plasticity and self-regulation is consistent with the idea that Sox9 is part of Turing network and it is more difficult to reconcile with the idea that Sox9 is a downstream marker. In summary, the detailed analysis of the Sox9 expression patterns together with the high throughput analysis, the gene expression time-courses and analysis of the distribution of the active pathways supported the hypothesis that the Turing network which controlled digit patterning was implemented by Sox9, Bmps, and Wnts.

4.1.3) A realistic computational model of digit patterning

A third aspect that was crucial to characterize the Turing network was to develop a computational model of digit patterning. In contrast to previous theoretical studies that developed Turing models with only two diffusible molecules, we developed a 3-node model with two diffusible nodes implemented by Bmp and Wnt signaling and one non-diffusible node implemented by Sox9. The choice of building a 3-node model was motivated by the observation that a more detailed model would be easier to relate to the experimental data. A systematic theoretical analysis of all possible interactions between Bmp, Sox9 and Wnt, revealed that 19 different 3-node topologies were able to form a Turing pattern and were consistent with the known interactions between Sox9 and Bmp on one side and Sox9 and Wnt signaling on the other. The theoretical analysis also showed that each of the 3-node topologies formed different in-phase and out-of-phase patterns that reflected the patterns formed by the two simplest Gierer-Meinhardt models: the Activator-Inhibitor model or the Substrate-Depleted model. This suggested that although the two classical Gierer-Meinhardt models are interpreted as a set of chemical reactions (e.g. depletion of a substrate), the same Turing mechanisms could be extended in a number of different ways depending on the positive and negative interactions between the nodes of the network. Only five of the 19 topologies identified by the analysis produced a Sox9 pattern that was out of phase of Bmp and Wnt patterns as observed in the experimental data. Among these topologies, two had a very small Turing parameter space and therefore were not consistent with the high robustness shown by the real digit patterning process. The BSW model was chosen among the three remaining topologies as the simplest network that did not required any cross-regulation between Bmp and Wnt signaling.

The BSW topology can be related to a Substrate-Depleted model by observing that the Wnt and the Sox9 node act together as the "activator", while the Bmp node act as the "substrate", see Figure 38. Indeed, the mutual inhibition between Wnt and Sox9 implements the necessary auto-activation associated with the activator node, while the positive interaction from Bmp to Sox9 and the negative interaction from Sox9 to Bmp underlies the promotion of the activator and the consumption of the substrate respectively.

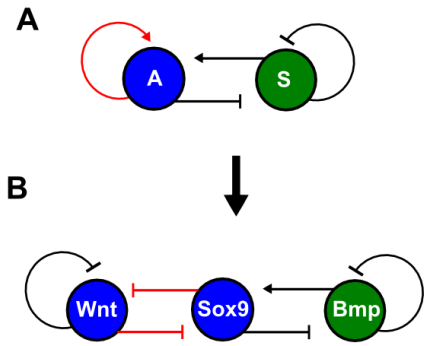

Figure 38. The BSW model relates to a Substrate-Depleted topology.
A) The Substrate-Depleted topology is implemented by a diffusible activator (A) that activates itself and consumes its diffusible substrate (S). B) The mutual inhibition between Wnt and Sox9 (red lines) is equivalent to the autoactivation of the activator (red arrow in A), therefore Wnt and Sox9 togheter play the role of the activator. Bmp plays the role of the substrate, since it shares with Sox9 the same interactions shown between the substrate and the activator in the simple Substrate-Depleted model.

If Wnt diffuses less than Bmp, these interactions create out-of-phase patterns similar to the one created by the Substrate-Depleted model where the negative feedback from Sox9 to Bmp can explain why the Bmp and the Sox9 pattern are out of phase despite the positive effect of BMP signaling on Sox9. A realistic two-dimensional simulation of digit patterning, further demonstrated that the BSW model can reproduce the experimental digit pattern of Sox9 and the opposite Bmp expression and Wnt signaling activity patterns. This simulation strengthened the hypothesis that the BSW model controlled digit patterning and represented an ideal starting point to predict the effect of perturbations.

Nevertheless, the other two networks identified by our theoretical analysis could also explain the formation of opposite patterns of Sox9 and Bmp/Wnt, (Figure 39).

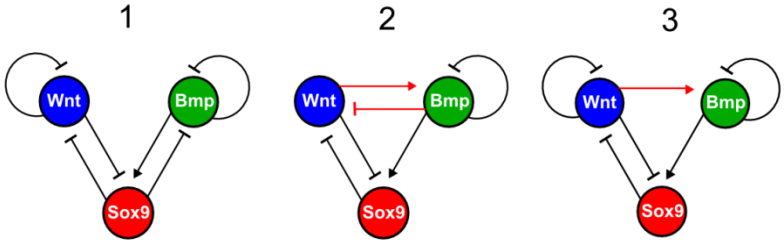

Figure 39. The three alternative topologies for the BSW model.

1)The topology chosen for the BSW model as the simplest network that does not required any cross-regulation between Bmp and Wnt signaling. 2-3) The two other topologies with cross-regulations between Bmp and Wnt signaling (red lines) that can form opposite patterns of Sox9 and Bmp/Wnt.

In these cases however, the out-of-phase patterns are formed by other mechanisms that depend on the cross regulatory interactions between Wnt and Bmp rather than on a negative feedback from Sox9 to Bmp. Since previous studies have highlighted a cross-talk between the Bmp and the Wnt pathway during limb development (Guo and Wang, 2008, Knobloch et al., 2007, Church and Francis-West, 2002), these two networks represent alternative plausible Turing models that may control the digit patterning process. However, designing experimental perturbations that will allow distinguishing which of the networks fits better the experimental data is not straightforward. This is due to the fact that the BSW model and the other two networks share similar feedbacks. Indeed, preliminary theoretical analysis suggests that simple down-regulations or up-regulations of Bmp or Wnt signaling will have similar effects in all the three models. For example, in all three cases an up-regulation of BMP signaling would results in Sox9 up-regulation and Wnt signaling down-regulation. The first effect is mediated by a direct positive interaction from Bmp to Sox9 in all three models. The second effect however is mediated by different interactions depending on the model: in the BSW and in the third model it is mediated by the Sox9 node, while in the second model it is mediated by a direct negative interaction from Bmp to Wnt. Nevertheless, the effects on the final patterns would be indistinguishable. A possible way to distinguish between these three models would be to accompany Sox9 inactivation/reduction with the Wnt or Bmp signaling perturbation. By analyzing Bmp expression or Wnt signaling levels, it will be possible to distinguish if the feedbacks between Wnt and Bmp are mediated by Sox9 or by direct interactions.

4.1.4) Analysis of the patterning dynamics upon perturbations

A fourth and last important aspect of the strategy presented in this study was the experimental set-up used to validate the Turing network. Because Turing networks are implemented by a set of incoherent feedbacks, it is usually difficult to predict the effect of perturbations without the use of modeling. Therefore, the best way to evaluate a Turing model is usually to compare the patterning dynamics predicted by simulations with the patterning dynamics observed upon experimental perturbations. However, performing and monitoring experimental perturbations during mouse development is challenging. This is due to two main problems: firstly because the mammalian embryo is difficult to access and has a low viability in culture, secondly because mouse development shows a high degree of redundancy/robustness which often results in no phenotypic changes when single genes are perturbed. An example of redundancy during limb development is showed by the fact that single Bmp knock-outs have almost no effect, while double knock-outs lead to loss of digits. To address these problems, I chose to perform experiments in Sox9-EGFP limb cultures and to apply perturbations using pharmacological inhibitors and bead experiments. By culturing E11.5 Sox9-EFGP limbs, I could observed that in the first 48h, although the growth of the limb was slightly reduced, the formation of the Sox9 periodic patterns reflected the digit patterning process observed in wild type limbs until E12.5. Thus, I used this in-vitro culture system to study the effect of different perturbations on digit patterning.

The BSW model predicted that the promotion of Sox9 by Bmp and the inhibition of Sox9 by Wnt were integrative parts of the Turing network and were required for digit patterning. Indeed, the inhibition of Bmp or Wnt signaling in the model predicted a loss of digits with low levels of and high levels of Sox9 respectively. Importantly, in the second case, the model predicted that the homogenous high expression of Sox9 was obtained by a progressive expansion of each digit that eventually fused into one domain of Sox9 expression. To perform similar perturbations in limb cultures, rather than applying ectopic extracellular protein inhibitors or using a genetic approach, I decided to use inhibitory drugs that prevented signaling. This choice had three main advantages: firstly, I could challenge the redundancy/robustness of the patterning system by targeting the activity of all the BMPs and all the WNTs, secondly I could apply the perturbations by simply adding the drugs into the limb culture medium and thirdly I could easily apply the WNT and BMP signaling inhibitors simultaneously. The close correspondence between the Sox9 patterns predicted by the model and the Sox9-EGFP patterns observed in the experimental perturbations strongly supported the idea that the BSW model controlled digit

patterning. In particular, the progressive expansion of each digit in the case of WNT signaling inhibition confirmed the idea that the inter-digital regions were established by high WNT signaling activity that inhibited Sox9. Moreover, the simultaneous inhibition of both WNT and BMP signaling promoted a Sox9 pattern re-arrangement that resulted in olygodactily with larger digits. These patterning dynamics are naturally predicted by a change in Turing wavelength and are more difficult to reconcile with a Positional Information model.

Although the pharmacological inhibitors clearly confirmed the involvement of BMP and WNT signaling in the BSW network, the identity of the main Bmp and Wnt ligands remains to be elucidated. In the case of BMPs, the striking out-of-phase patterns between *Bmp2* and *Sox9* suggests that *Bmp2* may play the most important role. This was also confirmed by the implantation of BMP2-soaked beads in limb culture, that in agreement with model predictions up-regulated Sox9 and down-regulated *Bmp2* expression. However, previous studies have also shown that Bmp4 and Bmp7 have a positive influence on Sox9 (Hoffman et al., 2006, Shea et al., 2003). Moreover, it has been shown that Bmp heterodimers can also signal through the canonical BMP pathway (Nishimatsu and Thomsen, 1998, Schmid et al., 2000). It is therefore possible that all three Bmps are playing an important role and a more detailed molecular model will be required to explore this hypothesis. This is further discussed in section 4.4.2. In the case of WNTs, my preliminary analysis showed that only the ectopic application of WNT3a in micromass and limb cultures was able to inhibit Sox9. This is consistent with previous studies (ten Berge et al., 2008) that have shown that WNT3 signaling from the ectoderm represses the expression of Sox9 in the mesenchyme of the limb. The role of Bmps and Wnts is further discussed in details in the next two sections.

4.2 The role of BMP and WNT signaling in the BSW model

4.2.1) The role of Bmps

In this study I provided experimental evidence for a new role for the BMP signaling pathway as a component of the Turing network that specifies the digits. This new role extends the other BMP signaling roles described in previous studies. In particular, it has been described that BMP signaling controls inter-digital apoptosis (Ganan et al., 1996, Zou et al., 1997, Bandyopadhyay et al., 2006), it is important for the SHH-GREM-FGF feedback loop that controls outgrowth (Bénazet et al., 2009) and that it induces chondrogenesis and regulates skeletogenesis, for

review see (Yoon and Lyons, 2004, Bandyopadhyay et al., 2006). The question that naturally arises is how one signaling pathway can achieve so many different functions. The answer to this question seems to lay in the complex details of the BMP pathway: the spatio-temporal regulation of the expression of Bmp genes, the sharing of the same receptors by many different BMP ligands (as well as other structurally related morphogens such as TGFbetas, and Activins/Inhibins) (Mueller and Nickel, 2012) and to some extent the BMP functional redundancy (Bandyopadhyay et al., 2006, Karsenty, 2003). The proposal that Bmps act as a node in the BSW network is nevertheless in agreement with the experimental evidences presented in previous studies. It has been shown that Bmps are necessary for the initiation of chondrogenesis (Capdevila et al., 1999, Pizette and Niswander, 2000) and that they directly activate Sox9 (Pan et al., 2008, Zehentner et al., 1999). This strongly supports the involvement of BMP signaling in the early digit patterning process. In addition, it has been shown that disruption of BMP signaling through conditional inactivation of the *BmprIA* receptor or *Smad4*, results in lack of *Sox9* in the autopod and in complete absence of the digits (Ovchinnikov et al., 2006, Bénazet et al., 2012). Furthermore, conditional *Bmp2/Bmp4* double mutants lack the two most posterior digits due to loss *Sox9* expression (Bandyopadhyay et al., 2006).

In this study I also showed that among the three Bmps expressed in the limb, *Bmp2* is the only one that shows an out-of-phase expression pattern with *Sox9* at all stages of digit patterning. As I mentioned in the previous section, this strongly suggests that Bmp2 plays an important role in the BSW network, however the fact that conditional *Bmp2* mutants do not show any digital phenotype (Bandyopadhyay et al., 2006) suggests that other Bmps may act redundantly (Bandyopadhyay et al., 2006, Karsenty, 2003). Moreover, it is possible that the digit patterning robustness observed in *Bmp2* mutants could be explained by an extended BSW Turing that includes other ligands that are structurally similar to BMPs, such as Activins and Tgf-βs since they modulate the BMP/SMAD-signaling as well (Montero et al., 2008).

The involvement of BMPs in the control of interdigital apoptosis is occurring at later stages (around E12.5-E13.5) after the digits have been specified (Pajni-Underwood et al., 2007) and therefore it is not temporally interfering with the role of Bmps in the BSW network. However, BMP signaling has also been proposed to participate in the SHH-GREM-FGF loop that controls growth from E10.5 to E12.0, and in particular, it has been described that a maintenance of a constant low BMP activity during early development is necessary for limb bud outgrowth. It was recently proposed that while SHH specifies the digits during limb outgrowth, a final raise in BMP activity is necessary to permit commitment of digit progenitors to chondrogenesis (Lopez-

Rios et al., 2012, Bénazet et al., 2009). This was proposed to be achieved by two different mechanisms, one acting in the posterior region of the limb and one in the anterior (Lopez-Rios et al., 2012). First, the termination of the SHH-GREM1-FGF loop around E12.0 inhibits *Grem1* expression in the posterior part of the limb, which leads to the rise of BMP activity posteriorly resulting in the commitment to chondrogenesis of the posterior digits (Lopez-Rios et al., 2012, Bénazet et al., 2009). On the other hand it was also shown that Gli3 is necessary to reduce *Grem1* expression in the anterior part of the limb, so that the final raise of BMP can induce digits anteriorly (Lopez-Rios et al., 2012). How does the BMP role in the SHH-GREM1-FGF feedback loop fit with our BSW network?

As I have described in section 1.2.5, experimental evidence shows that SHH is dispensable for digit specification, while its main role seems to be the control of the AP-expansion and digit identities (Litingtung et al., 2002). The work presented in this thesis has shown evidence that digit specification is under the control of the BSW network where the main role of BMP signaling is to promote Sox9. However, previous studies on the SHH-GREM1-FGF loop have suggested that GREM1, a main antagonist of BMP, is high during early limb development and allows BMP activity to rise only while the SHH-GREM1-FGF is in its termination phase and GREM1 is reduced (around E12.0). This contrasts with the idea that BMPs participate in the BSW that specify the digits before E12. There are several possibilities that could explain how the role of BMPs in the BSW network can be reconciled with the SHH-GREM1-FGF feedback loop. A first plausible explanation is that the low BMP activity necessary for the maintenance of the FGF expression in the AER (Bénazet et al., 2009) is sufficient to fulfill the role of BMPs in the BSW network. Indeed, it was suggested that only a minimal threshold of BMP signaling is necessary for the induction of chondrogenesis (Bandyopadhyay et al., 2006). Another possibility is that different BMPs are involved in different functions during limb development. It has been shown that BMP4 is the ligand that influences the most the SHH-GREM1-FGF feedback loop (Bénazet et al., 2009), therefore other BMPs (E.g. BMP2) could instead participate in the BSW network. Another possibility is that the low BMP4 activity is required only in the most distal part of the mesenchyme to maintain the AER, while higher BMP activity in the core mesenchyme could participate in the BSW network to induce *Sox9* expression. This hypothesis fits with the distal expression of *Bmp4* during digit specification and with the expression of *Grem1*, which is located in the ventral and dorsal mesenchyme but not in the core mesenchyme (see Figure 30 and 33). Finally, it is also possible that the rise of BMP activity from the posterior part to the anterior part of the limb (Lopez-Rios et al., 2012) is in reality starting earlier than expected, that is as soon as digit 4 is visible in the posterior region of the limb

around E11. This is in agreement with the BSW model that shows a posterior to anterior formation of the digits which depends on BMP signaling. This also suggests that the SHH-GREM1-FGF feedback loop could coordinate patterning and growth. This is discussed in more detail in section 4.4.1.

An aspect of BMP signaling that needs to be explored in future studies is the role of the non-canonical MAPK/p38 pathway for the induction of *Sox9*. Previously it has been shown that p38 MAPK act as positive regulator of chondrogenesis (Oh et al., 2000, Yoon et al., 2000) and is necessary for *Sox9* transcription (Pan et al., 2008). It would be interesting to analyze the spatial distribution of phosphorilated p38 as it was done for pSMAD1/5/8. This will show if the two pathways share the same distribution or underlie different regulations of BMP signaling. In addition, specific inhibition of the MAPK/p38 could be performed in Sox-EGFP limb cultures. Finally, a previous study in chick mesenchymal cells (Jin et al., 2006) proposed that a BMP/p38 signaling down-regulates *Wnt-7a* and decreases active β-catenin levels resulting in Sox9 up-regulation. This suggested a possible crosstalk between BMP and WNT signaling that act as positive and negative regulators of chondrogenesis to regulate Sox9 (Jin et al., 2006). A future direction would be to explore if this cross-talk implement a more complex and robust Turing network.

4.2.2) The role of WNT signaling

Contrary to the Bmp node, that reflects *Bmp2* expression, the Wnt node in the BSW model represents the active WNT ligand. During limb development, WNT signaling is important for the establishment of the dorso-ventral polarity (Riddle et al., 1995) and for the induction and maintenance of the AER (Kawakami et al., 2001). Moreover canonical-WNT signaling from the ectoderm was shown to be necessary for the restriction of Sox9 expression to the core mesenchyme and necessary for the commitment of cells underling the ectoderm to connective tissue lineage (ten Berge et al., 2008). In addition to these WNT roles, I proposed a new role for WNT ligands as part of the reaction-diffusion BSW network that specifies the digits.

The periodic interdigital WNT signaling pattern in our model is directly related with the interdigital distribution of active β-catenin revealed by immunohistochemistry analysis. The BSW model suggests that WNT signaling is not only restricting chondrogenesis to the core of the mesenchyme, but also restricts the expression of *Sox9* to the digits. Therefore, when I

inactivated WNT ligand secretion with the IWP2 inhibitor in limb culture, Sox9-EGFP expression was expanded in the interdigits fusing in a broad Sox9-EGFP expression which covered the whole autopod. This result is in agreement with previous studies that show how β-catenin inactivation results in the over-expression of Sox9 in the whole limb (Hill et al., 2005).

By applying different WNT ligands in limb culture, I have proposed that the main WNT ligand involved in the BSW network could be WNT3. Although this gene is expressed in the ectoderm, previous studies have shown that ectodermal Wnts can indeed regulate gene expression in the mesenchyme, eg. Wnt7a activates Lmx1b in the dorsal half of the mesenchyme (spanning from the sub-ectodermal tissue, to the core of the limb bud) (Riddle et al., 1995). Nevertheless the exact mechanism by which WNTs signal to the mesenchyme is still unknown. Further experiments are necessary to investigate the effect of WNT3 as part of the BSW network. Previous studies have shown that conditional inactivation of *Wnt3* in the ectoderm with the Msx2-Cre promoter or inhibition of its secretion by conditional inactivation of *Porcupine* with the same Cre-line, leads to limb bud truncations due to disruption of the AER (Barrott et al., 2011, Barrow, 2006). To study the role of *Wnt3* on digit patterning, it would be therefore necessary to remove *Wnt3* with a conditional Cre line that would not affect the induction of the AER by WNTs, permitting limb outgrowth. Another possible way to investigate the action of WNT3 would be to analyze its distribution in the limb mesenchyme, which will depend on the availability of good antibodies that are currently missing. Besides the analysis of Wnt3, a more detailed screening would also be necessary to investigate role of other WNT ligands in the BSW network. As in the case of BMPs, it is possible that WNTs are acting redundantly to add robustness to the BSW network. WNT14 for example is another good candidate as it is expressed in the interdigital mesenchyme of chick wings at day 5 (similar to mouse E11.5) and signals through the WNT/canonical pathway (Hartmann and Tabin, 2001, Guo et al., 2004). WNT14 is also expressed in the inter-joint region and is able to repress chondrogenic markers such as *Sox9*, *Col2a1*, *Noggin* and *Aggrecan* so that synovial joint formation can proceed though activation of a different set of joint markers such as *Gdf5* and autotoxin, see (Hartmann and Tabin, 2001). Since WNT14 can repress Sox9 in the joint region, it would be interesting to explore its interdigital activity at early stages. Nevertheless, the microarray analysis presented in this study did not show any differential expression of Wnt14 in Sox9-negative cells. In addition, previous studies suggest that in the mouse Wnt14 expression is not the interdigital during early limb development as compared to chick (Guo et al., 2004). However it is still possible that Wnt14 could be involved in the BSW network and that regulation of its activity rather in its expression play the important role in the Turing mechanism.

In this study, I have also analyzed the effect of WNT7a and WNT5a soaked beads in limb culture and showed that they did not have an inhibitory effect on Sox9-EGFP. Nevertheless, *Wnt5a* null mutants present a very similar phenotype to the one observed when WNT signaling is inhibited with IWP2: the formation of very broad digits. Therefore, despite the outcome of the bead experiments (which may depend on technical reasons), WNT5a is a possible candidate for the BSW network. However, this hypothesis is not supported by two observations. First, WNT5a signals through the non-canonical WNT pathway (namely Ror2 and JNK (Topol et al., 2003, Westfall et al., 2003, Gao, 2012) and it was proposed that it promotes β-catenin degradation in the distal limb (Topol et al., 2003). Therefore, WNT5A could not be responsible for the activation of β-catenin in the interdigits but rather seems to allow for the expression of *Sox9* in the distal region (Topol et al., 2003). The second observation is that Wnt5a is mainly known to control cell movements by regulating the planar cell polarity (PCP) pathway to drive the correct elongation during limb morphogenesis. Indeed, it has been proposed that the distally truncated digits in the *Wnt5a* null mutant are due to changes in chondrocyte elongation (Gao et al., 2011). In contrast to these studies, when I inhibited WNT signaling in limb cultures with IWP2, I observed strong distal over-expression of Sox9-EGFP. Therefore the phenotype observed in my experiments does not seem to be due to morphological changes of the chondrocytes, but rather as I proposed in my second article to an alteration of the BSW network. To strengthen this conclusion, a careful quantification of the morphology of the limb, as presented in (Gao et al., 2011), should be performed after WNT signaling inhibition. It will also be important to inhibit WNT signaling with other drugs that are specific for β-catenin like 2,4-diamino-quinazoline (Chen et al., 2009) or PKF115-584 (Lepourcelet et al., 2004). In the current study I have inhibited WNT signaling with IWP2 that prevents secretion of all WNTs and therefore it is likely to interfere also with Wnt5a signaling.

The role of Wnt7a should also be investigated in more in detail. However, a previous study (Tufan and Tuan, 2001) described that addition of WNT7a in micromass cultures inhibited chondrogenesis but did not alter Sox9 mRNA levels. This is in consistent with my observation that it does not alter Sox9-EGFP distribution and suggests that this WNT ligand may instead mediate later chondrogenic differentiation events (Tufan and Tuan, 2001).

The interdigital inhibition of Sox9 by canonical WNT signaling together with previous studies on Wnt-mediated cell adhesion, also suggest a possible link between digit patterning and the control of digit condensation. Previous studies have shown that specific modifications of β-

catenin can prevent the formation of membrane bound β-catenin-cadherins complexes that promote cell-adhesion (Brembeck et al., 2006, Brembeck et al., 2004). It is therefore possible that WNT signaling is not only promoting stabilization of β-catenin to inhibit Sox9 as proposed by the BSW model, but may also simultaneously modify β-catenin to reduce cell-adhesion in the interdigital tissue. This would suggest a mechanistic link between the initiation of condensation and the patterning promoted by the BSW network. A similar mechanism has been observed during cancer progression, where WNT signaling is associated to a decrease of cell adhesion (Birchmeier et al., 1994). However, the specific control of the β-catenin modification that prevents cell-adhesion in mesenchymal cells is still unkown. In the limb, it has been shown that Sox9 binds to β-catenin in the nucleus competing with β-catenin binding to TCF transcription factors as well as promoting β-catenin proteasome-degradation (Akiyama et al., 2004). In this way Sox9 promotes chondrogenesis and blocks β-catenin signaling and β-catenin-mediated transcription of CyclinD1 which results in delayed proliferation and hypertrophic chondrocyte differentiation. It could be interesting to explore if Sox9 or other genes induced during early chondrogenesis promote binding of β-catenin to membrane bound cadherin to form condensations. An important experiment to evaluate the overall mechanistic link between condensation and patterning mediated by WNT signaling will be to analyze the distribution of membrane bound β-catenin-cadherin complexes in the limb. High levels of β-catenin-cadherins in the digits would be consistent with previous studies in chick and in micromass cultures (DeLise et al., 2000, Delise and Tuan, 2002b, Oberlender and Tuan, 1994b, Oberlender and Tuan, 1994a, Denker et al., 1999, DeLise and Tuan, 2002a), that have suggested that N-cadherin is involved in the process of cell-cell contact and cell-cell adhesion necessary for mesenchymal condensations. However, while Ncadherin has been suggested to be a direct downstream target of Sox9 (Panda et al., 2001) it does not seem to be expressed in the forming digits (Luo et al., 2005). In agreement with this, my microarray analysis did not reveal any differential N-cadherin expression in Sox9-EGFP positive cells. Moreover N-cadherin is not altered in *Sox9*-deficient limbs that do not form mesenchymal condensations, suggesting that the regulation of cellular adhesion by Sox9 may involve other molecules (Akiyama et al., 2002). Future work could consist in defining which are these molecules and if β-catenin is involved in this process.

4.3 Shh and the BSW model

In the last two decades several studies have explained digit patterning with Positional Information models based on the SHH morphogen gradient, (Riddle et al., 1993), for review see

(Zeller et al., 2009). However, other studies have provided evidence for the dispensability of SHH signaling for digit specification (Litingtung et al., 2002, Ahn and Joyner, 2004). In this thesis I proposed that digit specification is instead controlled by a Turing network implemented by Bmp, Sox9 and Wnt. Since SHH signaling is not included directly in the Turing network but it has been shown that can influence digit specification, how does this important morphogen fit with our model?

To answer this question it is important to first recapitulate the role of SHH in the control of growth along the AP axis. It was shown that SHH signaling inhibits Gli3R repressor in the posterior regions of the autopod (Wang et al., 2000). The inhibition of Gli3R is essential to promote growth, since Gli3R directly inhibits expression of G1-S cell-cycle transition regulators and constrains S phase entry of cells in the anterior region of the autopod (Lopez-Rios et al., 2012). On the other hand, SHH signaling promotes growth by participating in the SHH-GREM-FGF feedback loop that guarantees the coordinated outgrowth of the limb and the expansion of Fgfs from the posterior to the anterior part of the limb. Although we did not explicitly model Shh in the Turing network, part of the experimental data used to build the two dimensional simulation of digit patterning implicitly included the effect of SHH signaling. First of all, the simulation used a realistic limb growth map that was derived from experimental data. Therefore the morphological changes promoted by Shh are implicitly included in the model. Secondly, our simulation of digit patterning used experimental expression time course of *Fgf4* and *Fgf8* to simulate a realistic FGF signaling gradient. In particular, the *Fgf4* expression patterns were used to map into the model the progressive expansion of the *Fgf4-9-17* from the posterior to the anterior part of the limb. This expansion is under the control of the SHH-GREM-FGF feedback loop, therefore the effect of SHH signaling on the progressive posterior to anterior expansion of Fgfs is implicitly included in the model.

Besides the control of AP expansion, it has been also proposed that SHH controls digit identity. However recent studies have shown that this process seems to occur later in development when the digital rays become condensed cartilage (Suzuki et al., 2008). Evidence also suggests that the interdigit posterior to each digit provides positional information to the phalanx forming regions at the digit tips which determines digit identity (Suzuki et al., 2008). This process is probably mediated by BMP signaling which appears to controls the number, size and morphology of the phalanxes in each digit. Previous studies have proposed that the cells in the limb could retain a "memory" downstream of SHH to control digit identity at later stages (Harfe et al., 2004). In the light of current experimental evidence, such memory would be retained not

by the digit progenitor cells but by the surrounding interdigit mesenchyme (Suzuki, 2013). This memory could be either a direct downstream target of the SHH signaling or a separate signaling pathway triggered by SHH. For example, it is well known that SHH signaling regulates the expression of 5´Hoxd genes in the autopod (Chiang et al., 2001, Ros et al., 2003), and that Gli3R inhibits Hoxd gene transcription (Wang et al., 2000, te Welscher et al., 2002, Litingtung et al., 2002). In addition, it has been proposed that Hoxd genes control the asymmetry of digit identities in the autopod (Zákány et al., 2004). Therefore a possible way in which SHH may control digit identities at early stages is through regulation of Hoxd gene expression that will in consequence control the positional value assigned to the interdigits, possibly through regulation of BMP signaling. This is in agreement with the evidence that Hoxd genes regulate transcription of *Bmp* genes (Salsi et al., 2008, Knosp et al., 2004, Suzuki et al., 2004). The digit patterning model presented in this study does not consider the specification of digit identities since the simulations do not go beyond E12.5. However, it is interesting to observe that in our model Hox genes, together with Fgfs, act as modulators of the Turing gene network to produce the correct digit pattern. It is therefore possible that the SHH gradient could be included as a modulator in a similar way to Fgfs/Hox to create different digit identities together with Hox. This suggests that the BSW Turing network could specify the digits as a repetitive periodic fate while the SHH positional information could act as modulator of the Turing mechanism to specify the different digit identities. This hypothesis is consistent with the combination of a Turing mechanism and a Positional Information model discussed in (Wolpert, 1989).

Nevertheless, the majority of the classic Shh Positional Information models that I reviewed in this study, implicitly assumed that SHH signaling controlled both digit specification and digit identity, see section 1.2.5. In addition, several studies have evaluated perturbations at very late time points (namely from E18.5 beyond) rather than observing early markers of digit specification, which makes more difficult to uncouple digit specification from digit identity. Finally, under the assumption that Shh controlled both digit specification and identity, many studies have interpreted that the formation of fewer digits in Shh manipulations was due to an impairment of digit specification rather than a change in AP expansion. In the following sections, I propose a re-interpretation of classic SHH manipulations and positional information models based on Shh signaling under the assumption that digit specification is controlled by the BSW model rather than by the SHH signaling gradient.

4.3.1) Classical experiments with grafting of the ZPA or ectopic expression of Shh in the anterior region of the limb bud

The mirror image digits duplication obtained by grafting ZPA cells on the anterior region of the limb (Saunders and Gasseling, 1968) has been traditionally interpreted as the result of the duplication of the positional information gradient of SHH, which was assumed to control digit specification. Taking into account that SHH is dispensable for digit specification, the digit duplication can be interpreted essentially by a change in autopod growth. Anterior ectopic Shh expression (Riddle et al., 1993) promotes tissue expansion which results in the formation of new peaks (digits) driven by the BSW Turing model. Since SHH also controls the later specification of digit identity (formation of phalanxes) the doubled gradient of SHH signaling is able to specify mirror image digit identities.

4.3.2) Knockout of *Shh* (Chiang et al., 2001)

In the *Shh* null mutant, forelimbs do not form digits while hindlimbs form only one digit which is commonly interpreted as digit 1. It was proposed that this digit is independent of SHH signaling and that the loss of other digits reflect the essential role of Shh in digit specification. Taking into account the experimental evidence that show the dispensability of SHH signaling for digit specification, the presence or lack of digits in the Shh mutant cannot be related to an impairment of digit specification. If we consider instead that digit specification is driven by the BSW model, then the loss of digits can be associated to a decrease of the AP tissue expansion which is normally promoted by the SHH signaling. In this case, upon *Shh* inactivation, the resulting decrease in AP growth reduces the size of the limb so that the BSW model will from fewer peaks (digit). In addition, in this mutant the SHH-GREM-FGF feedback loop is disrupted, reinforcing the idea that the lack of digits is due to reduced growth. According to the BSW model, the formation of only one digit in the hindlimb will depend on the reduced limb size and on the expression domain of Hoxd13 which is still present in the hindlimb of *Shh* mutants (Chiang et al., 2001) and defines the region where the BSW model is active.

4.3.3) Alteration of SHH morphogen diffusivity (Li et al., 2006, Chen et al., 2004b)

A previous study has shown that lack of cholesterol modification increased SHH diffusivity resulting in the formation of extra digits in the anterior part of the limb (Li et al., 2006). On the other side, it has been shown that lack of palmitoylation reduces SHH diffusivity, resulting in loss of digit 2 and fusion of digit 3 and 4 (Chen et al., 2004b). These studies hypothesized that the formation of extra digits and the lack of digits was a consequence of the altered SHH signaling necessary for digit specification. If we consider that digit specification is driven by the BSW model, while SHH signaling controls AP expansion and specification of digit identities, than the phenotypes can be explained again as the results of altered AP growth. Extended SHH signaling may result in larger limbs with more peaks formed by the BSW Turing model (digits), while reducing SHH diffusivity results in narrower limbs with less Turing peaks (digits). In both cases, the association of digit identities to the formed digits is still possible, since the SHH gradient is still present.

4.3.4) The Temporal–Gradient model (Harfe et al., 2004)

This study showed evidence that half of digit 3 and digits 4 and 5 were made by Shh descendent cells. It was also shown that more anterior ZPA descendent cells cease to express Shh before posterior cells. Moreover, a shallower gradient of SHH resulted in the loss of only digit 2. Based on these observation, it was proposed that digit 1 was independent of SHH signaling, as proposed by (Chiang et al., 2001), digit 2 was the only digit specified by long-range SHH gradient, while digit 3 to 5 were formed depending on the time they have been exposed to high SHH autocrine signaling.

Again, if we assume that SHH signaling is dispensable for digit specification, the fate of SHH descendent cells is not correlated with the formation of digit 3 to 5 but rather reflects the other roles of SHH signaling, which are the control of digit identity and expansion along the AP. The same study (Harfe et al., 2004) showed that by creating a shallower SHH gradient the expression of Fgf4 was restricted to the posterior part of the limb. This is possibly due to compromised SHH-GREM-FGF feedback loop and results in narrower limbs. If digits are specified by a Turing mechanism, the loss of digits is then associated to the reduction of growth.

Since SHH signaling is still present it can still attribute an identity to the remaining four digits. Nevertheless, it is difficult to identify the digits that are formed since digit 2, 3 or 4 have all the same number of phalanges and other morphological adjustments of the digit (E.g. length) can just derive from the overall change in limb morphology.

4.3.5) Exposure to low levels of SHH (Scherz et al., 2007)

A following study (Scherz et al., 2007) validated the temporal-gradient model, and more particularly the fact that the most posterior digits were specified by the time of SHH exposure, using two different sets of experiments. First, the SHH signaling was interrupted at different times during chick limb development by using a SHH specific inhibitor, secondly a transgenic mutants mice were developed with reduced SHH levels. Two different transgenic lines were made: one that produces low levels of SHH for a short time (*Prx1Cre; Shh*$^{c/c}$), and one that produces low levels of SHH for a longer time period (*Shhgfpcre/Shh*$^{c/c}$). From these experiments it was concluded that reducing the time of SHH exposure caused defects on digit patterning and that the specification of the posterior digits required longer exposure to Shh signaling. In the *Prx1Cre; Shh*$^{c/c}$ mice, the forelimbs lost two digits indentified as 4 and 5. In the case of *Shhgfpcre/Shh*$^{c/c}$ mice, the forelimbs lost only digit 2, and one phalanx in digit 5. The identification of each digit was based on the overall digit length (digit 3 being longer than either digit 2 or 4) as well as the length of the primary ossification centre of E18.5 metacarpal elements. The authors also showed that in all experiments the size of the limb was smaller than in the WT and this was associated with a reduction in SHH signaling and a possible disruption of the SHH-GREM-FGF feedback loop. Indeed, *Fgf4* expression was reduced and restricted posteriorly. The study concluded that, as predicted by the temporal-gradient model, the posterior digits were more dependent on the time of exposure to SHH signaling than on SHH concentration.

To re-interpret their results with our model, it is first necessary to point out that whenever a loss of digits was observed, the limbs were smaller. Again, this fits with the prediction that a Turing mechanism would form fewer peaks (digits) in a smaller limb. Therefore, according to the BSW model, the loss of digits is not associated directly to the reduced SHH signaling gradient but rather to a reduction of growth. Secondly it is also necessary to remember that although digit identities are dependent on SHH signaling, digit specification is not (Litingtung et al., 2002) and therefore it is not possible to give an identity to the digits that are lost, but it is sensible to

associate SHH signaling to the specification of the identities in the remaining digits. This process may indeed depend on the SHH gradient and time of exposure to SHH signaling. An interesting study shows that 5′ Hoxd genes exhibit differential temporal dependence on Shh depending, with *Hoxd13* requiring SHH signaling for the longest amount of time (Panman et al., 2006). This supports the hypothesis that SHH would control digit identities through control of Hoxd expression.

4.3.6) The biphasic model for SHH signaling (Zhu et al., 2008)

In this study, *Shh* was deleted at different times using a tamoxifen induced conditional Cre-line. By analyzing the final skeletal pattern, the authors propose that removal of *Shh* at successively earlier stages causes digit loss in a progressive sequence: digit 3 (d3) first, then digit 5 (d5), then digit 2 (d2) and finally digit 4 (d4). In addition, based on the number of phalanxes and digit morphologies, it was also proposed that the remaining digits did not change identity. To rule-out digit identity transformations, the identities were analyzed at early stages based on the AP position and shape of the digits marked by the *Noggin-lacZ*. It was concluded that the sequence of digit loss during early stages was the same as the one observed by skeletogenic analysis, suggesting that the digit identities were specified early. This study also observed that sequence of digit appearance in the WT, as shown by *Noggin-lacZ*, was opposite to the order of digit loss (d4-d2-d5-d3). Finally, it was showed that upon *Shh* inactivation, both cell survival and proliferation were affected in the limb mesenchyme. Based on these data, the authors proposed a model where SHH signaling was only required early and transiently for digit specification/identity but continuous SHH signaling was necessary to ensure sufficient cell number for the correct formation of the digits.

If we consider that SHH is dispensable for digit specification, which is instead controlled by the BSW model, then the progressive loss of digits upon earlier inactivation of SHH can simply be explained by a progressively more severe reduction of limb growth. In this case, less Turing peaks (digits) will be formed due to a reduction of AP expansion. In this study, the authors attributed identity to the digits based on the AP position and shape as revealed by *Noggin-lacZ*. In the context of a reaction-diffusion mechanism, were digits are all specified as a periodic pattern with identical fates, these two characteristics are determined only by the size and the geometry of the developmental field. To verify if SHH specifies digit identity at early times as proposed by the authors, suitable molecular markers for each digit (E.g. Hox genes) should be

instead analyzed. In addition, it would be necessary to describe the expression of the chondrogenic marker *Sox9* in detail as it is expressed earlier than *Noggin*. As I mentioned at the begging of this chapter, the authors compared the expression of *Sox9* and *Noggin-LacZ*, however they observed the same order of digit formation (d4-d2-d5-d3). This result contrasts with the detailed Sox9 expression analysis presented in section 3.1.1, which shows that digits are specified in the following order: d4-d3/d2-d5-d1.

4.3.7) Growth and morphogen model (Towers et al., 2008)

In this study, the authors analyzed clonal fate-map data (with injection of fluorescent dyes in the chick limb) in the WT and in limbs where SHH signaling or proliferation was inhibited. The WT situation showed that each digit was formed by proximal progenitor cells and that only the most posterior digit was populated by Shh-expressing cells, thus showing a different result then the fate-map data in mouse (Harfe et al., 2004). When SHH was inhibited, smaller limbs were formed and posterior digits were lost. On the other side, upon inhibition of proliferation the resulting smaller limbs lacked anterior digits. Altogether these experiments supported a model where SHH has a dual role both controling growth and the specification of the digits.

Once more, if we consider that SHH signaling is dispensable for digit specification, which is instead controlled by the BSW model, then the formation of fewer digits can be explained by a reduction of limb growth. Both in the case of SHH inhibition and the inhibition of proliferation, the smaller limbs buds lead to the formation of less Turing peaks (digits). On the other hand, this study also investigated the other two roles of SHH, that are the control of digit identities and the control of growth. By observing fate maps, the authors concluded that when the proliferation was inhibited, different clones along the AP axis remained equally viable and contributed to the same AP region later in development. Therefore, in contrast with previous studies (Harfe et al., 2004) it was concluded that posterior identities were acquired early and were uncoupled from the anterior-posterior expansion. However, it would be important to check if the posterior digit 4, which is formed upon inhibition of proliferation, is indeed constituted only from posterior clones rather than by a mixed population. This would be useful to distinguish between the hypothesis that the posterior identities are acquired early and the hypothesis that identities are specified by SHH signaling later in development.

In conclusion, many studies have shown that SHH signaling affects the growth of the limb along the AP axis. Therefore any change in SHH is going to be accompanied by a change of AP limb size which affects the number of periodic peaks created by the BSW model. It is also essential to keep in mind, that although at later stages digits have different phalanx number and morphology, at early stages, digits do not show discernible identities. Another important observation that must be taken into account is that previous studies have shown that SHH signaling is dispensable for digit specification and that beside the control of growth, its main role is to specify digit identities. The exact mechanism by which Shh specifies digit identities is unknown but appears to involve distal Hox genes. It is interesting to notice that in the Gli3 mutant (as in the Gli3-SHH mutant) distal Hox genes are up-regulated in the anterior region of the limb (Büscher et al., 1997, Litingtung et al., 2002). Moreover, when the SHH receptor *Ptch1* is conditionally inactivated in the forelimb mesenchyme, the specification of symmetric digits (Butterfield et al., 2009) is accompanied with an up-regulation of Hox genes in the anterior part of the autopod, which strongly suggest that SHH-Ptch1 mediates the control of AP asymmetry and digit identities through the regulation of Hox genes (Butterfield et al., 2009). Finally, in agreement with this hypothesis inactivation of Hoxa13 in the Gli3 mutant background results in a drastic recovery of the asymmetrical phenotype (Sheth et al., 2012).

4.4 Future directions

4.2.1) Modulation by morphogen gradients and coordination of growth and patterning

To reproduce the correct digit pattern, the BSW model had to be modulated by the Fgf signaling gradient and Hox genes. These two signals defined the autopod region where the BSW model was active and modulated the wavelength of the periodic pattern in a PD graded manner. Our model also suggested that, to form the correct digit pattern, the modulation by Hox genes and by Fgf signaling had to be coordinated. In particular, the proximal expansion of Hoxd13 had to be coupled with the anterior expansion of FGF signaling. This theoretical finding is consistent with previous studies that showed that FGFs control the expression of distal Hox genes (i.e. group 11 to 13), as revealed by the Fgf8 requirement for the sequential activation of *Hoxa11* and *Hoxa13* in limb mesenchymal cells in culture (Cooper et al., 2011, Roselló-Díez et al., 2011) and *Hoxd13* downregulation associated with a reduced dose of FGFs (Sun et al., 2002). Moreover,

it suggests that FGF signaling may act as a central node to coordinate patterning and growth by correlating three separate events: growth (Martin, 1998), specification and proximal expansion of distal PD markers as *Hoxd13* (Mercader et al., 2000) and promotion of a larger digit wavelength by modulating the BSW model (Sheth et al., 2012). Interestingly, the central role of FGF signaling is also consistent with the idea that the SHH-GREM1-FGF feedback loop, which controls expansion of FGFs from the posterior to the anterior part of the limb, plays an important role in the coordination of patterning and growth, see Figure 40. This feedback loop is also able coordinate growth and the specification of the digits, which are driven by Fgfs and by the BSW network respectively, and the specification of digit identities, which is controlled by SHH signaling (Figure 40). In summary, our model suggests that during limb development, interactions between SHH, FGFs, Hox genes and the BSW network coordinates growth, digit specification and specification of digit identities. By uncoupling these different processes it is possible to create limbs with different digit number, increased or reduced growth or without asymmetries along the AP. An example of how growth and digit specification can be uncoupled was presented in (Sheth et al., 2012). In this study, the Gli3 null mutant, which has an increased AP size, was used as a background to prevent the reduction of growth observed upon the progressive removal of Hoxa13 and Hoxd11-13. This strategy was successful to highlight that removal of Hox genes caused more severe polydactyly with thinner digits, which suggested that one of the main roles of Hox genes was to control the wavelength of the Turing mechanism to specify the number of digits.

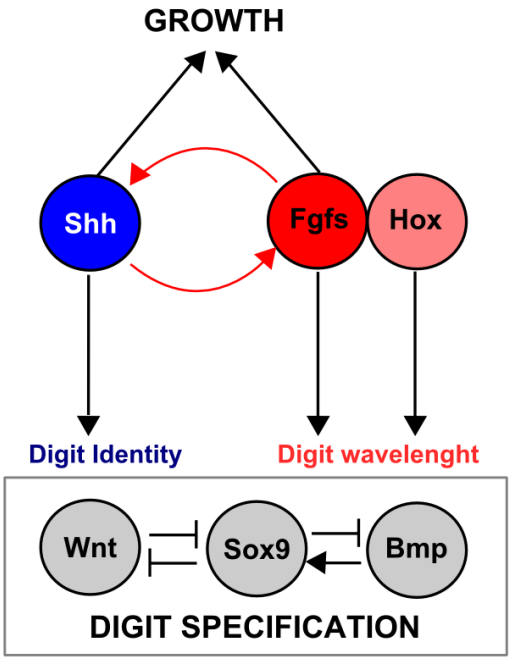

Figure 40. Coordination of patterning and growth by SHH and FGF signaling.
In this model SHH controls digit identity and growth; FGFs control growth and together with distal Hox genes controls digit wavelength. Digit specification *per-se* is controlled by the BSW model. Therefore the SHH-GREM1-FGF feedback loop coordinates digit specification, growth and specification of digit identity by uniting SHH and FGFs activities (red arrows).

On the other hand, in this study we have also shown that the wavelength can be altered by directly perturbing the BSW network by lowering BMP and WNT signaling to obtain larger digits. Therefore a possible way to alter the number of the digits without changing the AP size is also by perturbing the feedbacks of Turing network itself. By contrast, if the AP-expansion is changed and the wavelength remains unchanged, this can lead to alteration of digit number. In the *Shh/Gli3* double mutant and in the *Gli3* mutant for example, the lack of Gli3R repressor which inhibits growth, leads to the formation of bigger limbs with extra digits. On the other side, in the *Shh* null mutant the expansion of the Gli3R reduces growth allowing only one or no digits to form. By interpreting all these perturbations in the context of the BSW model and the SHH-GREM1-FGF feedback loop, it is possible to elucidate the mechanism by which evolution has constrained the tetrapod limb to the pentadactyl state. For example, the striking resemblance of the polydactyly phenotype in the mouse *Gli3* mutant with reduced distal *Hox* genes and the fin ray in the pectoral fin of sharks, suggested that the correct equilibrium of SHH/Gli3 signaling, Hox dosage and tuning of the Turing mechanism could have been an evolutionary strategy for the fin to limb transition (Sheth et al., 2012). In relation to this, two recent studies

have showed how different developmental mechanisms could underlie the reduction of digits from the pentadactyl state (Cooper et al., 2014, Lopez-Rios et al., 2014). One of these mechanisms is the expansion of anterior and posterior cell death that results in the active degradation of digits which were temporarily patterned in 3-toed species of jerboa, 2-toed camel and 1-toed horse. On the other hand, reduction of *Ptch1* expression was found responsible for the loss of digits in the cow and the pig, and seems one of the evolutionary steps that can lead to artiodactylous digits (even-toed digits). Ptch1 is the receptor of SHH that when inactivated leads to a negative feedback on SHH signaling, which maintains SHH activity in a gradient from posterior to anterior (Briscoe et al., 2001, Chen and Struhl, 1996, Marigo et al., 1996). Thus in the cow, as in the conditional *Ptch1* mouse mutant, SHH signaling is activated throughout the developing limb leading to loss of the AP asymmetry and a creation of to even-toed digits. The alteration of the SHH signaling leads to alteration in the cross-regulations of the SHH-GREM1-FGF feedback loop as well as to a change in the expression of distal Hox genes (e.g. Hoxd13 becomes expressed symmetrically) (Lopez-Rios et al., 2014, Butterfield et al., 2009). This seems to be underlying the loss of digits and the formation of two long frontal digits III and IV in the cow (and digit 3 and 4 in the mouse *Ptch1* mutant) suggesting again how a different equilibrium between the limb signaling centers and master transcription factors can be changed during evolution to generate the different digital patterns. Finally, it is possible that the difference between the digit patterns of the cow, the pig, the camel, the horse, the jerboa and the mouse is not only the number of digits but also their width. It would be interesting to explore if these changes are correlated with changes in FGF signaling levels, distal Hox genes expression or and changes in the BSW network.

4.4.2) Future characterization of the BSW network

In this study I presented data that support the involvement of the BMP and the WNT pathways in the Turing network that controls digit specification. However, further experiments should be performed to better characterize how these two pathways implement the main feedback of the BSW network in conjunction with Sox9.

An important aspect that needs to be further investigated is the mechanism that creates the periodic distribution of WNT signaling with higher activity in the interdigital regions. Our theoretical analysis predicted that low WNT signaling activity in the digits depends on the extracellular inhibition of WNT signaling by Sox9. Considering that Sox9 is a non-secreted

transcription factor, this hypothesis suggests that the extracellular inhibition should be mediated by secreted molecules that are promoted by Sox9 and prevent the diffusion or activity of WNTs. In the supplementary material of my second article, I have presented the expression patterns of several WNT inhibitors that were identified as differentially expressed in Sox9 positve cells by the microarray analysis. Among these inhibitors, genes of the Sfrp family were identified as good candidates that may mediate WNT signaling inhibition. Indeed *Sfrp1*, *Sfrp2* and *Sfrp3* are expressed in the limb at early stages (Witte et al., 2009) and are well known inhibitors of WNTs (Cruciat and Niehrs, 2013). My analysis revealed that *Sfrp2* is indeed expressed in the autopod region at E11.5 and that at slightly later stages appears to be expressed in the digital region. This is consistent with previous studies (Wada et al., 1999, Baranski et al., 2000, Ladher et al., 2000, Esteve et al., 2000) that revealed that *Sfrps* are expressed in chondrogenic condensations in the chick. Therefore, my analysis suggests that these inhibitors could be promoted by Sox9 to inhibit WNT signaling. Nevertheless, additional experiments should be performed to better characterize *Sfrps* expression patterns and to investigate the digit patterning change promoted by gain and loss of function of Sfrps. For example, beads soaked in Sfrps recombinant protein could be implanted in the interdigital regions of E11.5 Sox9-EGFP limb cultures to check for potential down-regulation of WNT-signaling. Another potential WNT inhibitor identified by my preliminary analysis is the extracellular heparan sulfate endosulfatase *Sulf1*. This membrane-bound enzyme removes sulfate groups of heparin sulfate proteoglycans (HS) which are known to bind signaling molecules including BMPs and WNTs to control their signaling (Farach-Carson et al., 2005, Gorsi and Stringer, 2007). My gene expression analysis has revealed that Sulf1 is expressed in the digital region as soon as Sox9 shows a periodic pattern. This agrees with the hypothesis that Sox9 may promote *Sulf1* to limit the diffusion or the activity of WNTs in the developing digits. Interestingly, this idea fits with previous studies that showed that *Sulf1* inhibited WNT signaling in quail embryos (Sahota and Dhoot, 2009) and promoted chondrogenesis and mesenchymal condensation in micromass cultures (Zhao et al., 2006) . These observations should be re-evaluated by analyzing the Sox9 pattern and additional gain and loss of function experiments should be performed as in the case of *Sfrps*.

Additional experiments should also be performed to investigate the simultaneous perturbation of WNT and BMP signaling. My perturbation experiments have revealed that by lowering both BMP and WNT signaling with inhibitory drugs, the Turing network can be tuned to generate a pattern with fewer and wider digits. A future direction would be to modulate these pathways to increase the signaling activity and stimulates the opposite effect, which is the formation of thinner digits. A pharmacological approach similar to the one used to perform loss of function

experiments would be the ideal choice. However, although there are several drugs that can activate WNT signaling (Chen et al., 2010), very few drugs are available to activate BMP signaling (Vrijens et al., 2013). An alternative strategy to ectopically activate BMP signaling could be to generate mice with conditional misexpression of BMP signaling in the limb autopod. This could be done for example by taking advantage of the Hoxa13 Cre line (Scotti and Kmita, 2012) to express constitutively active BMP receptors (Zhang et al., 2000).

Future experiments should also be performed to investigate gain and loss of functions of Sox9. In this study, I have proposed that this important transcription factor is not only the earliest marker of the skeletal pattern but it is also an integrative part of the Turing network that controls digit specification. Therefore, it will be important to investigate how the digit pattern changes upon *Sox9* perturbations. Complete *Sox9* loss of function (Akiyama et al., 2002) causes the disruption of the digit pattern. On the other hand, *Sox9* gain of function in mouse (Akiyama et al., 2007a) causes polydactyly in agreement with similar experiments in chick (Healy et al., 1999). It will be interesting to investigate how the BMP and the WNT pathways are affected in these mutants.

Last but not least, experiments should also be used to explore the modulation of Hox and Fgfs proposed by the BSW model. In particular, misexpression of Hoxd13 or Hoxa13 should be performed to verify if fewer larger digits would be formed in agreement with the increase in wavelength predicted by the BSW model. Finally, FGF signaling perturbation should be performed to investigate changes on the wavelength and on the control of digit bifurcations. In this case, as I have discussed in the previous section, experiments should be designed in order to uncouple the effect of FGF signaling on growth and on patterning.

4.4.3) Extension of the BSW model in 3D

In this study I have presented a 2D model of digit patterning which successfully recapitulates the expression patterns of *Sox9*, *Bmp2* and the distribution of active WNT canonical signaling, in the wildtype and in the perturbation experiments. However, digit patterning is a three-dimensional process which is coordinated with morphogenesis along the AP, PD and DV axis. We chose to build a 2D model to reduce the complexity of the theoretical analysis and the computational load required to run simulations. In addition, most of the experimental data was analyzed in 2D. A next challenge would be to extend the digit patterning model in 3D. For that

purpose, it would be essential to gather new experimental data that describes the dynamics of digit patterning in 3D. Optical projection tomography could be used to analyze gene expression patterns and protein distributions. I have started a preliminary analysis of gene expression with the OPT that shows an interesting distribution of the *Bmps* in comparison to the *Sox9* expression pattern. At E11.5, at the level of the autopod, *Bmp2* is expressed out-of-phase of *Sox9*, while *Bmp7* and *Bmp4* are expressed in the mesenchyme that underlies the ectoderm in a localized manner. These localized expression patterns could determine where the different BMP ligands interact. Previous studies have shown that *Bmp2/Bmp4*, and *Bmp2/Bmp7* heterodimers can activate the BMP signaling more efficiently than homodimers (Schmid et al., 2000, Nishimatsu and Thomsen, 1998). This could suggest that the regions of localized *Bmp* expression together with diffusion could lead to localized synergistic interactions between BMPs that may underlie different levels of BMP signaling along the space. This could modulate the BSW network in a similar manner as done by Hox genes and FGFs to generate the specific digit pattern. Moreover it has been shown that Bmps act redundantly in the limb, as the conditional inactivation of Bmp2/Bmp4 or the conditional inactivation of Smad4 leads to loss of digits (Bandyopadhyay et al., 2006, Bénazet et al., 2012). This reflects that even though the expression of Bmps is localized and not always overlapping, they can act redundantly sharing the same functions.
The analysis of the 3D expression patterns of the BMP inhibitors, namely *Chordin* and *Chrdl2*, shows an interesting pattern in the autopod (see Figure 35 and Figure 36): *Chordin* is expressed out-phase of the digits while *Chrdl2* is expressed in the digital rays at E12. This suggests that they could be implicated in the digit patterning process by regulating BMP levels. Studies in vertebrate bodies have shown that *Chordin* and *Crossveinless-2* create a system that potentiates the flow of BMP proteins from the intervertebral discs to the vertebral bodies (Zakin et al., 2010). A similar system could be explored in the limb where the players could be *Chordin* and *Chrdl2*, and direct the flow of BMP proteins from interdigital to the digital region. On the other side, my analysis showed a high proximal dorsal and ventral expression of the *Bmps* and their inhibitors, *Noggin*, *Chrdl2*, and *Chordin*. This suggests their involvement in the myogenic differentiation that occurs in these regions in the limb (Francis-West et al., 2003). Indeed it has been shown that high BMP signaling inhibits myogenic progenitors whereas low BMP signaling potentiates myogenic differentiation (Duprez, 2002). Therefore a tight regulation of BMP levels could be implemented by *Noggin*, *Chrdl2*, and *Chordin*.

To develop a 3D model it would be also necessary to analyze the results of experimental perturbations in 3D. To analyze pattern dynamics with the Sox9-EGFP reporter line in 3D and over time, the limb culture system and live OPT imaging could be used similarly as in (Boot et

al., 2008). This 4D imaging technique could also be used to analyze other reporter lines for WNT and BMP signaling (Currier et al., 2010, Jho et al., 2002, Monteiro et al., 2008). Immunohistochemistry protocols for specific antibodies and OPT imaging could also be used to analyze protein distributions (E.g. pSMAD1/5/8, act-βcat). Alternatively immunohistochemistry could be performed on serial sections and the 3D protein distribution pattern reconstructed successively. In general, not just for the 3D model but for the 2D model as well, it would be interesting to analyze the distribution of BMP and WNT ligands. Analysis of ligands co-localization will be important to investigate the role of BMP heterodimers and their distribution and to quantify the diffusion of ectodermally expressed genes. However, no good antibodies are available for BMP and WNT ligands and the development of functional transgenic lines with fusion-proteins is challenging. An interesting extension to this work would be to explore the possibility of creating a 3D micromass culture of the Sox9-EGFP limb mesenchyme to mimic a more biologically realistic micro-environment. This would also be useful for imaging cell dynamics such as cell adhesion and migration as well as analyzing the formation of the chondrogenic pattern in 3D. Protocols described in (Ivascu and Kubbies, 2006, Lorenzo et al., 2011) could be adapted for spheroid micromass cultures and imaging at a cellular level resolution could be performed with light sheet microscopy as in (Lorenzo et al., 2011).

4.3 Conclusion

In summary, this thesis has provided experimental and theoretical evidences that Bmps, Sox9 and Wnts implement the Turing network that controls digit patterning during limb development. This has strengthened the hypothesis that a Turing mechanism rather than a positional information model controls digit specification. On the other side, our model has also showed that positional information signals like FGF signaling are required to modulate the Turing network to form the correct digit pattern. Our digit patterning model shows that the dynamics of *Sox9* expression during early limb development can be robustly recapitulated by a process that coordinates a Turing network with growth and positional information signals. This suggests that the variation in digit number and morphologies observed during evolution may have arisen by modulating the different parts of this process. To conclude, it is possible that similar mechanisms which combine Positional Information and a Turing mechanism may underlies pattern formation in other developmental systems.

BIBLIOGRAPHY

AHN, K., MISHINA, Y., HANKS, M. C., BEHRINGER, R. R. & CRENSHAW, E. B. 2001. BMPR-IA signaling is required for the formation of the apical ectodermal ridge and dorsal-ventral patterning of the limb. *Development,* 128**,** 4449-4461.

AHN, S. & JOYNER, A. L. 2004. Dynamic changes in the response of cells to positive hedgehog signaling during mouse limb patterning. *Cell,* 118**,** 505-516.

AKAM, M. 1987. The molecular basis for metameric pattern in the Drosophila embryo. *Development,* 101**,** 1-22.

AKIYAMA, H. 2008. Control of chondrogenesis by the transcription factor Sox9. *Modern Rheumatology,* 18**,** 213-219.

AKIYAMA, H., CHABOISSIER, M.-C., MARTIN, J. F., SCHEDL, A. & DE CROMBRUGGHE, B. 2002. The transcription factor Sox9 has essential roles in successive steps of the chondrocyte differentiation pathway and is required for expression of Sox5 and Sox6. *Genes & development,* 16**,** 2813-2828.

AKIYAMA, H., KIM, J.-E., NAKASHIMA, K., BALMES, G., IWAI, N., DENG, J. M., ZHANG, Z., MARTIN, J. F., BEHRINGER, R. R. & NAKAMURA, T. 2005. Osteo-chondroprogenitor cells are derived from Sox9 expressing precursors. *Proceedings of the National Academy of Sciences of the United States of America,* 102**,** 14665-14670.

AKIYAMA, H., LYONS, J. P., MORI-AKIYAMA, Y., YANG, X., ZHANG, R., ZHANG, Z., DENG, J. M., TAKETO, M. M., NAKAMURA, T. & BEHRINGER, R. R. 2004. Interactions between Sox9 and β-catenin control chondrocyte differentiation. *Genes & development,* 18**,** 1072-1087.

AKIYAMA, H., STADLER, H. S., MARTIN, J. F., ISHII, T. M., BEACHY, P. A., NAKAMURA, T. & DE CROMBRUGGHE, B. 2007a. Misexpression of Sox9 in mouse limb bud mesenchyme induces polydactyly and rescues hypodactyly mice. *Matrix Biol,* 26**,** 224-33.

AKIYAMA, H., STADLER, H. S., MARTIN, J. F., ISHII, T. M., BEACHY, P. A., NAKAMURA, T. & DE CROMBRUGGHE, B. 2007b. Misexpression of Sox9 in mouse limb bud mesenchyme induces polydactyly and rescues hypodactyly mice. *Matrix biology,* 26**,** 224-233.

AMBLER, C. A., NOWICKI, J. L., BURKE, A. C. & BAUTCH, V. L. 2001. Assembly of trunk and limb blood vessels involves extensive migration and vasculogenesis of somite-derived angioblasts. *Developmental biology,* 234**,** 352-364.

BADUGU, A., KRAEMER, C., GERMANN, P., MENSHYKAU, D. & IBER, D. 2012. Digit patterning during limb development as a result of the BMP-receptor interaction. *Scientific reports,* 2.

BANDYOPADHYAY, A., TSUJI, K., COX, K., HARFE, B. D., ROSEN, V. & TABIN, C. J. 2006. Genetic analysis of the roles of BMP2, BMP4, and BMP7 in limb patterning and skeletogenesis. *PLoS genetics,* 2**,** e216.

BARANSKI, M., BERDOUGO, E., SANDLER, J. S., DARNELL, D. K. & BURRUS, L. W. 2000. The Dynamic Expression Pattern of< i> frzb-1</i> Suggests Multiple Roles in Chick Development. *Developmental biology,* 217**,** 25-41.

BARD, J. & LAUDER, I. 1974. How well does Turing's theory of morphogenesis work? *Journal of Theoretical Biology,* 45**,** 501-531.

BARNA, M. & NISWANDER, L. 2007. Visualization of cartilage formation: insight into cellular properties of skeletal progenitors and chondrodysplasia syndromes. *Developmental cell,* 12**,** 931-941.

BARROTT, J. J., CASH, G. M., SMITH, A. P., BARROW, J. R. & MURTAUGH, L. C. 2011. Deletion of mouse Porcn blocks Wnt ligand secretion and reveals an ectodermal etiology of human focal dermal hypoplasia/Goltz syndrome. *Proceedings of the National Academy of Sciences,* 108**,** 12752-12757.

BARROW, J. R. < i> Wnt</i>/PCP signaling: A veritable polar star in establishing patterns of polarity in embryonic tissues. Seminars in cell & developmental biology, 2006. Elsevier, 185-193.

BARROW, J. R., THOMAS, K. R., BOUSSADIA-ZAHUI, O., MOORE, R., KEMLER, R., CAPECCHI, M. R. & MCMAHON, A. P. 2003. Ectodermal Wnt3/β-catenin signaling is required for the establishment and maintenance of the apical ectodermal ridge. *Genes & development,* 17**,** 394-409.

BASTIDA, M. F., SHETH, R. & ROS, M. A. 2009. A BMP-Shh negative-feedback loop restricts Shh expression during limb development. *Development,* 136**,** 3779-3789.

BAZZI, H., FANTAUZZO, K. A., RICHARDSON, G. D., JAHODA, C. A. & CHRISTIANO, A. M. 2007. The Wnt inhibitor, Dickkopf 4, is induced by canonical Wnt signaling during ectodermal appendage morphogenesis. *Dev Biol,* 305**,** 498-507.

BEALS, C. R., SHERIDAN, C. M., TURCK, C. W., GARDNER, P. & CRABTREE, G. R. 1997. Nuclear export of NF-ATc enhanced by glycogen synthase kinase-3. *Science,* 275**,** 1930-1933.

BÉNAZET, J.-D., BISCHOFBERGER, M., TIECKE, E., GONÇALVES, A., MARTIN, J. F., ZUNIGA, A., NAEF, F. & ZELLER, R. 2009. A self-regulatory system of interlinked signaling feedback loops controls mouse limb patterning. *Science,* 323**,** 1050-1053.

BÉNAZET, J.-D., PIGNATTI, E., NUGENT, A., UNAL, E., LAURENT, F. & ZELLER, R. 2012. Smad4 is required to induce digit ray primordia and to initiate the aggregation and differentiation of chondrogenic progenitors in mouse limb buds. *Development,* 139**,** 4250-4260.

BÉNAZET, J.-D. & ZELLER, R. 2009. Vertebrate limb development: moving from classical morphogen gradients to an integrated 4-dimensional patterning system. *Cold Spring Harbor perspectives in biology,* 1**,** a001339.

BEPPU, H., KAWABATA, M., HAMAMOTO, T., CHYTIL, A., MINOWA, O., NODA, T. & MIYAZONO, K. 2000. BMP type II receptor is required for gastrulation and early development of mouse embryos. *Developmental biology,* 221**,** 249-258.

BI, W., HUANG, W., WHITWORTH, D. J., DENG, J. M., ZHANG, Z., BEHRINGER, R. R. & DE CROMBRUGGHE, B. 2001. Haploinsufficiency of Sox9 results in defective cartilage primordia and premature skeletal mineralization. *Proceedings of the National Academy of Sciences,* 98**,** 6698-6703.

BIRCHMEIER, W., HÜLSKEN, J. & BEHRENS, J. 1994. Adherens junction proteins in tumour progression. *Cancer surveys,* 24**,** 129-140.

BOEHM, B., RAUTSCHKA, M., QUINTANA, L., RASPOPOVIC, J., JAN, Ž. & SHARPE, J. 2011. A landmark-free morphometric staging system for the mouse limb bud. *Development,* 138**,** 1227-1234.

BOOT, M. J., WESTERBERG, C. H., SANZ-EZQUERRO, J., COTTERELL, J., SCHWEITZER, R., TORRES, M. & SHARPE, J. 2008. In vitro whole-organ imaging: 4D quantification of growing mouse limb buds. *Nature methods,* 5**,** 609-612.

BOULET, A. M., MOON, A. M., ARENKIEL, B. R. & CAPECCHI, M. R. 2004. The roles of< i> Fgf4</i> and< i> Fgf8</i> in limb bud initiation and outgrowth. *Developmental biology,* 273**,** 361-372.

BOUTROS, M., PARICIO, N., STRUTT, D. I. & MLODZIK, M. 1998. Dishevelled Activates JNK and Discriminates between JNK Pathways in Planar Polarity and< i> wingless</i> Signaling. *Cell,* 94**,** 109-118.

BRAND-SABERI, B., MÜLLER, T., WILTING, J., CHRIST, B. & BIRCHMEIER, C. 1996. Scatter Factor/Hepatocyte Growth Factor (SF/HGF) Induces Emigration of Myogenic Cells at Interlimb Level< i> in Vivo</i>. *Developmental biology,* 179**,** 303-308.

BREMBECK, F. H., ROSÁRIO, M. & BIRCHMEIER, W. 2006. Balancing cell adhesion and Wnt signaling, the key role of β-catenin. *Current opinion in genetics & development,* 16**,** 51-59.

BREMBECK, F. H., SCHWARZ-ROMOND, T., BAKKERS, J., WILHELM, S., HAMMERSCHMIDT, M. & BIRCHMEIER, W. 2004. Essential role of BCL9-2 in the switch between β-catenin's adhesive and transcriptional functions. *Genes & development,* 18**,** 2225-2230.

BRIDGEWATER, L. C., LEFEBVRE, V. & DE CROMBRUGGHE, B. 1998. Chondrocyte-specific Enhancer Elements in the Col11a2Gene Resemble the Col2a1 Tissue-specific Enhancer. *Journal of Biological Chemistry,* 273**,** 14998-15006.

BRISCOE, J., CHEN, Y., JESSELL, T. M. & STRUHL, G. 2001. A hedgehog-insensitive form of patched provides evidence for direct long-range morphogen activity of sonic hedgehog in the neural tube. *Mol Cell,* 7**,** 1279-91.

BURKE, A. C., NELSON, C. E., MORGAN, B. A. & TABIN, C. 1995. Hox genes and the evolution of vertebrate axial morphology. *Development,* 121**,** 333-346.

BÜSCHER, D., BOSSE, B., HEYMER, J. & RÜTHER, U. 1997. Evidence for genetic control of Sonic hedgehog by Gli3 in mouse limb development. *Mechanisms of development,* 62**,** 175-182.

BUTTERFIELD, N. C., METZIS, V., MCGLINN, E., BRUCE, S. J., WAINWRIGHT, B. J. & WICKING, C. 2009. Patched 1 is a crucial determinant of asymmetry and digit number in the vertebrate limb. *Development,* 136**,** 3515-3524.

CAPDEVILA, J. & JOHNSON, R. L. 1998. Endogenous and Ectopic Expression of< i> noggin</i> Suggests a Conserved Mechanism for Regulation of BMP Function during Limb and Somite Patterning. *Developmental biology,* 197**,** 205-217.

CAPDEVILA, J., TSUKUI, T., ESTEBAN, C. R., ZAPPAVIGNA, V. & BELMONTE, J. C. I. 1999. Control of Vertebrate Limb Outgrowth by the Proximal Factor< i> Meis2</i> and Distal Antagonism of BMPs by Gremlin. *Molecular cell,* 4**,** 839-849.

CAPELLINI, T. D., DI GIACOMO, G., SALSI, V., BRENDOLAN, A., FERRETTI, E., SRIVASTAVA, D., ZAPPAVIGNA, V. & SELLERI, L. 2006. Pbx1/Pbx2 requirement for distal limb patterning is mediated by the hierarchical control of Hox gene spatial distribution and Shh expression. *Development,* 133**,** 2263-2273.

CARKETT, M. & LOGAN, M. 2011. 1, 2, 3: Counting the fingers on a chicken wing. *Genome biology,* 12**,** 130.
CASTETS, V. V., DULOS, E., BOISSONADE, J. & DE KEPPER, P. 1990. Experimental evidence of a sustained standing Turing-type nonequilibrium chemical pattern. *Phys Rev Lett,* 64**,** 2953-2956.
COHN, M. J. 2000. Developmental biology: Giving limbs a hand. *Nature,* 406**,** 953-954.
COHN, M. J., IZPISÚA-BELMONTE, J. C., ABUD, H., HEATH, J. K. & TICKLE, C. 1995. Fibroblast growth factors induce additional limb development from the flank of chick embryos. *Cell,* 80**,** 739-746.
COHN, M. J. & TICKLE, C. 1999. Developmental basis of limblessness and axial patterning in snakes. *Nature,* 399**,** 474-479.
COOPER, K. L., HU, J. K.-H., TEN BERGE, D., FERNANDEZ-TERAN, M., ROS, M. A. & TABIN, C. J. 2011. Initiation of proximal-distal patterning in the vertebrate limb by signals and growth. *Science,* 332**,** 1083-1086.
COOPER, K. L., SEARS, K. E., UYGUR, A., MAIER, J., BACZKOWSKI, K.-S., BROSNAHAN, M., ANTCZAK, D., SKIDMORE, J. A. & TABIN, C. J. 2014. Patterning and post-patterning modes of evolutionary digit loss in mammals. *Nature,* 511**,** 41-45.
COTTRILL, C. P., ARCHER, C. W. & WOLPERT, L. 1987. Cell sorting and chondrogenic aggregate formation in micromass culture. *Developmental biology,* 122**,** 503-515.
CROSSLEY, P. H. & MARTIN, G. R. 1995. The mouse Fgf8 gene encodes a family of polypeptides and is expressed in regions that direct outgrowth and patterning in the developing embryo. *Development,* 121**,** 439-451.
CRUCIAT, C.-M. & NIEHRS, C. 2013. Secreted and transmembrane wnt inhibitors and activators. *Cold Spring Harbor perspectives in biology,* 5**,** a015081.
CURRIER, N., CHEA, K., HLAVACOVA, M., SUSSMAN, D. J., SELDIN, D. C. & DOMINGUEZ, I. 2010. Dynamic expression of a LEF-EGFP Wnt reporter in mouse development and cancer. *genesis,* 48**,** 183-194.
CYGAN, J. A., JOHNSON, R. L. & MCMAHON, A. P. 1997. Novel regulatory interactions revealed by studies of murine limb pattern in Wnt-7a and En-1 mutants. *Development,* 124**,** 5021-5032.
CHEN, B., DODGE, M. E., TANG, W., LU, J., MA, Z., FAN, C.-W., WEI, S., HAO, W., KILGORE, J. & WILLIAMS, N. S. 2009. Small molecule–mediated disruption of Wnt-dependent signaling in tissue regeneration and cancer. *Nature chemical biology,* 5**,** 100-107.
CHEN, D., ZHAO, M. & MUNDY, G. R. 2004a. Bone morphogenetic proteins. *Growth factors,* 22**,** 233-241.
CHEN, H., LUN, Y., OVCHINNIKOV, D., KOKUBO, H., OBERG, K. C., PEPICELLI, C. V., CAN, L., LEE, B. & JOHNSON, R. L. 1998. Limb and kidney defects in Lmx1b mutant mice suggest an involvement of LMX1B in human nail patella syndrome. *Nature genetics,* 19**,** 51-55.
CHEN, M.-H., LI, Y.-J., KAWAKAMI, T., XU, S.-M. & CHUANG, P.-T. 2004b. Palmitoylation is required for the production of a soluble multimeric Hedgehog protein complex and long-range signaling in vertebrates. *Genes & development,* 18**,** 641-659.

CHEN, W., CHEN, M. & BARAK, L. S. 2010. Development of small molecules targeting the Wnt pathway for the treatment of colon cancer: a high-throughput screening approach. *Am J Physiol Gastrointest Liver Physiol,* 299**,** G293-300.
CHEN, Y. & SCHIER, A. F. 2002. Lefty proteins are long-range inhibitors of squint-mediated nodal signaling. *Curr Biol,* 12**,** 2124-8.
CHEN, Y. & STRUHL, G. 1996. Dual roles for patched in sequestering and transducing Hedgehog. *Cell,* 87**,** 553-63.
CHEVALLIER, A., KIENY, M. & MAUGER, A. 1977. Limb-somite relationship: origin of the limb musculature. *Journal of embryology and experimental morphology,* 41**,** 245-258.
CHIANG, C., LITINGTUNG, Y., HARRIS, M. P., SIMANDL, B. K., LI, Y., BEACHY, P. A. & FALLON, J. F. 2001. Manifestation of the limb prepattern: limb development in the absence of sonic hedgehog function. *Developmental biology,* 236**,** 421-435.
CHILD, C. M. 1941. Patterns and problems of development.
CHIMAL-MONROY, J. & DÍAZ, D. L. L. 1997. Differential effects of transforming growth factors beta 1, beta 2, beta 3 and beta 5 on chondrogenesis in mouse limb bud mesenchymal cells. *The International journal of developmental biology,* 41**,** 91-102.
CHRIST, B., JACOB, M. & JACOB, H. 1983. On the origin and development of the ventrolateral abdominal muscles in the avian embryo. *Anatomy and embryology,* 166**,** 87-101.
CHURCH, V. L. & FRANCIS-WEST, P. 2002. Wnt signalling during limb development. *International Journal of Developmental Biology,* 46**,** 927-936.
DA SILVA, S. M., GATES, P. B. & BROCKES, J. P. 2002. The newt ortholog of CD59 is implicated in proximodistal identity during amphibian limb regeneration. *Developmental cell,* 3**,** 547-555.
DAHN, R. D. & FALLON, J. F. 2000. Interdigital regulation of digit identity and homeotic transformation by modulated BMP signaling. *Science,* 289**,** 438-441.
DAY, T. F., GUO, X., GARRETT-BEAL, L. & YANG, Y. 2005. Wnt/β-catenin signaling in mesenchymal progenitors controls osteoblast and chondrocyte differentiation during vertebrate skeletogenesis. *Developmental cell,* 8**,** 739-750.
DE KEPPER, P. & EPSTEIN, I. R. 1982. Mechanistic study of oscillations and bistability in the Briggs-Rauscher reaction. *Journal of the American Chemical Society,* 104**,** 49-55.
DEGENKOLBE, E., KÖNIG, J., ZIMMER, J., WALTHER, M., REIßNER, C., NICKEL, J., PLÖGER, F., RASPOPOVIC, J., SHARPE, J. & DATHE, K. 2013. A GDF5 Point Mutation Strikes Twice-Causing BDA1 and SYNS2. *PLoS genetics,* 9**,** e1003846.
DELISE, A., FISCHER, L. & TUAN, R. 2000. Cellular interactions and signaling in cartilage development. *Osteoarthritis and cartilage,* 8**,** 309-334.
DELISE, A. M. & TUAN, R. S. 2002a. Alterations in the spatiotemporal expression pattern and function of N-Cadherin inhibit cellular condensation and chondrogenesis of limb mesenchymal cells in vitro. *Journal of cellular biochemistry,* 87**,** 342-359.
DELISE, A. M. & TUAN, R. S. 2002b. Analysis of N-cadherin function in limb mesenchymal chondrogenesis in vitro. *Developmental dynamics,* 225**,** 195-204.

DENKER, A. E., HAAS, A. R., NICOLL, S. B. & TUAN, R. S. 1999. Chondrogenic differentiation of murine C3H10T1/2 multipotential mesenchymal cells: I. Stimulation by bone morphogenetic protein-2 in high-density micromass cultures. *Differentiation,* 64**,** 67-76.

DEWULF, N., VERSCHUEREN, K., LONNOY, O., MOREN, A., GRIMSBY, S., VANDE SPIEGLE, K., MIYAZONO, K., HUYLEBROECK, D. & TEN DIJKE, P. 1995. Distinct spatial and temporal expression patterns of two type I receptors for bone morphogenetic proteins during mouse embryogenesis. *Endocrinology,* 136**,** 2652-2663.

DRIESCH 1893. Zur Verlagerung der Blastomeren des Echinideneies. *Anat Anz,* 8**,** 348–357.

DRIEVER, W. & NÜSSLEIN-VOLHARD, C. 1988. The< i> bicoid</i> protein determines position in the Drosophila embryo in a concentration-dependent manner. *Cell,* 54**,** 95-104.

DUCY, P. & KARSENTY, G. 2000. The family of bone morphogenetic proteins. *Kidney international,* 57**,** 2207-2214.

DUDLEY, A. T., LYONS, K. M. & ROBERTSON, E. J. 1995. A requirement for bone morphogenetic protein-7 during development of the mammalian kidney and eye. *Genes Dev,* 9**,** 2795-807.

DUDLEY, A. T., ROS, M. A. & TABIN, C. J. 2002. A re-examination of proximodistal patterning during vertebrate limb development. *Nature,* 418**,** 539-544.

DÜNKER, N., SCHMITT, K. & KRIEGLSTEIN, K. 2002. TGF-β is required for programmed cell death in interdigital webs of the developing mouse limb. *Mechanisms of development,* 113**,** 111-120.

DUPREZ, D. 2002. Signals regulating muscle formation in the limb during embryonic development. *International Journal of Developmental Biology,* 46**,** 915-926.

DUPREZ, D. M., KOSTAKOPOULOU, K., FRANCIS-WEST, P. H., TICKLE, C. & BRICKELL, P. M. 1996. Activation of Fgf-4 and HoxD gene expression by BMP-2 expressing cells in the developing chick limb. *Development,* 122**,** 1821-1828.

DUTKO, J. A. & MULLINS, M. C. 2011. SnapShot: BMP signaling in development. *Cell,* 145**,** 636-636. e2.

ECONOMOU, A. D., OHAZAMA, A., PORNTAVEETUS, T., SHARPE, P. T., KONDO, S., BASSON, M. A., GRITLI-LINDE, A., COBOURNE, M. T. & GREEN, J. B. 2012. Periodic stripe formation by a Turing mechanism operating at growth zones in the mammalian palate. *Nat Genet,* 44**,** 348-51.

EIVERS, E., FUENTEALBA, L. C. & DE ROBERTIS, E. 2008. Integrating positional information at the level of Smad1/5/8. *Current opinion in genetics & development,* 18**,** 304-310.

ESTEVE, P., MORCILLO, J. & BOVOLENTA, P. 2000. Early and dynamic expression of< i> cSfrp1</i> during chick embryo development. *Mechanisms of development,* 97**,** 217-221.

FALLON, J. F., LOPEZ, A., ROS, M. A., SAVAGE, M. P., OLWIN, B. B. & SIMANDL, B. K. 1994. FGF-2: apical ectodermal ridge growth signal for chick limb development. *Science,* 264**,** 104-107.

FARACH-CARSON, M. C., HECHT, J. T. & CARSON, D. D. 2005. Heparan sulfate proteoglycans: key players in cartilage biology. *Critical Reviews™ in Eukaryotic Gene Expression,* 15.

FENG, X.-H. & DERYNCK, R. 2005. Specificity and versatility in TGF-β signaling through Smads. *Annu. Rev. Cell Dev. Biol.,* 21**,** 659-693.
FERNANDEZ-TERAN, M. & ROS, M. A. 2008. The Apical Ectodermal Ridge: morphological aspects and signaling pathways. *International Journal of Developmental Biology,* 52**,** 857-871.
FERNÁNDEZ-TERÁN, M., HINCHLIFFE, J. & ROS, M. 2006. Birth and death of cells in limb development: a mapping study. *Developmental dynamics,* 235**,** 2521-2537.
FLINIAUX, I., MIKKOLA, M. L., LEFEBVRE, S. & THESLEFF, I. 2008. Identification of dkk4 as a target of Eda-A1/Edar pathway reveals an unexpected role of ectodysplasin as inhibitor of Wnt signalling in ectodermal placodes. *Dev Biol,* 320**,** 60-71.
FOSTER, J. W., DOMINGUEZ-STEGLICH, M. A., GUIOLI, S., KWOK, C., WELLER, P. A., STEVANOVIC, M., WEISSENBACH, J., MANSOUR, S., YOUNG, I. D. & GOODFELLOW, P. N. 1994. Campomelic dysplasia and autosomal sex reversal caused by mutations in an SRY-related gene. *Nature,* 372**,** 525-529.
FRANCIS-WEST, P. H., ANTONI, L. & ANAKWE, K. 2003. Regulation of myogenic differentiation in the developing limb bud. *Journal of anatomy,* 202**,** 69-81.
FRANCO, C. A., LIEBNER, S. & GERHARDT, H. 2009. Vascular morphogenesis: a Wnt for every vessel? *Current opinion in genetics & development,* 19**,** 476-483.
FROHNHÖFER, H. G. & NÜSSLEIN-VOLHARD, C. 1986. Organization of anterior pattern in the Drosophila embryo by the maternal gene bicoid. *Nature,* 324**,** 120-125.
GALLOWAY, J. L., DELGADO, I., ROS, M. A. & TABIN, C. J. 2009. A reevaluation of X-irradiation-induced phocomelia and proximodistal limb patterning. *Nature,* 460**,** 400-404.
GAMER, L. W., TSUJI, K., COX, K., CAPELO, L. P., LOWERY, J., BEPPU, H. & ROSEN, V. 2011. BMPR-II is dispensable for formation of the limb skeleton. *genesis,* 49**,** 719-724.
GANAN, Y., MACIAS, D., DUTERQUE-COQUILLAUD, M., ROS, M. & HURLE, J. 1996. Role of TGF beta s and BMPs as signals controlling the position of the digits and the areas of interdigital cell death in the developing chick limb autopod. *Development,* 122**,** 2349-2357.
GAO, B. 2012. Wnt regulation of planar cell polarity (PCP). *Curr. Top. Dev. Biol,* 101**,** 263-295.
GAO, B., SONG, H., BISHOP, K., ELLIOT, G., GARRETT, L., ENGLISH, M. A., ANDRE, P., ROBINSON, J., SOOD, R. & MINAMI, Y. 2011. Wnt signaling gradients establish planar cell polarity by inducing Vangl2 phosphorylation through Ror2. *Developmental cell,* 20**,** 163-176.
GAVIN, B. J., MCMAHON, J. A. & MCMAHON, A. P. 1990. Expression of multiple novel Wnt-1/int-1-related genes during fetal and adult mouse development. *Genes & development,* 4**,** 2319-2332.
GEETHA-LOGANATHAN, P., NIMMAGADDA, S., CHRIST, B., HUANG, R. & SCAAL, M. 2010. Ectodermal Wnt6 is an early negative regulator of limb chondrogenesis in the chicken embryo. *BMC developmental biology,* 10**,** 32.

GEETHA-LOGANATHAN, P., NIMMAGADDA, S., HUANG, R., SCAAL, M. & CHRIST, B. 2006. Expression pattern of BMPs during chick limb development. *Anatomy and embryology,* 211**,** 87-93.
GIERER, A. 1981. Generation of biological patterns and form: some physical, mathematical, and logical aspects. *Prog Biophys Mol Biol,* 37**,** 1-47.
GIERER, A. & MEINHARDT, H. 1972. A theory of biological pattern formation. *Kybernetik,* 12**,** 30-9.
GLANSDORF, P. & PRIGOGINE, I. 1971. Structure, stability and fluctuations. *Interscience, New York.*
GORSI, B. & STRINGER, S. E. 2007. Tinkering with heparan sulfate sulfation to steer development. *Trends in cell biology,* 17**,** 173-177.
GROS, J., HU, J. K.-H., VINEGONI, C., FERUGLIO, P. F., WEISSLEDER, R. & TABIN, C. J. 2010. WNT5A/JNK and FGF/MAPK pathways regulate the cellular events shaping the vertebrate limb bud. *Current Biology,* 20**,** 1993-2002.
GU, Z., NOMURA, M., SIMPSON, B. B., LEI, H., FEIJEN, A., VAN DEN EIJNDEN-VAN RAAIJ, J., DONAHOE, P. K. & LI, E. 1998. The type I activin receptor ActRIB is required for egg cylinder organization and gastrulation in the mouse. *Genes & development,* 12**,** 844-857.
GUO, Q., LOOMIS, C. & JOYNER, A. L. 2003. Fate map of mouse ventral limb ectoderm and the apical ectodermal ridge. *Developmental biology,* 264**,** 166-178.
GUO, X., DAY, T. F., JIANG, X., GARRETT-BEAL, L., TOPOL, L. & YANG, Y. 2004. Wnt/beta-catenin signaling is sufficient and necessary for synovial joint formation. *Genes Dev,* 18**,** 2404-17.
GUO, X. & WANG, X.-F. 2008. Signaling cross-talk between TGF-β/BMP and other pathways. *Cell research,* 19**,** 71-88.
HAAS, A. R. & TUAN, R. S. 1999. Chondrogenic differentiation of murine C3H10T1/2 multipotential mesenchymal cells: II. Stimulation by bone morphogenetic protein-2 requires modulation of N-cadherin expression and function. *Differentiation,* 64**,** 77-89.
HABAS, R., DAWID, I. B. & HE, X. 2003. Coactivation of Rac and Rho by Wnt/Frizzled signaling is required for vertebrate gastrulation. *Genes & development,* 17**,** 295-309.
HABAS, R., KATO, Y. & HE, X. 2001. Wnt/Frizzled activation of Rho regulates vertebrate gastrulation and requires a novel Formin homology protein Daam1. *Cell,* 107**,** 843-854.
HALL, B. K. & MIYAKE, T. 2000. All for one and one for all: condensations and the initiation of skeletal development. *Bioessays,* 22**,** 138-147.
HAMADA, H. 2012. In search of Turing in vivo: understanding Nodal and Lefty behavior. *Dev Cell,* 22**,** 911-2.
HAMADA, H., MENO, C., WATANABE, D. & SAIJOH, Y. 2002. Establishment of vertebrate left-right asymmetry. *Nat Rev Genet,* 3**,** 103-13.
HARFE, B. D., SCHERZ, P. J., NISSIM, S., TIAN, H., MCMAHON, A. P. & TABIN, C. J. 2004. Evidence for an expansion-based temporal Shh gradient in specifying vertebrate digit identities. *Cell,* 118**,** 517-528.
HARTMANN, C. & TABIN, C. J. 2001. Wnt-14 plays a pivotal role in inducing synovial joint formation in the developing appendicular skeleton. *Cell,* 104**,** 341-351.

HATSELL, S., ROWLANDS, T., HIREMATH, M. & COWIN, P. 2003. β-Catenin and Tcfs in mammary development and cancer. *Journal of mammary gland biology and neoplasia,* 8**,** 145-158.
HE, X., SEMENOV, M., TAMAI, K. & ZENG, X. 2004. LDL receptor-related proteins 5 and 6 in Wnt/β-catenin signaling: arrows point the way. *Development,* 131**,** 1663-1677.
HEADON, D. J. & PAINTER, K. J. 2009. Stippling the skin: Generation of anatomical periodicity by reaction-diffusion mechanisms. *Mathematical Modelling of Natural Phenomena,* 4**,** 83-102.
HEALY, C., UWANOGHO, D. & SHARPE, P. T. 1999. Regulation and role of Sox9 in cartilage formation. *Developmental dynamics,* 215**,** 69-78.
HEISENBERG, C.-P., TADA, M., RAUCH, G.-J., SAÚDE, L., CONCHA, M. L., GEISLER, R., STEMPLE, D. L., SMITH, J. C. & WILSON, S. W. 2000. Silberblick/Wnt11 mediates convergent extension movements during zebrafish gastrulation. *Nature,* 405**,** 76-81.
HELDIN, C.-H., MIYAZONO, K. & TEN DIJKE, P. 1997. TGF-β signalling from cell membrane to nucleus through SMAD proteins. *Nature,* 390**,** 465-471.
HENTSCHEL, H., GLIMM, T., GLAZIER, J. A. & NEWMAN, S. A. 2004. Dynamical mechanisms for skeletal pattern formation in the vertebrate limb. *PROCEEDINGS-ROYAL SOCIETY OF LONDON B,* 271**,** 1713-1722.
HILL, T. P., SPÄTER, D., TAKETO, M. M., BIRCHMEIER, W. & HARTMANN, C. 2005. Canonical Wnt/β-catenin signaling prevents osteoblasts from differentiating into chondrocytes. *Developmental cell,* 8**,** 727-738.
HILL, T. P., TAKETO, M. M., BIRCHMEIER, W. & HARTMANN, C. 2006. Multiple roles of mesenchymal β-catenin during murine limb patterning. *Development,* 133**,** 1219-1229.
HIRAMATSU, K., IWAI, T., YOSHIKAWA, H. & TSUMAKI, N. 2011. Expression of dominant negative TGF-β receptors inhibits cartilage formation in conditional transgenic mice. *Journal of bone and mineral metabolism,* 29**,** 493-500.
HOFFMAN, L. M., GARCHA, K., KARAMBOULAS, K., COWAN, M. F., DRYSDALE, L. M., HORTON, W. A. & UNDERHILL, T. M. 2006. BMP action in skeletogenesis involves attenuation of retinoid signaling. *The Journal of cell biology,* 174**,** 101-113.
HOGAN, B. 1996. Bone morphogenetic proteins: multifunctional regulators of vertebrate development. *Genes & development,* 10**,** 1580-1594.
HÖRSTADIUS, S. 1935. Uber die Determination im Verlaufe der Eiachse bei Seeigeln. *Pubbl. Staz. zool.,* 14**,** 251-479.
HU, H., HILTON, M. J., TU, X., YU, K., ORNITZ, D. M. & LONG, F. 2005. Sequential roles of Hedgehog and Wnt signaling in osteoblast development. *Development,* 132**,** 49-60.
HUISKEN, J., SWOGER, J., DEL BENE, F., WITTBRODT, J. & STELZER, E. H. 2004. Optical sectioning deep inside live embryos by selective plane illumination microscopy. *Science,* 305**,** 1007-1009.
INABA, M., YAMANAKA, H. & KONDO, S. 2012. Pigment pattern formation by contact-dependent depolarization. *Science,* 335**,** 677-677.
INGHAM, P. W. 1988. The molecular genetics of embryonic pattern formation in Drosophila. *Nature,* 335**,** 25-34.

INOUE, Y. & IMAMURA, T. 2008. Regulation of TGF-β family signaling by E3 ubiquitin ligases. *Cancer science,* 99**,** 2107-2112.
IVASCU, A. & KUBBIES, M. 2006. Rapid generation of single-tumor spheroids for high-throughput cell function and toxicity analysis. *J Biomol Screen,* 11**,** 922-32.
JAEGER, J. 2011. The gap gene network. *Cell Mol Life Sci,* 68**,** 243-74.
JAEGER, J. & MARTINEZ-ARIAS, A. 2009. Getting the measure of positional information. *PLoS biology,* 7**,** e1000081.
JHO, E. H., ZHANG, T., DOMON, C., JOO, C. K., FREUND, J. N. & COSTANTINI, F. 2002. Wnt/beta-catenin/Tcf signaling induces the transcription of Axin2, a negative regulator of the signaling pathway. *Mol Cell Biol,* 22**,** 1172-83.
JIANG, T.-X., YI, J.-R., YING, S.-Y. & CHUONG, C.-M. 1993. Activin enhances chondrogenesis of limb bud cells: stimulation of precartilaginous mesenchymal condensations and expression of NCAM. *Developmental biology,* 155**,** 545-557.
JIN, E. J., LEE, S. Y., CHOI, Y. A., JUNG, J. C., BANG, O. S. & KANG, S. S. 2006. BMP-2-enhanced chondrogenesis involves p38 MAPK-mediated down-regulation of Wnt-7a pathway. *Mol Cells,* 22**,** 353-9.
JIN, E. J., LEE, S. Y., JUNG, J. C., BANG, O. S. & KANG, S. S. 2008. TGF-β3 inhibits chondrogenesis of cultured chick leg bud mesenchymal cells via downregulation of connexin 43 and integrin β4. *Journal of cellular physiology,* 214**,** 345-353.
JOHNSTON, D. S., DRIEVER, W., BERLETH, T., RICHSTEIN, S. & NÜSSLEIN-VOLHARD, C. 1989. Multiple steps in the localization of bicoid RNA to the anterior pole of the Drosophila oocyte. *Development,* 107**,** 13-19.
JUNG, H. S., FRANCIS-WEST, P. H., WIDELITZ, R. B., JIANG, T. X., TING-BERRETH, S., TICKLE, C., WOLPERT, L. & CHUONG, C. M. 1998. Local inhibitory action of BMPs and their relationships with activators in feather formation: implications for periodic patterning. *Dev Biol,* 196**,** 11-23.
JURAND, A. 1965. Ultrastructural aspects of early development of the fore-limb buds in the chick and the mouse. *Proceedings of the Royal Society of London. Series B, Biological Sciences***,** 387-405.
KAARTINEN, V., VONCKEN, J. W., SHULER, C., WARBURTON, D., BU, D., HEISTERKAMP, N. & GROFFEN, J. 1995. Abnormal lung development and cleft palate in mice lacking TGF–β3 indicates defects of epithelial–mesenchymal interaction. *Nature genetics,* 11**,** 415-421.
KAK, A. C. & SLANEY, M. Principles of computerized tomographic imaging. 1988. *IEEE, New York.*
KARAMBOULAS, K., DRANSE, H. J. & UNDERHILL, T. M. 2010. Regulation of BMP-dependent chondrogenesis in early limb mesenchyme by TGFβ signals. *Journal of cell science,* 123**,** 2068-2076.
KARSENTY, G. 2003. The complexities of skeletal biology. *Nature,* 423**,** 316-318.
KAWAKAMI, Y., CAPDEVILA, J., BÜSCHER, D., ITOH, T., ESTEBAN, C. R. G. & BELMONTE, J. C. I. 2001. WNT signals control FGF-dependent limb initiation and AER induction in the chick embryo. *Cell,* 104**,** 891-900.
KAWAKAMI, Y., ISHIKAWA, T., SHIMABARA, M., TANDA, N., ENOMOTO-IWAMOTO, M., IWAMOTO, M., KUWANA, T., UEKI, A., NOJI, S. & NOHNO, T. 1996. BMP signaling during bone pattern determination in the developing limb. *Development,* 122**,** 3557-3566.

KELLER, R. 2002. Shaping the vertebrate body plan by polarized embryonic cell movements. *Science,* 298**,** 1950-1954.
KENGAKU, M., CAPDEVILA, J., RODRIGUEZ-ESTEBAN, C., DE LA PEÑA, J., JOHNSON, R. L., BELMONTE, J. C. I. & TABIN, C. J. 1998. Distinct WNT pathways regulating AER formation and dorsoventral polarity in the chick limb bud. *Science,* 280**,** 1274-1277.
KHOKHA, M. K., HSU, D., BRUNET, L. J., DIONNE, M. S. & HARLAND, R. M. 2003. Gremlin is the BMP antagonist required for maintenance of Shh and Fgf signals during limb patterning. *Nature genetics,* 34**,** 303-307.
KIECKER, C. & NIEHRS, C. 2001. A morphogen gradient of Wnt/β-catenin signalling regulates anteroposterior neural patterning in Xenopus. *Development,* 128**,** 4189-4201.
KMITA, M., TARCHINI, B., ZÀKÀNY, J., LOGAN, M., TABIN, C. J. & DUBOULE, D. 2005. Early developmental arrest of mammalian limbs lacking HoxA/HoxD gene function. *Nature,* 435**,** 1113-1116.
KNOBLOCH, J., SHAUGHNESSY, J. D. & RÜTHER, U. 2007. Thalidomide induces limb deformities by perturbing the Bmp/Dkk1/Wnt signaling pathway. *The FASEB Journal,* 21**,** 1410-1421.
KNOSP, W. M., SCOTT, V., BÄCHINGER, H. P. & STADLER, H. S. 2004. HOXA13 regulates the expression of bone morphogenetic proteins 2 and 7 to control distal limb morphogenesis. *Development,* 131**,** 4581-4592.
KOHN, A. D. & MOON, R. T. 2005. Wnt and calcium signaling: β-catenin-independent pathways. *Cell calcium,* 38**,** 439-446.
KONDO, S. & ASAI, R. 1995. A reaction-diffusion wave on the skin of the marine angelfish Pomacanthus. *Nature,* 376**,** 765-768.
KONDO, S. & MIURA, T. 2010. Reaction-diffusion model as a framework for understanding biological pattern formation. *Science,* 329**,** 1616-20.
KOSHIBA-TAKEUCHI, K., TAKEUCHI, J. K., ARRUDA, E. P., KATHIRIYA, I. S., MO, R., HUI, C.-C., SRIVASTAVA, D. & BRUNEAU, B. G. 2005. Cooperative and antagonistic interactions between Sall4 and Tbx5 pattern the mouse limb and heart. *Nature genetics,* 38**,** 175-183.
KRAUS, P., FRAIDENRAICH, D. & LOOMIS, C. A. 2001. Some distal limb structures develop in mice lacking Sonic hedgehog signaling. *Mechanisms of development,* 100**,** 45-58.
KÜHL, M., SHELDAHL, L. C., PARK, M., MILLER, J. R. & MOON, R. T. 2000. The Wnt/Ca< sup> 2+</sup> pathway: a new vertebrate Wnt signaling pathway takes shape. *Trends in genetics,* 16**,** 279-283.
KUMAR, A., GATES, P. B. & BROCKES, J. P. 2007. Positional identity of adult stem cells in salamander limb regeneration. *Comptes rendus biologies,* 330**,** 485-490.
KUO, C. K., PETERSEN, B. C. & TUAN, R. S. 2008. Spatiotemporal protein distribution of TGF-βs, their receptors, and extracellular matrix molecules during embryonic tendon development. *Developmental Dynamics,* 237**,** 1477-1489.
LADHER, R., CHURCH, V., ALLEN, S., ROBSON, L., ABDELFATTAH, A., BROWN, N., HATTERSLEY, G., ROSEN, V., LUYTEN, F. & DALE, L. 2000. Cloning and Expression of the Wnt Antagonists< i> Sfrp-2</i> and< i> Frzb</i> during Chick Development. *Developmental biology,* 218**,** 183-198.

LE, Y. & SAUER, B. 2000. Conditional gene knockout using cre recombinase. *Developmental Biology Protocols: Volume II.* Springer.
LEE, S. M., TOLE, S., GROVE, E. & MCMAHON, A. P. 2000. A local Wnt-3a signal is required for development of the mammalian hippocampus. *Development,* 127**,** 457-67.
LEFEBVRE, V., HUANG, W., HARLEY, V. R., GOODFELLOW, P. N. & DE CROMBRUGGHE, B. 1997. SOX9 is a potent activator of the chondrocyte-specific enhancer of the pro alpha1 (II) collagen gene. *Molecular and cellular biology,* 17**,** 2336-2346.
LEONARD, C. M., FULD, H. M., FRENZ, D. A., DOWNIE, S. A., MASSAGUE, J. & NEWMAN, S. A. 1991. Role of transforming growth factor-beta in chondrogenic pattern formation in the embryonic limb: stimulation of mesenchymal condensation and fibronectin gene expression by exogenenous TGF-beta and evidence for endogenous TGF-beta-like activity. *Dev Biol,* 145**,** 99-109.
LEPOURCELET, M., CHEN, Y.-N. P., FRANCE, D. S., WANG, H., CREWS, P., PETERSEN, F., BRUSEO, C., WOOD, A. W. & SHIVDASANI, R. A. 2004. Small-molecule antagonists of the oncogenic Tcf/β-catenin protein complex. *Cancer cell,* 5**,** 91-102.
LESCHER, B., HAENIG, B. & KISPERT, A. 1998. sFRP-2 is a target of the Wnt-4 signaling pathway in the developing metanephric kidney. *Dev Dyn,* 213**,** 440-51.
LEWANDOSKI, M., SUN, X. & MARTIN, G. R. 2000. Fgf8 signalling from the AER is essential for normal limb development. *Nature genetics,* 26**,** 460-463.
LI, L., YUAN, H., WEAVER, C. D., MAO, J., FARR III, G. H., SUSSMAN, D. J., JONKERS, J., KIMELMAN, D. & WU, D. 1999. Axin and Frat1 interact with dvl and GSK, bridging Dvl to GSK in Wnt-mediated regulation of LEF-1. *The EMBO journal,* 18**,** 4233-4240.
LI, Y., ZHANG, H., LITINGTUNG, Y. & CHIANG, C. 2006. Cholesterol modification restricts the spread of Shh gradient in the limb bud. *Proceedings of the National Academy of Sciences,* 103**,** 6548-6553.
LITINGTUNG, Y., DAHN, R. D., LI, Y., FALLON, J. F. & CHIANG, C. 2002. Shh and Gli3 are dispensable for limb skeleton formation but regulate digit number and identity. *Nature,* 418**,** 979-983.
LOGAN, C., HORNBRUCH, A., CAMPBELL, I. & LUMSDEN, A. 1997. The role of Engrailed in establishing the dorsoventral axis of the chick limb. *Development,* 124**,** 2317-2324.
LOGAN, C. Y. & NUSSE, R. 2004. The Wnt signaling pathway in development and disease. *Annu. Rev. Cell Dev. Biol.,* 20**,** 781-810.
LOGAN, M., MARTIN, J. F., NAGY, A., LOBE, C., OLSON, E. N. & TABIN, C. J. 2002. Expression of Cre Recombinase in the developing mouse limb bud driven by a Prxl enhancer. *Genesis,* 33**,** 77-80.
LONG, F., CHUNG, U.-I., OHBA, S., MCMAHON, J., KRONENBERG, H. M. & MCMAHON, A. P. 2004. Ihh signaling is directly required for the osteoblast lineage in the endochondral skeleton. *Development,* 131**,** 1309-1318.
LOOMIS, C. A., HARRIS, E., MICHAUD, J., WURST, W., HANKS, M. & JOYNER, A. L. 1996. The mouse Engrailed-1 gene and ventral limb patterning.
LOOMIS, C. A., KIMMEL, R. A., TONG, C.-X., MICHAUD, J. & JOYNER, A. L. 1998. Analysis of the genetic pathway leading to formation of ectopic apical

ectodermal ridges in mouse Engrailed-1 mutant limbs. *Development,* 125**,** 1137-1148.
LOPEZ-RIOS, J., DUCHESNE, A., SPEZIALE, D., ANDREY, G., PETERSON, K. A., GERMANN, P., UNAL, E., LIU, J., FLORIOT, S., BARBEY, S., GALLARD, Y., MULLER-GERBL, M., COURTNEY, A. D., KLOPP, C., RODRIGUEZ, S., IVANEK, R., BEISEL, C., WICKING, C., IBER, D., ROBERT, B., MCMAHON, A. P., DUBOULE, D. & ZELLER, R. 2014. Attenuated sensing of SHH by Ptch1 underlies evolution of bovine limbs. *Nature,* 511**,** 46-51.
LOPEZ-RIOS, J., SPEZIALE, D., ROBAY, D., SCOTTI, M., OSTERWALDER, M., NUSSPAUMER, G., GALLI, A., HOLLÄNDER, G. A., KMITA, M. & ZELLER, R. 2012. GLI3 constrains digit number by controlling both progenitor proliferation and BMP-dependent exit to chondrogenesis. *Developmental cell,* 22**,** 837-848.
LORDA-DIEZ, C. I., MONTERO, J. A., DIAZ-MENDOZA, M. J., GARCIA-PORRERO, J. A. & HURLE, J. M. 2011. Defining the earliest transcriptional steps of chondrogenic progenitor specification during the formation of the digits in the embryonic limb. *PloS one,* 6**,** e24546.
LORDA-DIEZ, C. I., MONTERO, J. A., GARCIA-PORRERO, J. A. & HURLE, J. M. 2010. Tgfβ2 and 3 are coexpressed with their extracellular regulator Ltbp1 in the early limb bud and modulate mesodermal outgrowth and BMP signaling in chicken embryos. *BMC developmental biology,* 10**,** 69.
LORDA-DIEZ, C. I., MONTERO, J. A., MARTINEZ-CUE, C., GARCIA-PORRERO, J. A. & HURLE, J. M. 2009. Transforming growth factors beta coordinate cartilage and tendon differentiation in the developing limb mesenchyme. *J Biol Chem,* 284**,** 29988-96.
LORENZO, C., FRONGIA, C., JORAND, R., FEHRENBACH, J., WEISS, P., MAANDHUI, A., GAY, G., DUCOMMUN, B. & LOBJOIS, V. 2011. Live cell division dynamics monitoring in 3D large spheroid tumor models using light sheet microscopy. *Cell division,* 6**,** 22.
LU, P., MINOWADA, G. & MARTIN, G. R. 2006. Increasing Fgf4 expression in the mouse limb bud causes polysyndactyly and rescues the skeletal defects that result from loss of Fgf8 function. *Development,* 133**,** 33-42.
LUO, Y., KOSTETSKII, I. & RADICE, G. L. 2005. N-cadherin is not essential for limb mesenchymal chondrogenesis. *Developmental dynamics,* 232**,** 336-344.
MARCON, L. & SHARPE, J. 2012. Turing patterns in development: what about the horse part? *Current opinion in genetics & development,* 22**,** 578-584.
MARIANI, F. V., AHN, C. P. & MARTIN, G. R. 2008. Genetic evidence that FGFs have an instructive role in limb proximal–distal patterning. *Nature,* 453**,** 401-405.
MARIANI, F. V. & MARTIN, G. R. 2003. Deciphering skeletal patterning: clues from the limb. *Nature,* 423**,** 319-325.
MARIGO, V., DAVEY, R. A., ZUO, Y., CUNNINGHAM, J. M. & TABIN, C. J. 1996. Biochemical evidence that patched is the Hedgehog receptor. *Nature,* 384**,** 176-9.
MARLOW, F., TOPCZEWSKI, J., SEPICH, D. & SOLNICA-KREZEL, L. 2002. Zebrafish Rho kinase 2 acts downstream of Wnt11 to mediate cell polarity and effective convergence and extension movements. *Current biology,* 12**,** 876-884.

MARTIN, G. R. 1998. The roles of FGFs in the early development of vertebrate limbs. *Genes & Development,* 12**,** 1571-1586.
MASSAGUE, J. 1990. The transforming growth factor-beta family. *Annual review of cell biology,* 6**,** 597-641.
MASSAGUÉ, J. 2012. TGFβ signalling in context. *Nature reviews Molecular cell biology,* 13**,** 616-630.
MATZUK, M. M., KUMAR, T. R. & BRADLEY, A. 1995a. Different phenotypes for mice deficient in either activins or activin receptor type II.
MATZUK, M. M., KUMAR, T. R., VASSALLI, A., BICKENBACH, J. R., ROOP, D. R., JAENISCH, R. & BRADLEY, A. 1995b. Functional analysis of activins during mammalian development.
MEINHARDT, H. 2012. Turing's theory of morphogenesis of 1952 and the subsequent discovery of the crucial role of local self-enhancement and long-range inhibition. *Interface Focus,* 2**,** 407-16.
MENSHYKAU, D., KRAEMER, C. & IBER, D. 2012. Branch mode selection during early lung development. *PLoS computational biology,* 8**,** e1002377.
MERCADER, N., LEONARDO, E., AZPIAZU, N., SERRANO, A., MORATA, G., MARTÍNEZ-A, C. & TORRES, M. 1999. Conserved regulation of proximodistal limb axis development by Meis1/Hth. *Nature,* 402**,** 425-429.
MERCADER, N., LEONARDO, E., PIEDRA, M. E., MARTINEZ-A, C., ROS, M. & TORRES, M. 2000. Opposing RA and FGF signals control proximodistal vertebrate limb development through regulation of Meis genes. *Development,* 127**,** 3961-3970.
MERINO, R., GAÑAN, Y., MACIAS, D., ECONOMIDES, A. N., SAMPATH, K. T. & HURLE, J. M. 1998. Morphogenesis of digits in the avian limb is controlled by FGFs, TGFβs, and noggin through BMP signaling. *Developmental biology,* 200**,** 35-45.
MERINO, R., MACIAS, D., GANAN, Y., RODRIGUEZ-LEON, J., ECONOMIDES, A., RODRIGUEZ-ESTEBAN, C., IZPISUA-BELMONTE, J. & HURLE, J. 1999. Control of digit formation by activin signalling. *Development,* 126**,** 2161-2170.
MICHON, F., FOREST, L., COLLOMB, E., DEMONGEOT, J. & DHOUAILLY, D. 2008. BMP2 and BMP7 play antagonistic roles in feather induction. *Development,* 135**,** 2797-805.
MICHOS, O., PANMAN, L., VINTERSTEN, K., BEIER, K., ZELLER, R. & ZUNIGA, A. 2004. Gremlin-mediated BMP antagonism induces the epithelial-mesenchymal feedback signaling controlling metanephric kidney and limb organogenesis. *Development,* 131**,** 3401-3410.
MILAIRE, J. 1974. *Histochemical aspects of organogenesis in vertrebrates. Part I. The skeletal system. Limb morphogenesis. The sense organs.,* Stuttgart, Gustav Fischer Verlag.
MILLAN, F. A., DENHEZ, F., KONDAIAH, P. & AKHURST, R. J. 1991. Embryonic gene expression patterns of TGF beta 1, beta 2 and beta 3 suggest different developmental functions in vivo. *Development,* 111**,** 131-143.
MIN, H., DANILENKO, D. M., SCULLY, S. A., BOLON, B., RING, B. D., TARPLEY, J. E., DEROSE, M. & SIMONET, W. S. 1998. Fgf-10 is required for both limb and lung development and exhibits striking functional similarity to Drosophila branchless. *Genes & development,* 12**,** 3156-3161.

MISHINA, Y., CROMBIE, R., BRADLEY, A. & BEHRINGER, R. R. 1999. Multiple roles for activin-like kinase-2 signaling during mouse embryogenesis. *Developmental biology,* 213**,** 314-326.
MISHINA, Y., SUZUKI, A., UENO, N. & BEHRINGER, R. R. 1995. Bmpr encodes a type I bone morphogenetic protein receptor that is essential for gastrulation during mouse embryogenesis. *Genes & Development,* 9**,** 3027-3037.
MIURA, T. & SHIOTA, K. 2000. TGFβ2 acts as an "Activator" molecule in reaction-diffusion model and is involved in cell sorting phenomenon in mouse limb micromass culture. *Developmental Dynamics,* 217**,** 241-249.
MIURA, T. & SHIOTA, K. 2002. Depletion of FGF acts as a lateral inhibitory factor in lung branching morphogenesis in vitro. *Mechanisms of development,* 116**,** 29-38.
MIURA, T., SHIOTA, K., MORRISS-KAY, G. & MAINI, P. K. 2006. Mixed-mode pattern in< i> Doublefoot</i> mutant mouse limb—Turing reaction–diffusion model on a growing domain during limb development. *Journal of theoretical biology,* 240**,** 562-573.
MONTAVON, T., LE GARREC, J.-F., KERSZBERG, M. & DUBOULE, D. 2008. Modeling Hox gene regulation in digits: reverse collinearity and the molecular origin of thumbness. *Genes & development,* 22**,** 346-359.
MONTEIRO, R. M., DE SOUSA LOPES, S. M., BIALECKA, M., DE BOER, S., ZWIJSEN, A. & MUMMERY, C. L. 2008. Real time monitoring of BMP Smads transcriptional activity during mouse development. *Genesis,* 46**,** 335-46.
MONTERO, J. A., LORDA-DIEZ, C. I., GAÑAN, Y., MACIAS, D. & HURLE, J. M. 2008. Activin/TGFβ and BMP crosstalk determines digit chondrogenesis. *Developmental biology,* 321**,** 343-356.
MOON, A. M. & CAPECCHI, M. R. 2000. Fgf8 is required for outgrowth and patterning of the limbs. *Nature genetics,* 26**,** 455-459.
MOU, C., PITEL, F., GOURICHON, D., VIGNOLES, F., TZIKA, A., TATO, P., YU, L., BURT, D. W., BED'HOM, B., TIXIER-BOICHARD, M., PAINTER, K. J. & HEADON, D. J. 2011. Cryptic patterning of avian skin confers a developmental facility for loss of neck feathering. *PLoS Biol,* 9**,** e1001028.
MOUSTAKAS, A. & HELDIN, C.-H. 2005. Non-Smad TGF-β signals. *Journal of cell science,* 118**,** 3573-3584.
MUELLER, T. D. & NICKEL, J. 2012. Promiscuity and specificity in BMP receptor activation. *FEBS letters,* 586**,** 1846-1859.
MULLER, P., ROGERS, K. W., JORDAN, B. M., LEE, J. S., ROBSON, D., RAMANATHAN, S. & SCHIER, A. F. 2012. Differential diffusivity of Nodal and Lefty underlies a reaction-diffusion patterning system. *Science,* 336**,** 721-4.
MURPHY, L. L. S. & HUGHES, C. C. 2002. Endothelial cells stimulate T cell NFAT nuclear translocation in the presence of cyclosporin A: involvement of the wnt/glycogen synthase kinase-3β pathway. *The Journal of Immunology,* 169**,** 3717-3725.
MURRAY, J. D. 2012. Vignettes from the field of mathematical biology: the application of mathematics to biology and medicine. *Interface Focus,* 2**,** 397-406.
NAGORCKA, B. N. 1983. Evidence for a reaction-diffusion system as a mechanism controlling mammalian hair growth. *Biosystems,* 16**,** 323-32.
NAGORCKA, B. N. & MOONEY, J. R. 1985. The role of a reaction-diffusion system in the initiation of primary hair follicles. *J Theor Biol,* 114**,** 243-72.

NAGY, A. 2000. Cre recombinase: the universal reagent for genome tailoring. *genesis,* 26**,** 99-109.
NAKAMASU, A., TAKAHASHI, G., KANBE, A. & KONDO, S. 2009. Interactions between zebrafish pigment cells responsible for the generation of Turing patterns. *Proceedings of the National Academy of Sciences,* 106**,** 8429-8434.
NAKAMURA, T., MINE, N., NAKAGUCHI, E., MOCHIZUKI, A., YAMAMOTO, M., YASHIRO, K., MENO, C. & HAMADA, H. 2006. Generation of robust left-right asymmetry in the mouse embryo requires a self-enhancement and lateral-inhibition system. *Dev Cell,* 11**,** 495-504.
NEWMAN, S. A. 1996. Sticky fingers: Hox genes and cell adhesion in vertebrate limb development. *Bioessays,* 18**,** 171-174.
NEWMAN, S. A. & FRISCH, H. 1979. Dynamics of skeletal pattern formation in developing chick limb. *Science,* 205**,** 662-668.
NG, L.-J., WHEATLEY, S., MUSCAT, G. E., CONWAY-CAMPBELL, J., BOWLES, J., WRIGHT, E., BELL, D. M., TAM, P. P., CHEAH, K. S. & KOOPMAN, P. 1997. SOX9 binds DNA, activates transcription, and coexpresses with type II collagen during chondrogenesis in the mouse. *Developmental biology,* 183**,** 108-121.
NICOLIS, G. & PRIGOGINE, I. 1977. *Self-organization in nonequilibrium systems,* Wiley, New York.
NIEHRS, C. 2010. On growth and form: a Cartesian coordinate system of Wnt and BMP signaling specifies bilaterian body axes. *Development,* 137**,** 845-857.
NISHIMATSU, S.-I. & THOMSEN, G. H. 1998. Ventral mesoderm induction and patterning by bone morphogenetic protein heterodimers in< i> Xenopus</i> embryos. *Mechanisms of development,* 74**,** 75-88.
NISSIM, S., HASSO, S. M., FALLON, J. F. & TABIN, C. J. 2006. Regulation of< i> Gremlin</i> expression in the posterior limb bud. *Developmental biology,* 299**,** 12-21.
NISWANDER, L. 2002. Interplay between the molecular signals that control vertebrate limb development. *International Journal of Developmental Biology,* 46**,** 877-882.
NISWANDER, L., TICKLE, C., VOGEL, A., BOOTH, I. & MARTIN, G. R. 1993. FGF-4 replaces the apical ectodermal ridge and directs outgrowth and patterning of the limb. *Cell,* 75**,** 579-587.
NOMURA, M. & LI, E. 1998. Smad2 role in mesoderm formation, left–right patterning and craniofacial development. *Nature,* 393**,** 786-790.
NUSSE, R. 2005. Wnt signaling in disease and in development. *Cell research,* 15**,** 28-32.
OBERLENDER, S. A. & TUAN, R. S. 1994a. Expression and functional involvement of N-cadherin in embryonic limb chondrogenesis. *Development,* 120**,** 177-187.
OBERLENDER, S. A. & TUAN, R. S. 1994b. Spatiotemporal profile of N-cadherin expression in the developing limb mesenchyme. *Cell Communication and Adhesion,* 2**,** 521-537.
OH, C. D., CHANG, S. H., YOON, Y. M., LEE, S. J., LEE, Y. S., KANG, S. S. & CHUN, J. S. 2000. Opposing role of mitogen-activated protein kinase subtypes, erk-1/2 and p38, in the regulation of chondrogenesis of mesenchymes. *J Biol Chem,* 275**,** 5613-9.

OH, S. P., YEO, C.-Y., LEE, Y., SCHREWE, H., WHITMAN, M. & LI, E. 2002. Activin type IIA and IIB receptors mediate Gdf11 signaling in axial vertebral patterning. *Genes & development,* 16**,** 2749-2754.

OLSSON, L. 2007. A clash of traditions: the history of comparative and experimental embryology in Sweden as exemplified by the research of Gosta Jagersten and Sven Horstadius. *Theory Biosci,* 126**,** 117-29.

OVCHINNIKOV, D. A., SELEVER, J., WANG, Y., CHEN, Y.-T., MISHINA, Y., MARTIN, J. F. & BEHRINGER, R. R. 2006. BMP receptor type IA in limb bud mesenchyme regulates distal outgrowth and patterning. *Developmental biology,* 295**,** 103-115.

PAINTER, K., HUNT, G., WELLS, K., JOHANSSON, J. & HEADON, D. 2012. Towards an integrated experimental–theoretical approach for assessing the mechanistic basis of hair and feather morphogenesis. *Interface focus***,** rsfs20110122.

PAJNI-UNDERWOOD, S., WILSON, C. P., ELDER, C., MISHINA, Y. & LEWANDOSKI, M. 2007. BMP signals control limb bud interdigital programmed cell death by regulating FGF signaling. *Development,* 134**,** 2359-2368.

PAN, Q., YU, Y., CHEN, Q., LI, C., WU, H., WAN, Y., MA, J. & SUN, F. 2008. Sox9, a key transcription factor of bone morphogenetic protein-2-induced chondrogenesis, is activated through BMP pathway and a CCAAT box in the proximal promoter. *Journal of cellular physiology,* 217**,** 228-241.

PANDA, D. K., MIAO, D., LEFEBVRE, V., HENDY, G. N. & GOLTZMAN, D. 2001. The transcription factor SOX9 regulates cell cycle and differentiation genes in chondrocytic CFK2 cells. *Journal of Biological Chemistry,* 276**,** 41229-41236.

PANMAN, L., GALLI, A., LAGARDE, N., MICHOS, O., SOETE, G., ZUNIGA, A. & ZELLER, R. 2006. Differential regulation of gene expression in the digit forming area of the mouse limb bud by SHH and gremlin 1/FGF-mediated epithelial-mesenchymal signalling. *Development,* 133**,** 3419-28.

PARR, B. A., AVERY, E. J., CYGAN, J. A. & MCMAHON, A. P. 1998. The Classical Mouse Mutant Postaxial Hemimelia Results from a Mutation in the< i> Wnt</i> 7a Gene. *Developmental biology,* 202**,** 228-234.

PARR, B. A. & MCMAHON, A. P. 1995. Dorsalizing signal Wnt-7a required for normal polarity of D–V and A–P axes of mouse limb. *Nature,* 374**,** 350-353.

PARR, B. A., SHEA, M. J., VASSILEVA, G. & MCMAHON, A. P. 1993. Mouse Wnt genes exhibit discrete domains of expression in the early embryonic CNS and limb buds. *Development,* 119**,** 247-261.

PEIFER, M. & POLAKIS, P. 2000. Wnt signaling in oncogenesis and embryogenesis--a look outside the nucleus. *Science,* 287**,** 1606-1609.

PESCITELLI JR, M. J. & STOCUM, D. L. 1981. Nonsegmental organization of positional information in regenerating< i> Ambystoma</i> limbs. *Developmental biology,* 82**,** 69-85.

PINSON, K. I., BRENNAN, J., MONKLEY, S., AVERY, B. J. & SKARNES, W. C. 2000. An LDL-receptor-related protein mediates Wnt signalling in mice. *Nature,* 407**,** 535-538.

PIZETTE, S., ABATE-SHEN, C. & NISWANDER, L. 2001. BMP controls proximodistal outgrowth, via induction of the apical ectodermal ridge, and dorsoventral patterning in the vertebrate limb. *Development,* 128**,** 4463-4474.

PIZETTE, S. & NISWANDER, L. 2000. BMPs are required at two steps of limb chondrogenesis: formation of prechondrogenic condensations and their differentiation into chondrocytes. *Developmental biology,* 219**,** 237-249.
PRIGOGINE, I. & LEFEVER, R. 1968. Symmetry Breaking Instabilities in Dissipative Systems. II. *The Journal of Chemical Physics,* 48**,** 1695-1700.
PRYCE, B. A., WATSON, S. S., MURCHISON, N. D., STAVEROSKY, J. A., DÜNKER, N. & SCHWEITZER, R. 2009. Recruitment and maintenance of tendon progenitors by TGFβ signaling are essential for tendon formation. *Development,* 136**,** 1351-1361.
REINITZ, J., KOSMAN, D., VANARIO-ALONSO, C. E. & SHARP, D. H. 1998. Stripe forming architecture of the gap gene system. *Dev Genet,* 23**,** 11-27.
REVEST, J.-M., SPENCER-DENE, B., KERR, K., DE MOERLOOZE, L., ROSEWELL, I. & DICKSON, C. 2001. Fibroblast Growth Factor Receptor 2-IIIb Acts Upstream of< i> Shh</i> and< i> Fgf4</i> and Is Required for Limb Bud Maintenance but Not for the Induction of< i> Fgf8</i>,< i> Fgf10</i>,< i> Msx1,</i> or< i> Bmp4</i>. *Developmental biology,* 231**,** 47-62.
RIDDLE, R. D., ENSINI, M., NELSON, C., TSUCHIDA, T., JESSELL, T. M. & TABIN, C. 1995. Induction of the LIM homeobox gene< i> Lmx1</i> by WNT6a establishes dorsoventral pattern in the vertebrate limb. *Cell,* 83**,** 631-640.
RIDDLE, R. D., JOHNSON, R. L., LAUFER, E. & TABIN, C. 1993. < i> Sonic hedgehog</i> mediates the polarizing activity of the ZPA. *Cell,* 75**,** 1401-1416.
ROARK, E. F. & GREER, K. 1994. Transforming growth factor-β and bone morphogenetic protein-2 act by distinct mechanisms to promote chick limb cartilage differentiation in vitro. *Developmental dynamics,* 200**,** 103-116.
ROBERT, B. 2007. Bone morphogenetic protein signaling in limb outgrowth and patterning. *Development, growth & differentiation,* 49**,** 455-468.
ROS, M. A., DAHN, R. D., FERNANDEZ-TERAN, M., RASHKA, K., CARUCCIO, N. C., HASSO, S. M., BITGOOD, J. J., LANCMAN, J. J. & FALLON, J. F. 2003. The chick oligozeugodactyly (ozd) mutant lacks sonic hedgehog function in the limb. *Development,* 130**,** 527-537.
ROS, M. A., LÓPEZ-MARTÍNEZ, A., SIMANDL, B. K., RODRIGUEZ, C., BELMONTE, J. I., DAHN, R. & FALLON, J. F. 1996. The limb field mesoderm determines initial limb bud anteroposterior asymmetry and budding independent of sonic hedgehog or apical ectodermal gene expressions. *Development,* 122**,** 2319-2330.
ROSELLÓ-DÍEZ, A., ROS, M. A. & TORRES, M. 2011. Diffusible signals, not autonomous mechanisms, determine the main proximodistal limb subdivision. *Science,* 332**,** 1086-1088.
RUBIN, L. & SAUNDERS JR, J. W. 1972. Ectodermal-mesodermal interactions in the growth of limb buds in the chick embryo: constancy and temporal limits of the ectodermal induction. *Developmental biology,* 28**,** 94-112.
RUDNICKI, J. A. & BROWN, A. 1997. Inhibition of Chondrogenesis by< i> Wnt</i> Gene Expression< i> in Vivo</i> and< i> in Vitro</i>. *Developmental biology,* 185**,** 104-118.
SAHOTA, A. P. & DHOOT, G. K. 2009. A novel SULF1 splice variant inhibits Wnt signalling but enhances angiogenesis by opposing SULF1 activity. *Experimental cell research,* 315**,** 2752-2764.

SAIJOH, Y., ADACHI, H., SAKUMA, R., YEO, C. Y., YASHIRO, K., WATANABE, M., HASHIGUCHI, H., MOCHIDA, K., OHISHI, S., KAWABATA, M., MIYAZONO, K., WHITMAN, M. & HAMADA, H. 2000. Left-right asymmetric expression of lefty2 and nodal is induced by a signaling pathway that includes the transcription factor FAST2. *Mol Cell,* 5**,** 35-47.

SALSI, V., VIGANO, M. A., COCCHIARELLA, F., MANTOVANI, R. & ZAPPAVIGNA, V. 2008. Hoxd13 binds< i> in</i>< i> vivo</i> and regulates the expression of genes acting in key pathways for early limb and skeletal patterning. *Developmental biology,* 317**,** 497-507.

SANDERS, T. A., LLAGOSTERA, E. & BARNA, M. 2013. Specialized filopodia direct long-range transport of SHH during vertebrate tissue patterning. *Nature,* 497**,** 628-632.

SANFORD, L. P., ORMSBY, I., GITTENBERGER-DE GROOT, A. C., SARIOLA, H., FRIEDMAN, R., BOIVIN, G. P., CARDELL, E. L. & DOETSCHMAN, T. 1997. TGFbeta2 knockout mice have multiple developmental defects that are non-overlapping with other TGFbeta knockout phenotypes. *Development,* 124**,** 2659-2670.

SANZ-EZQUERRO, J. J. & TICKLE, C. 2003. Fgf signaling controls the number of phalanges and tip formation in developing digits. *Current biology,* 13**,** 1830-1836.

SAUNDERS, J. W. 1948. The proximo-distal sequence of origin of the parts of the chick wing and the role of the ectoderm. *Journal of Experimental Zoology,* 108**,** 363-403.

SAUNDERS, J. W. & GASSELING, M. T. 1968. Ectodermal-mesenchymal interaction in the origin of limb symmetry. *EpithelialMesenchymal Interaction,* 78–97.

SCOTTI, M. & KMITA, M. 2012. Recruitment of 5′ Hoxa genes in the allantois is essential for proper extra-embryonic function in placental mammals. *Development,* 139**,** 731-739.

SCHERZ, P. J., HARFE, B. D., MCMAHON, A. P. & TABIN, C. J. 2004. The limb bud Shh-Fgf feedback loop is terminated by expansion of former ZPA cells. *Science,* 305**,** 396-399.

SCHERZ, P. J., MCGLINN, E., NISSIM, S. & TABIN, C. J. 2007. Extended exposure to Sonic hedgehog is required for patterning the posterior digits of the vertebrate limb. *Developmental biology,* 308**,** 343-354.

SCHMID, B., FURTHAUER, M., CONNORS, S. A., TROUT, J., THISSE, B., THISSE, C. & MULLINS, M. C. 2000. Equivalent genetic roles for bmp7/snailhouse and bmp2b/swirl in dorsoventral pattern formation. *Development,* 127**,** 957-967.

SCHOFIELD, J. N. & WOLPERT, L. 1990. Effect of TGF-β1, TGF-β2, and bFGF on chick cartilage and muscle cell differentiation. *Experimental cell research,* 191**,** 144-148.

SEEMANN, P., SCHWAPPACHER, R., KJAER, K. W., KRAKOW, D., LEHMANN, K., DAWSON, K., STRICKER, S., POHL, J., PLÖGER, F. & STAUB, E. 2005. Activating and deactivating mutations in the receptor interaction site of GDF5 cause symphalangism or brachydactyly type A2. *Journal of Clinical Investigation,* 115**,** 2373-2381.

SEKINE, K., OHUCHI, H., FUJIWARA, M., YAMASAKI, M., YOSHIZAWA, T., SATO, T., YAGISHITA, N., MATSUI, D., KOGA, Y. & ITOH, N. 1999. Fgf10 is essential for limb and lung formation. *Nature genetics,* 21**,** 138-141.

SEKIYA, I., TSUJI, K., KOOPMAN, P., WATANABE, H., YAMADA, Y., SHINOMIYA, K., NIFUJI, A. & NODA, M. 2000. SOX9 enhances aggrecan gene promoter/enhancer activity and is up-regulated by retinoic acid in a cartilage-derived cell line, TC6. *Journal of Biological Chemistry,* 275**,** 10738-10744.

SELEVER, J., LIU, W., LU, M.-F., BEHRINGER, R. R. & MARTIN, J. F. 2004. < i> Bmp4</i> in limb bud mesoderm regulates digit pattern by controlling AER development. *Developmental biology,* 276**,** 268-279.

SEO, H.-S. & SERRA, R. 2007. Deletion of< i> Tgfbr2</i> in Prx1-cre expressing mesenchyme results in defects in development of the long bones and joints. *Developmental biology,* 310**,** 304-316.

SETTLE JR, S. H., ROUNTREE, R. B., SINHA, A., THACKER, A., HIGGINS, K. & KINGSLEY, D. M. 2003. Multiple joint and skeletal patterning defects caused by single and double mutations in the mouse< i> Gdf6</i> and< i> Gdf5</i> genes. *Developmental biology,* 254**,** 116-130.

SHARPE, J. 2003. Optical projection tomography as a new tool for studying embryo anatomy. *Journal of anatomy,* 202**,** 175-181.

SHARPE, J., AHLGREN, U., PERRY, P., HILL, B., ROSS, A., HECKSHER-SØRENSEN, J., BALDOCK, R. & DAVIDSON, D. 2002. Optical projection tomography as a tool for 3D microscopy and gene expression studies. *Science,* 296**,** 541-545.

SHEA, C. M., EDGAR, C. M., EINHORN, T. A. & GERSTENFELD, L. C. 2003. BMP treatment of C3H10T1/2 mesenchymal stem cells induces both chondrogenesis and osteogenesis. *Journal of cellular biochemistry,* 90**,** 1112-1127.

SHELDAHL, L. C., PARK, M., MALBON, C. C. & MOON, R. T. 1999. Protein kinase C is differentially stimulated by wnt and frizzled homologs in aG-protein-dependent manner. *Current Biology,* 9**,** 695-S1.

SHEN, M. M. 2007. Nodal signaling: developmental roles and regulation. *Development,* 134**,** 1023-34.

SHETH, R., MARCON, L., BASTIDA, M. F., JUNCO, M., QUINTANA, L., DAHN, R., KMITA, M., SHARPE, J. & ROS, M. A. 2012. Hox genes regulate digit patterning by controlling the wavelength of a Turing-type mechanism. *Science,* 338**,** 1476-1480.

SHI, Y. & MASSAGUÉ, J. 2003. Mechanisms of TGF-β signaling from cell membrane to the nucleus. *Cell,* 113**,** 685-700.

SHORE, E. M., XU, M., FELDMAN, G. J., FENSTERMACHER, D. A., CHO, T.-J., CHOI, I. H., CONNOR, J. M., DELAI, P., GLASER, D. L. & LEMERRER, M. 2006. A recurrent mutation in the BMP type I receptor ACVR1 causes inherited and sporadic fibrodysplasia ossificans progressiva. *Nature genetics,* 38**,** 525-527.

SHUKUNAMI, C., OHTA, Y., SAKUDA, M. & HIRAKI, Y. 1998. Sequential progression of the differentiation program by bone morphogenetic protein-2 in chondrogenic cell line ATDC5. *Experimental cell research,* 241**,** 1-11.

SHULL, M. M., ORMSBY, I., KIER, A. B., PAWLOWSKR, S., DIEBOLD, R. J., YIN, M., ALLEN, R., SIDMAN, C., PROETZEL, G. & CALVINT, D. 1992.

Targeted disruption of the mouse transforming growth factor-β1 gene results in multifocal inflammatory disease. *Nature,* 359**,** 693.
SICK, S., REINKER, S., TIMMER, J. & SCHLAKE, T. 2006. WNT and DKK determine hair follicle spacing through a reaction-diffusion mechanism. *Science,* 314**,** 1447-50.
SLUSARSKI, D. C., CORCES, V. G. & MOON, R. T. 1997. Interaction of Wnt and a Frizzled homologue triggers G-protein-linked phosphatidylinositol signalling. *Nature,* 390**,** 410-413.
SLUSARSKI, D. C. & PELEGRI, F. 2007. Calcium signaling in vertebrate embryonic patterning and morphogenesis. *Developmental biology,* 307**,** 1-13.
SMITS, P., LI, P., MANDEL, J., ZHANG, Z., DENG, J. M., BEHRINGER, R. R., DE CROMBRUGGHE, B. & LEFEBVRE, V. 2001. The transcription factors L-Sox5 and Sox6 are essential for cartilage formation. *Developmental cell,* 1**,** 277-290.
SOLNICA-KREZEL, L. 2003. Vertebrate development: taming the nodal waves. *Curr Biol,* 13**,** R7-9.
SONG, J., OH, S. P., SCHREWE, H., NOMURA, M., LEI, H., OKANO, M., GRIDLEY, T. & LI, E. 1999. The type II activin receptors are essential for egg cylinder growth, gastrulation, and rostral head development in mice. *Developmental biology,* 213**,** 157-169.
SORRENTINO, A., THAKUR, N., GRIMSBY, S., MARCUSSON, A., VON BULOW, V., SCHUSTER, N., ZHANG, S., HELDIN, C.-H. & LANDSTRÖM, M. 2008. The type I TGF-β receptor engages TRAF6 to activate TAK1 in a receptor kinase-independent manner. *Nature cell biology,* 10**,** 1199-1207.
SOSHNIKOVA, N., ZECHNER, D., HUELSKEN, J., MISHINA, Y., BEHRINGER, R. R., TAKETO, M. M., CRENSHAW, E. B. & BIRCHMEIER, W. 2003. Genetic interaction between Wnt/β-catenin and BMP receptor signaling during formation of the AER and the dorsal–ventral axis in the limb. *Genes & development,* 17**,** 1963-1968.
SPIROV, A., FAHMY, K., SCHNEIDER, M., FREI, E., NOLL, M. & BAUMGARTNER, S. 2009. Formation of the bicoid morphogen gradient: an mRNA gradient dictates the protein gradient. *Development,* 136**,** 605-14.
STORM, E. E., HUYNH, T., COPELAND, N., JENKINS, N. A., KINGSLEY, D. M. & LEE, S. 1994. Limb alterations in brachypodism mice due to mutations in a new member of the TGFb-superfamily. *Nature,* 368**,** 639-642.
STORM, E. E. & KINGSLEY, D. M. 1996. Joint patterning defects caused by single and double mutations in members of the bone morphogenetic protein (BMP) family. *Development,* 122**,** 3969-3979.
STOTT, N. S., JIANG, T. & CHUONG, C. M. 1999. Successive formative stages of precartilaginous mesenchymal condensations in vitro: modulation of cell adhesion by Wnt-7A and BMP-2. *Journal of cellular physiology,* 180**,** 314-324.
SUMMERBELL, D., LEWIS, J. H. & WOLPERT, L. 1973. Positional information in chick limb morphogenesis. *Nature,* 244**,** 492-6.
SUMMERHURST, K., STARK, M., SHARPE, J., DAVIDSON, D. & MURPHY, P. 2008. 3D representation of Wnt and Frizzled gene expression patterns in the mouse embryo at embryonic day 11.5 (Ts19). *Gene Expression Patterns,* 8**,** 331-348.

SUN, X., MARIANI, F. V. & MARTIN, G. R. 2002. Functions of FGF signalling from the apical ectodermal ridge in limb development. *Nature,* 418**,** 501-508.
SUZUKI, T. 2013. How is digit identity determined during limb development? *Development, Growth & Differentiation,* 55**,** 130-138.
SUZUKI, T., HASSO, S. M. & FALLON, J. F. 2008. Unique SMAD1/5/8 activity at the phalanx-forming region determines digit identity. *Proceedings of the National Academy of Sciences,* 105**,** 4185-4190.
SUZUKI, T., TAKEUCHI, J., KOSHIBA-TAKEUCHI, K. & OGURA, T. 2004. < i> Tbx</i> Genes Specify Posterior Digit Identity through Shh and BMP Signaling. *Developmental cell,* 6**,** 43-53.
SZALAI, I., CUINAS, D., TAKACS, N., HORVATH, J. & DE KEPPER, P. 2012. Chemical morphogenesis: recent experimental advances in reaction-diffusion system design and control. *Interface Focus,* 2**,** 417-32.
TABIN, C. & WOLPERT, L. 2007. Rethinking the proximodistal axis of the vertebrate limb in the molecular era. *Genes & development,* 21**,** 1433-1442.
TARCHINI, B. & DUBOULE, D. 2006. Control of< i> Hoxd</i> Genes' Collinearity during Early Limb Development. *Developmental cell,* 10**,** 93-103.
TE WELSCHER, P., ZUNIGA, A., KUIJPER, S., DRENTH, T., GOEDEMANS, H. J., MEIJLINK, F. & ZELLER, R. 2002. Progression of vertebrate limb development through SHH-mediated counteraction of GLI3. *Science,* 298**,** 827-830.
TEN BERGE, D., BRUGMANN, S. A., HELMS, J. A. & NUSSE, R. 2008. Wnt and FGF signals interact to coordinate growth with cell fate specification during limb development. *Development,* 135**,** 3247-3257.
THEILER, K. 1972. *The House Mouse: Development and Normal Stages from Fertilization to 4 Weeks of Age,* Berlin, Germany, Springer-Verlag.
TICKLE, C. 1981. The number of polarizing region cells required to specify additional digits in the developing chick wing.
TICKLE, C. 2005. Making digit patterns in the vertebrate limb. *Nature Reviews Molecular Cell Biology,* 7**,** 45-53.
TICKLE, C., SUMMERBELL, D. & WOLPERT, L. 1975. Positional signalling and specification of digits in chick limb morphogenesis. *Nature,* 254**,** 199-202.
TOPOL, L., JIANG, X., CHOI, H., GARRETT-BEAL, L., CAROLAN, P. J. & YANG, Y. 2003. Wnt-5a inhibits the canonical Wnt pathway by promoting GSK-3–independent β-catenin degradation. *The Journal of cell biology,* 162**,** 899-908.
TOWERS, M., MAHOOD, R., YIN, Y. & TICKLE, C. 2008. Integration of growth and specification in chick wing digit-patterning. *Nature,* 452**,** 882-886.
TOWERS, M. & TICKLE, C. 2009. Growing models of vertebrate limb development. *Development,* 136**,** 179-190.
TSUIKI, H. & KISHI, K. 1999. Retinoid-induced limb defects 2: Involvement of TGF-β2 in retinoid-induced inhibition of limb bud development. *Reproductive Toxicology,* 13**,** 113-122.
TUFAN, A. C., DAUMER, K. M., DELISE, A. M. & TUAN, R. S. 2002a. AP-1 transcription factor complex is a target of signals from both WnT-7a and N-cadherin-dependent cell–cell adhesion complex during the regulation of limb mesenchymal chondrogenesis. *Experimental cell research,* 273**,** 197-203.

TUFAN, A. C., DAUMER, K. M. & TUAN, R. S. 2002b. Frizzled-7 and limb mesenchymal chondrogenesis: Effect of misexpression and involvement of N-cadherin. *Developmental dynamics,* 223**,** 241-253.
TUFAN, A. C. & TUAN, R. S. 2001. Wnt regulation of limb mesenchymal chondrogenesis is accompanied by altered N-cadherin-related functions. *The FASEB Journal,* 15**,** 1436-1438.
TURING, A. M. 1990. The chemical basis of morphogenesis. 1953. *Bull Math Biol,* 52**,** 153-97; discussion 119-52.
URIST, M. R. 1965. Bone: formation by autoinduction. *Science,* 150**,** 893-899.
VAN AMERONGEN, R. & NUSSE, R. 2009. Towards an integrated view of Wnt signaling in development. *Development,* 136**,** 3205-3214.
VARGAS, A. O. & FALLON, J. F. 2005. The digits of the wing of birds are 1, 2, and 3. A review. *Journal of Experimental Zoology Part B: Molecular and Developmental Evolution,* 304**,** 206-219.
VERHEYDEN, J. M. & SUN, X. 2008. An Fgf/Gremlin inhibitory feedback loop triggers termination of limb bud outgrowth. *Nature,* 454**,** 638-641.
VERSCHUEREN, K., DEWULF, N., GOUMANS, M.-J., LONNOY, O., FEIJEN, A., GRIMSBY, S., VANDE SPIEGLE, K., TEN DIJKE, P., MOREN, A. & VANSCHEEUWIJCK, P. 1995. Expression of type I and type IB receptors for activin in midgestation mouse embryos suggests distinct functions in organogenesis. *Mechanisms of development,* 52**,** 109-123.
VOGEL, A., RODRIGUEZ, C., WARNKEN, W. & IZPISUA BELMONTE, J. 1995. Dorsal cell fate specified by chick Lmx1 during vertebrate limb development. *Nature,* 378**,** 716-720.
VOKES, S. A., JI, H., MCCUINE, S., TENZEN, T., GILES, S., ZHONG, S., LONGABAUGH, W. J., DAVIDSON, E. H., WONG, W. H. & MCMAHON, A. P. 2007. Genomic characterization of Gli-activator targets in sonic hedgehog-mediated neural patterning. *Development,* 134**,** 1977-1989.
VOKES, S. A., JI, H., WONG, W. H. & MCMAHON, A. P. 2008. A genome-scale analysis of the cis-regulatory circuitry underlying sonic hedgehog-mediated patterning of the mammalian limb. *Genes & development,* 22**,** 2651-2663.
VRIJENS, K., LIN, W., CUI, J., FARMER, D., LOW, J., PRONIER, E., ZENG, F. Y., SHELAT, A. A., GUY, K., TAYLOR, M. R., CHEN, T. & ROUSSEL, M. F. 2013. Identification of small molecule activators of BMP signaling. *PLoS One,* 8**,** e59045.
WADA, N., KAWAKAMI, Y., LADHER, R., FRANCIS-WEST, P. H. & NOHNO, T. 1999. Involvement of Frzb-1 in mesenchymal condensation and cartilage differentiation in the chick limb bud. *INTERNATIONAL JOURNAL OF DEVELOPMENTAL BIOLOGY,* 43**,** 495-500.
WAGNER, T., WIRTH, J., MEYER, J., ZABEL, B., HELD, M., ZIMMER, J., PASANTES, J., BRICARELLI, F. D., KEUTEL, J. & HUSTERT, E. 1994. Autosomal sex reversal and campomelic dysplasia are caused by mutations in and around the< i> SRY</i>-related gene< i> SOX9</i>. *Cell,* 79**,** 1111-1120.
WANEK, N., MUNEOKA, K., HOLLER-DINSMORE, G., BURTON, R. & BRYANT, S. 1989. A staging system for mouse limb development. *Journal of Experimental Zoology,* 249**,** 41-49.

WANG, B., FALLON, J. F. & BEACHY, P. A. 2000. Hedgehog-regulated processing of Gli3 produces an anterior/posterior repressor gradient in the developing vertebrate limb. *Cell,* 100**,** 423-434.
WANG, E., ISRAEL, D., KELLY, S. & LUXENBERG, D. 1993. Bone morphogenetic protein-2 causes commitment and differentiation in C3Hl0T1/2 and 3T3 cells. *Growth Factors,* 9**,** 57-71.
WATANABE, M., IWASHITA, M., ISHII, M., KURACHI, Y., KAWAKAMI, A., KONDO, S. & OKADA, N. 2006. Spot pattern of leopard Danio is caused by mutation in the zebrafish connexin41. 8 gene. *EMBO reports,* 7**,** 893-897.
WEISER, D. C., PYATI, U. J. & KIMELMAN, D. 2007. Gravin regulates mesodermal cell behavior changes required for axis elongation during zebrafish gastrulation. *Genes & development,* 21**,** 1559-1571.
WESTFALL, T. A., BRIMEYER, R., TWEDT, J., GLADON, J., OLBERDING, A., FURUTANI-SEIKI, M. & SLUSARSKI, D. C. 2003. Wnt-5/pipetail functions in vertebrate axis formation as a negative regulator of Wnt/β-catenin activity. *The Journal of cell biology,* 162**,** 889-898.
WHITELAW, V. & HOLLYDAY, M. 1983. Position-dependent motor innervation of the chick hindlimb following serial and parallel duplications of limb segments. *The Journal of Neuroscience,* 3**,** 1216-1225.
WIDELITZ, R. B., JIANG, T. X., NOVEEN, A., CHEN, C. W. & CHUONG, C. M. 1996. FGF induces new feather buds from developing avian skin. *J Invest Dermatol,* 107**,** 797-803.
WILBY, O. 1977. A model for the control of limb growth and development. *Vertebrate limb and somite morphogenesis.*
WINNIER, G., BLESSING, M., LABOSKY, P. A. & HOGAN, B. 1995. Bone morphogenetic protein-4 is required for mesoderm formation and patterning in the mouse. *Genes & development,* 9**,** 2105-2116.
WITTE, F., DOKAS, J., NEUENDORF, F., MUNDLOS, S. & STRICKER, S. 2009. Comprehensive expression analysis of all Wnt genes and their major secreted antagonists during mouse limb development and cartilage differentiation. *Gene Expression Patterns,* 9**,** 215-223.
WOLPERT, L. 1969. Positional information and the spatial pattern of cellular differentiation. *J Theor Biol,* 25**,** 1-47.
WOLPERT, L. 1971. Positional information and pattern formation. *Curr Top Dev Biol,* 6**,** 183-224.
WOLPERT, L. 1989. Positional information revisited. *Development,* 107 Suppl**,** 3-12.
WOLPERT, L., TICKLE, C., SAMPFORD, M. & LEWIS, J. 1979. The effect of cell killing by x-irradiation on pattern formation in the chick limb. *Journal of embryology and experimental morphology,* 50**,** 175-198.
WOODS, C., STRICKER, S., SEEMANN, P., STERN, R., COX, J., SHERRIDAN, E., ROBERTS, E., SPRINGELL, K., SCOTT, S. & KARBANI, G. 2006. Mutations in< i> WNT7A</i> Cause a Range of Limb Malformations, Including Fuhrmann Syndrome and Al-Awadi/Raas-Rothschild/Schinzel Phocomelia Syndrome. *The American Journal of Human Genetics,* 79**,** 402-408.
WOTTON, D. & MASSAGUE, J. 2001. Smad transcriptional corepressors in TGFβ family signaling. *Transcriptional Corepressors: Mediators of Eukaryotic Gene Repression.* Springer.

WOZNEY, J. M., ROSEN, V., CELESTE, A. J., MITSOCK, L. M., WHITTERS, M. J., KRIZ, R. W., HEWICK, R. M. & WANG, E. A. 1988. Novel regulators of bone formation: molecular clones and activities. *Science,* 242**,** 1528-1534.

WRIGHT, E., HARGRAVE, M. R., CHRISTIANSEN, J., COOPER, L., KUN, J., EVANS, T., GANGADHARAN, U., GREENFIELD, A. & KOOPMAN, P. 1995. The Sry-related gene Sox9 is expressed during chondrogenesis in mouse embryos. *Nature genetics,* 9**,** 15-20.

WUNDERLE, V. M., CRITCHER, R., HASTIE, N., GOODFELLOW, P. N. & SCHEDL, A. 1998. Deletion of long-range regulatory elements upstream of SOX9 causes campomelic dysplasia. *Proceedings of the National Academy of Sciences,* 95**,** 10649-10654.

XU, X., WEINSTEIN, M., LI, C., NASKI, M., COHEN, R. I., ORNITZ, D. M., LEDER, P. & DENG, C. 1998. Fibroblast growth factor receptor 2 (FGFR2)-mediated reciprocal regulation loop between FGF8 and FGF10 is essential for limb induction. *Development,* 125**,** 753-765.

YAMAGUCHI, M., YOSHIMOTO, E. & KONDO, S. 2007. Pattern regulation in the stripe of zebrafish suggests an underlying dynamic and autonomous mechanism. *Proceedings of the National Academy of Sciences,* 104**,** 4790-4793.

YAMAGUCHI, T. P., BRADLEY, A., MCMAHON, A. P. & JONES, S. 1999. A Wnt5a pathway underlies outgrowth of multiple structures in the vertebrate embryo. *Development,* 126**,** 1211-1223.

YAMAJI, N., CELESTE, A. J., THIES, R. S., SONG, J. J., BERNIER, S. M., GOLTZMAN, D., LYONS, K. M., NOVE, J., ROSEN, V. & WOZNEY, J. M. 1994. A mammalian serine/threonine kinase receptor specifically binds BMP-2 and BMP-4. *Biochemical and biophysical research communications,* 205**,** 1944-1951.

YAMASHITA, M., FATYOL, K., JIN, C., WANG, X., LIU, Z. & ZHANG, Y. E. 2008. TRAF6 mediates Smad-independent activation of JNK and p38 by TGF-β. *Molecular cell,* 31**,** 918-924.

YANG, X., LI, C., HERRERA, P. L. & DENG, C. X. 2002. Generation of Smad4/Dpc4 conditional knockout mice. *Genesis,* 32**,** 80-81.

YANG, Y., DROSSOPOULOU, G., CHUANG, P., DUPREZ, D., MARTI, E., BUMCROT, D., VARGESSON, N., CLARKE, J., NISWANDER, L. & MCMAHON, A. 1997. Relationship between dose, distance and time in Sonic Hedgehog-mediated regulation of anteroposterior polarity in the chick limb. *Development,* 124**,** 4393-4404.

YI, S. E., DALUISKI, A., PEDERSON, R., ROSEN, V. & LYONS, K. M. 2000. The type I BMP receptor BMPRIB is required for chondrogenesis in the mouse limb. *Development,* 127**,** 621-630.

YOKOYAMA, H., ENDO, T., TAMURA, K., YAJIMA, H. & IDE, H. 1998. Multiple Digit Formation in< i> Xenopus</i> Limb Bud Recombinants. *Developmental biology,* 196**,** 1-10.

YOON, B. S. & LYONS, K. M. 2004. Multiple functions of BMPs in chondrogenesis. *Journal of cellular biochemistry,* 93**,** 93-103.

YOON, Y.-M., OH, C.-D., KIM, D.-Y., LEE, Y.-S., PARK, J.-W., HUH, T.-L., KANG, S.-S. & CHUN, J.-S. 2000. Epidermal growth factor negatively regulates chondrogenesis of mesenchymal cells by modulating the protein kinase C-α,

Erk-1, and p38 MAPK signaling pathways. *Journal of Biological Chemistry,* 275**,** 12353-12359.
YU, K., XU, J., LIU, Z., SOSIC, D., SHAO, J., OLSON, E. N., TOWLER, D. A. & ORNITZ, D. M. 2003. Conditional inactivation of FGF receptor 2 reveals an essential role for FGF signaling in the regulation of osteoblast function and bone growth. *Development,* 130**,** 3063-3074.
ZÁKÁNY, J., KMITA, M. & DUBOULE, D. 2004. A dual role for Hox genes in limb anterior-posterior asymmetry. *Science,* 304**,** 1669-1672.
ZAKIN, L., CHANG, E. Y., PLOUHINEC, J. L. & DE ROBERTIS, E. M. 2010. Crossveinless-2 is required for the relocalization of Chordin protein within the vertebral field in mouse embryos. *Dev Biol,* 347**,** 204-15.
ZEHENTNER, B. K., DONY, C. & BURTSCHER, H. 1999. The Transcription Factor Sox9 Is Involved in BMP-2 Signaling. *Journal of Bone and Mineral research,* 14**,** 1734-1741.
ZEHENTNER, B. K., HAUSSMANN, A. & BURTSCHER, H. 2002. The bone morphogenetic protein antagonist Noggin is regulated by Sox9 during endochondral differentiation. *Development, growth & differentiation,* 44**,** 1-9.
ZELLER, R. 2004. It takes time to make a pinky: unexpected insights into how SHH patterns vertebrate digits. *Science Signaling,* 2004**,** pe53.
ZELLER, R., LÓPEZ-RÍOS, J. & ZUNIGA, A. 2009. Vertebrate limb bud development: moving towards integrative analysis of organogenesis. *Nature Reviews Genetics,* 10**,** 845-858.
ZHANG, H. & BRADLEY, A. 1996. Mice deficient for BMP2 are nonviable and have defects in amnion/chorion and cardiac development. *Development,* 122**,** 2977-2986.
ZHANG, X., ZIRAN, N., GOATER, J. J., SCHWARZ, E. M., PUZAS, J. E., ROSIER, R. N., ZUSCIK, M., DRISSI, H. & O'KEEFE, R. J. 2004. Primary murine limb bud mesenchymal cells in long-term culture complete chondrocyte differentiation: TGF-β delays hypertrophy and PGE2 inhibits terminal differentiation. *Bone,* 34**,** 809-817.
ZHANG, Y., TOMANN, P., ANDL, T., GALLANT, N. M., HUELSKEN, J., JERCHOW, B., BIRCHMEIER, W., PAUS, R., PICCOLO, S., MIKKOLA, M. L., MORRISEY, E. E., OVERBEEK, P. A., SCHEIDEREIT, C., MILLAR, S. E. & SCHMIDT-ULLRICH, R. 2009. Reciprocal requirements for EDA/EDAR/NF-kappaB and Wnt/beta-catenin signaling pathways in hair follicle induction. *Dev Cell,* 17**,** 49-61.
ZHANG, Y. E. 2008. Non-Smad pathways in TGF-β signaling. *Cell research,* 19**,** 128-139.
ZHANG, Z., YU, X., ZHANG, Y., GERONIMO, B., LØVLIE, A., FROMM, S. H. & CHEN, Y. 2000. Targeted Misexpression of Constitutively Active BMP Receptor-IB Causes Bifurcation, Duplication, and Posterior Transformation of Digit in Mouse Limb. *Developmental Biology,* 220**,** 154-167.
ZHAO, Q., EBERSPAECHER, H., LEFEBVRE, V. & DE CROMBRUGGHE, B. 1997. Parallel expression of Sox9 and Col2a1 in cells undergoing chondrogenesis. *Developmental Dynamics,* 209**,** 377-386.
ZHAO, W., SALA-NEWBY, G. B. & DHOOT, G. K. 2006. Sulf1 expression pattern and its role in cartilage and joint development. *Developmental dynamics,* 235**,** 3327-3335.

ZHAO, X., SIRBU, I. O., MIC, F. A., MOLOTKOVA, N., MOLOTKOV, A., KUMAR, S. & DUESTER, G. 2009. Retinoic acid promotes limb induction through effects on body axis extension but is unnecessary for limb patterning. *Current Biology,* 19**,** 1050-1057.

ZHU, J., NAKAMURA, E., NGUYEN, M.-T., BAO, X., AKIYAMA, H. & MACKEM, S. 2008. Uncoupling Sonic hedgehog control of pattern and expansion of the developing limb bud. *Developmental cell,* 14**,** 624-632.

ZHU, Y., RICHARDSON, J. A., PARADA, L. F. & GRAFF, J. M. 1998. < i> Smad3</i> Mutant Mice Develop Metastatic Colorectal Cancer. *Cell,* 94**,** 703-714.

ZIMMERMAN, L. B., DE JESÚS-ESCOBAR, J. M. & HARLAND, R. M. 1996. The Spemann organizer signal noggin binds and inactivates bone morphogenetic protein 4. *Cell,* 86**,** 599-606.

ZOU, H., CHOE, K.-M., LU, Y., MASSAGUE, J. & NISWANDER, L. BMP signaling and vertebrate limb development. Cold Spring Harbor symposia on quantitative biology, 1997. Cold Spring Harbor Laboratory Press, 269-272.

ZUZARTE-LUıS, V., MONTERO, J., RODRIGUEZ-LEON, J., MERINO, R., RODRıGUEZ-REY, J. & HURLE, J. 2004. A new role for BMP5 during limb development acting through the synergic activation of Smad and MAPK pathways. *Developmental biology,* 272**,** 39-52.

ZWILLING, E. 1964. Development of fragmented and of dissociated limb bud mesoderm. *Developmental biology,* 9**,** 20-37.